Proton transfer, electron binding and electronegativity in ammonium-containing systems

Alexander Whiteside

Thesis submitted for the qualification of Doctor of Philosophy,
Heriot-Watt University, Department of chemistry

September 2012

Abstract

Using modern electronic structure methods, the ammonia-hydrogen halide complexes and their anions are characterised to determine the number, type, and properties of their minima, and their electron binding energies. Methodological issues of determining the potential energy surfaces of reactive monomers are addressed in the course of this investigation. The energetic origins of the hydrogen-bonded minima are determined by evaluation of the one-body and two-body terms composing the total energy of the complexes, and a rationale for the drive to proton transfer is presented. It is concluded that the systems have qualitatively similar potential surfaces, and that the balance of the one-body and two-body forces determines the number and depth of minima, while the electron acts as a perturbing agent on the one- or two-body energy, depending upon the nature of the minimum encountered. The halogen-bonded structures of ammonia-hydrogen bromide, iodide, and astatide complexes are shown to be stable, and one may perhaps bind an electron. The concept of the ammonium radical as a pseudo-atom is presented and tested. It is found to show competing pseudo-atomic and molecular properties.

For Andréa

Acknowledgements

The author gratefully acknowledges the EPSRC for their PhD studentship funding. The majority of computer resources were provided by Heriot-Watt University. Additional computer resources were provided by Pacific Northwest National Laboratory / the Department of Energy's Office of Biological and Environmental Research under Grand Challenge project GC20901, "Reliable Electronic Structure Prediction of Molecular Properties".

For untold hours of intellectual support and camaraderie I would like to thank my supervisor, Maciej Gutowski; our collaborators at Johns Hopkins, in particular (but not limited to) Kit Bowen, Soren Eustis, Jing Chen, and Angela Buonaugurio; Maciej Haranczyk; Sotiris Xantheas, my host at PNNL for the 2008 Summer Research Institute; my colleagues in the Gutowski, Paterson, and Macgregor groups at Heriot-Watt; and our past and present project students Elisa Ruhland, Mikaela Nash, Calum Sloan, David Grist and Brian Cox.

I would like to express my gratitude to my family and friends for their companionship, support and patience over the last five years, not least my wife. Thank you.

ACADEMIC REGISTRY
Research Thesis Submission

Name*:*	Alexander Whiteside		
School/PGI:	Chemistry		
Version: *(i.e. First, Resubmission, Final)*	Final	Degree Sought (Award **and** Subject area)	PhD Computational Chemistry

Declaration

In accordance with the appropriate regulations I hereby submit my thesis and I declare that:

1) the thesis embodies the results of my own work and has been composed by myself
2) where appropriate, I have made acknowledgement of the work of others and have made reference to work carried out in collaboration with other persons
3) the thesis is the correct version of the thesis for submission and is the same version as any electronic versions submitted*.
4) my thesis for the award referred to, deposited in the Heriot-Watt University Library, should be made available for loan or photocopying and be available via the Institutional Repository, subject to such conditions as the Librarian may require
5) I understand that as a student of the University I am required to abide by the Regulations of the University and to conform to its discipline.

* *Please note that it is the responsibility of the candidate to ensure that the correct version of the thesis is submitted.*

Signature of Candidate*:*		Date:	

Submission

Submitted By *(name in capitals):*	
Signature of Individual Submitting:	
Date Submitted:	

For Completion in the Student Service Centre (SSC)

Received in the SSC by *(name in capitals):*			
Method of Submission *(Handed in to SSC; posted through internal/external mail):*			
E-thesis Submitted (mandatory for final theses)			
Signature:		Date:	

Table of Contents

Chapter 1: Introduction

This thesis assembles work performed on evaluating the hydrogen-bonded complexes NH_3HX, their anions, and the implicit pseudo-alkali-metal unit NH_4 (ammonium). While the opening sections of the chapters summarise the pertinent literature associated with that research, those discussions are necessarily brief. This introductory chapter provides a broader overview of the literature on proton transfer in the NH_3HX systems, on molecular anions, on electronegativity, and on electron-triggered reactions.

1.1. The Hydrogen Bond and Proton Transfer

The hydrogen bond is the attractive interaction between an acceptor atom in one site A, classically electron-rich, and a hydrogen atom donor in a second site, classically a hydrogen atom bonded to an electronegative atom H-D.[1,2] (Hereafter denoted A···H-D or similar.) A simple electrostatic model appears sensible; however hydrogen bonds are now known to be somewhat covalent in character.[3,4] In fact, hydrogen bonds are characterised by the degree to which the electrostatic and polarisation, charge-transfer (covalent), dispersion (van der Waals) and exchange repulsion dominate the interaction. Electrostatic, polarisation and charge transfer terms dominate in strong bonds, while exchange repulsion and dispersion interactions are the most significant terms in weak bonds.[1,5,6]

The hydrogen bond has several effects upon the donor, the most prominent of which make hydrogen bonding a kind of "incipient proton transfer".[1] Prototypically, the H-D bond is extended and the corresponding stretching mode is softened, moreso as the hydrogen bond becomes stronger (and the distance between the heavy atoms reduces).[1-3,7,8] This is ascribed to the electrostatic hyperconjugate interaction between the donor and acceptor; the proton is attracted to the other heavy atom, and electron density is contributed to the vacant sigma* orbital corresponding to this bond. This charge transfer is present in all hydrogen bonds, and correlates closely with bond strength.[3,9] However this effect is in balance with the Pauli repulsion of the atoms and a rehybridization of the donor which leads to a shortening and strengthening of the bond. Where hyperconjugation is small, as in very weak hydrogen bonds (sometimes argued to be van der Waals interactions[1]), a blue shift and bond shortening may, paradoxically, be observed.[9]

Kock and Popelier established criteria for the definition of hydrogen bonds in the Atoms in Molecules (AIM) model. In that model, chemical structures are described in terms of the topology of the electron density, particularly those points where the gradient is zero (critical points). Chemical bonds are identified as critical points (bond critical points, BCP) where the curvature is negative along an internuclear axis, and positive perpendicular to this axis. Covalent (electron-sharing) interactions exist where there is an accumulation of density (the Laplacian of the density is negative), while closed-shell interactions (such as ionic bonds) exist where there is a deficit of electron density (the Laplacian of the density is positive; see Figure 1.1).[10] Hydrogen bonds were defiend by Kock and Popelier as existing where there is a BCP between the donor and acceptor, with a density between 0.002 and 0.034 a.u. and a local curvature that is positive, from 0.024 to 0.139 a.u., indicating a closed-shell interaction.[11] The density at the critical point is positively correlated with the strength of the interaction, and with the degree of proton transfer.[1,3] The criteria are necessarily equivocal as a consequence, and strong hydrogen bonds exhibit a negative curvature at the BCP, due to an increasing degree of covalency.[1,3]

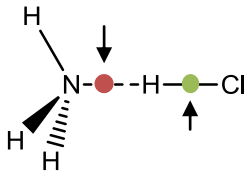

Figure 1.1: Location of the bond critical points (BCPs) in the hydrogen-bonded complex $H_3N^{\cdots}HCl$. The red BCP has a positive Laplacian, indicating the closed-shell closed-shell hydrogen-bonding interaction; the green BCP has a negative Laplacian, indicating the electron-sharing covalent bond.

If the position of a proton is varied across the hydrogen bond, the topological properties of the bond critical points between donor, acceptor, and proton vary continuously. As an example, consider with the hydrogen bonded complex between NH_3 and H-Cl from Figure 1.1, which we label "N". The proton moves toward NH_3. The density at the $NH_3^{\cdots}H^+$ BCP increases, while the Laplacian (second derivative) of the density increases from its original positive value to a peak near the (free-molecule) $NH_3^{\cdots}H^+$ dissociation limit. As the proton approaches NH_3 more closely, the Laplacian drops rapidly below zero. In other words, a covalent bond between NH_3 and H^+ replaces the hydrogen bond. Meanwhile, the reverse occurs at the BCP between H and Cl; the covalent bond is replaced with a hydrogen bond $NH_3\text{-}H^{+\cdots}Cl^-$. We have transferred a proton; as a consequence of moving the charge, we haveformed a zwitterionic complex which we shall label Z.[4,12-15] In the cited studies (which dealt with a different set of systems)

these changes in the topology around the bond critical points occur irrespective of whether this transfer is actually favourable.

Given that the proton seems to be able to bond at the acceptor or donor depending on its position, that hydrogen bonds are an "incipient proton transfer",[1] and that external perturbations can *drive* hydrogen bonded systems along a continuum from weakly interacting to completely proton-transferred,[4] it is worth investigating the circumstances which make a proton transfer across a hydrogen bond favourable or unfavourable. An important test system is the hydrogen-bonded dimer $NH_3\cdots HX$, where X is a halide (the aforementioned NH_3HCl is its most notorious member). The degree of proton transfer in this system has been of theoretical interest to chemists for decades (as this chapter will demonstrate), providing an insight into proton transfer, and is of practical significance for understanding the chemistry of gas giants, where pressures are low and free hydrogen halides have an important role.[16]

The problem of proton transfer in hydrogen-bonded systems can be divided into the contributions from one-body and two-body terms; by evaluating these terms, we can rationalise the role of monomer and two-body properties in controlling proton transfer, and predict what changes will drive or impede proton transfer (Chapter 4). Furthermore, we can investigate whether the perturbation from a third body – an electron in this instance – works through the one or two body terms, or independently of them (Chapters 3 and 5).

The one-body term comes from the balalance of the proton donor and proton acceptor character of the monomers. The hydrogen bond acceptor, A, is typically also a good proton acceptor. However, the conjugate base D^- of the donor DH is also typically a good proton acceptor. If the two monomers are infinitely separated from one another, but able to exchange a proton, the proton is more favourably localised at the species with the greatest proton affinity, and the difference between the proton affinities decides how strong this preference is. This is the one-body energy component of the problem, and it raises the energy of the system with respect to the two free monomers: both species would prefer to be protonated, but only one may be. The balance of the one-body energies nigh-universally favours N.[17,18]

There is also an attractive two-body term, due to the hydrogen-bonding, electrostatic and van der Waals interactions between the monomers. This term is always greater in magnitude than the destabilising one-body energy, because otherwise the N-type structure would not exist. The electrostatic interaction between the ions in Z is always larger than the sum of the weaker interactions in the N, and therefore this two-body term favours Z.

The balance between the one- and two-body terms, then, determines whether the N or Z structure is preferred in isolation. (Matrix effects and outside perturbations can shift this balance, as discussed in section 1.1.5). By computing the values of these terms, and comparing them for different species, it is possible to evaluate which structure is favoured and whether the one- or two-body energy is the dominant contribution. Furthermore, the one- and two-body terms are not constants but are functions of the proton position in the monomers (D-H or A-H^+ bond length) and in the complex (the proton transfer coordinate). By describing how the one- and two-body energies vary with these coordinates, we can gain an insight into the *shape* of the potential energy surface, and thereby several of the properties of the complex (see section 2.7).

1.1.1. The Structure of NH_3HCl

The theoretical study of NH_3HCl arguably begins with Mulliken. His early studies of charge transfer complexes created the categorization "outer complex" for interacting monomers which do not transfer atoms in the formation of the dimer, and "inner complex" for interacting monomers which *do* transfer atoms in the dimer. In this case, N and Z structures would constitute the outer and inner complexes, respectively.[19] Mulliken highlighted the contemporary experimental data for the complex of NH_3 with HCl. In Rodebush and Michalek's study of thoroughly dried NH_3 and HCl vapours above NH_4Cl, the rate at which NH_4Cl condensed out was greatly reduced by drying, indicating that water was an important intermediary in proton transfer.[20] Similarly in Spotz and Hirschfelder's gas phase study, NH_4Cl crystals were formed from NH_3 and HCl gases in air,[21] but a follow-up by Johnston and Manno found that the exclusion of air and use of dry gases prevented precipitation.[22] Clearly, NH_3 and HCl did not undergo proton transfer, unperturbed, in the gas phase.

The early theoretical work was hamstrung by the limited computational resources of the time, but the difficulties encountered would ultimately grant an insight into the importance of electron correlation and basis set effects in these systems. Clementi performed important early theoretical work on the NH_3HCl complex, using the SCF method (see 2.2).[23-25] This study progressed from free NH_3 + H^+ and Cl^- + H^+ fragments, describing the one-body energies of the monomers, to a combined system of interacting units. This work predicted that the Z structure *would* be preferred, would be stable by 19 kcal mol^{-1} with respect to dissociation, and that no minimum would exist for the NH_3HCl N complex.[23] This conflicted with the experimental observation that NH_4Cl crystals are not formed between HCl and NH_3 gases in the vacuum gas phase.[22]

Clementi noted that the omission of electron correlation was likely to cause issues with the shape of the potential energy surface, specifically the presence or absence of a barrier, but did not extend these concerns to the relative stabilities (or existence) of the minima. He argued that NH_4Cl was thermodynamically stable, but that the equilibrium was strongly in favour of the NH_3 and HCl monomers, i.e. it was kinetically unstable.[23] His subsequent paper with Gayles computed that, principally due to the very low barrier to dissociation on the potential surface, the equilibrium did indeed lie far in favour of the neutral molecules, and only parts-per-thousand levels of NH_4Cl would be present in an equilibrium mixture of NH_3 and HCl at experimental temperatures.[25]

Indeed, Goldfinger and Verhaegen were able to detect small amounts of ND_4^+ above solid ND_4Cl and reasonably concluded that it arose from ionisation of ND_4Cl. On the basis of the temperature dependence of the signal they found a value for the dissociation energy of NH_4Cl of 15.2 kcal mol^{-1}, in close agreement to Clementi's value.[26] On the basis of subsequent results it is likely that they had observed a dissociation product of the NH_3HCl Z structure, perhaps as a result of ionisation in a vibrationally excited (and more highly proton-transferred) state.

The most convincing experimental data of this era came from Shibata who performed electron scattering experiments on NH_4Cl vapours and was not only able to pin down the structure of its product as the C_{3v} structure with one proton between N and Cl

(Figure 1.2), but also provide geometric parameters for the internuclear distances. His experimental value for the H-Cl distance of 1.54 Å was indicative of an N structure.[27]

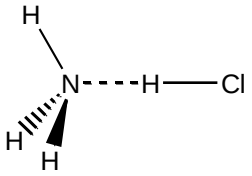

Figure 1.2: The C_{3v} structure of NH_3HCl

Note that Clementi also addressed the charge transfer between NH_3 and HCl in the complex. In this analysis, it was concluded that the interaction between the monomers causes charge transfer from the π orbitals associated with the H atoms on NH_3, to the nitrogen atom; and that subsequently this charge is transferred from the lone-pair σ orbital of NH_3 to Cl *via* the "shuttling" proton. He proposed the intriguing view that the nitrogen atom acted as a "transformer" of charge between the π and σ systems in the molecule in this instance.[24]

Improving computational resources and the dawn of computational chemistry as a field in its own right allowed Raffenetti and Phillips to compute the potential energy surface of NH_3HCl using a counterpoise treatment of BSSE (an issue in intermolecular interactions; see 2.6) and the CI method (for electron correlation; see 2.3.2.1), with large basis sets; this result concluded that the complex was likely to be NH_3HCl, and *not* NH_4Cl as previously believed.[28] An extensive study of the amine hydrogen halides by Brciz *et al*[29] reached the same conclusion, and their study and those by various other researchers established the effect of electron correlation[30-36] and of basis set quality[37] upon the number and type of minima computed for these hydrogen-bonded systems.

Essentially, the omission of electron correlation (see section 2.3 for a general overview) can lead to an underestimate of the intermolecular interaction energy for N (due to neglect of dispersion), which will tend to both unphysically stabilise Z with respect to the N, and lead to the appearance of an unphysical barrier between the two structures. In a significantly later study, Biczysko and Latajka established that the inclusion of very high level treatments of electron correlation – up to CCSD(T) – are required for the accurate quantitative description of the potential energy surfaces for the proton-transfer complex, e.g. the proton-shuttling vibrational frequency, in NH_3HF, NH_3HCl, and NH_3HBr, while cementing the view that NH_3HX takes the N structure.[38]

One particularly curious result was obtained by Famulari *et al*, using an *a priori* correction for BSSE, MCSCF, and a robust (Dunning-type TZ basis set (section 2.4). Their calculation of the NH_3HCl proton-transfer potential energy surface indicated a local minimum for the Z structure.[39] However this study used a rigid one-dimensional potential energy surface where only the position of the transferred proton was changed. It is now known that the "breathing" motion between the monomers is strongly coupled to the proton position, and so moving the proton without making the corresponding breathing motion artificially elevates the energy of the system. It is the author's opinion that this is the source of the barrier. (See also section 2.7.1). Such an issue was anticipated by Raffenetti and Phillips.[28] Regardless, the MCSCF method used in Famulari *et al*'s study provides information on how the N and Z "character" combines in the observed complex . A small amount NH_4Cl character in the N complex is responsible for the red-shift in the HCl vibrational frequency.[39]

Parallel experimental studies had issues of their own that shed light on the sensitivity of the proton transfer process in hydrogen bonds, in this case the issue of matrix effects. Interim experimental IR studies established quite definitively that NH_3HCl had a C_{3v} hydrogen-bonded structure,[40] but could not determine well the degree of proton transfer. This is now believed to be due to the role of matrix effects (specifically, the polarizability of the matrix, and the resultant field) in triggering proton transfer.[41,42] A 15 K infrared spectroscopy study in nitrogen by Ault *et al* suggested that the structure of NH_3HCl was intermediate between N and Z, for example,[40,43] An attempt to disentangle the contradictory theoretical and experimental results was made by Barnes *et al*, who moved to a less polar argon matrix and found greatly reduced proton transfer in NH_3HCl and the other amine-HCl complexes.[44,45] Modern studies in even more inert matrices continue to show a higher degree of proton transfer than that seen in the gas phase.[46]

The definitive experimental work on the structure of NH_3HCl was performed by Goodwin, Howard and Legon, using gas phase microwave spectroscopy. Their studies thoroughly characterised the NH_3HCl system as hydrogen bonded,[47-49] with particular insight from isotopic substitution of the hydrogen in the acid.[47] They found that the nuclear quadrupole coupling constant for the chlorine atom and intermolecular force constant was quantitatively consistent with an HCl unit perturbed by NH_3, rather than NH_4Cl (assuming that the quadrupole coupling with NH_4 would be similar to that

of the alkali chlorides). Their data indicated an N-Cl distance close to that of the NH_3HCl structure originally report by Latajka *et al.*[30]

1.1.2. From NH_3HCl to NH_3HBr and NH_3HI

Contemporary to the revival of the issue of the structure of NH_3HCl by Raffenetti and Phillips, theoreticians and experimentalists had began exploring the issue of proton transfer in the other hydrogen halide-amine systems, with either more labile hydrogen halides or more basic amines. Similar experimental and theoretical issues were encountered to those in the NH_3HCl studies.

Early computational work suggested that the complexes containing halides heavier than Cl would be proton-transferred or intermediate in structure, but as noted in the previous section on NH_3HCl, these results did not account for electron correlation and thus were likely to overestimate the degree of proton transfer.[50-52] The addition of MP2 electron correlation (section 2.3.2.3) to NH_3HBr in Latajka *et al*'s study of NH_3HBr only succeeded in recharacterising the system from one capable of adopting both N and Z structures, to one having an intermediate structure between those extremes.[51] Brciz *et al* (correctly) characterised NH_3HBr as an N-typestructure by using a now-obscure electron correlation method called CEPA[53] (a sort of approximate coupled cluster) with double-zeta, polarised basis sets, but this result was not yet persuasive.[29] Later calculations by Latajka *et al* with superior basis sets convincingly characterised NH_3HBr as the an N structure.[38,52]

Continuing on this theme, Kollman *et* al studied NH_3HI at the SCF level using an *ad-hoc* correction to the NH_3 proton affinity but obtained inconclusive results.[50] However a particularly strong early study was performed by Jasien and Stevens, who applied electron correlation by CCD (see 2.3.2.2) and zero-point corrections to establish the existence of a single N-type minimum for NH_3HCl and NH_3HBr, but two minima for NH_3HI, the N-type one being more stable than the Z-type.[35] Latajka *et al* attempted to characterise the potential energy surface of NH_3HI at the MP2 level, and found two shallow minima, perhaps coalescing into a very broad well with complete sharing of the proton. However given that the N was increasingly favoured when moving to the MP4 level, there is reason to suppose that a higher-level treatment may find just a single N-type minimum.[52]

Experimentalists found NH_3HBr and NH_3HI as challenging as their lighter counterpart. Nitrogen matrix IR studies initially suggested that NH_3HBr was proton-transferred,[43] but the argon matrix work of Barnes *et al* again pointed towards a system which would adopt an N-typestructure in the gas phase butwas being perturbed by the matrix to favour a Z-type structure.[54] Comprehensive studies by Schriver *et al*,[55] Andrews *et al*,[41,56,57] Barnes *et al*,[58,59] Liu *et al*[60] and del Bene *et al*[61] show that the measured degree of proton transfer in NH_3HX is strongly matrix-dependent, to the extent that changing matrix by one step in the sequence gas-Ne-Ar-N_2 causes a change in degree of proton transfer equal to substituting for the next halide in the series F-Cl-Br-I.

Howard and Legon followed up their seminal microwave study of NH_3HCl with an equivalent analysis (albeit without isotopic labelling of hydrogen) of NH_3HBr, in search of a proton-transferred complex.[62] Early computational studies had suggested the existence of such a minimum. Given the soft intermonomer stretching mode and the value of the quadrupole coupling between the nitrogen and the bromine (i.e. similar arguments to those for NH_3HCl), they concluded that this was also an N structure with a small amount of charge transfer and little geometric perturbation. Legon confirmed that this extended to NH_3HI with an analogous study.[63]

1.1.3. Modelling and generalisation to other hydrogen-bonded systems

As theoretical tools began to assign the correct qualitative structure to the ammonia-hydrogen halide complexes, investigation into the electronic structure of these systems began in earnest. One of the most extensive computational studies is that performed by Alkorta *et al*, with the specific goal of addressing the driving force for proton transfer.[17] Their systematic DFT study crossing the hydrogen halides with a variety of bases (including NH_3 and the methylamines) drew several useful conclusions. Most pertinent to this section was the observation that the strength of the N complexes grew with the electronegativity of the halogen, while the strength of the Z complexes dropped. The N complex becomes more stable because of the increase in the polarisation of H-X, and thus the electrostatic intermolecular interaction. The Z complex becomes less stable because the one-body term to dissociate the H-X bond increases, while the counterbalancing electrostatic two-body interaction does not increase as rapidly.[17]

Secondly, and most importantly, Alkorta *et al*. deduced a simple model for whether proton transfer will occur with a given acid and base. For a pair of ions A^- and HB^+, there is a distance R_c where the electrostatic interaction between these ions (which varies with the inverse of the distance) becomes so large that it is greater than the difference between the proton affinities of the free molecules, and these ions (the Z structure) are favoured over the neutral molecules (the N structure). Note that the difference between the proton affinities of the free molecules is the asymptotic limit of the "difficulty" in forming the ion pair; in reality, proton transfer is slightly easier because the proton is still near *both* molecules On the other hand, the model assumes that the interaction between the neutral molecules is zero, but it is actually finite. Alkorta *et al* supposed that two molecules could not come closer than 2.8 Å, and therefore the electrostatic interaction at that distance had to be greater than the difference in two-body energies if proton transfer was to occur. They computed the electrostatic energy between two point charges at that distance, giving a critical value of 120 kcal mol^{-1}. If the difference in one-body energies is greater than this value, then the molecules cannot approach close enough for the electrostatic two-body term to rise enough to overcome it.[17]

A similar treatment had been suggested by Ault and Pimentel in the publication of one of their matrix isolation studies, which put the threshold at 124 kcal mol^{-1}, and forecast the critical internuclear distances for the NH_3HBr and NH_3HI complexes at 2.90 Å and 3.17 Å, respectively.[40] These models were borne out by their computational data points, although of particular note was the fact that NH_3HI was found to be a borderline case. These models are grossly simplified in a manner that does not consistently favour the neutral molecules or the ions. For example, omitting valence repulsion will oppose the approach of the ions, disfavouring Z at any internuclear distance, while hyperconjugation which will act to weaken the A-H bond and thereby make proton transfer more favourable. However these approaches provided some of the first reliable benchmarks for the likelihood of proton transfer between acids and bases.

1.1.4. NH_3HF: an outlier

NH_3HF poses a number of experimental issues, not least the corrosiveness of HF, which have limited the experimental research into the structure of NH_3HF. Notwithstanding this difficulty some studies went ahead, and fortunately unlike the other NH_3HX systems, there was little ambiguity about its structure in either experimental or theoretical studies, due to fluoride's great affinity for the system's proton. Shibata's electron scattering studies reportedly found the C_{3v} structure seen in NH_3HCl (see [27]). Johnson and Andrews' argon matrix IR study characterised the complex as HF only modestly perturbed by NH_3, albeit with a large amount of charge transfer.[64] Even SCF-level theoretical calculations indicated a very small amount of proton transfer.[65] Szczesniak *et al* performed later computational studies on NH_3HF at the MP2 and MP3 levels, and found that correlation, while not necessary for the qualitative description of the NH_3HF complex, reduced the already small degree of proton transfer and perturbation.[66] However, measurements of the complex's dipole moment and the geometric parameters have unfortunately remained unpublished. (See ref.s 10 and 11 in [64]).

1.1.5. Additional degrees of freedom: variation of the base or environment

Although beyond the remit of this thesis, we may also consider the situation in which we change the other one-body term by varying the base. Adding methyl groups to ammonia will increase its proton affinity, increase the degree of proton transfer in the system, and ultimately should "tip the balance" in favour of the proton-transferred structure, as indicated by experimental[43,45,48,54,67-69] and computational studies.[17,29,30,51,52,67,70] In their DFT analysis of the hydrogen halides (up to iodine) versus a variety of nitrogen- and phosphorus-containing bases, Alkorta *et al* found that the use of strong bases was expected to create the Z structure in many cases.[17] As expected, strong acids and bases tended to favour Z, while weak acids and bases tended to favour the N structure. HBr, being a strong acid, had a Z structure in all cases, although given that this includes NH_3 there is likely some degree of overestimation. HF, meanwhile, made N favourable in all but two cases, congruent with Szczesniak's *et al*'s earlier study that the methylamines are simply not strong enough bases given HF's poor acidity.[66] With one exception, only a single minimum

was found on the potential energy surface, *i.e.* either N or Z structure weas obtained,[17] as anticipated for correlated calculations.[30]

Proton transfer may also be triggered by an outside perturbation. In a similar manner to the effect of polarisable matrices, the addition of a polar solvent leads to increased proton transfer, as a microscopic example of solvation,[36,71-78] while the addition of other NH_3HX dimers can also make proton transfer possible as a microscopic form of crystal formation.[79,80] Even on ice, the hydrogen chloride is ionised to a hydrated chloride anion and a hydrated proton, which can then find and react with hydrated NH_3 to form ammonium.[81]

Related to matrix effects, proton transfer can also be facilitated by the application of an outside electric field, which favours the formation of a large dipole on the complex by proton transfer.[82,83] As well as providing a way to model matrix effects,[83] such fields allow experimental and computational studies of one system with an arbitrary intermediate degree of proton transfer determined by the field strength.[82,83]

In the gas phase hydration of NH_3HX, the acidity of the halide controls the rate at which additional water molecules enhance proton transfer. Recall that it is the difference in one-body proton affinities of the monomers that must be overcome; the more acidic the hydrogen halide, the smaller the imbalance is. (Some of this imbalance is reduced by the two-body energy term.) Correspondingly, one molecule of water has been shown in simulations to drive NH_3HBr to proton transfer, two water molecules to drive transfer in NH_3HCl, and three to cause transfer in NH_3HF.[71-73,77] The addition of water molecules stabilises tZ (which is ionic) more favourably than the N, and ultimately moves the balance in favour of proton transfer. Contrary to the above, only one additional *ammonia* is needed to drive proton transfer in the halides heavier than F.[75]

Mulliken proposed that the clustering of many NH_4Cl units could ultimately construct a local environment where the electrostatic stabilisation by the other NH_4Cl would lead to the thermodynamic favourability of proton transfer.[19] However, the kinetic improbability of forming these NH_4Cl units and bringing them together in clusters in the first place would require high pressures.[19] This problem was revisited by Cheurng and Tao, who studied the clusters $(NH_3HX)_n$ at the DFT and MP2 level, where X is F, Cl, or Br.[79,80] For n=1, the hydrogen bonded structure with only a mild perturbation

of the H-X bond was predicted. For *n*=2 and above and X=Cl and Br, a wholly ionic cluster was predicted and for *n*=4, even fluorine was expected to form a microscopic salt crystal. Naturally, at very large *n*, we have the macroscopic crystal.

Cheurng and Tao made the interesting proposal that the observed proton transfer was due to the strengths of the intermolecular interactions (i.e. the 2-body term) but also the rate at which those terms increased. For increasing *n*, a single new hydrogen-bonding interaction is available to each dimer, but n new ionic interactions can be obtained. They forecast that the ionic advantage would become saturated once the halides were fully surrounded by base units (and *vice versa*). Therefore an amine-hydrogen halide which did not undergo proton transfer with a sufficiently large number of other dimers would *never* undergo proton transfer.[79,80]

1.1.6. Summary

In summation, the NH_3HX systems are a prime example of the careful balancing act of the intermolecular forces behind proton transfer, which both makes them an excellent test case and a theoretical and experimental challenge. A great deal of progress has been made through a combination of Legon and collaborators' experimental ingenuity in gaining true gas phase studies, and the improvement of computational techniques to the point where they could describe the underappreciated non-electrostatic effects involved. Principally, the use of poor theoretical tools tends to favour the more electrostatic Z structure, and exaggerate or create barriers between the Z and N structures.

That said, this thesis has two primary themes. Firstly, it determines the role of one- and two-body energy terms in the overall favourability of proton transfer in the ammonia-hydrogen halide hydrogen bonded complexes. This is the subject of Chapter 4. Secondly, itinvestigates the effect of a very simple chemical perturbation – the binding of an electron, to create the molecular anion – upon the degree of proton transfer in these systems, which is discussed in Chapters 3 and 5.

1.2. Anions

To understand the anions of the NH_3HX systems, it is vital to first understand the nature of anions in general.[1] At the simplest level, an anion is any chemical system in which the number of electrons is greater than the number of protons, the singly-charged anion being most commonplace due to the Coulombic repulsion between a singly-charged anion and an electron[84] (although multiply-charged anions are not out of the realm of possibility,[85] that research often focuses on providing many discrete sites for the electrons to bind[86,87]). These may be classified by the mechanism by which the excess electron is bound, and the ultimate fate of the anion once created.

1.2.1. Methods of Binding an Excess Electron

The simplest anions are valence anionsof open-shell parents, for example the chloride anion or the hydroxide anion, where the inclusion of an additional electron in the valence orbital satisfies the valence of the system and closes the shell. However the modern study of molecular anions is typically focussed upon those in which an "extra" electron has been added to a system which already has a closed shell. The nature of the interaction and the consequences categorise the anions. In this review, anions where the incident electron has negligible kinetic energy shall be considered (i.e. we shall study the properties of *anions*, not of the electron impact).

The first and simplest such anion is, as mentioned above, the valence anion, where the excess electron appears in a valence orbital of a molecule which may or may not have a closed shell. As valence electrons are closely bound to the system, their orbitals typically exhibit nodal structure within the nuclear framework (Figure 1.3), and consequently the binding of an electron can lead to a change in the nuclear structure, the bond strengthening or weakening that undergraduate chemists learn to associate with bonding and antibonding orbitals.[88] More unoccupied orbitals are antibonding than bonding as they accumulate ever greater numbers of nodes to satisfy their orthogonality with the remainder of the molecule, and therefore bond weakening is more commonplace.

[1] This section of the review is addressed primarily with the phenomenology of dipole-bound anions; the relevant theory of anions is discussed in Chapter 2.

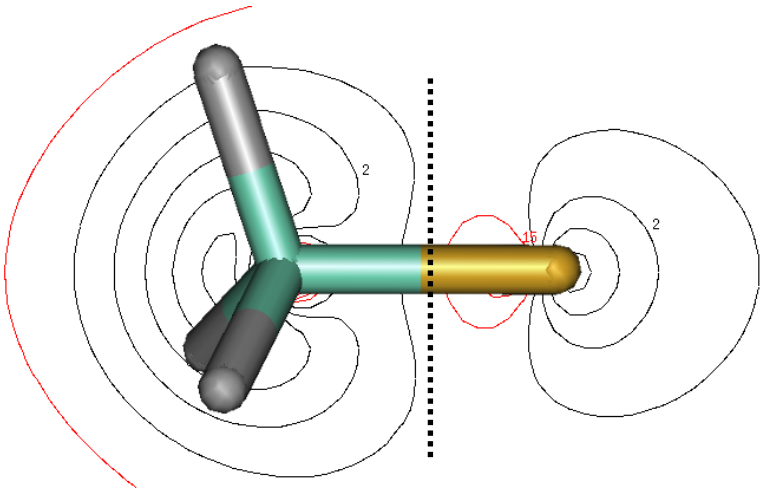

Figure 1.3: The lowest unoccupied orbital (red and black contour lines, denoting phase) of CH_3F, which has a node (dashed line) between C and F. If an electron occupies this antibonding valence orbital to form the CH_3F anion, the C-F bond will weaken.

The second and, for this thesis, most relevant type of anion is the multipole-bound anion. In this class of systems the positive regions of the multipole on a molecule – such as "N" the end of the dipole that exists across NH_3HX - bind an excess electron.[89] Due to the rate of decay of the multipole interaction (r^{-2} for a dipole, r^{-3} for a quadrupole, *etc.*) dipole-bound anions are the most common.[84] The resulting electron density is diffuse, and therefore although orthogonality must be satisfied, the interaction between the dipole-bound electron and the nuclear framework is weak.

A notable strong early study by Miller *et al* addressed the alkali halide anions MX^-. This study sought to understand whether the electronis bound by the dipole, *i.e.* $[M^{+\cdots}X^-]^-$ or the electron simply occupyies the diffuse *s* orbital of the alkali metal ion, with some polarisation by the halide anion, *i.e.* $M^{0\cdots}X^-$. Their study hypothesised that in the "valence" scheme the vertical detachment energy of the anion would be correlated with the polarizability of the alkali metal atom and the inverse square of the internuclear distance (α/r^2). Their data indicated no strong correlation between the dipole moment and the vertical detachment energy, but a clear correlation with α/r^2, validating this "valence" picture.[90]

The solvated electron is closely related to the dipole-bound anion. In these systems, an electron is not bound by the sum multipole of a group of molecules. Instead, the multipoles (typically dipoles) of the solvent molecules arrange such that their positive ends are directed towards the electron. Although the total dipole of the group is near zero by cancellation of the dipole vectors, there exists a local region of positive electrostatic potential where the electron may reside (Figure 1.4).[84,89,91]

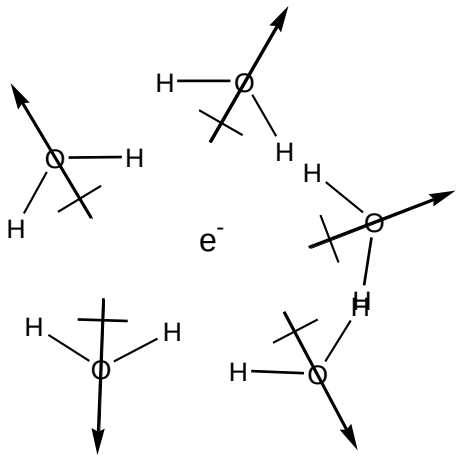

Figure 1.4: Schematic illustration of a solvated electron in water

The classic example of a solvated electron is the blue solution of an alkali metal in ammonia, where the blue colour arises from visible-light absorption by the solvated electrons. Similar principles lie behind the proper description of species such as dipole-bound anions and the less-electronegative halide anions in solution, where the charge on the solute is distributed into the solvent.[84] There is an ongoing lively debate about whether the solvated electron, and its solid-state peer, the electride (an electron occupying an anion site in a crystal lattice),[92] constitute anions in their own right. There is computational evidence of electron density maxima in the vicinity of solvated electrons; which in the AIM formalism, which attempts to describe molecular systems entirely in terms of the electron density (see also section 1.1) electron density maxima are defined as nuclear attractors, i.e. the nuclei of atoms.[93]

The most curious of the bound anions is known as the Rydberg anion.[84] These states, analogous to the Rydberg series of orbitals of the hydrogen atom, bind electrons due to the long-range potential of the molecule, out where the valence repulsion to the excess electron is weak and dispersion and other higher-order interactions can have a significant effect.[84] Such species typically find a use as very soft electron sources for the formation of anions of other species.[94]

The terms “correlation-bound anion” and “dispersion-bound anion” have been coined for anions of any of the foregoing types which are bound primarily through the correlation effects in general and dispersion interaction in particular between the extra electron and its neutral host, rather than the electrostatic interactions which are typically used to rationalise them.[95-97]

1.2.2. Unbound Anions

There exists a third class of anion, the anionic resonance or unbound anion, in which the electron interacts with a molecule (*e.g.* by scattering) but is adiabatically unbound: the resulting anion is higher in energy than the relaxed neutral molecule .[88,89] These are divided into shape resonances, so named because the electron is bound by the "shape" of the molecule-electron potential which temporarily blocks its escape (*e.g.* a centrifugal barrier),[88,89,98] and excited resonances, in which the mixing of excited vibrational and/or electronic states creates an anion state that is higher in energy than the associated vibrationally excited neutral ("vertical detachment" is exothermic), but not with respect to the neutral ground state.[88,89,98] Vibrationally-excited resonances are known as Feshbach resonances; electronically-excited resonances in the vibrational ground state are known as core-excited shape resonances (where the core is the parent molecule),[88,89] and finally electronically- and vibrationally-excited resonances are termed core-excited Feshbach resonances.[88]

1.2.3. The Fates of Anions

The fates of the anions are determined by two factors. First, each of the anion classes outlined in the previous section can couple to the others, including the unbound states. Secondly, and importantly for chemistry, structural changes can occur that bind the electron more permanently,[99-101] or which lead to the breakdown of the molecular framework, or even aggregation.[88] This is dependent upon the electron's lifetime being large. It is infinite in the case of bound electrons, and for shape resonances is strongly dependent upon the coupling to bound states, for example.

In dipole-bound anions, as noted previously, the interaction with the molecular framework are not strong and the geometric perturbations are typically mild.[102] However, a system may undergo a geometric change which produces a more stable anion. In the alkali halide and dipole-bound anions, the system relaxes by increasing the alkali-halogen distance, congruent with both an increase in the stability of the excess electron, and the weakly antibonding nature of the SOMO.[90,103] This raises the question: are these the effect of the SOMO's antibonding nature, or the enhancement of the electron binding that these changes provide?

The effect is more pronounced in cyanoacetylene, which has a linear dipole-bound anion, while a significantly more stable valence anion with a "zig-zag" state is

available,[99,100] while $(HF)_3$ prefers a cyclic structure which restricts its dipole moment, and its anion prefers a "zig-zag" structure to maximise the dipole moment (Figure 1.5).[104] The lowest-energy tautomers of several nucleic acid base anions are not the lowest-energy ("canonical") tautomers of the neutrals, as the need to stabilise the excess electron adds an additional term.[105-110]

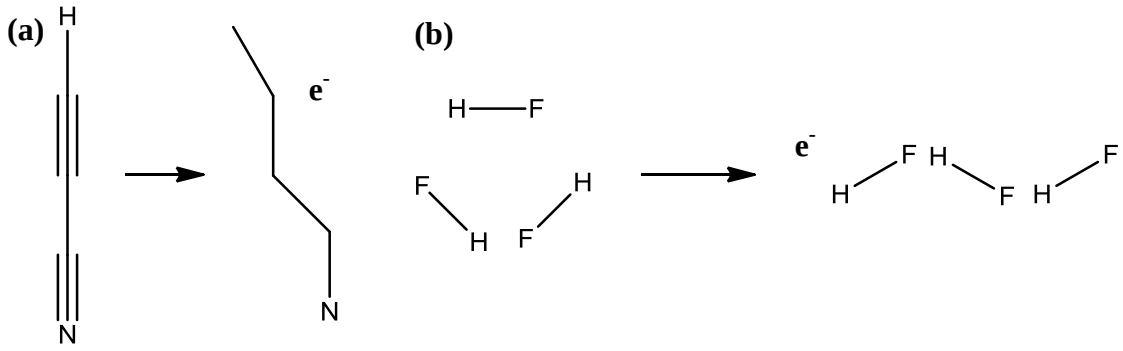

Figure 1.5 (a): Cyanoacetylene neutral structure and zig-zag valence anion; bond orders in the anion are ambiguous. (b): Cyclic, dipole-minimising structure of the HF trimer, and the linear dipole-maximising structure of its anion.

Hydrogen bonds provide a particularly appealing target. The hydrogen-bonded complexes $H_2O^{\cdots}HCl$ and $HOH^{\cdots}NH_3$ show a weakening and softening of the bond between the donor and the hydrogen upon binding of the electron, with the addition of an extension of the distance between the two heavy atoms that further enhances the dipole.[111,112] In NH_3HCl, binding the excess electron drives complete proton transfer to the ammonia, producing an $(NH_4Cl)^-$ complex reminiscent of the alkali halide anions.[113] In the thymine-glycine dimer anion, proton transfer is similarly triggered upon binding of an extra electron,[114] More generally, dipole-bound anions exhibit a softening and lengthening of any bond, be it intra- or inter-molecular, which can be characterised as providing the dipole moment, so that the dipole is enhanced.[102]

Dissociative electron attachment (DEA), wherein a molecule decomposes upon the binding of an excess electron, is a well-studied class of reactions. DEA is of particular interest as a way to chemically process surfaces with electron beams as a form of lithography for nanotechnology. A little-appreciated counterpart exists, known as associative attachment, in which an electron can bind two fragments together that would not otherwise be stable. Such a three-body interaction is an unlikely process but has nevertheless been proposed in the case of heterogeneous and homogeneous clusters.[88,98]

DEA is traditionally associated with valence anions, particularly the occupation of antibonding valence orbitals associated with the bonds to be broken.[115-118] Alternatively, the exotherm associated with the electron affinity and any electron kinetic energy may be greater than the dissociation energy of the molecule. If the molecule has no way to disperse this energy, it may fragment.[94] Regardless, the lifespan of the anion between electron binding and dissociation is dependent upon the dissociation pathway. For a polyatomic molecule, it may be a matter of milliseconds before the molecule samples the region of the potential energy surface that allows it to dissociate; for diatomic molecules the lifespan is no more than a vibrational period.[88]

The final possible fate of an anion is, of course, electron autodetachment, which is possible under a variety of circumstances. In resonances, this is a matter of course; ultimately electronic and/or nuclear relaxation leads to the escape of the electron or decay into another state.[88,89]

1.2.4. Low energy electron attachment to DNA

Given the previous discussion, it is worth highlighting one of the most practically-revevant electron-triggered reactions, which happens to involve the whole spectrum of anions: the reductive DNA damage caused by secondary electrons from ionising radiation. This radiation is so named because the energy of a single incident particle or quantum of radiation is sufficient to eject completely electrons from molecules and atoms, forming cations. As implied previously, the majority of electrons in a stable molecule are to be found in the stable bonding orbitals, therefore there is a high likelihood that the radiation will cause a weakening of the bonding framework of the molecule, possibly leading to dissociation. At any rate, the bonding framework will change, *i.e.*chemical damage has been initiated by the physical ionisation process. The incident radiation may also dump significant energy into the molecule's vibrational or rotational modes.

Where the ionised molecule is a DNA strand, this leads to damage which, if left unrepaired, may cause problems in proper cell functioning and replication, leading to disease and possibly cancer. When high-energy radiation passes through an aqueous medium, it does not simply dump all of its energy onto the first molecule it encounters. The nucleus or photon dumps energy into the medium gradually, ionising the water and producing streams of relatively high-energy secondary electrons.[119,120]

The journey through our medium has, in 10^{-16} to 10^{-18} seconds, produced a wake of sites containing low energy electrons, ionised water molecules, excited water molecules, protons, hydroxyl anions, and aqueous radicals. Although the other species are important in creating a variety of radiation products, the low-energy electrons dominate. Thermalisation and solvation, resulting in almost-zero-energy electrons is rapid, and recombination with the water cations is considered unlikely.[119]

These electrons have low energies, but they are by no means benign. As discussed previously, electron attachment can lead to processes such as DEA. One particular area of interest is low-energy electron attachment to DNA, for example Sanche and coworkers' seminal paper in 2000.[121] Their experimental work demonstrated that low-energy electrons (< 20 eV) can cause single- or double-strand breaks in the DNA chain, with clear peaks indicating some resonant process above a monotonous background (*i.e.* some precise electron-capture process is involved). In other words, the kinetic energy of the elecron need not be large for damage to occur. Since then, there has been a great interest in exploring low-energy or zero-energy electron damage to DNA, including finding the mechanisms for this strand breaking process.

Much research has been concerned with discussing valence- and dipole-bound anions, considering metastable anions to simply be "doorways" to these states, rather than reactive intermediates in themselves.[122,123] DNA bases, for example, can form dipole-bound anions in isolation and valence anions when they dimerize.[124] However, the significance of shape resonances in these processes is now being appreciated.[125,126] It is interesting to note that although the nucleic acid bases can bind electrons more strongly than the backbone, and large chains of guanine resides appear to be efficient at capturing electrons (either with the guanine dipole or *via* resonance states) the electrons may not be ultimately localised on the bases themselves.[123]

Calculations on phosphate fragments have suggested that binding of very low-energy (< 5 eV) electrons can simply break the sugar-phosphate backbone by DEA.[127] This is a simplistic model, but even more comprehensive calculations have suggested that such incompletely thermalised (2-3 eV) electrons may attach directly to the phosphate group in the backbone,[128] and perform some DEA process.

Below energies of a few eV, binding of an electron to the backbone at the equilibrium geometry is considered unlikely, as with the exception of guanine, binding to the base

should be favoured.[128,129] It has been suggested that base excision may occur directly by DEA of low energy electrons to the base itself. This is not just a structural failure in the strand and a loss of a "bit" of genetic information, as the resultant sugar radical can cleave the backbone. A reactive hydrogen radical is then produced, and the excised base can itself abstract hydrogen from its surroundings on the DNA strand.[130]

Electron attachment to the base is one of the most significant low-energy processes, in comparison to dissociative attachment *via* the backbone.[131] It is widely suggested that < 5 eV electrons can perform DEA to the nucleic acid bases to release hydrogen radicals or hydride ions, which can then further react to cause damage to the DNA molecule.[122,132,133][134-136] This process may be highly selective, with the electron energy determining the hydrogen removed, yet it appears to be indirect.[137,138] It has been suggested that by replacing the target hydrogen with a halogen, haloradicals could be released during radiation exposure, which are much more reactive. Therefore halo-nucleotides could act as novel sensitizers for radiation therapy.[139,140]

While these DEA processes are interesting and *create* reactive species which may damage the backbone, metastable resonances may be very important in inducing strand breaks directly. It has been suggested that a π* shape resonance (see 1.2.2; in this case the "shape" capturing the electron is associated with a π* orbital) of the base may temporarily bind an electron, and then stretching of the C-O bond can make the π*-anion and the backbone-based σ* C-O anion degenerate. The electron can then transfer into the σ* orbital, and therefore the anion equilibrium C-O bond length is greatly increased and the barrier to dissociation is significantly lower. This is unlikely in the gas phase due to the high probability of autoejection of the electron from the π* orbital and the inhibition of electron transfer by base stacking, but becomes plausible in the solution phase, where the π* orbital may become bound or, at least, more stable.[125,126,141] The term "indirect dissociative electron attachment" has been coined for such processes.[142]

It is interesting to note that there exists a weakly-bound π* valence anion of uracil which becomes bound with respect to the anion when the ring is puckered;[106] this may be related to the π* shape resonance discussed above. Sommerfeld noted a *Feshbach* resonance of uracil that coupled a highly-vibrationally-excited form of its

dipole-bound anion to its valence anion. The resultant valence anion would have significant internal energy, which could induce DEA.[101]

It has been shown that certain tautomers of the nucleic acid base anions (formed by transfer of hydrogen from an abasic nitrogen to one of the carbon atoms, for example) are more stable than the "canonical" anion. As mentioned previously, the "canonical" valence anions of the nucleic acid bases may not be stable at their equilibrium geometries at all, and therefore fragment.[106] The tautomers, once formed, may not base pair correctly, leading to transcription and replication errors, *i.e.* mutations. The relative stabilities of the "non-canonical" tautomers is believed to be due to the stabilisation of the excess electron's orbital. [105-110,114] In this case, the origin and energy of the excess electron is not particularly significant, provided that it can bind long enough for the tautomerisation to occur.

1.3. Proton-coupled electron transfer

Tautomerisation or proton transfer triggered by an excess electron may be considered as a proton transfer process coupled to the position of an electron. It therefore belongs to the class of reactions known as "proton-coupled electron transfer", or PCET. The proton transfer we hope to induce in NH_3HX by addition of an excess electron would also fall under this umbrella. A generous definition of an electron transfer coupled to a proton transfer would include the entire sphere of hydrogen transfer reactions,[143] but it is more typical to consider coupled proton and electron motions where the electron and proton are not moving *together*, whether they be moving along the same axis (collinear PCET) or in different regions (orthogonal PCET).[144] Proton transfer events are typically short-range, and electron-transfer events long-range, but there remains the possibility of long-range proton "transfer" by a relay of short proton-transfer events, as is important in biological systems.[145]

PCET has been implicated in charge transfer through the DNA chain, due to the existence of many (Watson-Crick) hydrogen bonds between the nucleic acid bases.[146] The long-range charge transfer properties of DNA (both hole transfer and electron transfer) are believed to be important in the detection of DNA damage and its subsequent repair.[147-149] PCET is also important in the charge transport chains in photosynthesis and respiration, and the redox action of various enzymes[144,150] as well as artificial charge-transport systems.[151,152]

It is important to consider whether this process is concerted or stepwise. The stepwise case is perhaps intuitively more likely, as the probability of transfer of both species at the same time is lower than the probability that one will transfer, and then drive the motion of the other. For example, transient solvent fluctuations could shift the electron potential energy surface such that it transfers, and then the resultant change in the proton potential energy surface drives its transfer which "fixes" the product. The reverse, where solvent fluctuations make proton transfer favourable which then stimulates electron transfer, is also plausible.[153]

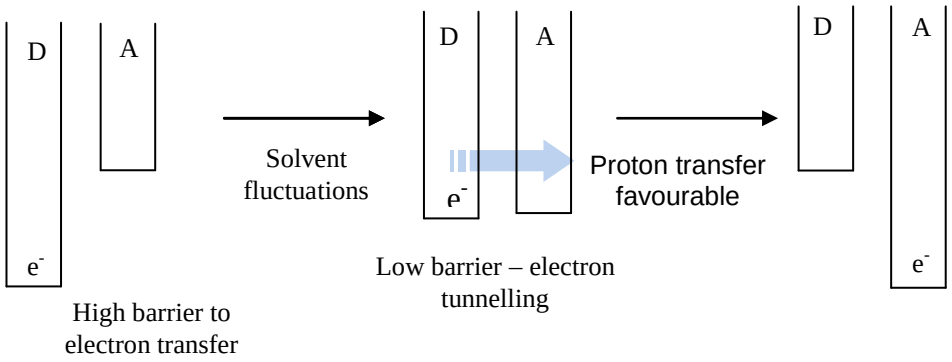

Figure 1.6: Diagram of changes in electron potential energy surface for PCET, D is electron donor, A is electron acceptor

On the other hand, the stepwise process may be unfavourable in free-energy terms, as it is for a hydrogen transfer reaction, due to the high-energy intermediates (or in the solution phase, the kinetic difficulty in obtaining the correct solvent fluctuation). The concerted reaction exploits the quantum mechanical nature of the proton, coupling the proton and electron motions and avoiding the barrier on the potential energy surface defined by the proton or electron position (see 2.7) that must be invoked in a stepwise mechanism (although the transfer of the electron and proton is not necessarily simultaneous). [143,145,153] By using a proton relay, the proton transfer can occur over a surprisingly long distance, a property exploited by enzyme activity.[145]

Such processes are curious from a theoretical perspective because, while the proton is a much more "quantum-mechanical" body than the rest of the molecule, the electron is even moreso in comparison to the proton, moving relatively rapidly. The process may be modelled as an uncoupled electron, proton, and rest-of-system reaction, each occurring on a different timescale and uncoupled from the rest.[145,152,154] However situations can even arise in collinear PCET where the proton transfer occurs faster than the electron transfer, and proton and electron motions must be treated as coupled.[155]

In summation, the addition of an excess electron can have a significant effect upon the structure of a chemical system, with this change being most obvious in the potential energy surface associated with the position of a proton. Proton and electron motions can be extremely closely coupled. These couplings have important roles in biochemistry, both constructively and destructively, and mimickry of these processes is a promising area of research for materials science.

1.4. Halogen bonding

Halogen bonding is a counterintuitive noncovalent intermolecular interaction. It is an attraction between a halogen atom in a donor molecule R-X and an electron-rich acceptor A, it is principally electrostatic in nature, in which the van der Waals surfaces intersect and the R-X bond and X-A are collinear.[156-158] At first glance, the idea that two characteristically electronegative species would interact electrostatically is absurd. However such interactions are extant in nature, and in fact have many properties that are directly analogous to hydrogen bonds.[159] Halogen bonding requires a more nuanced picture of the way molecules "talk to" one another. Given the involvement of the hydrogen halides in our research, it is natural to ask: will the hydrogen halides H-X also form halogen bonds with NH_3, in the "backwards" complex $H_3N\cdots X\text{-}H$?

The definitive picture of the halogen bond is that the halogen atom – although negatively charged overall – has a region where the negative charge is depleted by its bonding to another atom. For example, in a CH_3Cl molecule, this region would be on the Cl atom along the axis of – but on the other side of the Cl atom from – the Cl-C bond. This "σ hole" is satisfied by interaction with an electron-rich region on another molecule, known in the nomenclature as the halogen bond *acceptor*, as vividly illustrated by various publications by Politzer and coworkers.[156,158,160] (This is illustrated in Figure 1.7). In other words, this is a *local* electrostatic interaction, where the goal is not simply to align monopoles, but to bring electron density "holes" together with electron density "lumps".[161] The resultant interactions can be quite strong, and have proven to be an appealing new tool for structural chemists.[157,162] The theoretical study of these systems continues apace.[162]

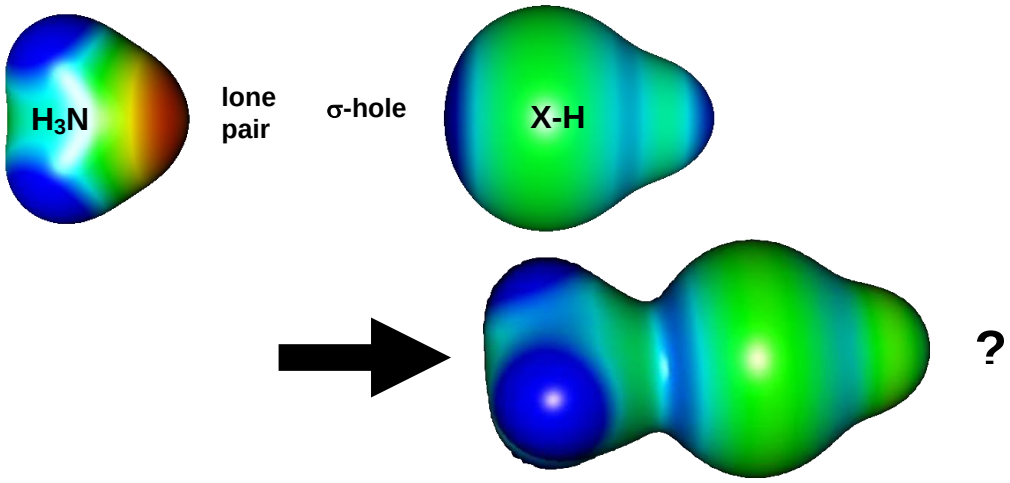

Figure 1.7: Electrostatic potential maps of NH_3, HCl, and hypothetical $H_3N^{\cdots}ClH$ halogen bonded structure

The σ hole can be thought of as a region of depleted charge along the bond axis. This certainly contributes to the effectiveness of halogen bonds – adding more electronegative substituents R to R_3C-X halogen bond donors increases their donor ability, while adding electropositive substituents reduces it.[163] However halogen bonds do not require that the group attached to the halogen is more electronegative than the halogen. It has been proposed by NBO analysis that the depletion occurs because a *p* electron is involved in the covalent bond with the neighbouring atom, along the bond axis, and is not available to "fill out" the electron density around the halogen. This is supported by the trend in the strength of halogen bonds; the smaller the halogen, the more *s*-*p* hybridisation occurs, the more the σ hole is mixed across the *p* orbitals, and the less distinct it is.[158,160] Note that in $H_3N^{\cdots}XH$, the hydrogen atom has no *p* orbitals, and therefore *s*-*p* hybridisation cannot quench the σ hole, suggesting that halogen bonding is plausible.

It has also been proposed that halogen bonding is not simply an electrostatic interaction; where the donor halogen is bonded to particularly electronegative groups (*e.g.* in HOX or XY donors, where Y is also a halogen) there is a high degree of charge transfer from the acceptor to donor, and the degree of charge transfer correlates positively with the bond strength.[163,164] SAPT analyses suggest that dispersion interactions are very important in halogen bonds involving the lighter halogens (Cl, F) where the electrostatic term is small.[165]

AIM analysis of the charge density of hydrogen- and halogen-bonded systems has provided some particular insights (see 1.1). In this formalism, the Laplacian of the electron density is positive at a critical point in a region where the electron density is depleted, as is the case for σ holes, and negative at a critical point in a region where the electron density is accumulated, such as in lone pairs on halogen bond acceptors; the magnitude of the Laplacian is correlated with the strength of the resultant halogen bond.[161,164] A critical point is established between the donor and acceptor in the complex; in halogen bonds the Laplacian of the electron density at the critical point is positive, indicative of a closed-shell interaction.[164] While, similarly to hydrogen bonds, the density of charge at the critical point and amount of charge transfer are positively correlated with the strength of the bond, the Laplacian of the density at the critical point becomes *increasingly* positive as the halogen bond becomes stronger, *i.e.* more closed-shell, whereas hydrogen bonds tend to show increasing covalency.[164,166]

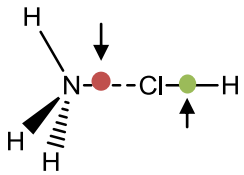

Figure 1.8: The halogen-bonded $H_3N^{\cdots}ClH$ structure, and its critical points; positive between nitrogen and chlorine, indicating a closed-shell interaction and negative inside the hydrogen chloride molecule, where there is a covalent bond.

In an X-Y$^{\cdots}$A halogen bond, where X and Y are both halogens, as the electron-donating nature of the halogen bond acceptor increases, the bond becomes stronger, shorter, and more electrostatic. Complicating this, the X-Y distance increases, and there is a corresponding redshift in the X-Y stretching vibrational mode, just as is observed in the hydrogen bond.[167] Furthermore, as in the hydrogen bond these changes arise from hyperconjugation, the donation of charge into the σ* orbital of X-Y.[168,169] In bonds where there is a very significant amount of charge transfer from the acceptor A, and usually where Y is chlorine, this can ultimately lead to a chlorine-shared or chlorine-transferred, "ion-pair" halogen bond AY$^{+\cdots}$X^{-}, in a similar manner to particularly strong hydrogen bonds leading to proton transfer.[159,170,171]

For some weak, long halogen bonds, the amount of charge transfer is small; in these cases a blue shift of the X-Y stretching mode and a shortening of the corresponding X-

Y bond may be observed. This is due to an electrostatic repulsion between the electron-rich halogen and the acceptor atom that is not offset by the red-shifting effect of the charge transfer to σ*. This phenomenon is similar in nature to blue-shifted hydrogen bonds.[168] It has been argued that this effect is more ubiquitous in halogen bonds because the halogen may redistribute this back-donated charge to its *p* orbitals, a mechanism not available to the hydrogen atom in a hydrogen bond.

One of the promising uses of halogen bonds in structural chemistry is as an orthogonal interaction to hydrogen bonds; that is, where a halogen is used as a hydrogen bond acceptor, it can also be used as a halogen bond donor in another direction, without disrupting the hydrogen bond, due to the distinctly different methods of bonding. The energetic independence of the two interactions has been suggested by a recent review.[172] However in the three-centre complexes NH_3-XY-HF, where the halogen X is acting as both a halogen bond donor and a hydrogen bond acceptor, the halogen bond may enhance the hydrogen bonds, and *vice versa*, due to the polarisation of the X-Y bond through charge transfer.[173] Furthermore halogen and hydrogen bonds may compete for the same site in the crystallisation of small molecules. In polar solvents, the halogen bond tends to be favoured, *in spite* of the electrostatic favourability of the hydrogen bond.[174-177] Tuning the competition between these interactions may thus open new avenues in molecular self-assembly.[157,166]

1.5. Electronegativity

In section 1.1.1 , it was noted that the structure of the ammonium halides was established, in part, by comparison of the ammonium halide quadrupole coupling constants to the equivalent alkali halides. The body of this thesis shall make the case that ammonium is a genuine "pseudo-alkali metal" with pseudo-alkali-metal-like properties, specifically electronegativity.

Electronegativity (χ) is a property intimately tied into the modern history of our understanding of chemistry. Avogadro was the first to propose such an idea in an attempt to formalise the discussion of oxidising and reducing materials (oxygenicity, in their terms), in the era between the demise of alchemy and the arrival of the concept of molecules; Berzelius ultimately coined the term we use today.[178,179] The term gained widespread acceptance as a sense of the "electron-attracting ability" of an atom

when the atomic and molecular model of chemistry began to be widely appreciated and adopted. In particular, it offers a rationalisation for the formation of polar bonds and the tendency of organic reactions to prefer one pathway and set of products over another.

1.5.1. Pauling and Mulliken: The Physics of Electronegativity

Electronegativity was not quantitative, however, until Linus Pauling set out a theoretical study of and empirical scale for electronegativity in the 1930s, in one of the first issues of the *Journal of the American Chemical Society*.[180] In the paper, Pauling describes the additivity of the energies of chemical bonds: that the energy E_{AB} of the bond AB is equal to one half of the energy E_{AA} of an A-A bond and one half of the energy E_{BB} of a B-B bond:

$$E_{AB} \cong \frac{1}{2}(E_{AA} + E_{BB}) \qquad (1)$$

This principle holds for weakly-polar bonds, but for polar bonds the total bond energy is (almost) always *greater* than predicted by additivity, to a degree that increases with increasing polarity. This is due to the additional electrostatic attraction between the oppositely charged atoms on each end of the polar bond. The polarity of these bonds and the "extra" nonadditive component of the energy arise because of the electronegativity difference. Pauling established a mapping between the square of the differences in the electronegativities of the two atoms (χ_A and χ_B) and the surplus bond energy, chose a sign for differences by chemical intuition, and thereby created an empirical quantitative scale.

$$E_{AB} = \frac{1}{2}(E_{AA} + E_{BB}) + (\chi_A - \chi_B)^2 \qquad (2)$$

Pauling suggested that using the geometric mean might be superior in consistency to simple additivity (the arithmetic mean), naming it the "postulate of the geometric mean".[181,182] In fact the Pauling electronegativity computed in this way, using modern thermochemical data, is not significantly better.[183]

Note that Mulliken came up with a theoretically superior scale by supposing that the energies, and thus contributions, of the two different ionic resonance structures were equal to the difference between the ionisation energy (*IE*) of one atom and the electron affinity (*EA*) of the other.[184]

$$A^+B^-(1) \leftrightarrow AB \leftrightarrow A^-B^+(2)$$

$$E_1 = IE_A - EA_B \quad (3)$$

$$E_2 = IE_A - EA_B$$

Where the electronegativities are equal, the contributions are equal, and therefore the energies of the two resonance structures must be equal:

$$E_1 = E_2 \quad (4)$$

$$IE_A - EA_B = IE_A - EA_B \quad (5)$$

By simple rearrangement and adding an arbitrary factor of ½, he concluded that the electronegativity of an atom is equal to the arithmetic mean of the ionisation energy and electron affinity.

$$\chi_A = \frac{IE_A + EA_A}{2} \quad (6)$$

Mulliken invoked an important caveat: the atom in the molecule is not the same as the atom in the gas phase, and the necessity of forming a bond puts the atom into a valence state. Therefore it is the ionisation energy and electron affinity of *this* state which must be calculated. [184]

Mulliken's scale correlates well with Pauling's, indicating that they are both measures of the same implicit property; a proper correlation with the Pauling electronegativity, or sometimes Allred and Rochow's (see below) is a historical criterion for the worthiness of an electronegativity scale. A recent review of correlations between the Pauling and Mulliken schemes has suggested that the connections between Pauling's and Mulliken's scale might be improved by attempting to understand the tangable link between the bond energies and the electronic energies of molecules, *i.e.* by making sense of correlations using valence bond theory.[185]

A significant issue is that the Pauling and Mulliken scale have different units; Pauling's the square root of energy, and Mulliken's the energy itself. Given that the Mulliken scale has now been identified as a potential per unit electron (see the discussion on DFT, below), one would expect the energy units to be correct. A recent evaluation suggests that Pauling electronegativities are indeed superior if the "excess energy" is taken as the electronegativity difference, rather than its square root.[183]

1.5.2. The Application of Electronegativity

These papers by Pauling[180] and Mulliken[184] launched what would appear to be an ongoing operation to define the electronegativity in terms of every available chemical property. Schemes can be divided into two rough groups: post-Pauling scales which correlate the electronegativity with some property of bond strength, such as Gordy's famously successful relation of the electronegativity product to the bond force constant and bond strength[186]; and post-Mulliken scales with correlate the electronegativity to some property of the electronic structure of the system.

The latter are of the most theoretical interest to the quantum chemist, however not all provide immediate insight. Gordy proposed a scale based upon the electrostatic potential,[187] and Allred and Rochow created a popular scale based upon the electrostatic force.[188] Both are measured using the covalent radius for an atom in a particular bonding state, but use different measures for the effective nuclear charge. Both are ultimately simply related to the orbital energy.

Allen proposed that the electronegativity is simply the mean of the energies of the valence electrons in a ground-state atom in the gas phase, as determined by experiment.[189] Although appealing, such a scheme is clearly just an effective approximation to the established Mulliken scheme. Similarly Nagle suggested a scheme based on atomic polarisabilities, which are of course intimately related to the frontier orbital energies.[190] In that publication, he proposed that such a scheme would not require a correction for the valence state, as the polarizability (to some extent) describes the ease with which electrons may be excited to such states.

The diversification of the two lineages continues to this day. The theory of electronegativity has comparatively been slow to advance, and exclusively in the region of post-Mulliken definitions. The first step was the impressive case made by Hinze and Jaffe that the Mulliken electronegativity, being defined for an electron removed from the valence state of an atom, is only well-defined *for a specific electron*, and therefore *a specific electronic orbital*.[191] This clarification was of such importance that the Mulliken electronegativity is often commonly referred to as the "Mulliken-Hinze-Jaffe" electronegativity, or simply the "Hinze-Jaffe orbital electronegativity. (This is not to

ignore their remarkable effort in computing the Mulliken electronegativities of the elements and their ions.[191-194])

1.5.3. The Electronegativity of Groups

It should not be surprising that the electronegativity as a tool in describing organic reactions was soon linked to substituent constants, which are taken as descriptors of the donating or withdrawing power of a chemical group. However such a concept requires the idea of group electronegativity.

Most efforts lead from where electronegativity scales had progressed. Clifford, after relating the solubility of metal salts to the electronegativity of the constituent ions, established the electronegativities of chemical ions *via* the known electronegativity of the metal.[195,196] He made the observation, and proposed a generalised principle, that negative ions tended to have an electronegativity similar to the mean of the constituent atoms, while positively-charged, metal-containing ions tended to have an electronegativity similar to that of the metal. Datta *et al* took a direct route (as evaluated negatively in Pritchard and Skinner's review decades earlier)[197] and computed group electronegativities on the basis of thermochemical data for bond dissociation energies, and found the results to correlate well with NMR spin coupling constants (one potential electronegativity scale).[198]

Analyses in terms of molecular structure were suggestive of later developments. Huheey demonstrated the ability to properly account for the charge placed on a chemical group in computing its electronegativity, by introducing a parameter which varies the electronegativity with the charge,[199,200] a concept rigorously defined in terms of atomic charges, hardnesses, and electronegativities by Komorowski *et al*, who obtained a strong correlation with the Hammett constants of organic chemistry.[201] Following up on comments in Allen's original publication of his electronegativity scheme, Reed and Allen devised an electronegativity scale based upon the "bond polarity index", a property comparing the average energy of the valence electrons in two bonded atoms, which they had previously shown to compare well to experimental measures of polarity such as substituent constants and chemical shifts.[202,203] Mullay proposed a scheme based upon the calculated energy of the orbital involved in a bond,

using a combination of semi-empirical estimates of orbital energies and the electronegativity equalisation scheme.[204,205]

It was Sanderson who ultimately laid the groundwork for the conception of molecular or group electronegativity by suggesting that scheme. Given that two atoms of differing electronegativity will transfer electron density, and that putting electron density on an atom reduces its electronegativity, he proposed the "equalisation principle", stating that electron density will be rearranged within a molecule until all the electronegativities are equal, and that this can be approximated by the geometric mean of the constituent electronegativities.[206,207] This suggests that the idea of a whole molecule, or a functional group, having a well-defined electronegativity *distinct from that of the constituent atoms* is not only plausible but necessary. Hinze and Jaffe applied this idea productively in computing the electronegativity of chemical bonds or groups from first principles.[192]

1.5.4. The Modern Synthesis of Electronegativity and DFT

The issue of electronegativity equalisation was "brought into the fold" of modern electronic structure theory by Parr *et al*. Iczkowski and Margave had deduced that the electronegativity is simply the finite difference approximation to the derivative of the energy with respect to the gain or loss of electrons by a system.[208] Parr *et al* used density functional theory (DFT, an electronic structure method with deep links to chemical properties) to rigorously show that the electronegativity is the negative of the electronic chemical potential (the potential related to the addition or removal of electrons to/from a chemical system), a parameter which is already present in the DFT implimentation as the Lagrange multiplier.[209] Given that a potential is equal across any closed system in a stationary state, the equalisation principle must hold. From this work, the group were able to deduce the conditions under which Sanderson's "geometric mean" principle was valid. They found that it was related specifically to an expontential decay of the valence state energy as more electrons are added to an atom (which happens to be true in many common cases).[210]

It is now known that two other quantities are closely related to electronegativity through DFT. The first is the global absolute hardness, a counterpart to electronegativity which was originally defined as equal to the difference (or half of the difference) between the

ionisation energy and electron affinity of the species in question, but can be shown to be the second derivative of the energy with respect to addition or loss of electrons; where the electronegativity is a gradient, the hardness is a curvature.[211] It also has a local value, equal to the derivative of the density with respect to the global electronegativity. Furthermore, the Fukui function, a local parameter used to predict reactivity, is equal to the derivative of the local density with respect to a change in the total number of electrons, but is also equivalent to the derivative of the electronegativity with respect to an applied potential.[212,213] Komorowski demonstrated that such a definition allows one to describe the electronegativity as varying with the chemical and physical environment to a degree controlled by the hardness, with Mulliken's definition for a lone atom in the valence state as a special case and approximation.[214]

Modern computational approaches create the tantalising possibility of probing electronegativity in situations which are not experimentally tractable, and are too complex to succumb to the traditional theoretical tools that enabled the classical definitions to be devised. Marriott *et al* made the reasonable observation that the electronegativity of an atom X is correlated with $1-q_H$, where q_H is the calculated charge on the hydrogen atom in the molecule HX. From this they proposed and tested a definition of electronegativity for organic *groups* R, $\chi_R = 1-q_H$ where q_H is the calculated charge on the hydrogen atom in HR.[215] Boyd and Edgecombe made the tantalising suggestion that the electronegativity relative to hydrogen could be related to the ratio of the position of and charge density at the bond critical point between a given group and a hydrogen atom (*i.e.* RH) suggesting that electronegativity could be probed experimentally.[216]

Drawing together the foregoing, it is clear that the Mulliken electronegativity is a justified measure of an inherent, physically meaningful property of a chemical group or molecule. De Proft *et al* made a significant step forward when, on the basis of Parr's definition, they computed the electronegativity and hardness of chemical groups by computing the calculated ionisation energy and electron affinity of the associated radicals; the results compared well with previous scales and chemical intuition.[217] Leyssens *et al*, applied modern computational chemistry techniques to compute the Mulliken electronegativity of component parts of a molecule as they are exposed to point charges.[218] It is in this context that we have evaluated the ammonium radical.

1.6. Summary

To summarise, the key outstanding issues from the above literature which are addressed in this thesis:

- In the NH_3HX complexes, where X = F or Cl, the proton transfer potential energy surfaces have been ambiguously characterised in the past, and the shapes of the surfaces have been found to be highly dependent upon the quality of the theoretical method.
- For heavier halogens, the shapes of the surfaces and the structures of the complexes become increasingly ambiguously characterised.
- The anions of the NH_3HX neutral pair complexes may undergo proton transfer, for reasons that have not been fully elucidated.
- The electronegativity of groups and molecules has been justified, but its usefulness in a practical context has not yet been established.
- The NH_4 group, widely regarded (implicitly and explicitly) as a "pseudo-atom", could be assigned the atomic property of electronegativity and evaluated as both a pseudo-atom and a molecule.
- It is likely that the hydrogen halides can form a "backwards" structure using halogen bonding.

1.7. References

[1] T. Steiner, *The hydrogen bond in the solid state*, Angew. Chem. Int. Ed., **41**, 48-76 (2002)
[2] G. C. Pimentel and A. L. McClellan, *Hydrogen Bonding*, Annu. Rev. Phys. Chem., **22**, 347-385 (1971)
[3] S. J. Grabowski, *What Is the Covalency of Hydrogen Bonding?*, Chem. Rev., **111**, 2597-2625 (2011)
[4] I. Mata, I. Alkorta, E. Espinosa and E. Molins, *Relationships between interaction energy, intermolecular distance and electron density properties in hydrogen bonded complexes under external electric fields*, Chem. Phys. Lett., **507**, 185-189 (2011)
[5] K. Morokuma, *Why Do Molecules Interact - Origin of Electron Donor-Acceptor Complexes, Hydrogen-Bonding, and Proton Affinity*, Acc. Chem. Res., **10**, 294-300 (1977)
[6] H. Umeyama and K. Morokuma, *The Origin of Hydrogen Bonding. An Energy Decomposition Study*, J. Am. Chem. Soc., **99**, 1316-1322 (1977)

[7] R. H. McKenzie, *A diabatic state model for donor-hydrogen vibrational frequency shifts in hydrogen-bonded complexes*, Chem. Phys. Lett., **535**, 196-200 (2012)
[8] K. Morokuma and J. R. Winick, *Molecular Orbital Studies of Hydrogen Bonds - Dimeric H_2O with Slater Minimal Basis Set*, J. Chem. Phys., **52**, 1301-1306 (1970)
[9] P. P. Zhou and W. Y. Qiu, *Red-Shifted Hydrogen Bonds and Blue-Shifted van der Waals Contact in the Standard Watson-Crick Adenine-Thymine Base Pair*, J. Phys. Chem. A, **113**, 10306-10320 (2009)
[10] R. F. W. Bader, *Atoms in Molecules*, Acc. Chem. Res., **18**, 9-15 (1985)
[11] U. Koch and P. L. A. Popelier, *Characterization of C-H-O Hydrogen Bonds on the Basis of the Charge-Density*, J. Phys. Chem., **99**, 9747-9754 (1995)
[12] L. F. Pacios, O. Galvez and P. C. Gomez, *Variation of geometries and electron properties along proton transfer in strong hydrogen-bond complexes*, J. Chem. Phys., **122**, 214307 (2005)
[13] J. A. Platts and K. E. Laidig, *Proton transfer in ionic hydrogen bonds*, J. Phys. Chem., **100**, 13455-13461 (1996)
[14] E. Espinosa, I. Alkorta, J. Elguero and E. Molins, *From weak to strong interactions: A comprehensive analysis of the topological and energetic properties of the electron density distribution involving X-H···F-Y systems*, J. Chem. Phys., **117**, 5529-5542 (2002)
[15] O. Galvez, P. C. Gomez and L. F. Pacios, *Variation with the intermolecular distance of properties dependent on the electron density in hydrogen bond dimers*, J. Chem. Phys., **115**, 11166-11184 (2001)
[16] A. P. Showman, *Hydrogen halides on Jupiter and Saturn*, Icarus, **152**, 140-150 (2001)
[17] I. Alkorta, I. Rozas, O. Mo, M. Yanez and J. Elguero, *Hydrogen bond vs proton transfer between neutral molecules in the gas phase*, J. Phys. Chem. A, **105**, 7481-7485 (2001)
[18] E. D. Raczynska, J. F. Gal, P. C. Maria and M. Szelag, *Proton Transfer Chemistry in the Gas Phase. Is a Spontaneous 'Neutralization' Reaction a Myth or a Reality?*, Croat. Chem. Acta, **82**, 87-103 (2009)
[19] R. S. Mulliken, *Molecular Compounds and Their Spectra. III. The Interaction of Electron Donors and Acceptors*, J. Phys. Chem., **56**, 801-822 (1952)
[20] W. H. Rodebush and J. C. Michalek, *The Vapor Pressure and Vapor Density of Intensively Dried Ammonium Chloride*, J. Am. Chem. Soc., **51**, 748-759 (1929)
[21] E. L. Spotz and J. O. Hirschfelder, *Liesegang Ring Formation Arising from Disffusion of Ammonia and Hydrogen Chlorine Gases through Air*, J. Am. Chem. Soc., **19**, 1215 (1951)
[22] W. H. Johnston and P. J. Manno, *Liesegang Rings of Ammonium Chloride*, Ind. Eng. Chem., **44**, 1304-1305 (1952)
[23] E. Clementi, *Study of the Electronic Structure of Molecules. II. Wavefunctions for the NH_3+HCl → NH_4Cl Reaction*, J. Chem. Phys., **46**, 3851-3880 (1967)
[24] E. Clementi, *Study of the Electronic Structure of Molecules. VI. Charge Transfer Mechanism for the NH_3+HCl → NH_4Cl reaction*, J. Chem. Phys., **47**, 2323-2334 (1967)
[25] E. Clementi and J. N. Gayles, *Study of the Electronic Structure of Molecules. VII. Inner and Outer Complex in the NH_4Cl Formation from NH_3 and HCl*, J. Chem. Phys., **47**, 3837-3841 (1967)
[26] P. Goldfinger and G. Verhaegen, *Stability of the Gaseous Ammonium Chloride Molecule*, J. Chem. Phys., **50**, 1467-1471 (1969)
[27] S. Shibata, *Structure of Gaseous Ammonium Chloride*, Acta Chem. Scand., **24**, 705-706 (1970)

[28] R. C. Raffenetti and D. H. Phillips, *Gaseous NH_4Cl revisited: A computational investigation of the potential energy surface and properties*, J. Chem. Phys., **71**, 4534-4540 (1979)
[29] A. Brciz, A. Karpfen, H. Lischka and P. Schuster, *A Candidate for an Ion-Pair in the Vapor-Phase - Proton-Transfer in Complexes $R_3N{\cdot}HX$*, Chem. Phys., **89**, 337-343 (1984)
[30] Z. Latajka, S. Sakai, K. Morokuma and H. Ratajczak, *Possible Gas-Phase Ion-Pairs in Amine-HCl Complexes - an Ab initio Theoretical Study*, Chem. Phys. Lett., **110**, 464-468 (1984)
[31] S. Scheiner, *Theoretical Studies of Proton Transfers*, Acc. Chem. Res., **18**, 174-180 (1985)
[32] S. Scheiner and L. B. Harding, *Proton Transfers in Hydrogen-Bonded Systems. 2. Electron Correlation Effects in $(N_2H_7)^+$*, J. Am. Chem. Soc., **103**, 2169-2173 (1981)
[33] S. Scheiner and L. B. Harding, *Molecular Orbital Study of Proton Transfer in $(H_3NHOH_2)^+$*, J. Phys. Chem., **87**, 1145-1153 (1983)
[34] Y. Bouteiller, C. Mijoule, A. Karpfen, H. Lischka and P. Schuster, *Theoretical Vibrational Investigation of Hydrogen-Bonded Complexes - Application to $ClH-NH_3$, $ClH-NH_2CH_3$, and $BrH-NH_3$*, J. Phys. Chem., **91**, 4464-4466 (1987)
[35] P. G. Jasien and W. J. Stevens, *Theoretical Studies of Potential Gas-Phase Charge-Transfer Complexes: NH_3+HCl,NH_3+HBr,NH_3+HI*, Chem. Phys. Lett., **130**, 127-131 (1986)
[36] C. Chipot, D. Rinaldi and J. L. Rivail, *Intramolecular Electron Correlation in the Self-Consistent Reaction Field Model of Solvation - a MP2/6-31g** Ab Initio Study of the NH_3-HCl Complex*, Chem. Phys. Lett., **191**, 287-292 (1992)
[37] Z. Latajka and S. Scheiner, *Influence of Basis Set on the Calculated Properties of (H_3N-HCl)*, J. Chem. Phys., **82**, 4131-4134 (1985)
[38] M. Biczysko and Z. Latajka, *Accuracy of theoretical potential energy profiles along proton-transfer coordinate for $XH-NH_3$ (X = F, Cl, Br) hydrogen-bonded complexes*, J. Phys. Chem. A, **106**, 3197-3201 (2002)
[39] A. Famulari, M. Sironi and M. Raimondi *BSSE-Free MCSCF method for strong hydrogen bonds: Investigation of H_2O-HCl and NH_3-HCl complexes* in *Quantum Systems in Chemistry and Physics, Vol. 1: Basic Problems and Model Systems*; Hernández-Laguna, A.; Maruani, J.; McWeeny, R.; Wilson, S., Eds.; Kluwer Academic Publishers: London, 2000, p 361-379.
[40] B. S. Ault and G. C. Pimentel, *Infrared Spectra of the Ammonia-Hydrochloric Acid Complex in Solid Nitrogen*, J. Phys. Chem., **77**, 1649-1653 (1973)
[41] L. Andrews and X. F. Wang, *Infrared spectrum of the H_3N-HI complex in solid Ne, Ar, Ne/Ar, Kr, and N_2. Comparisons of matrix effects on hydrogen-bonded complexes*, J. Phys. Chem. A, **105**, 7541-7550 (2001)
[42] M. J. T. Jordan and J. E. Del Bene, *Unraveling environmental effects on hydrogen-bonded complexes: Matrix effects on the structures and proton-stretching frequencies of hydrogen-halide complexes with ammonia and trimethylamine*, J. Am. Chem. Soc., **122**, 2101-2115 (2000)
[43] B. S. Ault, E. Steinback and G. C. Pimentel, *Matrix Isolation Studies of Hydrogen Bonding. The Vibrational Correlation Diagram.*, J. Phys. Chem., **79**, 615-620 (1975)
[44] A. J. Barnes, T. R. Beech and Z. Mielke, *Strongly Hydrogen-Bonded Molecular-Complexes Studied by Matrix-Isolation Vibrational Spectroscopy .1. The Ammonia Hydrogen-Chloride Complex*, J. Chem. Soc., Faraday Trans. 2, **80**, 455-463 (1984)
[45] A. J. Barnes, J. N. S. Kuzniarski and Z. Mielke, *Strongly Hydrogen-Bonded Molecular-Complexes Studied by Matrix-Isolation Vibrational Spectroscopy .2. Amine-Hydrogen Chloride Complexes*, J. Chem. Soc., Faraday Trans. 2, **80**, 465-476 (1984)

[46] L. Andrews, X. F. Wang and Z. Mielke, *Infrared spectrum of the H_3N-HCl complex in solid neon*, J. Am. Chem. Soc., **123**, 1499-1500 (2001)
[47] N. W. Howard and A. C. Legon, *Nature, Geometry, and binding strength of the ammonia-hydrogen chloride dimer determined from the rotational spectrum of the ammonium-chloride vapor*, J. Chem. Phys., **88**, 4694-4701 (1988)
[48] A. C. Legon, *The Nature of Ammonium and Methylammonium Halides in the Vapor-Phase - Hydrogen-Bonding Versus Proton-Transfer*, Chem. Soc. Rev., **22**, 153-163 (1993)
[49] E. J. Goodwin, N. W. Howard and A. C. Legon, *The Rotational Spectrum of N-15-Ammonium Chloride Vapor - Characterization of the Hydrogen-Bonded Dimer $H_3N^{\cdots}HCl$*, Chem. Phys. Lett., **131**, 319-324 (1986)
[50] P. Kollman, A. Dearing and E. Kochanski, *Ab Initio Self-Consistent Fieid Calculations on I_2-NH_3 and HI-NH_3. The Classic "Charge-Transfer" Interaction, an Example of Gas-Phase Proton Transfer, and the Duality of Lewis Acid Sites on HI*, J. Phys. Chem., **86**, 1607-1610 (1982)
[51] Z. Latajka, S. Scheiner and H. Ratajczak, *The Proton Position in Hydrogen Halide-Amine Complexes - BrH-NH_3 and BrH-NH_2CH_3*, Chem. Phys. Lett., **135**, 367-372 (1987)
[52] Z. Latajka, S. Scheiner and H. Ratajczak, *The Proton Position in Amine HX (X = Br, I) Complexes*, Chem. Phys., **166**, 85-96 (1992)
[53] R. Ahlrichs, H. Lischka, V. Staemmler and W. Kutzelnigg, *Pno-Ci (Pair Natural Orbital Configuration Interaction) and Cepa-Pno (Coupled Electron Pair Approximation with Pair Natural Orbitals) Calculations of Molecular Systems .1. Outline of Method for Closed-Shell States*, J. Chem. Phys., **62**, 1225-1234 (1975)
[54] A. J. Barnes and M. P. Wright, *Strongly Hydrogen-Bonded Molecular-Complexes Studied by Matrix-Isolation Vibrational Spectroscopy .3. Ammonia-Hydrogen Bromide and Amine-Hydrogen Bromide Complexes*, J. Chem. Soc., Faraday Trans. 2, **82**, 153-164 (1986)
[55] L. Schriver, A. Schriver and J. P. Perchard, *Spectroscopic Evidence for Proton-Transfer within the Bimolecular Complex HI-NH_3 Trapped in Cryogenic Matrices*, J. Am. Chem. Soc., **105**, 3843-3848 (1983)
[56] L. Andrews and X. F. Wang, *Infrared spectra of the H_3N-HBr complex in solid Ne, Ne/Ar, Ar, Kr, and N_2. Strong matrix effects on a hydrogen-bonded complex*, J. Phys. Chem. A, **105**, 6420-6429 (2001)
[57] L. Andrews, X. F. Wang and Z. Mielke, *Infrared spectrum of the H_3N-HCl complex in solid Ne, Ne/Ar, Ar, and Kr. Matrix effects on a strong hydrogen-bonded complex*, J. Phys. Chem. A, **105**, 6054-6064 (2001)
[58] A. J. Barnes, Z. Latajka and M. Biczysko, *Proton transfer in strongly hydrogen-bonded molecular complexes: matrix effects*, J. Mol. Struct., **614**, 11-21 (2002)
[59] A. J. Barnes and A. C. Legon, *Proton transfer in amine-hydrogen halide complexes: comparison of low temperature matrices with the gas phase*, J. Mol. Struct., **448**, 101-106 (1998)
[60] G. Q. Liu, Y. M. Zhao and Y. Yang, *Modeling Ar and Kr matrix effect on the ν_s (Cl - H) and ν_l (Cl - H) of Cl-H $^{\cdots}$ NH_3 by the IEF-PCM method*, Struct. Chem., **19**, 659-663 (2008)
[61] J. E. Del Bene, M. J. T. Jordan, P. M. W. Gill and A. D. Buckingham, *An ab initio study of anharmonicity and matrix effects on the hydrogen-bonded BrH:NH_3 complex*, Mol. Phys., **92**, 429-439 (1997)
[62] N. W. Howard and A. C. Legon, *An investigation of the hydrogen-bonded dimer H_3N-HBr by pulsed-nozzle, fourier-transform microwave spectroscopy of the ammonium bromide vapor.*, J. Chem. Phys., **86**, 6722-6730 (1987)

[63] A. C. Legon and D. Stephenson, *Is Ammonium Iodide an Ion Pair $H_3N^+H^{\cdots}I^-$ or a Hydrogen-bonded Species $H_3N^{\cdots}HI$ in the Gas Phase?*, J. Chem. Soc., Faraday Trans., **88**, 761-762 (1992)

[64] G. L. Johnson and L. Andrews, *Matrix Infrared Spectrum of the H_3N-HF Hydrogen-Bonded Complex*, J. Am. Chem. Soc., **104**, 3043-3047 (1982)

[65] P. Kollman and L. C. Allen, *The Nature of the Hydrogen Bond. Dimers Involving Electronegative Atoms of the First Row.*, J. Am. Chem. Soc., **93**, 4991-5000 (1971)

[66] M. M. Szczesniak, P. Hobza, Z. Latajka, H. Ratajczak and K. Skowronek, *The Methylation Effect in Amine-HF Hydrogen-Bonded Systems. Quantum Chemical and Statistical Thermodynamic Study*, J. Phys. Chem., **88**, 5923-5927 (1984)

[67] C. S. Brauer, M. B. Craddock, J. Kilian, E. M. Grumstrup, M. C. Orilall, Y. R. Mo, J. L. Gao and K. R. Leopold, *Amine-hydrogen halide complexes: Experimental electric dipole moments and a theoretical decomposition of dipole moments and binding energies*, J. Phys. Chem. A, **110**, 10025-10034 (2006)

[68] A. C. Legon, A. L. Wallwork and C. A. Rego, *The Rotational Spectrum and Nature of the Heterodimer in Trimethylammonium Bromide Vapor*, J. Chem. Phys., **92**, 6397-6407 (1990)

[69] A. C. Legon and C. A. Rego, *Rotational Spectrum of the Trimethylamine-Hydrogen Iodide Dimer - an Ion-Pair $(CH_3)_3NH^{+\cdots}I^-$ in the Gas-Phase*, J. Chem. Phys., **99**, 1463-1468 (1993)

[70] M. M. Szczesniak, Z. Latajka, H. Ratajczak and W. J. Orville-Thomas, *Properties of Strong Hydrogen-Bonded Systems. The Formation of Hydrogen-Bonded Ion Pair in Amine - HCl Systems*, Chem. Phys. Lett., **72**, 115-118 (1980)

[71] R. Cazar, A. Jamka and F. M. Tao, *Proton transfer reaction of hydrogen chloride with ammonia: is it possible in the gas phase?*, Chem. Phys. Lett., **287**, 549-552 (1998)

[72] J. A. Snyder, R. A. Cazar, A. J. Jamka and F. M. Tao, *Ab initio study of gas-phase proton transfer in ammonia-hydrogen halides and the influence of water molecules*, J. Phys. Chem. A, **103**, 7719-7724 (1999)

[73] M. Biczysko and Z. Latajka, *The influence of water molecules on the proton position in H_3N-HX (X = F, Cl, Br) complexes*, Chem. Phys. Lett., **313**, 366-373 (1999)

[74] P. Kollman and I. Kuntz, *Hydration of NH_4F*, J. Am. Chem. Soc., **98**, 6820-6825 (1976)

[75] J. T. Cheung, D. A. Dixon and D. R. Herschbach, *Cluster Beam Chemistry - Adducts of Hydrogen Halides with Ammonia Clusters*, J. Phys. Chem., **92**, 2536-2541 (1988)

[76] A. Abkowicz-Bienko, M. Biczysko and Z. Latajka, *Solvent effect on hydrogen bonded ammonia-hydrogen halide complexes: continuum medium versus cluster models*, Comput Chem, **24**, 303-309 (2000)

[77] R. A. Cazar, A. J. Jamka and F. M. Tao, *Ab initio investigation of proton transfer in ammonia hydrogen chloride and the effect of water molecules in the gas phase*, J. Phys. Chem. A, **102**, 5117-5123 (1998)

[78] M. F. Ruiz-Lopez, F. Bohr, M. T. C. Martins-Costa and D. Rinaldi, *Studies of Solvent Effects Using Density Functional Theory. Cooperative Interactions in $H_3N^{\cdots}HBr$ Proton Transfer*, Chem. Phys. Lett., **221**, 109-116 (1994)

[79] B. Cherng and F. M. Tao, *Formation of ammonium halide particles from pure ammonia and hydrogen halide gases: A theoretical study on small molecular clusters $(NH_3\text{-}HX)_n$ (n=1, 2, 4; X = F, Cl, Br)*, J. Chem. Phys., **114**, 1720-1726 (2001)

[80] F. M. Tao, *Direct formation of solid ammonium chloride particles from HCl and NH_3 vapors*, J. Chem. Phys., **110**, 11121-11124 (1999)

[81] C. J. Pursell, M. Zaidi, A. Thompson, C. Fraser-Gaston and E. Vela, *Acid-base chemistry on crystalline ice: HCl+NH_3*, J. Phys. Chem. A, **104**, 552-556 (2000)
[82] Z. J. Zhou, X. P. Li, Z. B. Liu, Z. R. Li, X. R. Huang and C. C. Sun, *Electric Field-Driven Acid Base Chemistry: Proton Transfer from Acid (HCl) to Base (NH_3/H_2O)*, J. Phys. Chem. A, **115**, 1418-1422 (2011)
[83] M. Ramos, I. Alkorta, J. Elguero, N. S. Golubev, G. S. Denisov, H. Benedict and H. H. Limbach, *Theoretical study of the influence of electric fields on hydrogen-bonded acid-base complexes*, J. Phys. Chem. A, **101**, 9791-9800 (1997)
[84] J. Simons, *Molecular anions*, J. Phys. Chem. A, **112**, 6401-6511 (2008)
[85] M. Gutowski, A. I. Boldyrev, J. V. Ortiz and J. Simons, *Vertical Electron Detachment Energies for Octahedral Closed-Shell Multiply-Charged Anions*, J. Am. Chem. Soc., **116**, 9262-9268 (1994)
[86] M. Gutowski, P. Skurski and J. Simons, *Bi-dipole-bound anions*, Int. J. Mass spectrom., **201**, 245-252 (2000)
[87] J. Kalcher and A. F. Sax, *Gas-Phase Stabilities of Small Anions - Theory and Experiment in Cooperation*, Chem. Rev., **94**, 2291-2318 (1994)
[88] O. Ingolfsson, F. Weik and E. Illenberger, *The reactivity of slow electrons with molecules at different degrees of aggregation: Gas phase, clusters and condensed phase*, Int. J. Mass Spectrom. Ion Processes, **155**, 1-68 (1996)
[89] J. Simons and K. D. Jordan, *Ab Initio Electronic Structure of Anions*, Chem. Rev., **87**, 535-550 (1987)
[90] T. M. Miller, D. G. Leopold, K. K. Murray and W. C. Lineberger, *Electron affinities of the alkali halides and the structure of their negative ions*, J. Chem. Phys., **85**, 2368-2375 (1986)
[91] M. Gutowski, C. S. Hall, L. Adamowicz, J. H. Hendricks, H. L. de Clercq, S. A. Lyapustina, J. M. Nilles, S. J. Xu and K. H. Bowen, *Solvated electrons in very small clusters of polar molecules: $(HF)_3^-$*, Phys. Rev. Lett., **88**, 143001 (2002)
[92] J. L. Dye, *Electrons as anions*, Science, **301**, 607-608 (2003)
[93] Q. K. Timerghazin, I. Rizvi and G. H. Peslherbe, *Can a Dipole-Bound Electron Form a Pseudo-Atom? An Atoms-In-Molecules Study of the Hydrated Electron*, J. Phys. Chem. A, **115**, 13201-13209 (2011)
[94] H. S. Carman, C. E. Klots and R. N. Compton, *Rydberg Electron-Transfer to Hydrogen Iodide - Dissociative and Nondissociative Electron-Capture*, J. Chem. Phys., **99**, 1734-1743 (1993)
[95] P. Skurski, I. Dabkowska, A. Sawicka and J. Rak, *Dipole-bound and dispersion-bound anions supported by the asymmetric tautomers of aminophosphine: H_3NPH and $HNPH_3$*, Chem. Phys., **279**, 101-110 (2002)
[96] T. Sommerfeld, B. Bhattarai, V. P. Vysotskiy and L. S. Cederbaum, *Correlation-bound anions of NaCl clusters*, J. Chem. Phys., **133**, 114301 (2010)
[97] P. Skurski, J. Rak and J. Simons, *Is 9-acridinamine anion a dispersion-bound anion?*, J. Chem. Phys., **115**, 11193-11199 (2001)
[98] E. Illenberger, *Electron-Attachment Reactions in Molecular Clusters*, Chem. Rev., **92**, 1589-1609 (1992)
[99] D. J. Goebbert, D. Khuseynov and A. Sanov, *Laboratory observation of the valence anion of cyanoacetylene, a possible precursor for negative ions in space*, J. Chem. Phys., **131**, 161102 (2009)
[100] T. Sommerfeld and S. Knecht, *Electronic interaction between valence and dipole-bound states of the cyanoacetylene anion*, Eur. Phys. J. D, **35**, 207-216 (2005)
[101] T. Sommerfeld, *Dipole-bound state as doorways in (dissociative) electron attachment*, Journal of Physics: Conference Series, **4**, 245-250 (2005)
[102] M. Gutowski, K. D. Jordan and P. Skurski, *Electronic Structure of Dipole-Bound Anions*, J. Phys. Chem. A, **102**, 2624-2633 (1998)

[103] J. Tong, Y. Li, D. Wu, S. H. Cui, Z. R. Li and X. R. Huang, *Dipole-bound states of the alkali-superhalogen anions: $LiBeX_3^-$ (X = F, Cl, Br)*, Chem. Phys. Lett., **496**, 20-24 (2010)
[104] M. Gutowski and P. Skurski, *Dispersion Stabilization of Solvated Electrons and Dipole-Bound Anions*, J. Phys. Chem. B, **101**, 9143-9146 (1997)
[105] R. A. Bachorz, J. Rak and M. Gutowski, *Stabilization of very rare tautomers of uracil by an excess electron*, PCCP, **7**, 2116-2125 (2005)
[106] R. A. Bachorz, W. Klopper and M. Gutowski, *Coupled-cluster and explicitly correlated perturbation-theory calculations of the uracil anion*, J. Chem. Phys., **126**, 085101 (2007)
[107] K. Mazurkiewicz, R. Bachorz, M. Gutowski and J. Rak, *On the unusual stability of valence anions of thymine based on very rare tautomers: A computational study*, J. Phys. Chem. B, **110**, 24696-24707 (2006)
[108] M. Harańczyk, J. Holliday, P. Willett and M. Gutowski, *Structure and Singly Occupied Molecular Orbital Analysis of Anionic Tautomers of Guanine*, J. Comput. Chem., **29**, 1277-1291 (2007)
[109] M. Harańczyk, M. Gutowski, X. Li and K. H. Bowen, *Adiabatically Bound Valence Anions of Guanine*, J. Phys. Chem. B, **111**, 14073-14076 (2007)
[110] M. Harańczyk, M. Gutowski, X. Li and K. H. Bowen, *Bound anionic states of adenine*, Proc. Natl. Acad. Sci. U. S. A., **104**, 4804-4807 (2007)
[111] P. Skurski and M. Gutowski, *Theoretical study of the dipole-bound anion $(H_2O...NH_3)^-$*, J. Chem. Phys., **108**, 6303-6311 (1998)
[112] P. Skurski and M. Gutowski, *Ab initio study of the dipole-bound anion $(H_2O...HCl)^-$*, J. Chem. Phys., **111**, 3004-3011 (1999)
[113] S. N. Eustis, D. Radisic, K. H. Bowen, R. A. Bachorz, M. Haranczyk, G. K. Schenter and M. Gutowski, *Electron-Driven Acid-Base Chemistry: Proton Transfer from Hydrogen Chloride to Ammonia*, Science, **319**, 936-939 (2008)
[114] I. Dąbkowska, J. Rak, M. Gutowski, J. M. Nilles, S. T. Stokes, D. Radisic and K. H. Bowen, *Barrier-free proton transfer in anionic complex of thymine with glycine*, PCCP, **6**, 4351-4357 (2004)
[115] R. Balog, M. N. Hedhili, F. Bournel, M. Penno, M. Tronc, R. Azria and E. Illenberger, *Synthesis of Cl_2 induced by low energy (0-18 eV) electron impact to condensed 1,2-$C_2F_4Cl_2$ molecules*, PCCP, **4**, 3350-3355 (2002)
[116] I. I. Fabrikant and H. Hotop, *Low-energy behavior of exothermic dissociative electron attachment*, Phys Rev A, **63**, (2001)
[117] A. Pelc, W. Sailer, P. Scheier, N. J. Mason, E. Illenberger and T. D. Mark, *Electron attachment to simple organic acids*, Vacuum, **70**, 429-433 (2003)
[118] P. Tegeder and E. Illenberger, *Electron stimulated desorption of F^- from condensed NF_3: unexpected narrow resonances in the low energy (0-4 eV) desorption yield*, PCCP, **1**, 5197-5201 (1999)
[119] A. K. Pikaev *The Hydrated Electron* in *The Solvated Electron in Radiation Chemistry* 1971.
[120] B. C. Garrett, D. A. Dixon, D. M. Camaioni, D. M. Chipman, M. A. Johnson, C. D. Jonah, G. A. Kimmel, J. H. Miller, T. N. Rescigno, P. J. Rossky, S. S. Xantheas, S. D. Colson, A. H. Laufer, D. Ray, P. F. Barbara, D. M. Bartels, K. H. Becker, H. Bowen, S. E. Bradforth, I. Carmichael, J. V. Coe, L. R. Corrales, J. P. Cowin, M. Dupuis, K. B. Eisenthal, J. A. Franz, M. S. Gutowski, K. D. Jordan, B. D. Kay, J. A. LaVerne, S. V. Lymar, T. E. Madey, C. W. McCurdy, D. Meisel, S. Mukamel, A. R. Nilsson, T. M. Orlando, N. G. Petrik, S. M. Pimblott, J. R. Rustad, G. K. Schenter, S. J. Singer, A. Tokmakoff, L. S. Wang, C. Wittig and T. S. Zwier, *Role of water in electron-initiated processes and radical chemistry: Issues and scientific advances*, Chem. Rev., **105**, 355-389 (2005)

[121] B. Boudaïffa, P. Cloutier, D. Hunting, M. A. Huels and L. Sanche, *Resonant Formation of DNA Strand Breaks by Low-Energy (3 to 20 eV) Electrons*, Science, **287**, 1658-1660 (2000)
[122] I. Dąbkowska, J. Rak and M. Gutowski, *DNA strand breaks induced by concerted interaction of H radicals and low-energy electrons: A computational study on the nucleotide cytosine*, The European Physical Journal D, **35**, 429-435 (2005)
[123] S. Ray, S. Daube and R. Naaman, *On the capturing of low-energy electrons by DNA*, Proc. Natl. Acad. Sci. U. S. A., **102**, 15-19 (2005)
[124] A. F. Jalbout and L. Adamowicz, *Electron attachment to DNA base complexes*, Adv Quantum Chem, **52**, 231-251 (2007)
[125] R. Barrios, P. Skurski and J. Simons, *Mechanism for Damage to DNA by Low-Energy Electrons*, J. Phys. Chem. B, **106**, 7991 (2002)
[126] W. Anusiewicz, J. Berdys, M. Sobczyk, P. Skurski and J. Simons, *Effects of base pi-stacking on damage to DNA by low-energy electrons*, J. Phys. Chem. A, **108**, 11381-11387 (2004)
[127] C. Konig, J. Kopyra, I. Bald and E. Illenberger, *Dissociative electron attachment to phosphoric acid esters: The direct mechanism for single strand breaks in DNA*, Phys. Rev. Lett., **97**, 018105 (2006)
[128] J. Berdys, I. Anusiewicz, P. Skurski and J. Simons, *Damage to model DNA fragments from very low-energy (< 1 eV) electrons*, J. Am. Chem. Soc., **126**, 6441-6447 (2004)
[129] J. Gu, Y. Xie and H. Schaefer, *Near 0 eV electrons attach to nucleotides*, J. Am. Chem. Soc., **128**, 1250-1252 (2006)
[130] H. Abdoul-Carime, S. Gohlke, E. Fischbach, J. Scheike and E. Illenberger, *Thymine excision from DNA by subexcitation electrons*, Chem. Phys. Lett., **387**, 267-270 (2004)
[131] J. Gu, Y. Xie and H. F. Schaefer, *Electron attachment to DNA single strands: gas phase and aqueous solution*, Nucleic Acids Res., **35**, 5165-5172 (2007)
[132] S. Ptasinska, S. Denifl, S. Gohlke, P. Scheier, E. Illenberger and T. Mork, *Decomposition of thymidine by low-energy electrons: Implications for the molecular mechanisms of single-strand breaks in DNA*, Angew. Chem. Int. Ed., **45**, 1893-1896 (2006)
[133] H. Abdoul-Carime, S. Gohlke and E. Illenberger, *Site-specific dissociation of DNA bases by slow electrons at early stages of irradiation*, Phys. Rev. Lett., **92**, 168103 (2004)
[134] S. Gohlke, H. Abdoul-Carime and E. Illenberger, *Dehydrogenation of adenine induced by slow (< 3 eV) electrons*, Chem. Phys. Lett., **380**, 595-599 (2003)
[135] S. Denifl, S. Ptasinska, G. Hanel, B. Gstir, P. Scheier, M. Probst, B. Farizon, M. Farizon, S. Matejcik, E. Illenberger and T. D. Märk, *Electron Attachment to Uracil, Thymine and Cytosine*, Phys. Scr., **T110**, 252-255 (2004)
[136] G. Hanel, B. Gstir, S. Denifl, P. Scheier, M. Probst, B. Farizon, M. Farizon, E. Illenberger and T. Mark, *Electron attachment to uracil: Effective destruction at subexcitation energies*, Phys. Rev. Lett., **90**, 188104 (2003)
[137] S. Ptasinska, S. Denifl, P. Scheier, E. Illenberger and T. Mark, *Bond- and site-selective loss of H atoms from nucleobases by very-low-energy electrons (< 3 eV)*, Angew. Chem. Int. Ed., **44**, 6941-6943 (2005)
[138] S. Ptasinska, S. Denifl, B. Mroz, M. Probst, V. Grill, E. Illenberger, P. Scheier and T. Mark, *Bond selective dissociative electron attachment to thymine*, J. Chem. Phys., **123**, 124302 (2005)
[139] H. Abdoul-Carime, M. Huels, E. Illenberger and L. Sanche, *Sensitizing DNA to secondary electron damage: Resonant formation of oxidative radicals from 5-halouracils*, J. Am. Chem. Soc., **123**, 5354-5355 (2001)

[140] H. Abdoul-Carime, M. Huels, E. Illenberger and L. Sanche, *Formation of negative ions from gas phase halo-uracils by low-energy (0-18 eV) electron impact*, Int. J. Mass spectrom., **228**, 703-716 (2003)
[141] J. Simons, *How very low-energy (0.1-2 eV) electrons cause DNA strand breaks*, Adv Quantum Chem, **52**, 171-188 (2007)
[142] I. Anusiewicz, M. Sobczyk, J. Berdys-Kochanska, P. Skurski and J. Simons, *A theoretical model for indirect dissociative electron attachment*, J. Phys. Chem. A, **109**, 484-492 (2005)
[143] J. Mayer, *Proton-coupled electron transfer: A reaction chemist's view*, Annu. Rev. Phys. Chem., **55**, 363-390 (2004)
[144] S. Y. Reece, J. M. Hodgkiss, J. Stubbe and D. G. Nocera, *Proton-coupled electron transfer: the mechanistic underpinning for radical transport and catalysis in biology*, Philos T R Soc B, **361**, 1351-1364 (2006)
[145] J. Bonin, C. Costentin, M. Robert, J. M. Saveant and C. Tard, *Hydrogen-Bond Relays in Concerted Proton-Electron Transfers*, Acc. Chem. Res., **45**, 372-381 (2012)
[146] J. Rak, J. Makowska and A. Voityuk, *Effect of proton transfer on the electronic coupling in DNA*, Chem. Phys., **325**, 567-574 (2006)
[147] H.-A. Wagenknecht, *Electron transfer processes in DNA: mechanisms, biological relevance and applications in DNA analytics*, Nat. Prod. Rep., **23**, 973-1006 (2006)
[148] S. Kelley, E. Boon, J. Barton, N. Jackson and M. Hill, *Single-base mismatch detection based on charge transduction through DNA*, Nucleic Acids Res., **27**, 4830-4837 (1999)
[149] A. Trifonov, I. Buchvarov, H. A. Wagenknecht and T. Fiebig, *Real-time observation of hydrogen bond-assisted electron transfer to a DNA base*, Chem. Phys. Lett., **409**, 277-280 (2005)
[150] S. Hammes-Schiffer and N. Iordanova, *Theoretical studies of proton-coupled electron transfer reactions*, Biochim. Biophys. Acta, **1655**, 29-36 (2004)
[151] T. Wang, G. Brudvig and V. S. Batista, *Characterization of Proton Coupled Electron Transfer in a Biomimetic Oxomanganese Complex: Evaluation of the DFT B3LYP Level of Theory*, J. Chem. Theory Comput., **6**, 755-760 (2010)
[152] C. Costentin, M. Robert and J. M. Saveant, *Concerted Proton-Electron Transfers: Electrochemical and Related Approaches*, Acc. Chem. Res., **43**, 1019-1029 (2010)
[153] R. I. Cukier and D. G. Nocera, *Proton-Coupled Electron Transfer*, Annu. Rev. Phys. Chem., **49**, 337-369 (1998)
[154] C. Costentin, M. Robert and J. M. Saveant, *Adiabatic and non-adiabatic concerted proton-electron transfers. Temperature effects in the oxidation of intramolecularly hydrogen-bonded phenols*, J. Am. Chem. Soc., **129**, 9953-9963 (2007)
[155] G. Villani, *Quantum dynamics of proton-coupled electron transfer in model systems*, Chem. Phys., **302**, 309-322 (2004)
[156] P. Politzer, J. S. Murray and T. Clark, *Halogen bonding: an electrostatically-driven highly directional noncovalent interaction*, PCCP, **12**, 7748-7757 (2010)
[157] P. Metrangolo and G. Resnati, *Halogen bonding: A paradigm in supramolecular chemistry*, Chem-Eur J, **7**, 2511-2519 (2001)
[158] P. Politzer, P. Lane, M. C. Concha, Y. G. Ma and J. S. Murray, *An overview of halogen bonding*, J. Mol. Model., **13**, 305-311 (2007)
[159] A. C. Legon, *The interaction of dihalogens and hydrogen halides with Lewis bases in the gas phase: An experimental comparison of the halogen bond and the hydrogen bond*, Struct Bond, **126**, 17-64 (2008)
[160] T. Clark, M. Hennemann, J. S. Murray and P. Politzer, *Halogen bonding: the σ-hole*, J. Mol. Model., **13**, 291-296 (2007)

[161] K. Eskandari and H. Zariny, *Halogen bonding: A lump-hole interaction*, Chem. Phys. Lett., **492**, 9-13 (2010)
[162] A. C. Legon, *The halogen bond: an interim perspective*, PCCP, **12**, 7736-7747 (2010)
[163] J. W. Zou, Y. J. Jiang, M. Guo, G. X. Hu, B. Zhang, H. C. Liu and Q. S. Yu, *Ab initio study of the complexes of halogen-containing molecules RX (X = Cl, Br, and I) and NH_3: Towards understanding the nature of halogen bonding and the electron-accepting propensities of covalently bonded halogen atoms*, Chem-Eur J, **11**, 740-751 (2005)
[164] N. J. M. Amezaga, S. C. Pamies, N. M. Peruchena and G. L. Sosa, *Halogen Bonding: A Study based on the Electronic Charge Density*, J. Phys. Chem. A, **114**, 552-562 (2010)
[165] K. E. Riley and P. Hobza, *Investigations into the nature of halogen bonding including symmetry adapted perturbation theory analyses*, J. Chem. Theory Comput., **4**, 232-242 (2008)
[166] M. Fourmigue, *Halogen bonding: Recent advances*, Curr Opin Solid St M, **13**, 36-45 (2009)
[167] W. Z. Wang, Y. Zhang, B. M. Ji and A. M. Tian, *On the correlation between bond-length change and vibrational frequency shift in halogen-bonded complexes*, J. Chem. Phys., **134**, 224303 (2011)
[168] W. Z. Wang and P. Hobza, *Origin of the X-Hal (Hal = Cl, Br) bond-length change in the halogen-bonded complexes*, J. Phys. Chem. A, **112**, 4114-4119 (2008)
[169] S. J. Grabowski, *Halogen Bond and Its Counterparts: Bent's Rule Explains the Formation of Nonbonding Interactions*, J. Phys. Chem. A, **115**, 12340-12347 (2011)
[170] I. Alkorta, G. Sanchez-Sanz, J. Elguero and J. E. Del Bene, *FCl:PCX Complexes: Old and New Types of Halogen Bonds*, J. Phys. Chem. A, **116**, 2300-2308 (2012)
[171] J. E. Del Bene, I. Alkorta and J. Elguero, *Do nitrogen bases form chlorine-shared and ion-pair halogen bonds?*, Chem. Phys. Lett., **508**, 6-9 (2011)
[172] A. R. Voth, P. Khuu, K. Oishi and P. S. Ho, *Halogen bonds as orthogonal molecular interactions to hydrogen bonds*, Nat Chem, **1**, 74-79 (2009)
[173] P. P. Zhou, W. Y. Qiu, S. Liu and N. Z. Jin, *Halogen as halogen-bonding donor and hydrogen-bonding acceptor simultaneously in ring-shaped $H_3N \cdot X(Y) \cdot HF$ (X = Cl, Br and Y = F, Cl, Br) Complexes*, PCCP, **13**, 7408-7418 (2011)
[174] P. Metrangolo and G. Resnati, *Chemistry - Halogen versus hydrogen*, Science, **321**, 918-919 (2008)
[175] Q. Z. Li, X. S. Xu, T. Liu, B. Jing, W. Z. Li, J. B. Cheng, B. A. Gong and J. Z. Sun, *Competition between hydrogen bond and halogen bond in complexes of formaldehyde with hypohalous acids*, PCCP, **12**, 6837-6843 (2010)
[176] M. G. Sarwar, B. Dragisic, L. J. Salsberg, C. Gouliaras and M. S. Taylor, *Thermodynamics of Halogen Bonding in Solution: Substituent, Structural, and Solvent Effects*, J. Am. Chem. Soc., **132**, 1646-1653 (2010)
[177] Q.-Z. Li, B. Jing, R. Li, Z.-B. Liu, W.-Z. Li, F. Luan, J.-B. Cheng, B.-A. Gong and J. Z. Sun, *Some measures for making halogen bonds stronger than hydrogen bonds in H_2CS-HOX (X= F, Cl, and Br) complexes*, PCCP, **13**, 2266-2271 (2011)
[178] W. Jensen, *Electronegativity from Avogadro to Pauling. Part 1: Origins of the electronegativity concept*, J. Chem. Educ., **73**, 11-20 (1996)
[179] W. Jensen, *Electronegativity from Avogadro to Pauling: II. Late nineteenth- and early twentieth-century developments*, J. Chem. Educ., **80**, 279-287 (2003)
[180] L. Pauling, *The Nature of the Chemical Bond. IV. The Energy of Single Bonds and the Relative Electronegativity of Atoms.*, J. Am. Chem. Soc., **54**, 3570-3582 (1932)

[181] L. Pauling *The Partial Ionic Character of Covalent Bonds and the Relative Electronegativity of Atoms* in *The Nature of the Chemical Bond*; Third ed.; Cornell University Press: Ithaca New York, 1960.
[182] L. Pauling and J. Sherman, *A Quantitative Discussion of Bond Orbitals*, J. Am. Chem. Soc., **59**, 1450-1456 (1937)
[183] L. R. Murphy, T. L. Meek, A. L. Allred and L. C. Allen, *Evaluation and test of Pauling's electronegativity scale*, J. Phys. Chem. A, **104**, 5867-5871 (2000)
[184] R. S. Mulliken, *A New Electroaffinity Scale; Together with Data on Valence States and on Valence Ionization Potentials and Electron Affinities*, J. Chem. Phys., **2**, 782-791 (1934)
[185] D. R. Herrick, *Connecting Pauling and Mulliken electronegativities*, J. Chem. Theory Comput., **1**, 255-260 (2005)
[186] W. Gordy, *A Relation between Bond Force Constants, Bond Orders, Bond Lengths, and the Electronegativities of the Bonded Atoms*, J. Chem. Phys., **14**, 305-320 (1946)
[187] W. Gordy, *A New Method of Determining Electronegativity from Other Atomic Properties*, Physical Review, **69**, 604-607 (1946)
[188] A. L. Allred and E. G. Rochow, *A Scale of Electronegativity Based on Electrostatic Force*, J. Inorg. Nucl. Chem., **5**, 264-268 (1958)
[189] L. C. Allen, *Electronegativity Is the Average One-Electron Energy of the Valence-Shell Electrons in Ground-State Free Atoms*, J. Am. Chem. Soc., **111**, 9003-9014 (1989)
[190] J. K. Nagle, *Atomic Polarizability and Electronegativity*, J. Am. Chem. Soc., **112**, 4741-4747 (1990)
[191] J. Hinze and H. H. Jaffe, *Electronegativity. I. Orbital Electronegativity of Neutral Atoms*, J. Am. Chem. Soc., **84**, 540-546 (1962)
[192] J. Hinze, M. A. Whitehead and H. H. Jaffe, *Electronegativity. II. Bond and Orbital Electronegativities.*, **85**, 148-154 (1962)
[193] J. Hinze and H. H. Jaffe, *Electronegativity: III. Orbital Electronegativities and Electron Affinities of Transition Metals*, Can. J. Chem., **41**, 1315-1328 (1963)
[194] J. Hinze and H. H. Jaffe, *Electronegativity: IV. Orbital Electronegativities of Neutral Atoms of the Periods Three A and Four A and of the Positive Ions of Periods One and Two*, J. Phys. Chem., **67**, 1501-1506 (1963)
[195] A. F. Clifford, *The Prediction of Solubility Product Constants*, J. Am. Chem. Soc., **79**, 5404 (1957)
[196] A. F. Clifford, *The Electronegativity of Groups*, J. Am. Chem. Soc., **63**, 1227-1231 (1959)
[197] H. O. Pritchard and H. A. Skinner, *The Concept of Electronegativity*, Chem. Rev., **55**, 745-786 (1955)
[198] D. Datta and S. N. Singh, *Evaluation of Group Electronegativity by Pauling Thermochemical Method*, J. Phys. Chem., **94**, 2187-2190 (1990)
[199] J. E. Huheey, *The Electronegativity of Groups*, J. Phys. Chem., **69**, 3284-3291 (1965)
[200] J. E. Huheey, *The Electronegativity of Multiply Bonded Groups*, J. Phys. Chem., **70**, 2086-2092 (1966)
[201] L. Komorowski, J. Lipinski and M. J. Pyka, *Electronegativity and Hardness of Chemical Groups*, J. Phys. Chem., **97**, 3166-3170 (1993)
[202] L. C. Allen, D. A. Egolf, E. T. Knight and C. X. Liang, *Bond Polarity Index*, J. Phys. Chem., **94**, 5602-5607 (1990)
[203] L. H. Reed and L. C. Allen, *Bond Polarity Index - Application to Group Electronegativity*, J. Phys. Chem., **96**, 157-164 (1992)

[204] J. Mullay, *Calculation of Group Electronegativity*, J. Am. Chem. Soc., **107**, 7271-7275 (1985)
[205] J. Mullay, *Atomic and Group Electronegativities*, J. Am. Chem. Soc., **106**, 5842-5847 (1984)
[206] R. T. Sanderson, *Electronegativities in inorganic chemistry (II)*, J. Chem. Educ., **31**, 2-7 (1954)
[207] R. T. Sanderson, *Principles of Electronegativity .1. General Nature*, J. Chem. Educ., **65**, 112-118 (1988)
[208] R. P. Iczkowski and J. L. Margrave, *Electronegativity*, J. Am. Chem. Soc., **83**, 3547-3551 (1961)
[209] R. G. Parr, R. A. Donnelly, M. Levy and W. E. Palke, *Electronegativity: The density functional viewpoint*, J. Chem. Phys., **68**, 3801-3807 (1978)
[210] R. G. Parr and L. J. Bartolotti, *On the Geometric Mean Principle for Electronegativity Equalization*, J. Am. Chem. Soc., **104**, 3801-3803 (1982)
[211] R. G. Parr and R. G. Pearson, *Absolute Hardness: Companion Parameter to Absolute Electronegativity*, J. Am. Chem. Soc., **105**, 7512-7516 (1983)
[212] P. Geerlings, F. De Proft and W. Langenaeker, *Conceptual density functional theory*, Chem. Rev., **103**, 1793-1873 (2003)
[213] M. V. Putz, N. Russo and E. Sicilia, *About the Mulliken electronegativity in DFT*, Theor. Chem. Acc., **114**, 38-45 (2005)
[214] L. Komorowski, *Electronegativity and Hardness in the Chemical Approximation*, Chem. Phys., **114**, 55-71 (1987)
[215] S. Marriott, W. F. Reynolds, R. W. Taft and R. D. Topsom, *Substituent Electronegativity Parameters*, J. Org. Chem., **49**, 959-965 (1984)
[216] R. J. Boyd and K. E. Edgecombe, *Atomic and Group Electronegativities from the Electron-Density Distributions of Molecules*, J. Am. Chem. Soc., **110**, 4182-4186 (1988)
[217] F. De Proft, W. Langenaeker and P. Geerlings, *Ab initio Determination of Substituent Constants in a Density Functional Theory Formalism - Calculation of Intrinsic Group Electronegativity, Hardness, and Softness*, J. Phys. Chem., **97**, 1826-1831 (1993)
[218] T. Leyssens, P. Geerlings and D. Peeters, *The Importance of the External Potential on Group Electronegativity*, J. Phys. Chem. A, **109**, 9882-9889 (2005)

Chapter 2: Theory

As established in Chapter 1, the proper calculation of the potential energy surfaces of the NH_3HX systems requires a high-quality treatment of electron correlation and good basis sets. Furthermore, the description of dipole-bound molecular anions has its own theoretical hurdles. Modern electronic structure methods, which used quantum mechanics to predict the properties of chemical systems, must be used. This chapter describes the theories and methods used in this thesis, and an evaluation of their advantages and limitations.

2.1. The Born-Oppenheimer Approximation

Suppose we wish to describe a chemical system by quantum mechanics. One fundamental approach is to determine the wavefunction of the system. Given the wavefunction, we would then be able to calculate the properties of that system.

We know that the wavefunction of the system must satisfy the Schrödinger equation:

$$\hat{H}\psi = E\psi \tag{7}$$

Where $\hat{H}$ is the Hamiltonian, ψ is the wavefunction, and E is the energy. The eigenfunctions and eigenvalues of this equation are the quantum states and the respective energies available to the system. For our complete chemical system, we have:

$$\hat{H}_{tot} = \hat{T}_n + \hat{T}_e + \hat{V}_{ne} + \hat{V}_{ee} + \hat{V}_{nn} \tag{8}$$

Where $\hat{T}_n$ is the nuclear kinetic energy operator, $\hat{T}_e$ is the electronic kinetic energy operator, $\hat{V}_{ne}$ is the nucleus-electron interaction operator, $\hat{V}_{ee}$ is the electron-electron interaction operator, and $\hat{V}_{nn}$ is the nucleus-nucleus interaction operator.[1] In this form, the nuclear and electronic motions are strongly coupled. However, the electrons and nuclei have very different masses, and therefore we would expect that the electronic motions would be more strongly coupled to each other than they are to the motions of the nuclei, and *vice versa*.

Without getting into any further technical detail, it is possible to separate the expression for the wavefunction into the product of an electronic wavefunction $\psi(r;R)$ at a given

set of nuclear coordinates *R*, and a function describing the nuclei moving in the electronic potential $E_e(R)$. This process splits the Hamiltonian into the sum of a "clamped nuclei" Hamiltonian for the electrons, with the nuclear positions as a parameter, and a corrective Hamiltonian for nuclear motion.[2]

A linear combination of the eigenfunctions of the clamped nuclei Hamiltonian gives us a (useful) exact form of the wavefunction. Taking a *single* eigenfunction of the clamped nuclei Hamiltonian decouples the different solutions and gives us the *adiabatic approximation*, which still incorporates a small correction for nuclear motion. Finally, we can remove the small correction for nuclear motion, and obtain the *Born-Oppenheimer approximation*.[2] We are no longer calculating the total wavefunction of the system, but just the electronic wavefunction, ψ_e. Given a set of nuclear coordinates *R*, and labelling the electronic coordinates as *r*, we must solve:

$$(\hat{T}_e + \hat{V}_{ne} + \hat{V}_{ee} + \hat{V}_{nn})\psi_e(r;R) = E(R)\psi_e(r;R) \tag{9}$$

2.2. The Hartree-Fock Method

So far we have not defined a form for the wavefunction $\psi(r;R)$, but we do know that it must be in terms of the electronic coordinates. We also know that it must be antisymmetric with respect to exchange of any two electrons, because they are fermions. We achieve this by defining the wavefunction as a (normalised) Slater determinant of orthonormal molecular spinorbitals[3]:

$$\psi = \frac{1}{\sqrt{N!}}\begin{vmatrix} \phi_1(1) & \phi_2(1) & \ldots & \phi_N(1) \\ \phi_1(2) & \phi_2(2) & \ldots & \phi_N(2) \\ \ldots & \ldots & \ldots & .. \\ \phi_1(N) & \phi_2(N) & \ldots & \phi_N(N) \end{vmatrix} \tag{10}$$

Each term $\phi_i(n)$ is the molecular spinorbital "i" occupied by electron "n". As the name suggests, these terms are the product of a spatial function ($\theta_i(r)$) and a spin function ($\alpha(s)$ or $\beta(s)$) denoting up or down spin:

$$\phi_i = \theta_i(r)\alpha(s) \tag{11}$$

It can be seen by writing out the determinant in full that exchange of any two particles changes the sign of the wavefunction:

$$\begin{aligned}\psi_O &= \frac{1}{\sqrt{N!}}(\phi_1(1)\phi_2(2)... - \phi_1(2)\phi_2(1)... + ...) \\ \psi_P &= \frac{1}{\sqrt{N!}}(\phi_1(2)\phi_2(1)... - \phi_1(1)\phi_2(2)... + ...) \\ \psi_O &= -\psi_P\end{aligned} \tag{12}$$

Jensen provides a useful trick to handling the Slater determinant which is applied to the remainder of this section.[4] It is more convenient to write the Slater determinant in terms of a product of one-electron wavefunctions, and an operator called the "antisymmetriser" $\hat{A}$. This idempotent, Hermitian operator generates all of the possible permutations of the electrons *via* a permutation operator $\hat{P}$, where the subscripts *i*, *ij*, *ijk* etc. indicate the permutation of 1, 2, 3 or more electrons, and π indicates the parity of the permutation[4]:

$$\begin{aligned}\psi &= \sqrt{N!}\hat{A}\left[\phi_1(1)\phi_2(2)\phi_3(3)\phi_4(4)...\phi_N(N)\right] = \sqrt{N!}\hat{A}\prod \\ \hat{A} &= \frac{1}{N!}\sum_P (-1)^\pi \hat{P} = \frac{1}{N!}\left[1 - \sum_{ij}\hat{P}_{ij} + \sum_{ijk}\hat{P}_{ijk} - ...\right]\end{aligned} \tag{13}$$

With the Hamiltonian and wavefunction well-defined, we are now ready to begin. Assuming atomic units (*i.e.* the mass and charge of the electron are implicit), the definitions of the components of the electronic Hamiltonian $\hat{H}_e$ are straightforward[3,4]:

$$\begin{aligned}\hat{H}_e &= \hat{T}_e + \hat{V}_{ne} + \hat{V}_{ee} + \hat{V}_{nn} \\ \hat{T}_e &= -\sum_i^{N_{elec}} \frac{1}{2}\nabla_i^2 \\ \hat{V}_{ne} &= -\sum_a^{N_{nuc}}\sum_i^{N_{elec}} \frac{Z_a}{|R_a - r_i|} \\ \hat{V}_{ee} &= +\sum_i^{N_{elec}}\sum_{j>i}^{N_{elec}} \frac{1}{|r_i - r_j|} \\ \hat{V}_{nn} &= +\sum_a^{N_{nuc}}\sum_{b>a}^{N_{nuc}} \frac{Z_a Z_b}{|R_a - R_b|}\end{aligned} \tag{14}$$

Note the sums, where *i* runs over all the electrons and all nuclei. We can gather the operators according to how many electrons they act upon. There is a no-electron operator, $\hat{V}_{nn}$, which comes out as a constant V_{nn}. This is simply the Coulomb repulsion of the nuclei from each other and is calculated using Coulomb's law for the electrostatic potential. There is a one-electron operator $\hat{h}_i$:

$$\hat{h}_i = -\frac{1}{2}\nabla_i^2 - \sum_a^{N_{nuc}} \frac{Z_a}{|R_a - r_i|} \tag{15}$$

The physical interpretation of this operator is one electron *i* moving (kinetic energy $-\frac{1}{2}\nabla_i^2$) in the field of all the nuclei (electrostatic potential energy $-\sum_a^{N_{nuc}} \frac{Z_a}{|R_a - r_i|}$).

Finally there is a two-electron operator $\hat{g}_{ij}$:

$$\hat{g}_{ij} = \frac{1}{|r_i - r_j|} \tag{16}$$

The physical interpretation of this operator is the Coulomb interaction between two electrons *i* and *j*.

So therefore (in the Born-Oppenheimer approximation) our total Hamiltonian becomes:

$$\hat{H} = \sum_i^{N_{elec}} \hat{h}_i + \sum_i^{N_{elec}} \sum_{j>i}^{N_{elec}} \hat{g}_{ij} + \hat{V}_{nn} \tag{17}$$

Now the reason for our use of the antisymmetriser will become apparent. If we define the energy in terms of the determinant, we can exploit the properties of the antisymmetriser to define the energy in terms of the Hamiltonian, and the permutations *P* of the electrons in the product:

$$\begin{aligned} E &= \left\langle \psi \middle| \hat{H} \middle| \psi \right\rangle \\ &= N! \left\langle \hat{A}\Pi \middle| \hat{H} \middle| \hat{A}\Pi \right\rangle \\ &= \sum_P (-1)^\pi \left\langle \Pi \middle| \hat{H} \middle| \hat{P}\Pi \right\rangle \end{aligned} \tag{18}$$

In other words, the energy is now defined in terms of permutations upon a simple product of singly-occupied spinorbitals.[4]

We now have a sum of integrals involving ever-higher orders of permutation operator $\hat{P}$. The integral involving $\hat{h}_i$ and $\hat{P}$ can be simplified, because orthonormalisation removes many of its parts. For $\hat{P}_i$=1, h_1 only operates upon each of the spinorbitals in which electron 1 resides, $\phi_i(1)$. In each case, we can gather that spinorbital in an integral around the operator, and leave the remaining operators in their own integral. The spinorbitals are normalised, and therefore the integrals involving the overlap of the other spinorbitals with themselves must be 1:

$$\begin{aligned}
&\left\langle \Pi \middle| \hat{h}_1 \middle| \Pi \right\rangle \\
&= \left\langle \phi_1(1) \middle| \hat{h}_1 \middle| \phi_1(1) \right\rangle \left\langle \phi_2(2)\phi_3(3)...\phi_N(N) \middle| \phi_2(2)\phi_3(3)...\phi_N(N) \right\rangle \\
&= \left\langle \phi_1(1) \middle| \hat{h}_1 \middle| \phi_1(1) \right\rangle \left\langle \phi_2(2) \middle| \phi_2(2) \right\rangle \left\langle \phi_3(3). \middle| \phi_3(3) \right\rangle ... \left\langle \phi_N(N) \middle| \phi_N(N) \right\rangle \\
&= \left\langle \phi_1(1) \middle| \hat{h}_1 \middle| \phi_1(1) \right\rangle = h_1
\end{aligned} \tag{19}$$

For integrals involving $\hat{h}_1$ and $\hat{P}_{ij}$ (or higher permutations), orthonormalisation means that the integral on the right is always equal to 0. This is because the permutation inevitably creates an integral involving the overlap of two different spinorbitals, which we know to be orthogonal. For example with $\hat{P}_{12}$

$$\begin{aligned}
&\left\langle \Pi \middle| \hat{h}_1 \middle| \hat{P}_{12} \Pi \right\rangle \\
&= \left\langle \phi_1(1)\phi_2(2)...\phi_N(N) \middle| \hat{h}_1 \middle| \phi_2(1)\phi_1(2)...\phi_N(N) \right\rangle \\
&= \left\langle \phi_1(1) \middle| \hat{h}_1 \middle| \phi_2(1) \right\rangle \left\langle \phi_2(2) \middle| \phi_1(2) \right\rangle ... \left\langle \phi_N(N) \middle| \phi_N(N) \right\rangle = 0
\end{aligned} \tag{20}$$

For integrals involving $\hat{g}_{ij}$ and $\hat{P}_i$=1, most of the MO parts vanish by normality as before:

$$\begin{aligned}
&\left\langle \Pi \middle| \hat{g}_{12} \middle| \Pi \right\rangle \\
&= \left\langle \phi_1(1)\phi_2(2) \middle| \hat{g}_{12} \middle| \phi_1(1)\phi_2(2) \right\rangle \left\langle \phi_3(3)...\phi_N(N) \middle| \phi_3(3)...\phi_N(N) \right\rangle \\
&= \left\langle \phi_1(1)\phi_2(2) \middle| \hat{g}_{12} \middle| \phi_1(1)\phi_2(2) \right\rangle \left\langle \phi_3(3). \middle| \phi_3(3) \right\rangle ... \left\langle \phi_N(N) \middle| \phi_N(N) \right\rangle \\
&= \left\langle \phi_1(1)\phi_2(2) \middle| \hat{g}_{12} \middle| \phi_1(1)\phi_2(2) \right\rangle = J_{12}
\end{aligned} \tag{21}$$

For integrals involving $\hat{g}_{ij}$ and $\hat{P}_{ij}$ the permutation of two electrons also gives a valid contribution to the integral, because the MOs holding the permuted electrons go into the integral with $\hat{g}_{ij}$ rather than just overlap. This term will appear with a negative sign because of the factor $(-1)^1$ in the sum:

$$\begin{aligned}
&\left\langle \Pi \middle| \hat{g}_{12} \middle| \hat{P}_{12} \Pi \right\rangle \\
&= \left\langle \phi_1(1)\phi_2(2)...\phi_N(N) \middle| \hat{g}_{12} \middle| \phi_2(1)\phi_1(2)...\phi_N(N) \right\rangle \\
&= \left\langle \phi_1(1)\phi_2(2) \middle| \hat{g}_{12} \middle| \phi_2(1)\phi_1(2) \right\rangle \left\langle \phi_3(3) \middle| \phi_3(3) \right\rangle ... \left\langle \phi_N(N) \middle| \phi_N(N) \right\rangle \\
&= \left\langle \phi_1(1)\phi_2(2) \middle| \hat{g}_{12} \middle| \phi_2(1)\phi_1(2) \right\rangle = K_{12}
\end{aligned} \tag{22}$$

For integrals with higher permutations, the integrals are all zero. The integral in the right now involves overlap of two different MOs, which are orthogonal.

$$\begin{aligned}&\left\langle \Pi \middle| \hat{g}_{12} \middle| \hat{P}_{123} \Pi \right\rangle \\ &= \left\langle \phi_1(1)\phi_2(2)\phi_3(3)...\phi_N(N) \middle| \hat{g}_{12} \middle| \phi_3(1)\phi_2(3)\phi_1(2)...\phi_N(N) \right\rangle \\ &= \left\langle \phi_1(1)\phi_2(2) \middle| \hat{g}_{12} \middle| \phi_3(1)\phi_1(2) \right\rangle \left\langle \phi_3(3) \middle| \phi_2(3) \right\rangle ... \left\langle \phi_N(N) \middle| \phi_N(N) \right\rangle = 0\end{aligned} \tag{23}$$

To summarise, we have the energy in terms of a sum of one-electron integrals, and a double-sum of two two-electron integrals, and the nucleus-nucleus repulsion:

$$E = \sum_{i=1}^{N_{elec}} h_i + \sum_{i=1}^{N_{elec}} \sum_{j>i}^{N_{elec}} (J_{ij} - K_{ij}) + V_{nn} \tag{24}$$

To simplify this a little, we can rewrite the double sum with a factor of one half to remove double-counting of the interactions:

$$E = \sum_{i=1}^{N_{elec}} h_i + \frac{1}{2} \sum_{i=1}^{N_{elec}} \sum_{j=1}^{N_{elec}} (J_{ij} - K_{ij}) + V_{nn} \tag{25}$$

The two-electron integrals J_{ij} and K_{ij} are known as the *Coulomb* and *exchange* integrals, respectively. It can be seen from inspection that the Coulomb integral describes the electrostatic (*i.e.* Coulombic) interaction between an electron *i* and another electron *j*, including an unphysical interaction between *i* and *i*. The exchange integral describes the quantum-mechanical exchange interaction between electrons *i* and *j*, which lacks a classical counterpart. The spurious exchange term for interaction between *i* and *i* exactly cancels the spurious Coulomb term.

We may also write this expression in terms of the "core Hamiltonian" operator $\hat{h}_i$, the nuclear-nuclear repulsion energy V_{nn}, and the coulomb and exchange operators $\hat{J}_i$ and $\hat{K}_i$:

$$E = \sum_{i=1}^{N_{elec}} \left\langle \phi_i \middle| \hat{h}_i \middle| \phi_i \right\rangle + \frac{1}{2} \sum_{ij}^{N_{elec}} \left(\left\langle \phi_j \middle| \hat{J}_i \middle| \phi_j \right\rangle - \left\langle \phi_j \middle| \hat{K}_i \middle| \phi_j \right\rangle \right) + V_{nn} \tag{26}$$

Where *e.g.*:

$$\begin{aligned}&\hat{J}_i \left| \phi_j(2) \right\rangle \\ &= \left\langle \phi_i(1) \middle| \hat{g}_{12} \middle| \phi_i(1) \right\rangle \left| \phi_j(2) \right\rangle \\ &\hat{K}_i \left| \phi_j(2) \right\rangle \\ &= \left\langle \phi_i(1) \middle| \hat{g}_{12} \middle| \phi_j(1) \right\rangle \left| \phi_i(2) \right\rangle\end{aligned} \tag{27}$$

The variational principle informs us that the wavefunction which provides us with the lowest energy will be the closest approximation to the wavefunction of this system (within the B-O approximation *etc.*).[4] Therefore we can now solve for the lowest

possible *E* given a set of MOs and nuclear coordinates, using the method of variations. By the method of Lagrange multipliers (to constrain orthonormality), it is possible to generate the set of Hartree-Fock equations:

$$\hat{F}\phi_i = \sum_j^{N_{elec}} \lambda_{ij}\phi_j \tag{28}$$

Where the one-electron Fock operator $\hat{F}$ is:

$$\hat{F} = \hat{h} + \sum_j^{n_{elec}} (\hat{J}_j - \hat{K}_j) \tag{29}$$

…and when λ_{ij} is diagonalised, this expression becomes the Fock equation:

$$\hat{F}\phi_i' = \varepsilon_i\phi_i' \tag{30}$$

Here the set of eigenfunctions is the set of the "canonical" molecular spinorbitals of the system, and the eigenvalues are the respective orbital energies.[4] The lowest-energy orbitals become occupied, and the remaining orbitals are "virtual" ones. However having come this far, we hit a snag. The one-electron Fock operator $\hat{F}$ includes the Coulomb and exchange operators. These operators are written in terms of all of the occupied spinorbitals *j*. Therefore, we cannot solve this eigenvalue problem unless we first know all of the spinorbitals. However we do not know the spinorbitals unless we solve the eigenvalue problem.

To bootstrap this, we must postulate a *guess* for the occupied molecular orbitals of the system. Then we can solve the problem. The Coulomb and exchange integrals will describe the interaction of the electron *i* with the approximate field of the other electrons *j*. The solution to this eigenvalue equation will not be ideal; however it will be better than the guess. We can then use this improved solution as the guess for another round of computation. This process can continue until we are satisfied with the results. Given the variational principle, we may impose a convergence criterion on the energy, which should drop with each iteration of the procedure. Or we may note that the exact solution would give us the same spinorbitals as output which were used in the original guess, and impose a self-consistency criterion. Computational methods use both in practice.[4,5]

To summarise, we now have an expression – the Hartree[6-8]-Fock equations – which can be solved to give a set of molecular orbitals and their energies. Now we must solve the equations. It is necessary to define the spinorbitals as a set of functions, in such a

way that we can computationally change their form. The problem is then one of finding the forms of the spinorbitals which satisfy the equations. One such approach is to express the spinorbitals as a linear combination of *basis functions*, where the basis functions are fixed and the coefficients used in their combination are varied. Expressing the Hartree-Fock equations in this way generates the *Roothaan-Hall equations*.[9,10]

*2.2.1. **The Roothaan-Hall Equations***

The Roothaan-Hall equations are deceptively simple, but very powerful. The closed-shell case is the simplest. Let us return to the one-electron pseudo-eigenvalue problem:

$$\hat{F}\phi_i' = \varepsilon_i\phi_i' \tag{31}$$

For a closed-shell molecule, there are an equal number of α and β electrons, paired in MOs. We can replace the spinorbital with a doubly-occupied spatial molecular orbital (MO) θ_i'. Once we redefine the $\hat{J}_j$ and $\hat{K}_j$ operators in terms of the new MOs, we get a simpler Fock operator thus:

$$\hat{F} = \hat{h} + \sum_{j}^{n_{elec}/2}(2\hat{J}_j - \hat{K}_j) \tag{32}$$

(NB: All electrons interact through the Coulomb operator, but only electrons of like spin interact through the exchange operator.)

Now we define the wholly spatial MO θ_i' as a linear combination of M_{basis} basis functions (spatial functions χ_α with a form which we will describe later):

$$\theta_i' = \sum_{\alpha}^{M_{basis}} C_{\alpha i}\chi_\alpha \tag{33}$$

So the problem is now:

$$\hat{F}\sum_{\alpha}^{M_{basis}} C_{\alpha i}\chi_\alpha = \varepsilon_i \sum_{\alpha}^{M_{basis}} C_{\alpha i}\chi_\alpha \tag{34}$$

If we multiply from the left by the complex conjugate of another basis function χ_β, integrate over the electron coordinates, and pull out the sum we get[4]:

$$\sum_{\alpha}^{M_{basis}} C_{\alpha i}\int dr\chi_\beta^*\hat{F}\chi_\alpha = \varepsilon_i \sum_{\alpha}^{M_{basis}} C_{\alpha i}\int dr\chi_\beta^*\chi_\alpha \tag{35}$$

We can denote the integral on the left hand side as:

$$F_{\alpha\beta} = \int dr\chi_\beta^*\hat{F}\chi_\alpha \tag{36}$$

This is the element $\alpha\beta$ of the "Fock matrix" F. The integral on the right hand side is denoted as:

$$S_{\alpha\beta} = \int dr \chi_\beta * \chi_\alpha \tag{37}$$

This is the element $\alpha\beta$ of the "overlap matrix" S.

If we gather all of the orbital coefficients into their own matrix C we can represent the Hartree-Fock equations in the basis set approximation. In this representation the equations are known as the Roothaan-Hall equations:

$$FC = SC\varepsilon \tag{38}$$

Note that the overlap matrix S, and the integrals involving the core Hamiltonian $\hat{h}$, do not involve the orbital coefficients, only the basis functions, which do not change in the course of the calculation. In contrast, the right hand side of each entry in the Fock matrix includes Coulomb and exchange operators, which invoke the MOs, and therefore involve the orbital coefficients. These can also be simplified.

$$F_{\alpha\beta} = \int dr \chi_\beta * \hat{F} \chi_\alpha \tag{39}$$

Returning to the space-saving bra-ket notation, this is:

$$\begin{aligned} F_{\alpha\beta} &= \langle \chi_\beta | \hat{F} | \chi_\alpha \rangle \\ F_{\alpha\beta} &= \langle \chi_\beta | \hat{h} | \chi_\alpha \rangle + \sum_j^{OccMOs} \langle \chi_\beta | 2\hat{J}_j - \hat{K}_j | \chi_\alpha \rangle \end{aligned} \tag{40}$$

Stating $\hat{J}_j$ and $\hat{K}_j$ explicitly in terms of the MO θ_j where *OccMOs* is the number of occupied MOs:

$$F_{\alpha\beta} = \langle \chi_\beta | \hat{h} | \chi_\alpha \rangle + \sum_j^{OccMOs} (2\langle \chi_\beta \phi_j | \hat{g} | \chi_\alpha \phi_j \rangle - \langle \chi_\beta \phi_j | \hat{g} | \phi_j \chi_\alpha \rangle) \tag{41}$$

Of course θ_j can be written in terms of the basis functions and its own set of orbital coefficients. Taking the utmost care with subscripts, we can deduce:

$$F_{\alpha\beta} = \langle \chi_\beta | \hat{h} | \chi_\alpha \rangle + \sum_j^{OccMOs} \sum_{\gamma\delta}^{M_{basis}} c_{\gamma j} c_{\delta j} (2\langle \chi_\beta \chi_\gamma | \hat{g} | \chi_\alpha \chi_\delta \rangle - \langle \chi_\beta \chi_\gamma | \hat{g} | \chi_\delta \chi_\alpha \rangle) \tag{42}$$

We can replace the sum over occupied MOs and the corresponding coefficients with a further matrix D[4]:

$$\begin{aligned} D_{\gamma\delta} &= \sum_j^{OccMOs} c_{\gamma j} c_{\delta j} \\ F_{\alpha\beta} &= \langle \chi_\beta | \hat{h} | \chi_\alpha \rangle + \sum_{\gamma\delta}^{M_{basis}} D_{\gamma\delta} (2\langle \chi_\beta \chi_\gamma | \hat{g} | \chi_\alpha \chi_\delta \rangle - \langle \chi_\beta \chi_\gamma | \hat{g} | \chi_\delta \chi_\alpha \rangle) \end{aligned} \tag{43}$$

These integrals, involving one or two electrons (in two or four basis functions), *do not change* in the course of the calculation. In practice one-electron integrals are computed once and kept in memory, while the two-electron integrals are typically too numerous to store in memory and are quicker to recompute when needed than retrieve from disk. The matrix *D*, known as the density matrix, provides information on the density of the electrons for the Coulomb and exchange interactions.

This is the key to solving the self-consistent field problem. Recall that in the Hartree-Fock method, the Fock operator was defined in terms of the solutions to the equation. It was suggested that we had to feed in a guess for the form of the MOs, so that the Coulomb and exchange parts of the Fock operator would be defined. The density matrix provides us with this opportunity.

$$FC = SC\varepsilon \tag{44}$$

We create a guess density matrix *D*, and use it with the one- and two-electron integrals to construct the Fock matrix *F*. Solving this matrix equation by diagonalising *F*, we obtain orbital coefficients in *C* and orbital energies in ε. The coefficients can then be used to compute a new density matrix, and thus construct a new Fock matrix *F* for the next iteration. This proceeds until self-consistency is achieved (*D* input into the equations approximately the same as *D* output by the equations) and the energy is converged.[3,4]

2.3. Beyond the Hartree-Fock method: Electron Correlation

The Hartree-Fock model is an elegant approach to predicting the electronic structure of chemical systems within the Born-Oppenheimer approximation, with one significant drawback. The Hartree-Fock method is predicated upon the assumption that a single Slater determinant is a good description of the wavefunction. However, the Slater determinant describes the wavefunction for a single electronic configuration. In reality, the wavefunction does not experience this restriction, and therefore the Hartree-Fock wavefunction – no matter how well-converged – is inaccurate.

The physical interpretation of this limitation is that the Hartree-Fock method only describes the Coulomb and exchange interaction between an electron and the *average field* of all of the electrons. The Hartree-Fock wavefunction is constructed in an effective Hamiltonian in which the electron-electron repulsion is dealt with as a mean

field, but its energy is evaluated in the nonrelativistic, Born-Oppenheimer model Hamiltonian. As a consequence the electrons do not "avoid" each other as successfully as they could. If the electrons were able to respond to each other instantaneously as the wavefunction was optimised, then a lower-energy solution could be found.

If the wavefunction could mix in additional electronic configurations, "excited" Slater determinants of higher energy, it would allow the electrons greater flexibility in "avoiding each other". (In a classical model we would say that their motions were correlated.) This flexibility would reduce the electron-electron potential energy and thereby lower the energy of the system. The extra stability gained by adding this flexibility is called the *electron correlation energy*. [11]The methods by which electron correlation is described are documented in a section 2.3.2

Note that providing electronic correlation only brings us one step closer to describing the "real" wavefunction of the system. We are still operating in the Born-Oppenheimer approximation, and with a nonrelativistic, time-independent Hamiltonian. If we were to turn on the adiabatic correction for nuclear motion, we would "step up" to the adiabatic approximation.[2] As mentioned in section 2.1, this approximation creates *one* of the eigenfunctions of the nonrelativistic, time-independent Hamiltonian, *i.e.* one electronic state. If we were to describe the wavefunction as a linear combination of these adiabatic wavefunctions, we could couple multiple electronic states, and describe the connection between nuclear and electronic motion (Figure 2.1). However these techniques are not of immediate importance to this study.

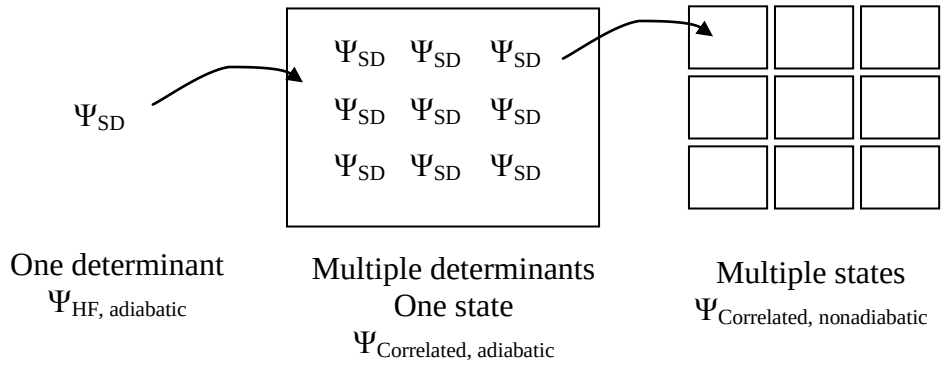

Figure 2.1: Relationship between determinants, states, and the nonadiabatic description of the system

2.3.1. The Post-Hartree-Fock methods

The Fock operator used in the Hartree-Fock method is hermitian, and therefore the eigenfunctions of the effective Hamiltonian – the sum of the Fock operators – form a complete set. These eigenfunctions are the Hartree-Fock wavefunction, and a series of excited configurations corresponding to exciting any number of electrons into virtual orbitals (*i.e.* replacing the occupied orbitals with virtual ones). We may express the wavefunction as a linear combination of a "reference" determinant obtained in Hartree-Fock and excited configurations thereof, and determine optimal linear combination coefficients.

This adds the flexibility that was lost by using a single-determinantal wavefunction. In particular, we can think of an electron being excited to a virtual orbital and another electron being excited to a different virtual orbital as a double-excitation, but also as a correlation between the motions of the two electrons. One electron can respond to the movement of the other. As the set of excited state determinants is complete, we can (if we use all the available determinants) produce an exact wavefunction within the limits of the model (a nonrelativistic Hamiltonian, in the Born-Oppenheimer approximation with a finite basis set). These methods – which use a Hartree-Fock reference as their starting point – are known as post-Hartree-Fock methods.

It is useful at this point to introduce a notation for the excitations. An interesting formulation of QM exists called the *second quantisation* which can be used to describe excitations tidily. In this notation, the excitation of an electron from one orbital *a* to another orbital *m* is equivalent to the simultaneous action of an annihilation operator $\hat{a}_a$, which destroys the electron in orbital *a*, and a creation operator $\hat{a}'_m$, which creates an electron in orbital *m*.

$$\hat{a}_a \hat{a}'_m \tag{45}$$

Double, triple *etc.* excitations simply involve a greater number of creation and annihilation operators.

$$\begin{gathered} \hat{a}_a \hat{a}_b \hat{a}'_m \hat{a}'_n \\ \hat{a}_a \hat{a}_b \hat{a}_c \hat{a}'_m \hat{a}'_n \hat{a}'_o \\ \textit{etc}. \end{gathered} \tag{46}$$

2.3.2. Three Related Approaches to Electron Correlation

There are many ways of expressing the correlated wave function using the excited determinants. It will be illustrative to discuss three approaches to the problem: Møller-Plesset perturbation theory of order *n* (MP*n*), the configuration interaction (CI) and the coupled cluster (CC) method. Assuming the MP*n* method converges, these methods would reach the same wave function if used to exhaustion. However they differ in important ways when they are truncated, which will always be the case in practice. One key issue to note is *size consistency*: a method should determine the same energy for two fragments at infinite separation, and the sum of the energy for each fragment calculated separately.

The CI method expresses the wavefunction as a linear combination of excited state determinants by applying an excitation operator $\hat{C}$ to the reference determinant Φ_0.[11]

$$\begin{aligned} H(1+\hat{C})\Phi_0 &= E(1+\hat{C})\Phi_0 \\ \hat{C} &= \hat{C}_1 + \hat{C}_2 + \hat{C}_3 + \hat{C}_4 + \ldots \end{aligned} \tag{47}$$

Where $\hat{C}_1$ creates all the singly-excited determinants, $\hat{C}_2$ generates all the doubly-excited determinants, *etc.* weighted by linear combination (CI) coefficients. We can solve this problem variationally in a manner analogous to that for SCF to get the coefficients. The truncation of the excitation operator determines the truncation of the method.

The CC method[12,13] also expresses the wavefunction as a linear combination of excited state determinants, but generates the wavefunction by acting on the reference wavefunction with a wave operator $e^{\hat{T}}$, where the cluster operator $\hat{T}$ has a similar form to the CI excitation operator $\hat{C}$.[14] This ansazt appears arbitrary, but has many desirable properties which we will discuss shortly. This method is also truncated by using a finite cluster operator.

$$He^{\hat{T}}\Phi_0 = Ee^{\hat{T}}\Phi_0 \tag{48}$$

MP*n* supposes that we can separate the Hamiltonian into a reference $\hat{H}_0$ and a perturbation $\hat{H}'$, and then generate *corrections* to the wavefunction by perturbation theory. The correction to the wavefunction is expressed as a linear combination of excited configurations, and ultimately the correction to the energy can also be expressed in terms of the same combination coefficients and integrals.[15]

*2.3.2.1. **The Configuration Interaction***

As mentioned previously, the CI method involves acting upon the reference wavefunction with an excitation operator $\hat{C}$, which contains terms to generate all the single, double, triple *etc.* excited configurations (Equation 47).

$$H(1+\hat{C})\Phi_0 = E(1+\hat{C})\Phi_0$$
$$\hat{C} = \hat{C}_1 + \hat{C}_2 + \hat{C}_3 + \hat{C}_4 + ... \tag{49}$$

Each of these terms $\hat{C}_n$ performs every possible n-tuple excitation, weighted by a coefficient, *e.g.* for single and double excitations:

$$\hat{C}_1 = \sum_{a,m} c_a^m \hat{a}_a \hat{a}'_m$$
$$\hat{C}_2 = \sum_{a,b,m,n} c_{ab}^{mn} \hat{a}_a \hat{a}_b \hat{a}'_m \hat{a}'_n \tag{50}$$

The goal is to optimise all of the coefficients.

The finite basis set means that there is a finite number of excitations, and in principle it can be solved exactly by including *all* of these excitations ("full CI"). However even for very small numbers of basis functions, the number of excitations is enormous. Therefore it is necessary to truncate the excitation operator, and this causes issues with size consistency.

Suppose we generate the wavefunction of the H_2 molecule using single and double excitations ($\hat{C} = \hat{C}_1 + \hat{C}_2$, which is denoted CISD). This is the full CI for the H_2 molecule, as there are no triple or higher excitations in a molecule with only two electrons. Two times this energy is, arithmetically, the energy of two isolated H_2 molecules. By doing this we include a doubly-excited configuration of each H_2 into the calculation of the energy, equivalent to a quadruply excited configuration of the dimer.

However, if we compute the energy of $(H_2)_2$ with an arbitrarily large intermolecular separation, using the same CISD method, we *do not have access to quadruple excitations*. Not only is the CISD method truncated with respect to $(H_2)_2$, now the monomer and dimer energies are being computed inconsistently! In other words, the CI energy is not additive, and does not scale linearly with the number of particles. CI is not size consistent.[16]

More formally, consider the form of the CID (no singles) wavefunction of the two H_2 molecules A and B in a minimal basis. With a minimal basis, the H_2 molecules have only two possible configurations, one with both electrons in bonding orbital (ψ_0), and some contribution *c* from an excited configuration (ψ_1) with both electrons in the antibonding orbital.

$$\begin{aligned} \Psi^A &= \psi_0^A + c_A \psi_1^A \\ \Psi^B &= \psi_0^B + c_B \psi_1^B \end{aligned} \tag{51}$$

At this stage it is useful to factorise these expressions, by introducing the excitation operator $\hat{C}_2$. By definition, $(1+\hat{C}_2)$ takes ψ_0 and creates a weighted combination of ψ_0 and ψ_1, which is exactly what we have in the above expression.

$$\begin{aligned} \Psi^A &= (1+\hat{C}_2^A)\psi_0^A \\ \Psi^B &= (1+\hat{C}_2^B)\psi_0^B \end{aligned} \tag{52}$$

If Ψ^A and Ψ^B do not overlap, the wavefunction for $(H_2)_2$ should be their antisymmetrised product[14]:

$$\begin{aligned} \Phi^{AB} &= \hat{A}\Psi^A\Psi^B \\ &= \hat{A}(1+\hat{C}_2^A)(1+\hat{C}_2^B)\psi_0^A\psi_0^B \\ &= (1+\hat{C}_2^A)(1+\hat{C}_2^B)\hat{A}\psi_0^A\psi_0^B \\ &= (1+\hat{C}_2^A+\hat{C}_2^B+\hat{C}_2^A\hat{C}_2^B)\phi_0^{AB} \end{aligned} \tag{53}$$

Clearly $\hat{C}_2^A\hat{C}_2^B$ is the troublesome quadruple excitation we encountered earlier. However the CID wavefunction for $(H_2)_2$ is:

$$\Phi_{CID}^{AB} = (1+\hat{C}_2^A+\hat{C}_2^B+\hat{C}_1^A\hat{C}_1^B)\phi_0^{AB} \tag{54}$$

This includes a double excitation $\hat{C}_1^A\hat{C}_1^B$ which does not appear in the product of the monomer CI wavefunctions (neither fragment has CI singles), and omits the quadruple excitation $\hat{C}_2^A\hat{C}_2^B$ (the interacting system has no quadruples). The former is not an issue, because the singly excited configurations are $\sigma_g\sigma_u$ and therefore overall ungerade, and thus cannot couple with ψ_0 (σ_g^2) or ψ_1 (σ_u^2) which are overall gerade. The latter is an important inconsistency. The size consistency failure in CID arises because it fails to provide excitations corresponding to the product of the excitation operators in the fragments.

*2.3.2.2. **The Coupled Cluster Method***

The product of the two CI wavefunctions suggests a solution to the size consistency issues in CI. Let us take an ansatz:

$$\Psi_{CC} = e^{\hat{T}}\Phi_0 \tag{55}$$

Why is this form of the wavefunction so useful? We can simply rewrite $e^{\hat{T}}$ (the "wave operator", where $\hat{T}$ is the "cluster operator") as a Maclaurin series[17]:

$$e^{\hat{T}} = 1 + \hat{T} + \frac{1}{2}\hat{T}^2 + \frac{1}{3!}\hat{T}^3 + \frac{1}{4!}\hat{T}^4 \ldots \tag{56}$$

We write the cluster operator in the same way as the CI excitation operator, truncating at some $\hat{T}_{\max}$ *e.g.* for CC singles and doubles:

$$\hat{T} = \hat{T}_1 + \hat{T}_2 \tag{57}$$

The cluster operator $\hat{T}_n$ is structured in a very similar way to the CI excitation operator $\hat{C}_n$. The difference is that its coefficients are known as "amplitudes". It is these amplitudes which the CC algorithm acts upon in order to find the wavefunction and the energy. [14]

$$\begin{aligned} \hat{T}_1 &= \sum_{a,m} t_a^m \hat{a}_a \hat{a}'_m \\ \hat{T}_2 &= \sum_{a,b,m,n} t_{ab}^{mn} \hat{a}_a \hat{a}_b \hat{a}'_m \hat{a}'_n \end{aligned} \tag{58}$$

The wave operator becomes:

$$e^{\hat{T}} = 1 + (\hat{T}_1 + \hat{T}_2) + \frac{1}{2}(\hat{T}_1 + \hat{T}_2)^2 + \frac{1}{3!}(\hat{T}_1 + \hat{T}_2)^3 + \frac{1}{4!}(\hat{T}_1 + \hat{T}_2)^4 ... \quad (59)$$

Which we can expand as:

$$e^{\hat{T}} = 1 + \hat{T}_1 + \hat{T}_2 + \frac{1}{2}\hat{T}_1^2 + \hat{T}_1\hat{T}_2 + \frac{1}{2}\hat{T}_2^2 + \frac{1}{6}\hat{T}_1^3 + \frac{1}{2}\hat{T}_1^2\hat{T}_2 + \frac{1}{2}\hat{T}_2^2\hat{T}_1 + \frac{1}{6}\hat{T}_2^3 ... \quad (60)$$

Then we gather terms by their total number of excitations:

$$e^{\hat{T}} = 1 + \hat{T}_1 + \left[\hat{T}_2 + \frac{1}{2}\hat{T}_1^2\right] + \left[\hat{T}_1\hat{T}_2 + \frac{1}{6}\hat{T}_1^3\right] + \left[\frac{1}{2}\hat{T}_2^2 + \frac{1}{2}\hat{T}_1^2\hat{T}_2 + \frac{1}{4!}\hat{T}_1^4\right] + ...$$

$$e^{\hat{T}}\Phi_0 = (1 + \hat{C}_1 + \hat{C}_2 + \hat{C}_3 + ...)\Phi_0$$

such that…

$$\hat{C}_1 = \hat{T}_1$$

$$\hat{C}_2 = \left[\hat{T}_2 + \frac{1}{2}\hat{T}_1^2\right] \quad (61)$$

$$\hat{C}_3 = \left[\hat{T}_1\hat{T}_2 + \frac{1}{6}\hat{T}_1^3\right]$$

$$\hat{C}_4 = \left[\frac{1}{2}\hat{T}_2^2 + \frac{1}{2}\hat{T}_1^2\hat{T}_2 + \frac{1}{4!}\hat{T}_1^4\right]$$

The first operator $\hat{C}_1$ groups terms which lead to single excitations. The second groups terms that create double excitations, and so on. Note that the truncation occurs in the cluster operator $\hat{T}$ and not the wave operator. Compare these operators to their CISD equivalents. Even at CC singles and doubles, with the cluster operator $\hat{T} = \hat{T}_1 + \hat{T}_2$, the wave operator includes terms for triple and higher excitations. [14] In this process we have generated not just single and double excitations $\hat{T}_1$ and $\hat{T}_2$, but a new $\hat{T}_1^2$ double excitation, and additional triple and quadruple and higher excitations. The term $\hat{T}_2^2$, for example, is exactly the product of two double excitations which we were deprived of when we did the CI calculation on the $(H_2)_2$ dimer. The coupled-cluster method is size consistent as a result of this form.[14,17,18]

The various terms are labelled connected or disconnected, to refer to their physical interpretation. The connected doubles term is $\hat{T}_2$, for example, and the connected quadruples term would be $\hat{T}_4$. These $\hat{T}_n$ terms represent the correlation between *N* electrons. However there is also a disconnected quadruples term $\hat{T}_2^2$, which represents

the mean-field interaction between two pairs of electrons, where the electrons in each pair are correlated with one another. In other words, the electrons in pair A move into excited orbitals to correlate their motions, but they happen to do so at the same time as pair B, and not as a result of the interaction between pair A and pair B. (The amplitude for that product of excitations is the product of the amplitudes of the excitations.)[19] Similarly, the disconnected triples term $\hat{T}_1\hat{T}_2$ represents a pair of correlated electrons ($\hat{T}_2$) and an electron interacting with the mean field of that pair ($\hat{T}_1$).[17]

Now that we have a rough theoretical justification for this ansatz, we must use the coupled cluster method to solve a quantum chemical problem. Recall that:

$$\hat{T}_2 = \sum_{a,b,m,n} t_{ab}^{mn} \hat{a}_a \hat{a}_b \hat{a}'_m \hat{a}'_n \tag{62}$$

The determinants generated by this connected doubles operator would be:

$$\left| \begin{matrix} mn \\ ab \end{matrix} \right\rangle \tag{63}$$

Let us take our ansatz:

$$\hat{H}e^{\hat{T}}\Phi_0 = Ee^{\hat{T}}\Phi_0 \tag{64}$$

We multiply from the left by $e^{-\hat{T}}$:

$$e^{-\hat{T}}\hat{H}e^{\hat{T}}\Phi_0 = E\Phi_0 \tag{65}$$

The left hand side of the equation can be expressed exactly in terms of the commutator[14] between H and T:

$$e^{-\hat{T}}\hat{H}e^{\hat{T}}\Phi_0 = \hat{H} + \left[\hat{H},\hat{T}\right] + \frac{1}{2!}\left[\left[\hat{H},\hat{T}\right],\hat{T}\right] + \frac{1}{3!}\left[\left[\left[\hat{H},\hat{T}\right],\hat{T}\right],\hat{T}\right] + \frac{1}{4!}\left[\left[\left[\hat{H},\hat{T}\right],\hat{T}\right],\hat{T}\right],\hat{T}\right] \tag{66}$$

If we substitute this back into the Schrödinger equation and multiply from the left by an excited determinant (in this example, a doubly-excited one):

$$\left\langle \begin{matrix} mn \\ ab \end{matrix} \middle| \hat{H} + \left[\hat{H},\hat{T}\right] + \frac{1}{2!}\left[\left[\hat{H},\hat{T}\right],\hat{T}\right] + \frac{1}{3!}\left[\left[\left[\hat{H},\hat{T}\right],\hat{T}\right],\hat{T}\right] + \frac{1}{4!}\left[\left[\left[\hat{H},\hat{T}\right],\hat{T}\right],\hat{T}\right],\hat{T}\right]\Phi_0 \right\rangle = E\left\langle \begin{matrix} mn \\ ab \end{matrix} \middle| \Phi_0 \right\rangle \tag{67}$$

Given that the excited determinants are orthogonal to the reference determinant, we have:

$$\left\langle \begin{matrix} mn \\ ab \end{matrix} \right| \hat{H} + \left[\hat{H},\hat{T}\right] + \frac{1}{2!}\left[\left[\hat{H},\hat{T}\right],\hat{T}\right] + \frac{1}{3!}\left[\left[\left[\hat{H},\hat{T}\right],\hat{T}\right],\hat{T}\right] + \frac{1}{4!}\left[\left[\left[\left[\hat{H},\hat{T}\right],\hat{T}\right],\hat{T}\right],\hat{T}\right]\Phi_0\right\rangle = 0 \quad (68)$$

There is one such equation for every excited determinant generated by the cluster operator. Now we must find the solutions: the cluster amplitudes in the cluster operator $\hat{T}$ that satisfy the set of all of these equations.

Without going into too much detail,[14,17] for CCD we can create an expression relating the energies of the orbitals involved, integrals between all of the orbitals, and the doubles amplitudes:

$$\begin{aligned}
&(\varepsilon_m + \varepsilon_n - \varepsilon_a - \varepsilon_b)t_{ab}^{mn} \\
&= \langle mn|ab\rangle - \sum_{p>q}\langle mn|pq\rangle t_{ab}^{pq} - \sum_{\gamma>\delta}\langle cd|ab\rangle t_{cd}^{mn} \\
&+ \sum_{c,p}\left[\langle cn|bp\rangle t_{ac}^{mp} - \langle cm|bp\rangle t_{ac}^{np} - \langle cn|ap\rangle t_{bc}^{mp} + \langle cm|ap\rangle t_{bc}^{np}\right] \\
&+ \sum_{c>d,p>q}\langle cd|pq\rangle\left[t_{ab}^{pq}t_{cd}^{mn} - 2(t_{ab}^{mp}t_{cd}^{nq} + t_{ab}^{nq}t_{cd}^{mp}) - 2(t_{ac}^{mn}t_{bd}^{pq} + t_{ac}^{pq}t_{bd}^{mn}) + 4(t_{ac}^{mp}t_{bd}^{nq} + t_{ac}^{nq}t_{bd}^{mp})\right]
\end{aligned} \quad (69)$$

Similar results exist for the singles, triples *etc*. These expressions can then be solved iteratively until self-consistency is achieved, bootstrapping the right hand side of the equation with a set of guessed amplitudes (zeros will suffice[14]). Then we can use the expression and the SCF orbital energies to determine the amplitudes for each excitation, and then plug those amplitudes into the right hand side of the equations to repeat the process.

*2.3.2.3. **Perturbation Theory.***

Perturbation theory is a ubiquitous method of approximation in which the exact solution to a problem is expressed as the known solution to a simpler problem, plus a correction to reach the solution to the true problem. The corrections are expanded in a series, which can be truncated to a desired level of accuracy. In this instance, we take a problematic Schrödinger equation:

$$\hat{H}\Psi = E\Psi \quad (70)$$

Where $\hat{H}$ is the many-electron Hamiltonian of the system (nonrelativistic and in the Born-Oppenheimer approximation for our purposes) and E and Ψ are the desired

solutions. We can re-express it in terms of a simpler Hamiltonian $\hat{H}_0$, and a correction $\hat{H}'$. The simpler *unperturbed Hamiltonian* $\hat{H}_0$ is the sum of the Fock operators from the Hartree-Fock procedure.:

$$(\hat{H}_0 + \lambda\hat{H}')\Psi = E\Psi$$
$$\hat{H}_0 = \sum_i^{n_{elec}} \hat{h}_i + \sum_i^{n_{elec}} \sum_j^{n_{elec}} \langle \hat{g}_{ij} \rangle \tag{71}$$

This is a mean field Hamiltonian – it assumes that the electrons move in a shared mean field of *all* of the electrons, and otherwise neglect each other's presence. This simpler problem is already solved, and being Hermitean has provided a *complete* set of wavefunctions Φ_n.[15,20]

$$\hat{H}_0\Phi_n = E_n\Phi_n \tag{72}$$

Φ_0 is the *unperturbed Hartree-Fock wavefunction*, which acts as a reference in this method (we are looking for the ground state wavefunction). E_0 is the sum of the occupied Hartree-Fock orbital energies. The other eigenfunctions are excited configurations obtained by replacing the occupied lowest-energy Hartree-Fock orbitals with virtual orbitals, and the energies of these configurations are also simply the sum of the constituent orbital energies.

The difference between the noninteracting Hamiltonian and the true Hamiltonian lies in the electron-electron interaction. By summing over every one-electron Fock operator, each of which includes the interaction between that electron and the mean field, the electron-electron interaction is counted twice.[15] Therefore the correction to the Hamiltonian is:

$$\hat{H} = \sum_i^{n_{elec}} \hat{h}_i + \sum_i^{n_{elec}} \sum_{j>i}^{n_{elec}} \hat{g}_{ij}$$
$$\hat{H} = \hat{H}_0 + \hat{H}'$$
$$\hat{H}' = \hat{H} - \hat{H}_0$$
$$\hat{H}' = \sum_i^{n_{elec}} \hat{h}_i + \sum_i^{n_{elec}} \sum_{j>i}^{n_{elec}} \hat{g}_{ij} - \sum_i^{n_{elec}} \hat{h}_i - \sum_i^{n_{elec}} \sum_j^{n_{elec}} \langle \hat{g}_{ij} \rangle \tag{73}$$
$$\hat{H}' = \sum_i^{n_{elec}} \sum_{j>i}^{n_{elec}} \hat{g}_{ij} - \sum_i^{n_{elec}} \sum_j^{n_{elec}} \langle \hat{g}_{ij} \rangle$$

$$\hat{H}' = V_{ee} - 2\langle V_{ee} \rangle$$

We introduce a parameter λ, where $0 \le \lambda \le 1$, which "turns on" the perturbation. This is a computational trick which allows us to express the problem as a Taylor series and gather terms in powers of λ :

$$(\hat{H}_0 + \lambda \hat{H}')\Psi = E\Psi$$

$$E = \lambda^0 W_0 + \lambda^1 W_1 + \lambda^2 W_2 + \ldots \tag{74}$$

$$\Psi = \lambda^0 \Psi_0 + \lambda^1 \Psi_1 + \lambda^2 \Psi_2 + \ldots$$

Where each term W_n and Ψ_n is the *n*th order correction to the energy or the wavefunction. Our hope is that the series converges rapidly towards the correct answer and can therefore be truncated to a small number of terms.[15,21]

$$(\hat{H}_0 + \lambda \hat{H}')(\lambda^0 \Psi_0 + \lambda^1 \Psi_1 + \lambda^2 \Psi_2 + \ldots) = (\lambda^0 W_0 + \lambda^1 W_1 + \lambda^2 W_2 + ..)(\lambda^0 \Psi_0 + \lambda^1 \Psi_1 + \lambda^2 \Psi_2 + \ldots) \tag{75}$$

If we multiply out and collect terms in λ^n:

$$\hat{H}_0 \Psi_0 = W_0 \Psi_0$$

$$(i.e.\ \ \hat{H}_0 \Phi_0 = E_0 \Phi_0)$$

$$\hat{H}_0 \Psi_1 + \hat{H}' \Psi_0 = W_0 \Psi_1 + W_1 \Psi_0$$

$$\hat{H}_0 \Psi_2 + \hat{H}' \Psi_1 = W_0 \Psi_2 + W_1 \Psi_1 + W_2 \Psi_0 \tag{76}$$

$$\hat{H}_0 \Psi_n + \hat{H}' \Psi_{n-1} = \sum_{i=0}^{n} W_i \Psi_{n-i}$$

etc.

This gives us *Rayleigh-Schrödinger* perturbation theory. Now we just need a basis in which to express the corrections Ψ_n to the wavefunction. Fortunately we already have one: the aforementioned complete set of eigenfunctions of the Schrödinger equation with the unperturbed Hamiltonian, the Slater determinants of the Hartree-Fock orbitals. We can express the wavefunction corrections as a linear combination of these determinants, using coefficients which are analogous to the CI coefficients and CC amplitudes. This model is known as *Møller-Plesset* perturbation theory.[15,22]

The solution to the zeroth-order of the perturbation equations is the unperturbed (Hartree-Fock) wavefunction and the sum of the orbital energies, which are already known. The first-order correction to the energy can then be calculated. The first order

correction exactly cancels the double-counting of electron-electron repulsion and provides the Hartree-Fock energy.

$$W_1 = -\langle V_{ee} \rangle \tag{77}$$

Now we can continue adding corrections of higher order to obtain the electron correlation energy.[15,21] In addition to the first-order correction to the energy, we can compute the first-order correction to the wavefunction. Then we can compute the second order correction to each, and so on up the hierarchy.(In fact we can compute the energy corrections up to (2*n*+1)th order given the *n*th order corrected wavefunction.)[15]

Note that we can obtain many of the coefficients for the MP corrections using amplitudes obtained on the first iteration of the CC cycle (where the self-consistency procedure starts with zero amplitudes). The MP2 amplitudes and energy (plus MP3, and some components of MP4) are "free" when we perform a CCSD calculation.[18] The second-order correction to the energy is (where c_i are the amplitudes):

$$W_2 = \sum_i c_i \langle \Phi_0 | H' | \Phi_i \rangle \tag{78}$$

We can express this energy without reference to the amplitudes at all:

$$W_2 = \sum_{i \neq 0} \frac{\langle \Phi_0 | H' | \Phi_i \rangle \langle \Phi_i | H' | \Phi_0 \rangle}{(E_0 - E_i)} \tag{79}$$

Single excitations do not couple to Φ_0 through the Hamiltonian by the Brillouin theorem, and higher excitations do not couple through two-electron operators at all, so this can be restricted to a sum over double excitations. Furthermore, given that the energies E_n are simply sums of MO energies, we can express the denominator in terms of the energies of the orbitals the electrons are excited from and to, which is information available at the Hartree-Fock level. Finally, the integrals between the excited determinants can be expressed as two-electron integrals between the orbitals involved in the excitation, which can be computed cheaply.[15,22]

$$E(MP2) = \sum_{i<j}^{occ} \sum_{a<b}^{vir} \frac{\left(\langle \phi_i \phi_j | \phi_a \phi_b \rangle - \langle \phi_i \phi_j | \phi_b \phi_a \rangle \right)^2}{\varepsilon_i + \varepsilon_j - \varepsilon_a - \varepsilon_b} \tag{80}$$

Note that the earlier assumption that our perturbation theory model would converge toward the correct answer at high order has been found to be inaccurate by numerical investigation. Although MP*n* becomes increasingly accurate at higher order for small values of *n* (less than 10), it soon displays oscillatory behaviour and ultimately

diverges.[22] Therefore it is common – as is the case in this work – to use MP2 as an early approximation, and switch to coupled cluster methods if higher accuracy is required.

2.3.3. Where Do We Truncate Expansions in Correlation Expressions?

We can use perturbation theory, or the CI expansion, to evaluate the importance of each set of excitations to the electron correlation, with excitations appearing in the lower-order corrections in the MP*n* energy (for $n>1$) being the most important. Clearly, the double excitations are of the highest importance, as they are the only contribution at MP2 (and even at MP3)[18] and they typically have large CI coefficients.[23] The double excitation describes the correlation of two electrons, which intuitively – and in practice – makes the largest single contribution to the correlation energy. Going to higher levels, *triple* excitations make an appearance as the next most important contribution. In all of these methods, single excitations enter only weakly, because they do not couple to the unperturbed configuration through the Hamiltonian, reflected in the fact that they do not appear in the MP*n* expansion below MP4.[18]

If we consider the CC method, then by the above rationale excitations involving $\hat{T}_2$ will tend to be important, such as the disconnected quadruples $\hat{T}_2^2$, while excitations involving $\hat{T}_1$ will tend to be small, such as the disconnected triples $\hat{T}_1\hat{T}_2$. As mentioned previously, the triple excitations become important, and by process of elimination the *connected* triples $\hat{T}_3$ must be the next most important contribution. It is omitted from CCSD. However, the CCSDT method is computationally very expensive, and is a rather wasteful way of getting at the connected triples (consider the many small terms involving $\hat{T}_1$ that will be generated). For this reason, the triples contribution to the CC energy is commonly calculated using perturbation theory, the so-called CCSD(T) method.[18,24]

2.4. The Form of the Basis Set

2.4.1. Choice of Functions

The Roothaan-Hall equations expand the molecular orbital in a basis of *basis functions*, however we have not yet addressed the form of these functions.[5,25] From intuitive ideas about atomic orbital overlap and LCAO theory we may conclude that a set of *atomic orbitals* might provide an efficient approximation for constructing molecular orbitals. Taking dilithium as an example, the basis set could consist of two identical groups of functions, one centred on each lithium atom. Each group would consist of two atomic orbitals, the *1s* and *2s* hydrogenic orbitals of the lithium atom, which are radial Slater-type functions:

$$\chi_s(r,\theta,\varphi) = NY_{l,m}(\theta,\varphi)r^{n-1}e^{-\zeta r} \tag{81}$$

(*Y* provides the spherical harmonics, while *N* is a normalisation constant; *n* and *l* are the principal and angular momentum quantum numbers; *r* is the nucleus-electron distance.) The Schrödinger equation, in considering the nucleus as a point charge, creates "cusp" in value of the wavefunction near the nucleus (nonzero gradient), and the wavefunction decays with e^{-r}. These properties are shared by Slater functions.[25] While these functions reproduce the solutions of the Schrödinger equation well, the two-electron integrals over these functions which are used in computational methods become computationally inconvenient.

Alternatively, we may choose to use Gaussian functions:

$$\chi_g(r,\theta,\varphi) = NY_{l,m}(\theta,\varphi)r^{2n-2-l}e^{-\zeta r^2} \tag{82}$$

These give integrals which are much quicker to compute. Gaussians do not have the cusp (the gradient is zero at the nucleus) or the right long-range behaviour, meaning that single Gaussians are not good approximations of single Slater functions. However, the two-electron integrals are so computationally cheap when performed upon these functions that we can simply use a fixed linear combination of *n* Gaussian functions ("*n*G") to approximate each Slater function without a significant performance cost.[25]

This linear combination constitutes a *contracted* basis function. More generally, any set of *primitive* functions (Gaussians in this case) may be collapsed into one contracted basis function by taking a linear combination of the primitives. The linear combination

coefficients (*contraction coefficients*) are optimised in the process of constructing the basis set then fixed, and are not manipulated during the subsequent molecular calculation. The contracted basis function acts as though it was just a single function.[5]

2.4.2. Basis Set Size and Convergence

Returning to our Li_2 example, the use of a basis set consisting of just two *s*-type Slater functions, or two "*n*G" approximations of these Slater functions, is somewhat restrictive. We can only create molecular orbitals with σ symmetry, and not π or δ. Instead, we could include enough functions to provide the complete core and valence shells of the lithium atom, *i.e.* two different *s* functions, and three identical *p* functions with different m_l values. This is known as a *minimal* basis set:

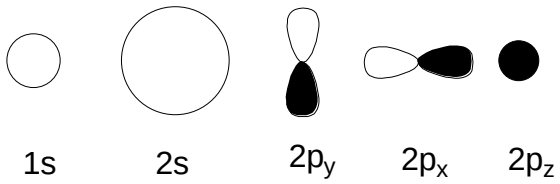

Figure 2.2: A minimal basis set for lithium

With these basis functions, we can now place nodes along the bond axis. We can now generate π orbitals:

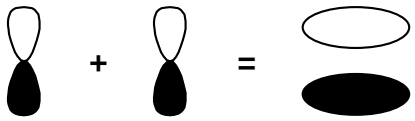

Figure 2.3: Constructing a π orbital

However there are still many limitations. We have little control over how compact or diffuse the molecular orbital is. While we can use a linear combination of the two *s* functions to approximate an *s* orbital of intermediate diffuseness, we cannot generate one which is more or less diffuse than either of the basis functions:

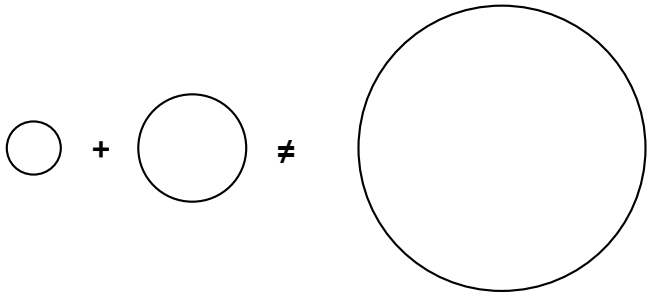

Figure 2.4: Limitations of basis function extent

A better basis set would provide some additional functions for flexibility. In the simplest case, we could add additional functions of the same symmetry but with different diffuseness, making the basis set *n*-tuply redundant (typically denoted as an "*n*-tuple zeta" basis set[5]). We can also add *polarisation* functions, of lower symmetry than the occupied atomic orbitals, to allow us to construct molecular orbitals of lower symmetry. As more basis functions are added, it becomes possible to approximate any arbitrarily chosen molecular orbital more closely.[5,25]

In this way the basis is said to progress toward *completeness*, where it would be able to exactly reproduce any arbitrary spatial function. Basis set completeness is an asymptote, and our ability to approach it is restricted by the availability of computational power and time. The time required for the Hartree-Fock method in the basis set approximation scales with N^3 or N^4, where N is the number of basis functions, and the time for correlated methods can scale with N^5 or higher. Therefore it is our best interest to use as few functions as possible. We most efficiently approach completeness when we add additional functions which fit the physics of the chemical system we are studying. Polarisation functions allow us to describe the polarisation of atomic orbitals, for example:

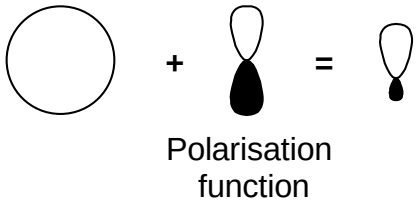

Figure 2.5: Polarisation functions

One of the most important families of basis sets is the Dunning-type *n*-tuple zeta correlation-consistent family, which is optimised to efficiently recover the correlation energy of a chemical system.[26] These basis sets drew primarily upon two previous

works. Almlöf and Taylor[27] proposed using a properly truncated set of atomic natural orbitals as basis functions. This was found to efficiently recover the correlation energy of the system.

Jankowski *et al* evaluated the effects of adding polarisation functions to *s* and *p* basis sets of fluorine, while performing high-level correlated calculations.[28] In their procedure, they added even-tempered sets of polarisation functions, where the exponents ζ of the functions go in a geometric progression:

$$\zeta_n = \alpha\beta^n \tag{83}$$

They then optimised the parameters of the even-tempered set as each additional function was added. They discovered that certain sets of functions recovered roughly equal amounts of correlation energy. For example, adding the first *d* function recovered around 130 milliHartrees (mH) of the correlation energy. Including a second *d* function recovered only 38mH. Adding the first *f* function recovered 40 mH of the correlation energy, which is similar to that recovered by the second *d* function. The third *d* function, second *f* function, and first *g* function all recover on the order of 10 mH. In this way a truncation scheme suggests itself: add groups of functions which recover similar amounts of the correlation energy.

Dunning adopted this idea, tested, and generalised it.[26] Starting with the oxygen atom, correlated calculations were performed to optimise even-tempered sets of polarisation functions. (The *1s* "core" orbitals were constrained to double occupancy in these calculations, with the effect that they were not able to correlate with the other, "valence" electrons.) As in Jankowski *et al*, it was found that the additional functions could be grouped according to their contributions to the correlation energy (specifically, as a function of their contribution to the total correlation energy that could be recovered using additional functions with that angular momentum). At each stage, one additional function of each existing angular momentum is added, plus one function of the next highest angular momentum. *2s1p* is superseded by *3s2p1d*, which is then replaced by *4s3p2d1f*. As all of the basis functions contribute roughly equally to the correlation at each stage, Dunning named these the *correlation consistent* basis sets. Dunning labelled these sets the "*N*-tuple zeta" sets ("double zeta", "triple zeta", *etc.*), where *N* is both the number of sets of Gaussians per valence orbital, and the maximum value of *l* in the set.

The orbitals occupied by the *s* and *p* electrons in the atomic ground state (the core orbitals, composed of core basis functions) have not been mentioned so far. The pre-Dunning studies used a contracted set of *s* and *p* functions for these orbitals. Dunning added *s* and *p* primitives as even-tempered sets of Gaussians, optimised through correlated calculations as before, with a fixed set of polarisation functions. He found that contractions of these primitives into pairs of a single *s* and a single *p* function were correlation-consistent with sets of polarisation functions. However he also discovered that contractions of Hartree-Fock orbitals could also be constructed which recovered similar amounts of correlation energy, and used these instead.

Dunning was able to construct similar basis sets for all of the first-row main-group elements in this paper. In later collaborations, Dunning and coworkers went on to develop sets for most of the periodic table.[29-31] Taking **c**orrelation-**c**onsistent, **p**olarised, **V**alence **N**-tuple **Z**eta, we have the notation:

cc-pVNZ

As noted earlier, the Dunning-type basis sets did not include correlation of the core electrons with the valence electrons (core-valence correlation), as these effects are often (but not always) minor. Later studies extended these basis sets by including additional "tight" functions which are optimised while allowing core-valence correlation. These are **C**ore-**V**alence basis sets:[31]

cc-pCVNZ

Calculations that include core-valence correlation may be less accurate than those that exclude it if these functions are omitted.[31]

Alternatively, we may wish to describe systems in which the electrons are much more diffuse than normal atomic orbitals. For example, Rydberg states and molecular anions often involve more diffuse orbitals. To describe these systems, we require functions with low exponents. Dunning and co-workers extended the basis set family by adding a single Gaussian function of each symmetry, and optimising its exponent to minimise the energy of the anion of the atom in question (at the SCF level for the core functions, and the CISD level for the polarisation functions).[32] Basis sets extended in such a fashion are "**aug**mented".

aug-cc-pVNZ

2.4.3. Limitations of Conventional Basis Sets

As the basis set is incomplete, the use of a basis set necessarily introduces an approximation. As noted above, we choose basis sets which fit the physics of the problem, in this case functions resembling atomic orbitals centred upon the atoms. Care must be taken to construct a basis set which is suited to the problem, and not a basis set which is suited to the answer we might like to obtain. For example, if we really wanted to demonstrate the electrons in water were mostly located on the hydrogens (which is obviously not true)), we could construct a basis set with no functions on oxygen at all.

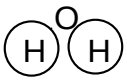

Figure 2.6: Schematic of water molecule with basis functions (circles) only on H.

Of course we are above begging the question in such a shameless way to obtain an unphysical result. Rather, we note when our basis set fails to properly describe the physics we are interested in, and extend it in an impartial manner to include that behaviour. An excellent example is in the description of dipole-bound anions. In these systems, electrons are contained in orbitals that are so diffuse that conventional basis sets simply do not have functions diffuse enough to describe them. The electron becomes unbound and the corresponding orbital makes use of the most diffuse basis functions available.

It is necessary to add diffuse functions to properly describe this excess electron. The tested and effective approach to this problem is to add an "even-tempered" set of basis functions.[33] These functions have exponents which undergo a geometric progression, from the most diffuse function in the standard Dunning basis out to a minimum exponent where the basis set is considered to be converged with respect to the properties of the neutral molecule's lowest unoccupied molecular orbital (LUMO). The properties in question are the energy of the LUMO, and the molecular orbital coefficients associated with the diffuse functions.

This can be better conveyed pictorially. Figure 2.7 shows the convergence of LUMO orbital energy of the neutral NH_3HCl with the addition of extra diffuse *s* and *p* functions (one of each added at each step, with the geometric progression ratio 2.5). Inset is an

overlay of the 0.9-electron isosurface of the LUMOs created with each set of extra functions. (Hartree-Fock/aug-cc-pvdz plus the extra functions, with a geometry optimised at MP2/aug-cc-pvdz plotted in VMD[34] with OpenCubeMan). [35] Figure 2.8 and Figure 2.9 plot MO coefficients against the negative of the natural logarithm of the exponent of the extra basis functions, for sets with 4, 5, 6, and 7 extra *s* and *p* diffuse functions. Smaller exponents correspond to Gaussian functions which decline at a slower rate – in other words, more diffuse wavefunctions. Therefore, an increase on the horizontal axis is an increase in orbital "diffuseness", on a logarithmic scale. Note that energy convergence (to five decimal places, or 0.57 mH) occurs before LCAO convergence.

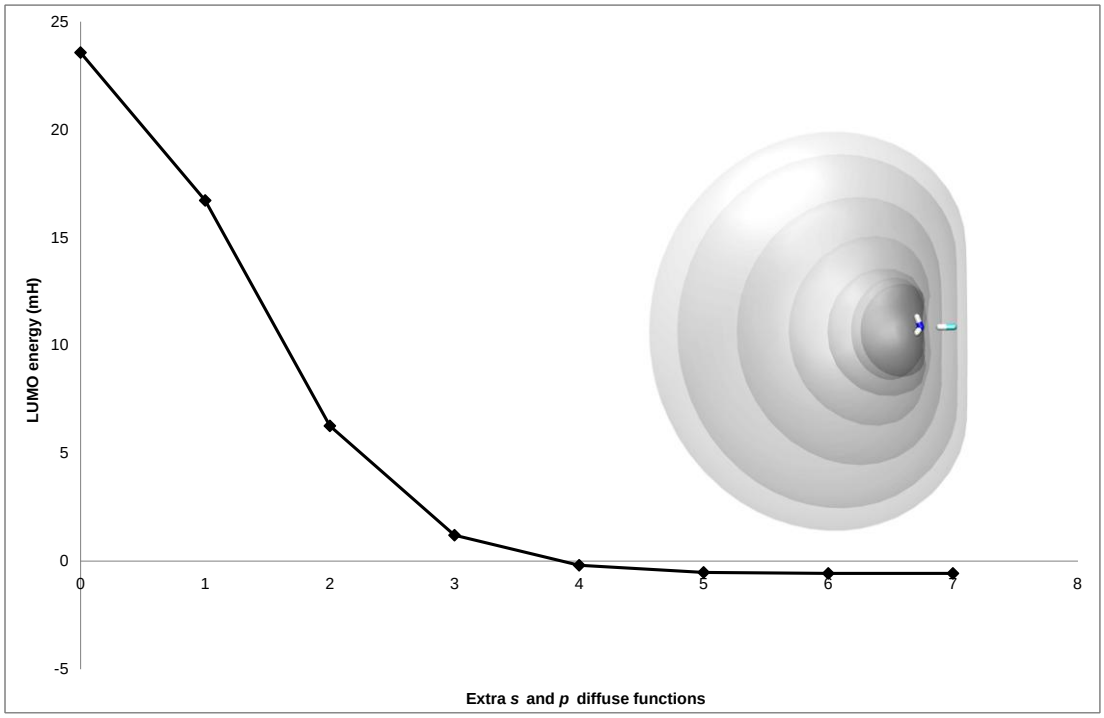

Figure 2.7: LUMO energy convergence with number of additional extra diffuse *s* and *p* functions for NH_3HCl neutral

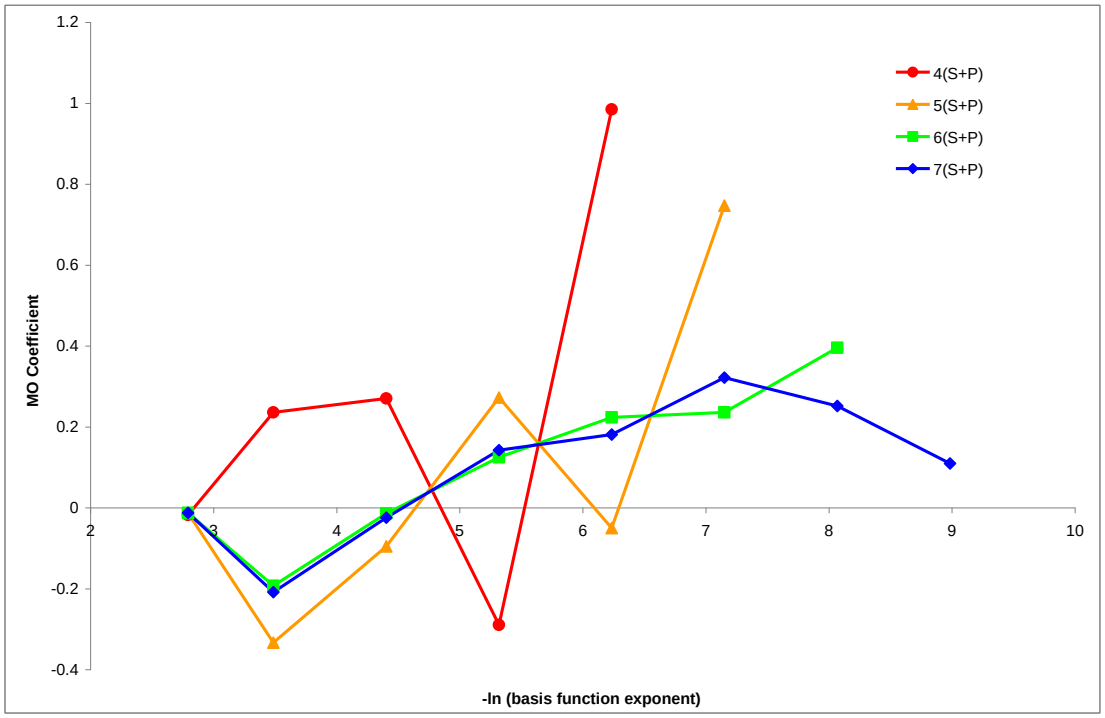

Figure 2.8: Variation of MO coefficients for additional diffuse *s* functions as additional functions are added to neutral NH_3HCl.

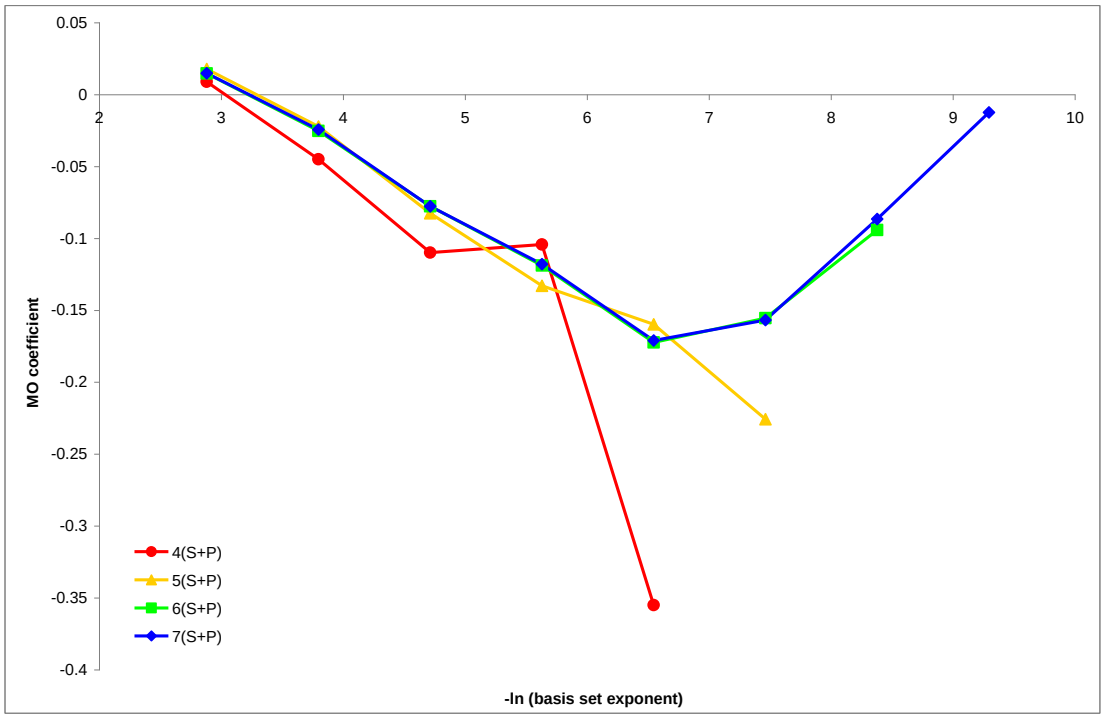

Figure 2.9: Variation of MO coefficients for additional diffuse *p* functions as additional functions are added to neutral NH_3HCl.

Once the LUMO properties have converged with respect to additional diffuse functions, the basis set is ready for use.

The lowest exponents for the diffuse functions (the exponents of the 7^{th} *s* and *p* functions in this case), can be used to estimate the lowest exponents required when studying the same system in a *different* basis set. Additional diffuse functions are added to the new basis set in the same way, but rather than starting from the standard basis set, we begin by adding an even-tempered set such that the lowest exponent is near the one found for the previous basis set. Then this set is tested to see if the LUMO properties are converged; if it is not, additional functions can then be added until convergence is achieved. If LCAO coefficients for the most diffuse functions are very small, these functions may be removed for efficiency.

Extending the basis set in this manner carries the assumption that the LUMO energy is a good measure of the anion electron binding energy. This approach, known as Koopmans' theorem (see 2.8.1), neglects orbital relaxation and therefore is an underestimate of the electron binding energy. This will only result in the addition of *more* diffuse functions than is actually needed. Therefore the method is conservative (the electron will bind at the Hartree-Fock level of theory if it is bound at the Koopmans' theorem level) but inefficient. The magnitude of the error is constrained, because the electronic relaxation caused by a weakly-bound electron is relatively small.[36]

2.5. Extrapolation to the Complete Basis Set Limit

The systematic growth of the Dunning type basis sets, and the consistent recovery of correlation energy, suggests an extrapolation scheme to a "basis set limit" when the cardinal number *N* in aug-cc-pVNZ is infinity. Helgaker *et al* noted that the Hartree-Fock energy and correlation energy would display different convergence with the increasing number of basis functions, as the former would be satisfied with a finite maximum *l* in the basis set (in principle, a finite number of basis functions could describe the single-determinant Hartree-Fock wavefunction) while correlated calculations benefit from arbitrarily large bases (to provide "headroom" for excitations).[37] This paper took Feller's suggestion of a three-point exponential extrapolation[38] (equation 84) and applied it to Hartree-Fock and correlated

calculations. They found that extrapolations to the limit with this model (which requires three points) were excellent for the Hartree-Fock theory.

$$E_N^{HF} = E_{cbs}^{HF} + Be^{(-AN)} \tag{84}$$

where E_{cbs}^{HF} is the Hartree-Fock energy at the complete basis set limit, which we wish to obtain, E_N^{HF} is the energy calculated with the N-tuple zeta basis set, and A and B are fitting parameters.

Halkier *et al* revisited the issue and evaluated exponential and power fits to the Hartree-Fock energy.[39] Their study found that exponential fits are superior, noting that the majority of the error in the extrapolated result arises due to the difference in the magnitude of the error between the highest and lowest extrapolation points.

Helgaker *et al* also attempted to determine the convergence of the *correlation* energy with respect to basis set size. Schwartz found that the correlation energy would converge with an inverse power in the highest *l* in the basis set, which he suggested to be between l_{max}^{-1} and l_{max}^{-4} and which at any rate is more slowly than Feller's scheme.[40] They performed extrapolations with a power form in N^{-3}, drawing on Schwartz's analysis of the correlation energy of the helium atom. The extrapolation assumes that the correlation energy with a given basis set has the form:

$$E_N^{corr} = E_{cbs}^{corr} + AN^{-3} \tag{85}$$

(A more general form, $E_N^{corr} = E_{cbs}^{corr} + A(N+B)^{(-3+C)}$, was also evaluated and found to be no better.)[37]

From these two schemes, expressions for the Hartree-Fock and correlation energy at the basis set limit have been proposed[41]:

$$\begin{aligned} E_{cbs}^{HF} &= \frac{E_N E_{N-2} - E_{N-1}^2}{E_{N-2} - 2E_{N-1} + E_N} \\ E_{cbs}^{corr} &= \frac{E_{N-1}(N-1)^3 - E_N N^3}{(N-1)^3 - N^3} \end{aligned} \tag{86}$$

2.6. Basis Set Superposition Error

The basis sets used in computational chemistry are never complete. Unlike the basis of orthogonal x, y, and z axes which could be used to exactly represent any vector in a 3-dimensional space, the basis sets of Gaussian atomic orbitals used in computational chemistry only allow us to create an approximation of the molecular orbitals. Although we try to ensure that the basis set lets us construct a wavefunction which properly captures the physics of the problem at hand, for example that the energy and geometry of a system are converged with respect to basis set size, this approximation has many subtle consequences that must be noted. The basis set superposition error is probably the most discussed and important issue.

Suppose we wish to describe the interaction energy between two monomers "A" and "B". The energy required to separate the two monomers is the energy for the following process:

$$AB \rightarrow A + B \tag{87}$$

We can compute the energies of A, B, and AB, (E_{AB}, E_A, and E_B) and then subtract the sum of the monomer energies from that of the dimer:

$$E_{AB} - E_A - E_B = E_{int} \tag{88}$$

This is known as a supermolecular calculation of the interaction energy. At first glance this is physically justifiable, but we must reconsider when operating in the basis set approximation. "A" has a set of basis functions a, and "B" has a set of basis functions b, and the dimer has both sets of functions $a \cup b$ (henceforth ab). Thus we have:

$$\begin{gathered} AB_{ab} \rightarrow A_a + B_b \\ E_{AB}^{ab} - E_A^a - E_B^b = E_{\text{int}} \end{gathered} \tag{89}$$

The energies of the monomers are computed with different, smaller basis sets than the energy of the dimer. In the dimer, monomer "A" can benefit from the basis functions b to lower its energy, and "B" can likewise benefit from the basis functions a. However in the monomer calculations, each monomer only has access to its own set of basis functions (Figure 2.10). As a consequence the dimer energy is artificially lowered relative to the monomers.

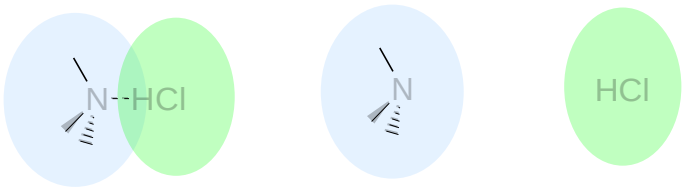

Figure 2.10: NH_3HCl complex (left) in dimer basis set; NH_3 (middle) and HCl (right) in monomer basis sets

This is known as the basis set superposition error – an additional stabilisation which results from the superposition of the basis sets of the monomers when they are assembled into the dimer.[5,25] The BSSE is dependent upon the intermolecular distance. Typically, the closer A and B are, the more one monomer can benefit from the basis set centred on the other. In the case of the supermolecular interaction energy of a typical chemical system, the BSSE is non-negligible for the equilibrium geometry of the dimer, and is zero when the monomers are infinitely separated. The BSSE varies continuously between these extremes, and distorts the energies, and gradients and higher derivatives of the energy with respect to geometric parameters.

2.6.1. The Counterpoise Correction to Basis Set Superposition Error

To correct for the BSSE in the supermolecular energy, we can apply what is known as the counterpoise correction. This method was developed by Boys and Bernardi,[42] and Jansen and Ros.[43] This quantifies the amount of the dimer energy which arises from BSSE, so that we may subtract it. The procedure is elegant. First, we compute the energy E_{AB}^{ab} as before.(Figure 2.11, left).

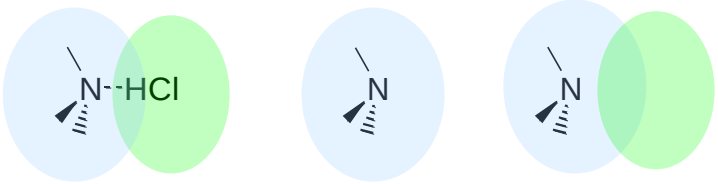

Figure 2.11: NH_3HCl in dimer basis set; NH_3 in dimer and monomer basis sets

Next, we compute the monomer energy for monomer A in its own basis set, E_A^a, as per the normal supermolecular interaction energy calculation (Figure 2.11, middle). At this stage, we take the dimer and remove the nuclei and electrons, *but not the basis functions*, from monomer B (Figure 2.11, right). The energy of this system is E_A^{ab}.

The basis functions b are still present at the original atomic coordinates, and still contribute to the wavefunction's variational flexibility. However the monomer B is missing. These are known as "ghost orbitals". The difference between E_A^a and E_A^{ab} is equal to the contribution to the basis set superposition error by monomer A using the basis functions b.

$$E_A^a - E_A^{ab} = BSSE_A \tag{90}$$

The same procedure is followed for monomer B. First E_B^b is calculated, and then E_B^{ab}.

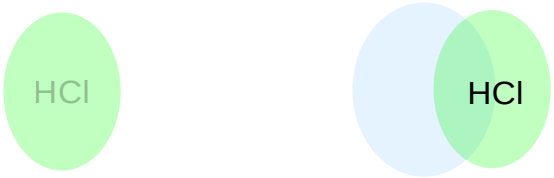

Figure 2.12: HCl in monomer (left) and dimer (right) basis sets

$$E_B^b - E_B^{ab} = BSSE_B \tag{91}$$

There total BSSE is now equal to the sum of these quantities:

$$BSSE_{AB} = BSSE_A + BSSE_B \tag{92}$$

We can add the BSSE to the energy of the dimer (or alternatively, subtract it from the interaction energy) to obtain the counterpoise-corrected energy. Using this energy, we can compute the interaction energy without BSSE:

$$\begin{aligned} E_{AB}^{ab} + BSSE_{AB} &= E_{AB}^{cpcorr} \\ E_{AB}^{cpcorr} - E_A^a - E_B^b &= E_{\text{int}}^{cpcorr} \end{aligned} \tag{93}$$

From this, it follows that there is a *counterpoise-corrected potential energy surface*, upon which chemical systems move and experience gradients and curvatures just as on the uncorrected surface as described in Equation 94 below. (Note that these are all partial derivatives, with *y* and *z* then the *z* coordinates respectively kept constant; the notation is omitted for clarity.)[44]

$$\begin{aligned} \frac{dE_{AB}^{cpcorr}}{dx} &= \frac{dE_{AB}^{ab}}{dx} + \left(\frac{dE_A^a}{dx} - \frac{dE_A^{ab}}{dx}\right) + \left(\frac{dE_B^b}{dx} - \frac{dE_B^{ab}}{dx}\right) \\ \frac{d^2E_{AB}^{cpcorr}}{dxdy} &= \frac{d^2E_{AB}^{ab}}{dxdy} + \left(\frac{d^2E_A^a}{dxdy} - \frac{d^2E_A^{ab}}{dxdy}\right) + \left(\frac{d^2E_B^b}{dxdy} - \frac{d^2E_B^{ab}}{dxdy}\right) \end{aligned} \tag{94}$$

2.6.2. Correcting BSSE for Reactive Monomers

Suppose we wish to describe a reaction profile for two monomers transferring a proton:

$$A^-H^+ + B^- \rightarrow A^- + H^+B^- \quad (95)$$

Furthermore, suppose we want to describe the strength of the interaction between the two monomers at any point across the reaction profile.

$$E_{\text{int}} = E_{AHB} - E_{monomer1} - E_{monomer2} \quad (96)$$

To compute the proper interaction energy, we should apply the counterpoise correction to E_{AHB}. However, we have two choices of monomers when defining the counterpoise correction. In one our monomers are the reactants AH and B^-, and the other with respect to the products A^- and HB. Which counterpoise correction should we choose?

We could simply impose the same correction across the reaction profile. However this would be unphysical in the region of the reactants or the products (depending on which we impose). So, we could impose the reactant counterpoise correction in the vicinity of the reactants, and the product counterpoise correction in the vicinity of the products. However we still have to choose a counterpoise correction for the intermediate region. Which is appropriate? And how do we handle the cross over?

It is possible and often necessary to redefine the counterpoise correction to consider more than two fragments. Turi and Dannenberg[45] treated a straight chain of *n* HF monomers by computing the CP correction between the *n*th monomer and the existing aggregate of (*n*-1) monomers. They observed that if an HF monomer is added to the molecule, it can be added to either end. While the counterpoise-uncorrected energy is identical for each process, the counterpoise corrections for each end differ (an inevitable consequence of the different basis functions involved), even though the same reactants and products are involved. This inconsistency arises because the Boys-Bernardi scheme does not consider the BSSE *within* the aggregate.

They proposed a scheme where the BSSE of an aggregate of *n* monomers is the sum of the BSSE of each monomer, and the BSSE of each monomer is the difference in energy between the monomer in its own basis set and its energy in the complete aggregate basis set.

$$E_{ABC}^{cpcorr} = E_{ABC} + BSSE_A + BSSE_B + BSSE_C$$
$$BSSE_A = E_A^a - E_A^{abc} \qquad (97)$$
$$etc.$$

In this model, the counterpoise correction to the energy for adding an additional monomer is equal to the difference in BSSE between a chain of *n* monomers and the BSSE of the resultant chain of *n*+1 monomers. This disregards the choice of where the HF molecule is added to the chain, returning consistency.

Valiron and Mayer highlighted some conceptual and practical limitations of the scheme, and improved upon it.[46] Refining work by White and Davidson,[47] they proposed that it is necessary to perform a counterpoise correction for each interaction between the monomers, and not simply the interaction between one monomer and the rest of the aggregate (although this is dominant). For example, in a three-body aggregate ABC, the counterpoise correction for monomer A must correct the A-BC interaction energy (as in Turi and Dannenberg), but also the A-B interaction energy, and the A-C interaction energy, in order for the energies to be consistent irrespective of the manner in which the complex is disconnected to its monomers. That is, the BSSE upon A consists of:

$$BSSE_A = BSSE_{A-BC} + BSSE_{A-B} + BSSE_{A-C}$$
$$BSSE_{A-BC} = E_A^a - E_A^{abc}$$
$$BSSE_{A-B} = E_A^a - E_A^{ab} \qquad (98)$$
$$BSSE_{A-C} = E_A^a - E_A^{ac}$$

(This quickly results in a very large number of terms. For the three-body counterpoise correction, 19 single-point energies are needed; for a four-body counterpoise correction, 125 energies are needed.)

Lendvay and Mayer evaluated the usefulness of two- and three-body counterpoise corrections in describing reactive surfaces.[48] They note the inevitable inconsistency between the surface determined if one takes the two-body counterpoise correction scheme using the reactant monomers, and one determined for the reverse reaction with *its* reactant counterpoise correction. However, they also note that the three-body counterpoise correction is not particularly physically sensible around the reactants or products, and consequently the energies in these regions are not accurate. Furthermore,

although the three-body counterpoise correction may be sensible with reference to a particular reaction pathway, it is arbitrary when we consider the space of other reactions available to the monomers. They make the case that ultimately, a compromise is necessary: either the surface must be discontinuous, or the conceptual demands placed upon the counterpoise correction must be relaxed.

2.7. Potential Energy Surfaces

2.7.1. Reducing the Dimensionality of Potential Energy Surfaces

The Born-Oppenheimer approximation imposes the idea of a potential energy surface within which the nuclei move, with each possible arrangement of nuclei having a particular potential energy associated with it. In the traditional chemist's view of the molecule, this corresponds to the energy involved in stretching, bending, making and breaking bonds. For a nonlinear system of N atoms, there are $3N$-6 degrees of freedom in the relative nuclear positions, and therefore the potential energy surface is $3N$-6-dimensional. However for high-symmetry systems, it is possible to reduce the dimensionality, and if we then express the positions in internal coordinates, we can construct potential surfaces that correspond to chemically intuitive bond lengths and angles. By restricting our search to just those degrees of freedom that are meaningful to the problem at hand, we can collapse the $3N$-6-dimensional surface to a comprehensible 1-, or 2-dimensional surface that can be given a 2- or 3-dimensional representation.[49]

As an example, consider the NH_3HX system which is at the heart of this project. If we wanted to describe its potential energy surface in absolute detail, we would need $3N$-6 = 12 coordinates for nuclear position. However, the for hydrogen bonded structure with C_{3v} symmetry (Figure 2.13), we can use just three bond lengths and one bond angle to completely describe the molecule.

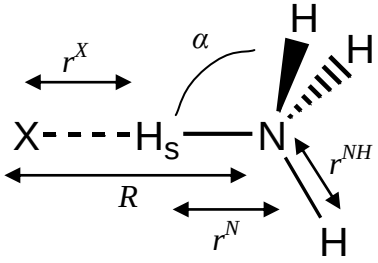

Figure 2.13: C_{3v} structure of a hydrogen bonded molecule

Note that the selection of these "internal coordinates" is not unique. We could equally use the N-H_s and H_s···X distances instead of N···X and H_s-X. These are still too many degrees of freedom to visualise. However given that we are interested in studying the H_s-X motion, and that the changes in the energy with respect to the NH_3 angle and N-H distance are small, we could neglect these coordinates and produce a two-dimensional potential energy surface such as Figure 2.14.

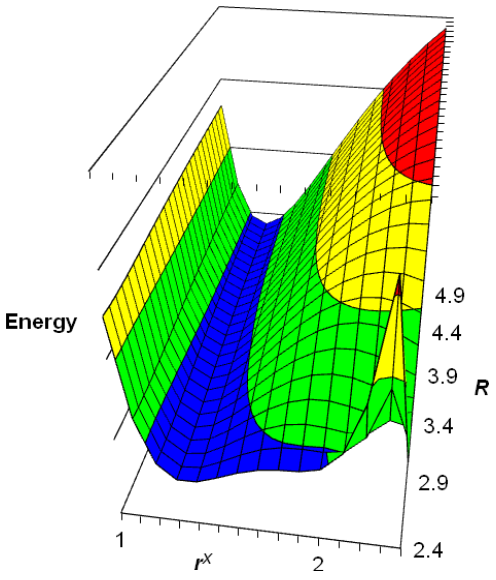

Figure 2.14: A two-dimensional potential energy surface for NH_3HCl neutral; Å and arbitrary energy scale

We could remove another dimension to obtain a one-dimensional surface describing only the proton motion (Figure 2.15), omitting the N-X distance entirely even though the energy changes meaningfully with respect to this coordinate.

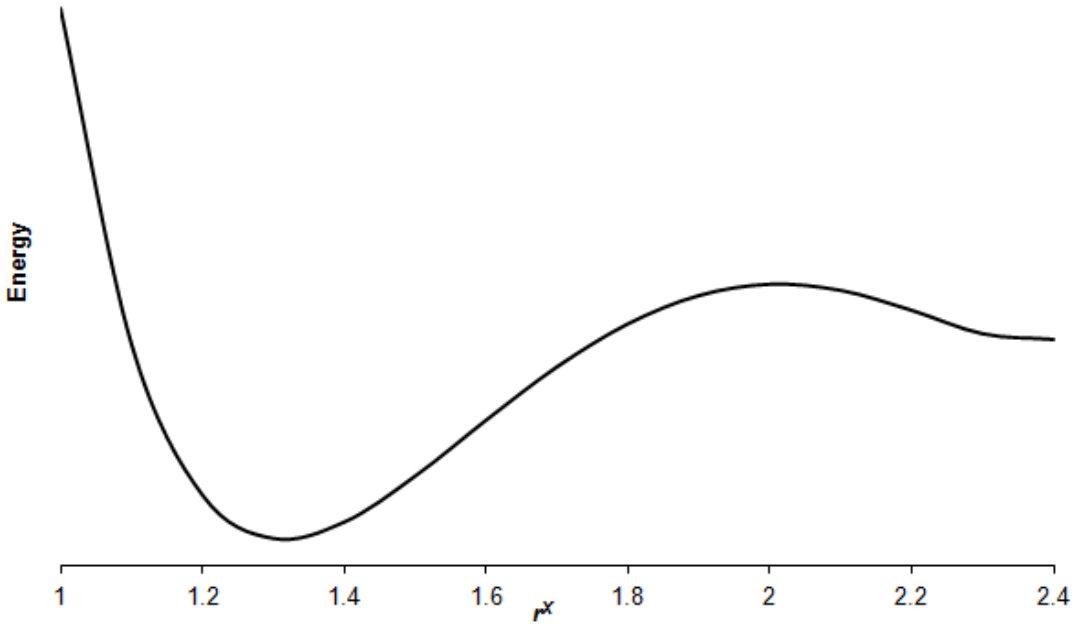

Figure 2.15: A one-dimensional potential energy surface (obtained for the same system as Figure 2.14) with fixed *R*=2.8. Units of Å and arbitrary energy scale

Dropping to lower dimensionality in this way adds complications. In order to neglect a coordinate, we must either fix that coordinate or relax it. In this case, fixing the coordinate corresponds to taking a straight slice through the 2D surface at some value of *R*, and the choice of value is important (e.g. the white line in Figure 2.16; the line would show a markedly different profile if it was shifted higher or lower). This can cause a misleading impression of the shape of the surface of interest (*e.g.* Famulari *et al* in Section 1.1.1, where the slice presented a nonexistent barrier). If we relax the coordinate, the resulting surface follows a curved path through the 2D potential energy surface and we lose some of our control of the specification of the molecule (red line in Figure 2.16).

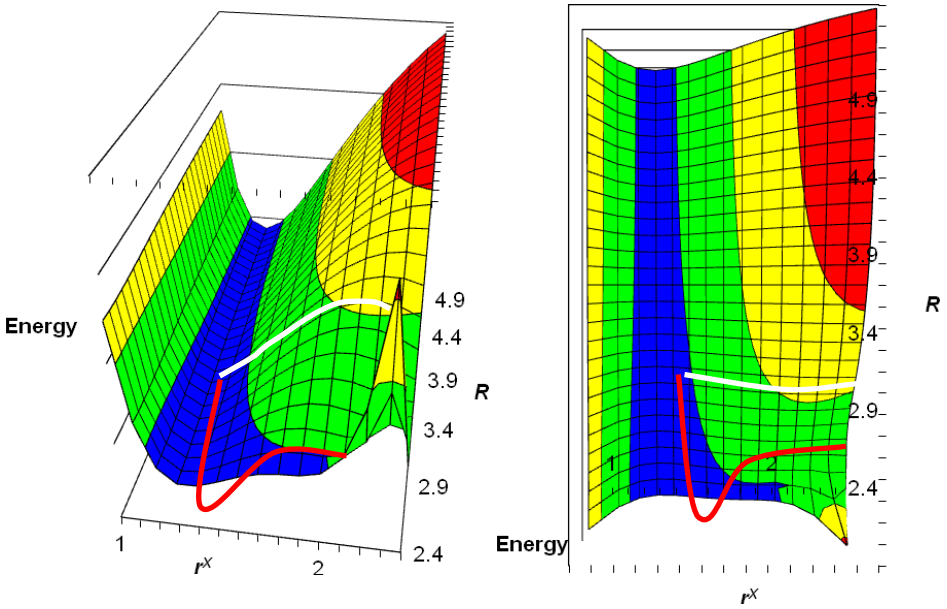

Figure 2.16: Example of the path a fixed (white) and a relaxed (red) 1D surface follows through the 2D surface for the same system as the previous figure. Å and arbitrary energy scale.

Supposing we vary r^X to study the motion of the proton and now relax all of the other coordinates. The resultant plot of energy against coordinate is a relaxed potential energy surface, shown by Figure 2.17 and the red line in Figure 2.16. Whereas the rigid plot (Figure 2.15) encounters the "hill" in the potential energy surface, the relaxed surface moves around it, following the lowest energy path, by changing *R*.

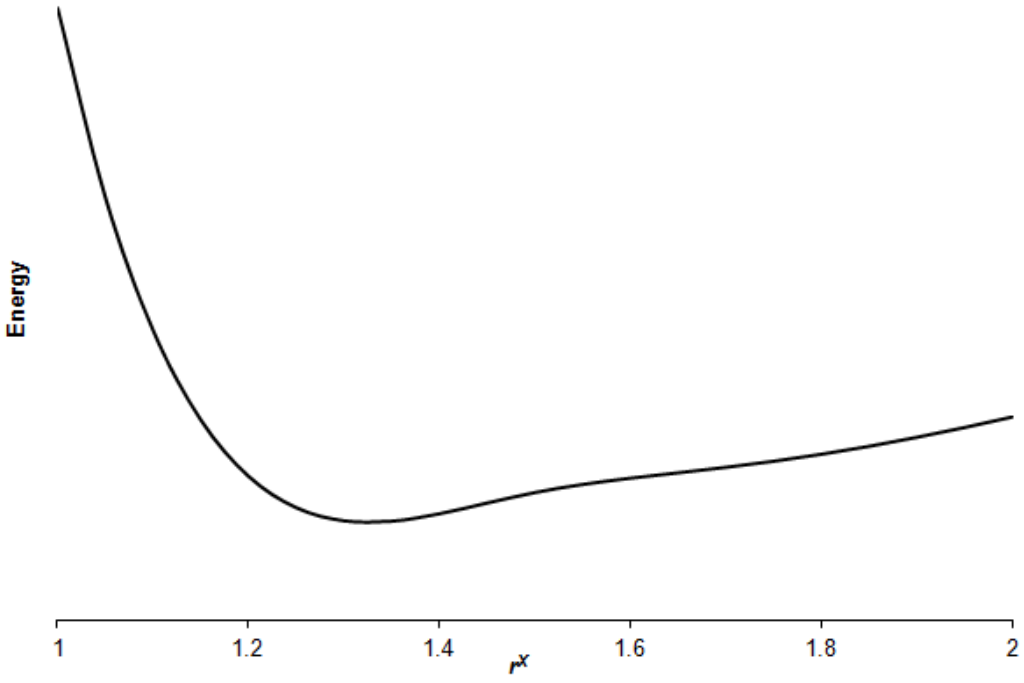

Figure 2.17: One-dimensional relaxed potential energy surface as in Figure 2.15. Å and arbitrary energy scale.

This is meaningful in the region near the halide X (small values of r^X). We can easily probe the repulsive wall around X. However the position of N is unrestricted with respect to X or H_s, and as H_s approaches the repulsive wall around N, the force that develops causes NH_3 to retreat. The change we apply to r^x does not affect r^N (which asymptotically approaches a fixed value) but instead increases R (Figure 2.18, Figure 2.19).

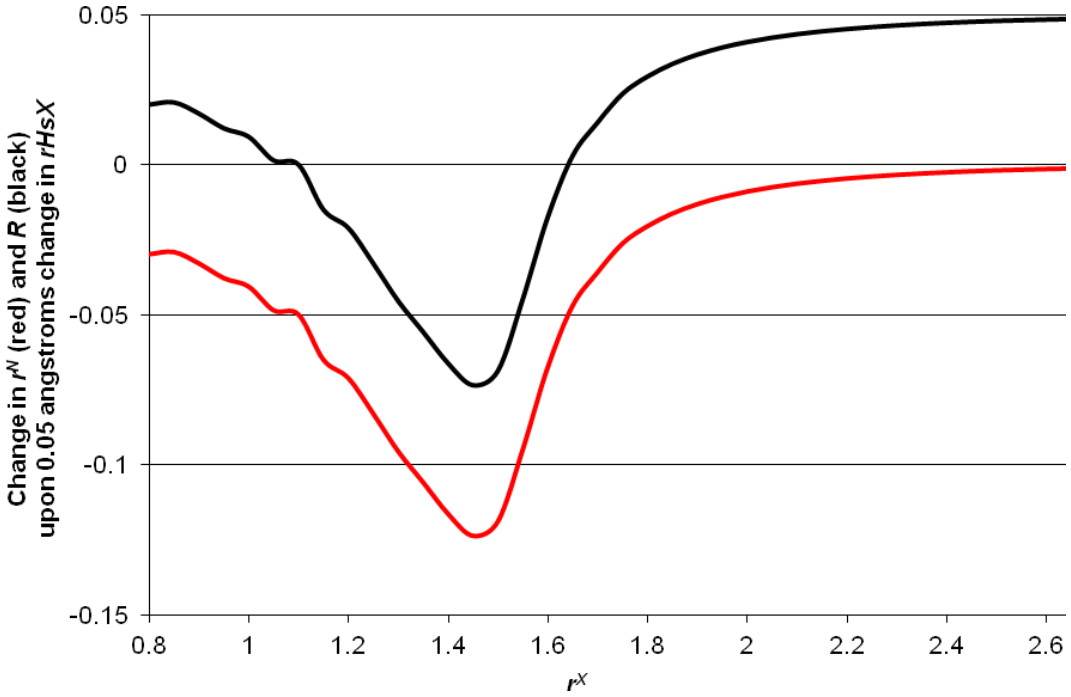

Figure 2.18: Effect of changing r^X upon r^N and R in NH_3HCl

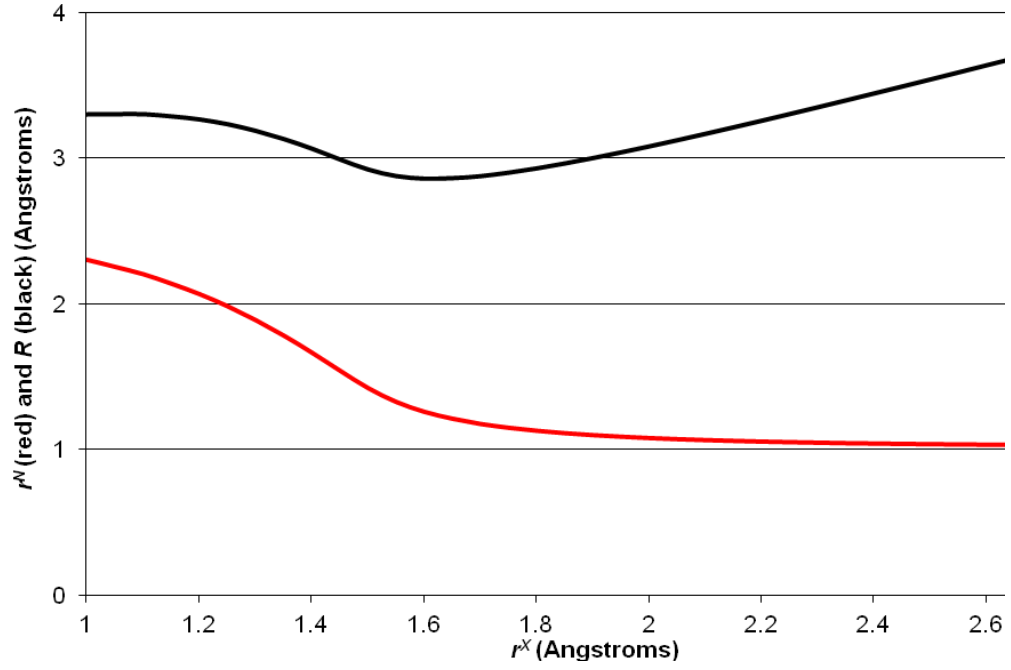

Figure 2.19: r^N and R versus r^X in NH_3HCl

An analogous situation arises if we describe the proton position with respect to N, and we try to probe the repulsive wall of X.

The solution in this study was to combine two complementary potential energy surfaces, one described with respect to N, one described with respect to X. At intermediate distances, the geometries obtained by the partial optimisation are the same regardless of the choice of coordinate, and so is the energy. Therefore the same surface is explored regardless of the choice of coordinate and the two surfaces coincide. When probing the repulsive wall of a heavy atom, the surface is chosen that specifies the proton position with respect to that atom, so that the heavy atom does not retreat.

For example, in Figure 2.20 the r^X distance is fixed at each step, and the other parameters are relaxed. This allows us to probe the repulsive wall near X. In Figure 2.21(a), r^N is fixed at each step, and all of the other parameters are relaxed, so we can probe the repulsive wall near N. We can also measure r^X at each step (Figure 2.21(b)) (which in the C_{3v} geometry is exactly the difference between R and r^X), and plot the energy at each point against that coordinate. We can then plot both surfaces on the same x axis (Figure 2.22).

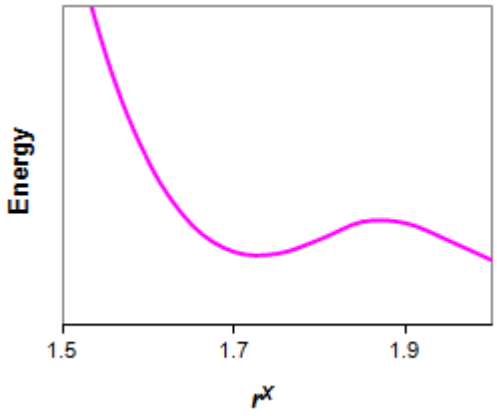

Figure 2.20: Relaxed potential energy surface of NH_3HAt with r^X as the coordinate (Å and arbitrary energy scale)

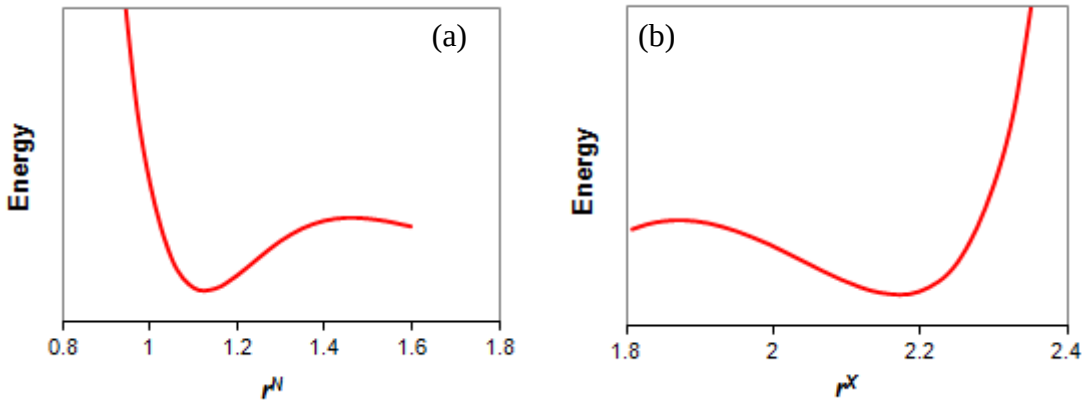

Figure 2.21: Relaxed potential energy surface of NH_3HAt with r^N as the coordinate, plotted against r^N (a) and against r^X (b) (Å and arbitrary energy scale)

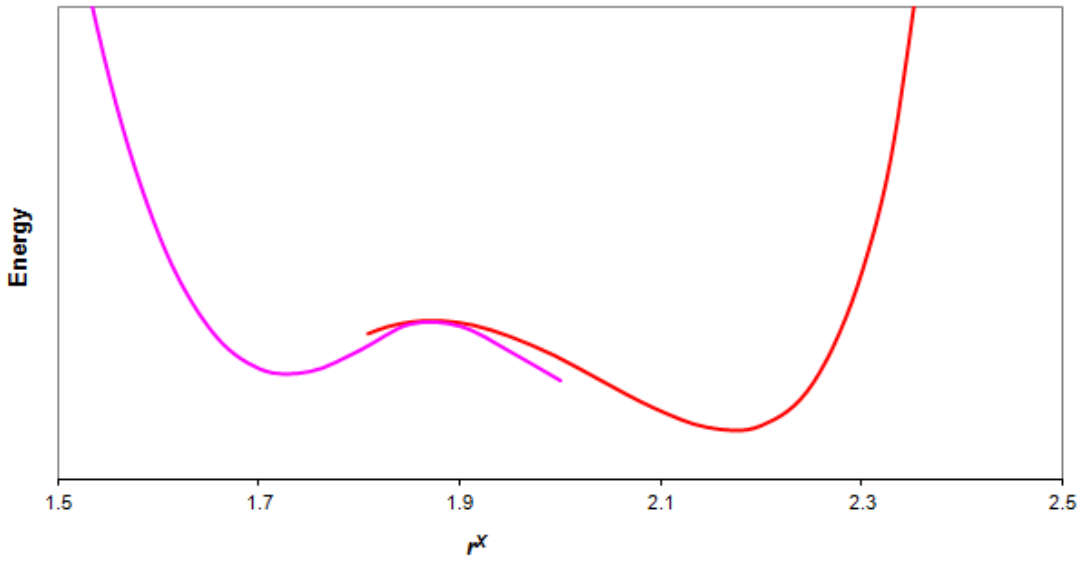

Figure 2.22: A combination of the two complementary 1D relaxed potential surfaces from Figure 2.20 and Figure 2.21(b) (i.e. NH_3HAt, Å and arbitrary energy scale)

As a final complication, note that the counterpoise correction applies an offset to the energy. If the same definition of counterpoise is used in correcting both of these surfaces, then the offsets will be equal and the two surfaces will still coincide as in Figure 2.22. However, if the choice of monomers is different, then a different correction will be applied and the resulting surfaces do not overlap. However, because the correction is simply an offset, the surfaces continue to be approximately parallel. In this study, proton transfer changed the identity of the monomers quite definitively and therefore the monomers *had* to be changed, giving a result like that shown in Figure 2.23.

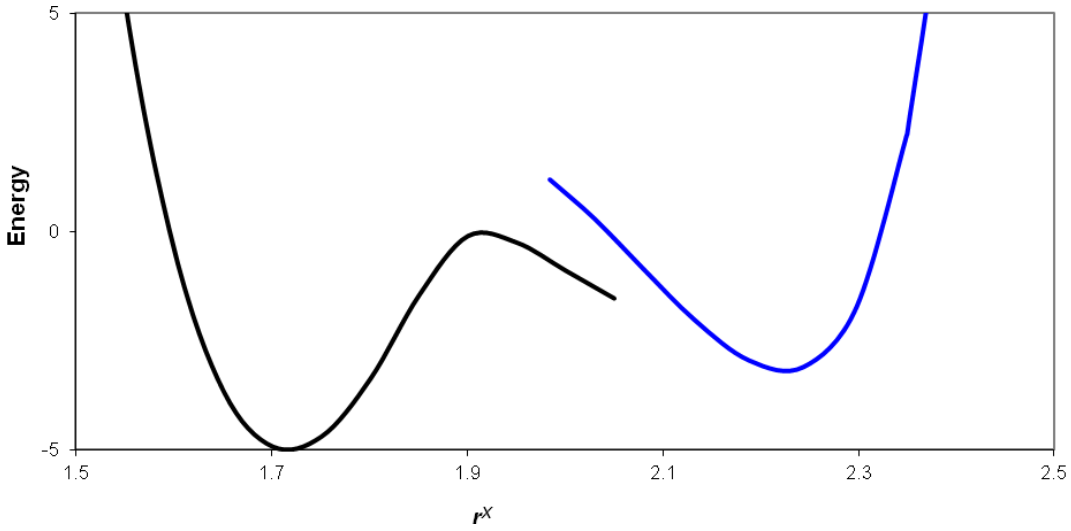

Figure 2.23: Complementary counterpoise-corrected 1D relaxed potential surfaces computed for the proton-transfer coordinate of NH_3HAt, at CCSD with a double-zeta basis set. (Å and mH)

2.7.2. The Significance of Stationary Points on the Surface

Geometries of key chemical importance lie at the stationary points upon the potential energy surface, the places where the derivatives of the energy with respect to the nuclear coordinates are zero. The negatives of these derivatives are more commonly and informatively known as forces. The stationary points are characterised by their second derivatives, also known as the curvatures (the matrix of these derivatives being the Hessian). These first and second derivatives are always available numerically, by varying nuclear coordinates by small amounts and recording the energy changes, but are also available analytically for certain methods.

For example, the gradients for a variational method such as Hartree-Fock can be computed directly from the derivatives of the one- and two-electron integrals, without reference to the basis set coefficients. When we try to introduce the coefficients into the expression for the gradient, the chain rule introduces terms which include first derivatives of the energy with respect to the coefficients, which for a variational method must be zero. Similarly, calculating the Hartree-Fock hessian involves only the first derivative of the coefficients with respect to nuclear coordinates, which can be obtained by an analytical method (coupled-perturbed Hartree-Fock).[50]

Where the second derivatives are all positive, the stationary point is a minimum. Minima correspond to chemically stable structures, inasmuch that any perturbation in the nuclear coordinates results in a restoring force, toward the original geometry. For the structure to be genuinely stable, its zero-point energy and any thermal energy must be smaller than the depth of the well around the minimum, otherwise the structure can "escape". Many such minima will exist for most potential surfaces; the most stable minimum is known as the global minimum, and the remainder are local minima.

When the second derivatives are all negative, the stationary point is a maximum, and the structure is unstable. Any perturbation will generate a nonzero force *away* from the stationary point.

Where *n* derivatives are negative and the remainder are positive, the stationary point is an *n*th order saddle point. First order saddle points are chemically important as they describe the lowest energy path between minima, which means that they are transition states when the two minima represent products, reactants, or intermediates, or barriers to intramolecular motion when the minima are multiple configurations or confirmations of the same molecule.

Finding the stationary points would be entirely trivial if we had an expression (derived or fitted) for the potential energy with respect to the nuclear coordinates that was easily soluble. Unfortunately this is usually not the case, and instead we must use the available energies, forces and curvatures to inform a search strategy. (This search will be much more efficient where analytical derivatives are available.) An algorithm can use this information to understand the shape of the surface and "plot a course" in a rational manner toward a stationary point.

Many such approaches are available for minima, from a simple steepest decent, which follows the gradient "downhill" (guaranteed to find a minimum, but inefficiently, and not necessary the global minimum)[49] through more nuanced methods involving the Hessian such as Newton-Raphson,[49] interpolated methods such as the GDIIS,[49] and elaborate artificial (and even human[51]) intelligence techniques used in protein folding.

Finding transition states (saddle points) is more challenging and typically involves investigating the path between a reactant and product structure (usually an interpolated series of coordinates between the two, e.g. linear and quadratic synchronous transit) and finding the maximum of energy on that path. This may then be further optimised by attempting to maximise the energy with respect to the parameters corresponding to the negative curvature(s), and minimise the energy in all other degrees of freedom.[49]

2.7.3. Defining Vibrational Frequencies with the PES

The second derivatives are useful for more than simply describing the curvature around stationary points. The matrix elements of the hessian are *force constants k* for the motions of the atoms in all available directions, *e.g.* k_{12} for the movement of an atom 1 along the *x* coordinate and atom 2 along the *y* coordinate. Therefore the hessian provides information on a harmonic approximation to the potential energy surface in which the nuclei move, from which the harmonic vibrational frequencies could be derived. The vibrational behaviour of the molecule, and its characteristic vibrational frequencies, can be obtained from this hessian by *normal mode analysis*.

First, the matrix *k* is re-expressed in a system of mass-weighted coordinates, such that for a basis vector *x* and atom *i*, we have a new basis vector:

$$q_i = m_i^{\frac{1}{2}} x_i \tag{99}$$

This mass-weighted Hessian is then diagonalised; the eigenvalues are the squares of the harmonic frequencies along a set of *normal modes*. The molecular motions related to these modes are described by the eigenvectors, which are linear combinations of the original mass-weighted coordinates.[50,52]

It is particularly informative to consider such a process when using internal coordinates, wherein the basis vectors are simply the bending and stretching motions of the molecule. In this case the eigenvectors are linear combinations of those basis vectors, which can be readily interpreted as the coupling of motions along different coordinates, *e.g.* a coupling between two stretching motions, a bend and a stretch, or two stretches in a single normal mode.[50,52]

The second derivatives encode useful information about the potential energy surface, such as the rigidity of the structure at a minimum, and the motion associated with crossing a transition state. The meaningfulness of the frequencies computed from these force constants depends upon the extent to which the harmonic approximation is valid, i.e. how closely the potential well approximates a parabola. If the potential surface is highly anharmonic, then the frequencies will not be properly described by this model. The double-well potentials in Figure 2.22 and Figure 2.23 are good examples. These surfaces are harmonic at low energies around the two minima, but increasingly anharmonic at higher energies.

2.8. Theoretical Aspects of Dipole-Bound Anions

Fermi and Teller in 1947 and Wightman in 1950 are jointly credited with the observation that in the Born-Oppenheimer approximation a point electric dipole of 1.625 Debyes or greater will bind an electron.[53,54] This implies that – neglecting rotation, or the Pauli exclusion principle – any molecule with a dipole moment greater than this value would bind an electron, even if it has no empty valence orbitals. However such a model results in an infinite number of bound states of infinite binding energy.[36] In practice, when molecular rotation and the repulsion between the molecule's valence orbitals and the excess electron are considered, a molecule with a dipole greater than about 2.4 Debyes will possess a dipole-bound state, usually only one such state, and able to bind only one electron.[55]

The most important descriptor of a weakly bound anion is, of course, the electron affinity of the species that binds the electron, and the strength with which the electron is bound. Given that the optimal geometry of the neutral will not be the optimal geometry of the anion, assuming the electron has any interaction with the molecule at all, we must define the electron binding energies in terms of the geometries of the anion and the neutral species.

The energy to go from the neutral species at its optimised geometry to the anion at that same geometry is the vertical attachment energy (VAC), "vertical" referring to the fixed horizontal position on the surface, with only a change in energy. Similarly, the energy to go from the anion at its optimised geometry to the neutral at that same geometry is

the vertical *detachment* energy (VDE). These energies inform us of the strength with which the electron is bound without accounting for geometric relaxation.

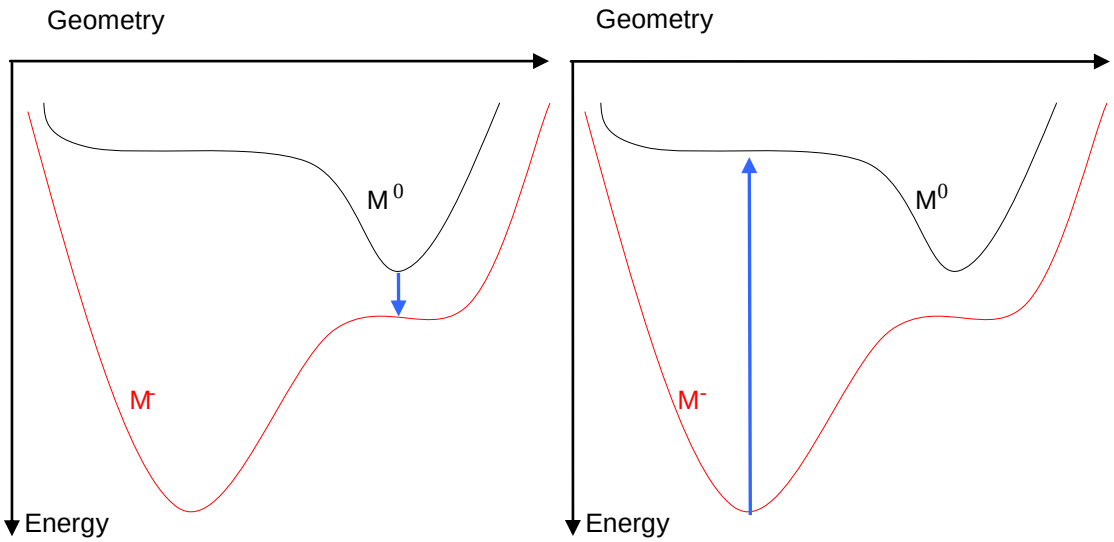

Figure 2.24: Vertical attachment (left) and detachment (right) energies (blue arrows)

Using the nomenclature $E_{M^C}(G)$ for the energy of the molecule "M" with charge "C" in geometry "G":

$$\begin{aligned} VAE &= E_{M^0}(Neutral) - E_{M^-}(Neutral) \\ VDE &= E_{M^0}(Anion) - E_{M^-}(Anion) \end{aligned} \tag{100}$$

Note the sign convention: the VAE and VDE are positive if the electron is bound, although the electron *attachment* process is exothermic and the electron *detachment* process is endothermic in that case.

The energy to go between the anion at its optimised geometry and the neutral at its optimised geometry – the electron affinity with geometric relaxation, in other words – is the adiabatic electron affinity EA_A.

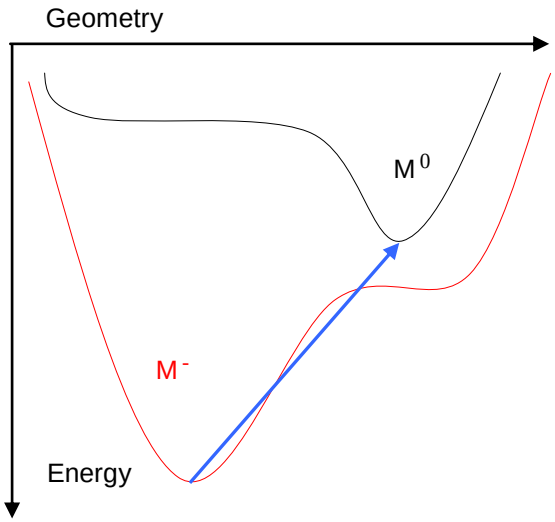

Figure 2.25: Adiabatic electron affinity (blue arrow)

$$EA_A = E_{M^0}(Neutral) - E_{M^-}(Anion) \tag{101}$$

These energies are calculated in a supermolecular method, *i.e.* the difference in energy between the anion and the neutral at a given geometry. The adiabatic electron affinity can be easily corrected for vibrational zero-point energy of the complex, as the ground vibrational states of the neutral and anion are well-defined around the minimum. However in the vertical energies, either the anion or neutral is away from its minimum energy structure, and therefore is vibrationally excited. In many of these NH_3HX systems, the neutral surfaces are highly anharmonic, and therefore the vibrational energy levels are difficult to compute.

2.8.1. Koopmans' Theorem for Electron Binding Energies

A convenient result of the Hartree-Fock method is that we have meaningful measures of the orbital energies. As a result it is possible to define the binding energy of an electron wholly in terms of the output of a single Hartree-Fock calculation. Once our Hartree-Fock orbitals are converged, the energy is:

$$E_{N_{elec}} = \sum_{i=1}^{N_{elec}} h_i + \sum_{i=1}^{N_{elec}} \sum_{j>i}^{N_{elec}} (J_{ij} - K_{ij}) + V_{nn} \tag{102}$$

Suppose we take the same orbitals, and remove an electron:

$$E_{N-1} = \sum_{i=1}^{N-1} h_i + \sum_{i=1}^{N-1} \sum_{j>i}^{N-1} (J_{ij} - K_{ij}) + V_{nn} \tag{103}$$

Taking the electron affinity as positive when the electron is bound, the difference between these two energies is:

$$E_{N-1} - E_N = -(h_k + \sum_{i=1}^{N_{elec}} (J_{ik} - K_{ik})) = -\varepsilon_k \quad (104)$$

This is Koopmans' theorem: the ionisation energy for removing a single electron from its Hartree-Fock orbital is equal to the Hartree-Fock orbital energy, and likewise the electron affinity for adding a single electron to an Hartree-Fock orbital is equal to the negative of the Hartree-Fock orbital energy.[4]

This measure of the electron binding energy, in which the same set of orbitals is used for the anion and the neutral, gives us a measure of electron affinity that neglects the relaxation of the orbitals. Therefore, if we predict the electron binding energy by taking the Hartree-Fock LUMO energy, we will obtain an underestimate.[5] It also has the limitation that while the occupied orbitals and their energies are well-defined, the *virtual* Hartree-Fock orbitals are not necessarily good descriptors of the unoccupied orbitals of the molecule.[4]

2.8.2. The Importance of Correlation in Electron Binding

Conveniently for the study of dipole-bound anions, the orbital relaxation caused by a weakly-bound electron is small, and therefore the difference between the KT and Hartree-Fock energies is also small.[36] However, the electron correlation effects are very important, and these must be included. The clearest *a priori* reason is that electron correlation in the anion and the neutral species will be different, as the two species have different numbers of electrons and different orbital occupancies, and therefore the correlation energy will not cancel when the two energies are subtracted.[36]

Furthermore, the very large polarizability of the diffuse dipole-bound electron means that the dispersion interaction between that electron and the neutral parent molecule is an important part of the description of the electron binding,[56] to the extent that dispersion can be the majority (sometimes the overwhelming majority[57-59]) of the binding energy.

2.9. Population Analysis: Defining the Charges of Atoms

The concept of an atom as a well-defined unit is a fundamental idea in chemistry. That the atom has particular physical properties, such as a certain amount of electron density, the ability to form bonds, *etc.* is implicit in the way chemical reactions are described, from simple structure drawings and Lewis diagrams to the theory of resonance. However, an atom within a molecule is not particularly well-defined in electronic structure, in particular having little concept of electron "ownership", and therefore evaluating the partial charges of atoms (to discuss polarity, charge transfer *etc.*) is nontrivial.

Suppose we have a homonuclear diatomic molecule H_2. It is intuitively sensible to assign the two electrons equally to each hydrogen atom (more accurately, to that nucleus) and obtain a structure of two neutrally charged atoms bonded together. For a heteronuclear diatomic molecule such as HF, we understand that fluorine has a higher electronegativity than hydrogen and will attract the electrons in the covalent bond and move them closer to F, *i.e.* it will polarise the bond. This results in an electric dipole across the molecule, as there is now more than nine electrons' worth of electron density "at F" and less than one electron's worth of density "at H". This forms an electric dipole. We express this understanding with the simple sketch:

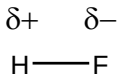

Figure 2.26: Schematic of a hydrogen fluoride molecule

Suppose we now wish to put values to these small partial charges δ+ and δ-. Using theoretical chemistry, we can determine the wavefunction of this system and thereby compute the density at any point in space. Now we have to integrate the electron density at F, add the nuclear charge, and we will obtain the partial charge at F. At this point our analysis comes to a halt as we realise that we do not know what "at F" means. Specifically, we do not have a way of assigning the electron density to a particular atom. The problem of partitioning the electron density between atoms is known as population analysis.

One of the easiest schemes of population analysis was devised by Mulliken, who proposed that the electrons in a given MO could be partitioned according to the

occupancy of the atomic basis functions.[60] Suppose we have a normalised molecular spinorbital ϕ_i of HF which is expanded in just two normalised basis functions χ_H and χ_F centred on H and F respectively. It is singly occupied and normalised, and therefore integrating the density over all space should give 1.

$$\begin{aligned} \phi_i &= c_H \chi_H + c_F \chi_F \\ \rho_i(r) = \phi_i(r)^2 &= {c_H}^2 \chi_H(r)^2 + 2c_H c_F \chi_H(r)\chi_F(r) + {c_F}^2 \chi_F(r)^2 \\ 1 = \int \rho_i d\tau &= \int {\phi_i}^2 d\tau = \int ({c_H}^2 {\chi_H}^2 + 2c_H c_F \chi_H \chi_F + {c_F}^2 {\chi_F}^2) d\tau \end{aligned} \tag{105}$$

Given that the basis functions are normalised, and knowing the identity of the overlap integral *S*, the following is obtained.

$$1 = {c_H}^2 + 2c_H c_F S_{HF} + {c_F}^2 \tag{106}$$

The first term indicates the amount of electron density in this orbital which is unambiguously assigned to the basis function on H, and the last term indicates the density assigned to F. The middle term indicates density which is shared between the two. Mulliken then generalised the expression to an arbitrary number of basis functions:

$$1 = (\sum_{k}^{basis} {c_k}^2 + \sum_{l \neq k}^{basis} c_k c_l S_{kl}) \tag{107}$$

The occupation numbers n_i of the molecular orbitals are then added, and now the number of electrons can be summed over the orbitals to give the total number of electrons:

$$\begin{aligned} N_{total} &= \sum_{i}^{orbitals} n_i (\sum_{k}^{basis} {c_k}^2 + \sum_{l \neq k}^{basis} c_k c_l S_{kl}) \\ &= \sum_{i}^{orbitals} (\sum_{k}^{basis} n_i {c_k}^2 + \sum_{l \neq k}^{basis} n_i c_k c_l S_{kl}) \end{aligned} \tag{108}$$

The first term indicates the electron density which is unambiguously assigned to a particular basis function *k*, while the second indicates electron density which is shared between the two functions *k* and *l*. Mulliken noted that this partitioning does not distinguish the two basis functions' contribution to this term, and therefore the two atoms must contribute equally to it. Instead of summing over the orbitals, we can take the same partitioning and sum over the basis functions $k \in A$ which are centred on a given atom *A*. Gathering all of these contributions gives the total number of electrons associated with atom *A*.[61]

$$N_A = \sum_{i}^{orbitals} (\sum_{k \in A}^{basis} n_i c_{ki}^{\ 2} + \sum_{k,l \in A, l \neq k}^{basis} n_i c_{ki} c_{li} S_{kl} + \sum_{k \in A, l \notin A} n_i c_{ki} c_{li} S_{kl}) \quad (109)$$

The connection to the Hartree-Fock results is clearer if the expression is written in terms of the density matrix *D* and the overlap matrix *S*. The diagonal elements provide for the first term for the above expression (diagonal elements of the overlap matrix are unity for a normalised basis) while off-diagonal elements provide the second two terms.[62]

$$\begin{aligned} S_{kl} &= \int \chi_k \chi_l d\tau \\ D_{kl} &= \sum_{i}^{orbitals} n_i c_{ki} c_{li} \\ N_A &= \sum_{k \in A} \sum_{l} D_{kl} S_{kl} \end{aligned} \quad (110)$$

This method has the advantage that it is simple to compute and uses only information that is already present in a calculation performed in an atomically-centred basis set. (It is meaningless when a non-atomically-centred basis set, is used *e.g.* plane waves or Gaussians centred anywhere other than a nucleus.) Unfortunately it is also completely beholden to the basis set and consequently subject to biases. Suppose we had a complete basis set for the H_2O molecule using *only* basis functions centred on the hydrogen atoms (inefficient, but possible; *c.f.* Section 2.4.3). In the Mulliken population analysis, the oxygen would always have a charge of +2, and each of the hydrogen atoms a charge of -1. This is unphysical. Subtler examples of the same bias limit the Mulliken population analysis' utility. There is also a limitation that the division of the overlap charge equally between the two centres is not accurate; this is addressed by other partitionings based on *D* and *S*, such as the Löwdin or natural population analysis schemes.[61,62]

A second method is to divide the molecule into a series of volumes, each associated with a particular atom, and to integrate the electron density over those volumes. A particularly broadly adopted partitioning was suggested by AIM theory (as raised in 1.1, 1.2.1, and 1.4). To revise, nuclei are maxima and chemical bonding is indicated by a second-order saddle point between nuclei.Atoms are volumes bounded by "zero-flux" surfaces where the electron density reaches a minimum with respect to distance from the nucleus, and the gradient is negative at a tangent to the surface. In Bader's model, the charge of an atom is obtained by integrating the electron density within the volume in which its nucleus lies.[62,63]

The topologies obtained by Bader's analysis are not strongly basis set or method dependent, provided that the wavefunction is well converged with respect to basis set size.[64] However charges obtained by Bader's analysis fail to properly recreate molecular dipole moments, because the analysis fails to account for the inhomogeneity of the electron density within the volume.[61]

The third approach is to assign charges which properly recreate the electrostatic potential of the whole molecule (and typically also the dipole moment). Merz-Kollman-Singh (MK), CHELP, and CHELPG schemes are based on this process.[65-67] All three schemes depend upon manipulating the point charges assigned to each atom until they accurately reproduce a subset of the true electrostatic potential of the molecule. These methods have the advantage that the electrostatic potential they reproduce is an important chemical property.The methods differ in how the electrostatic potential is sampled, and the fitting algorithm. The MK and CHELP schemes use nested surfaces beginning near the van der Waals surface and moving outward, while the CHELPG scheme uses a regular grid, excluding the van der Waals volume. Excluding the VdW volume is necessary because the electrostatic potential is not well-approximated by point charges when one is close to the molecule.[67] The MK scheme fits by an iterative least squares method, while CHELP and CHELPG use Lagrange multipliers.[65-67]

2.10. References

[1] F. Jensen *Introduction* in *Introduction to Computational Chemistry*; Second ed.; John Wiley & Sons: Chichester, 2007.
[2] L. Piela *Separation of Electronic and Nuclear Motions* in *Ideas of Quantum Chemistry*; 1st ed.; Elsevier: Oxford, 2007.
[3] C. J. Cramer *Foundations of Molecular Orbital Theory* in *Essentials of Computational Chemistry: Theories and Models*; Second ed.; John Wiley & Sons: Chichester, 2004.
[4] F. Jensen *Electronic Structure Methods: Independent-Particle Models* in *Introduction to Computational Chemistry*; Second ed.; John Wiley & Sons: Chichester, 2007.
[5] C. J. Cramer *Ab initio Implementations of Hartree-Fock Molecular Orbital Theory* in *Essentials of Computational Chemistry: Theories and Models*; Second ed.; John Wiley & Sons: Chichester, 2004.
[6] D. R. Hartree, *The Wave Mechanics of an Atom with a Non-Coulomb Central Field. Part I. Theory and Methods.*, Math. Proc. Cambridge Philos. Soc., **24**, 89-110 (1927)

[7] D. R. Hartree, *The Wave Mechanics of an Atom with a Non-Coulomb Central Field. Part II. Some Results and Discussion*, Math. Proc. Cambridge Philos. Soc., **24**, 111-132 (1927)
[8] D. R. Hartree, *The Wave Mechanics of an Atom with a Non-Coulomb Central Field. Part III. Term Values and Intensities in Series in Optical Spectra*, Math. Proc. Cambridge Philos. Soc., **24**, 426-437 (1928)
[9] G. G. Hall, *The Molecular Orbital Theory of Chemical Valency. VIII. A Method of Calculating Ionization Potentials*, Proc. R. Soc. London, Ser. A, **205**, 541-552 (1951)
[10] C. C. J. Roothaan, *New Developments in Molecular Orbital Theory*, Rev. Mod. Phys., **23**, 69-89 (1951)
[11] F. Jensen *Electron Correlation Methods* in *Introduction to Computational Chemistry*; Second ed.; John Wiley & Sons: Chichester, 2007.
[12] J. Čížek *On the Use of the Cluster Expansion and the Technique of Diagrams in Calculations of Correlation Effects in Atoms and Molecules* in *Advances in Chemical Physics*; P. C. Hariharan, Ed.; Wiley Interscience: New York, 1969; Vol. 14 p. 35-89
[13] J. Čížek, *On the Correlation Problem in Atomic and Molecular Systems. Calculation of Wavefunction Components in Ursell-Type Expansion Using Quantum Field Theoretical Methods*, J. Chem. Phys., **45**, 4256-4266 (1966)
[14] L. Piela *Coupled cluster (CC) method* in *Ideas of Quantum Chemistry*; 1st ed.; Elsevier: Oxford, 2007.
[15] F. Jensen *Many-Body Perturbation Theory* in *Introduction to Computational Chemistry*; Second ed.; John Wiley & Sons: Chichester, 2007.
[16] F. Jensen *Size Consitency and Size Extensivity* in *Introduction to Computational Chemistry*; Second ed.; John Wiley & Sons: Chichester, 2007.
[17] F. Jensen *Coupled Cluster* in *Introduction to Computational Chemistry*; Second ed.; John Wiley & Sons: Chichester, 2007.
[18] F. Jensen *Connections between Coupled Cluster, Configuration Interaction, and Perturbation Theory* in *Introduction to Computational Chemistry*; Second ed.; John Wiley & Sons: Chichester, 2007.
[19] H. Kummel, *Origins of the Coupled Cluster Method*, Theor Chim Acta, **80**, 81-89 (1991)
[20] L. Piela *Many body perturbation theory (MBPT)* in *Ideas of Quantum Chemistry*; 1st ed.; Elsevier: Oxford, 2007.
[21] C. J. Cramer *Perturbation Theory* in *Essentials of Computational Chemistry: Theories and Models*; Second ed.; John Wiley & Sons: Chichester, 2004.
[22] L. Piela *Møller-Plesset version of Rayleigh-Schrödinger perturbation theory* in *Ideas of Quantum Chemistry*; 1st ed.; Elsevier: Oxford, 2007.
[23] F. Jensen *Configuration Interaction* in *Introduction to Computational Chemistry*; Second ed.; John Wiley & Sons: Chichester, 2007.
[24] J. A. Pople, M. Head-Gordon and K. Raghavachari, *Quadratic configuration interaction - a general technique for determining electron correlation energies*, J. Chem. Phys., **87**, 5968-5975 (1987)
[25] F. Jensen *Basis Sets* in *Introduction to Computational Chemistry*; Second ed.; John Wiley & Sons: Chichester, 2007.
[26] T. H. Dunning, *Gaussian basis sets for use in correlated molecular calculations. I. The atoms boron through neon and hydrogen*, J. Chem. Phys., **90**, 1007-1023 (1989)
[27] J. Almlöf and P. R. Taylor, *General Contraction of Gaussian-Basis Sets .1. Atomic Natural Orbitals for 1st-Row and 2nd-Row Atoms*, J. Chem. Phys., **86**, 4070-4077 (1987)
[28] K. Jankowski, R. Becherer, P. Scharf, H. Schiffer and R. Ahlrichs, *The Impact of Higher Polarization Basis Functions on Molecular Ab initio Results .1. The Ground-State of F2*, J. Chem. Phys., **82**, 1413-1419 (1985)

[29] D. E. Woon and T. H. Dunning, *Gaussian basis sets for use in correlated molecular calculations. III. The atoms aluminum through argon*, J. Chem. Phys., **98**, 1358-1371 (1993)
[30] A. K. Wilson, D. E. Woon, K. A. Peterson and T. H. Dunning Jr., *Gaussian basis sets for use in correlated molecular calculations. IX. The atoms gallium through krypton*, J. Chem. Phys., **110**, 7667-7676 (1999)
[31] D. E. Woon and T. H. Dunning, *Gaussian basis sets for use in correlated molecular calculations. V. Core-valence basis-sets for boron through neon*, J. Chem. Phys., **103**, 4572-4585 (1995)
[32] R. A. Kendall, T. H. Dunning and R. J. Harrison, *Electron affinities of the first-row atoms revisited. Systematic basis sets and wave functions*, J. Chem. Phys., **96**, 6796-6806 (1992)
[33] P. Skurski, M. Gutowski and J. Simons, *How to choose a one-electron basis set to reliably describe a dipole-bound anion*, Int. J. Quantum Chem, **80**, 1024-1038 (2000)
[34] W. Humphrey, A. Dalke and K. Schulten, *VMD: Visual molecular dynamics*, J. Mol. Graphics Modell., **14**, 33-38 (1996)
[35] M. Haranczyk and M. Gutowski, *Visualization of molecular orbitals and the related electron densities*, J. Chem. Theory Comput., **4**, 689-693 (2008)
[36] J. Simons, *Molecular anions*, J. Phys. Chem. A, **112**, 6401-6511 (2008)
[37] T. Helgaker, W. Klopper, H. Koch and J. Noga, *Basis-set convergence of correlated calculations on water*, J. Chem. Phys., **106**, 9639-9646 (1997)
[38] D. Feller, *The Use of Systematic Sequences of Wave-Functions for Estimating the Complete Basis Set, Full Configuration-Interaction Limit in Water*, J. Chem. Phys., **98**, 7059-7071 (1993)
[39] A. Halkier, T. Helgaker, P. Jørgensen, W. Klopper and J. Olsen, *Basis-set convergence of the energy in molecular Hartree–Fock calculations*, Chem. Phys. Lett., **302**, 437-446 (1999)
[40] C. Schwartz, *Importance of Angular Correlations between Atomic Electrons*, Phys. Rev., **126**, 1015-1019 (1962)
[41] R. A. Bachorz, W. Klopper and M. Gutowski, *Coupled-cluster and explicitly correlated perturbation-theory calculations of the uracil anion*, J. Chem. Phys., **126**, 085101 (2007)
[42] S. F. Boys and F. Bernardi, *The calculation of small molecular interactions by the differences of separate total energies. Some procedures with reduced errors.*, Mol. Phys., **19**, 553-556 (1970)
[43] H. B. Jansen and P. Ros, *Non-empirical molecular orbital calculations on the protonation of carbon monoxide*, Chem. Phys. Lett., **3**, 140-143 (1969)
[44] S. Simon, M. Duran and J. J. Dannenberg, *How does basis set superposition error change the potential surfaces for hydrogen bonded dimers?*, J. Chem. Phys., **105**, 11024-11031 (1996)
[45] L. Turi and J. J. Dannenberg, *Correcting for Basis Set Superposition Error in Aggregates Containing More Than 2 Molecules - Ambiguities in the Calculation of the Counterpoise Correction*, J. Phys. Chem., **97**, 2488-2490 (1993)
[46] P. Valiron and I. Mayer, *Hierarchy of counterpoise corrections for N-body clusters: generalization of the Boys-Bernardi scheme*, Chem. Phys. Lett., **275**, 46-55 (1997)
[47] J. C. White and E. R. Davidson, *An Analysis of the Hydrogen Bond in Ice*, J. Chem. Phys., **93**, 8029-8035 (1990)
[48] G. Lendvay and I. Mayer, *Some difficulties in computing BSSE-corrected potential surfaces of chemical reactions*, Chem. Phys. Lett., **297**, 365-373 (1998)
[49] F. Jensen *Optimization Techniques* in *Introduction to Computational Chemistry*; Second ed.; John Wiley & Sons: Chichester, 2007.

[50] P. W. Atkins and R. S. Friedman *The calculation of electronic structure* in *Molecular Quantum Mechanics*; Third ed.; Oxford Univeristy Press: Oxford, 1997.
[51] F. Khatib, S. Cooper, M. D. Tyka, K. F. Xu, I. Makedon, Z. Popovic, D. Baker and F. Players, *Algorithm discovery by protein folding game players*, Proc. Natl. Acad. Sci. U. S. A., **108**, 18949-18953 (2011)
[52] P. W. Atkins and R. S. Friedman *Normal modes* in *Molecular Quantum Mechanics*; Third ed.; Oxford Univeristy Press: Oxford, 1997.
[53] E. Fermi and E. Teller, *The Capture of Negative Mesotrons in Matter*, Phys. Rev., **72**, 399-408 (1947)
[54] A. S. Wightman, *Moderation of Negative Mesons in Hydrogen I: Moderation from High Energies to Capture by an H_2 Molecule*, Phys. Rev., **77**, 521-528 (1950)
[55] K. D. Jordan and F. Wang, *Theory of dipole-bound anions*, Annu. Rev. Phys. Chem., **54**, 367-396 (2003)
[56] M. Gutowski, K. D. Jordan and P. Skurski, *Electronic Structure of Dipole-Bound Anions*, J. Phys. Chem. A, **102**, 2624-2633 (1998)
[57] S. Smuczynska, I. Gwarda, I. Anusiewicz and P. Skurski, *Is the p-chloroaniline anion bound almost entirely by correlation?*, J. Chem. Phys., **130**, 124316 (2009)
[58] P. Skurski, I. Dabkowska, A. Sawicka and J. Rak, *Dipole-bound and dispersion-bound anions supported by the asymmetric tautomers of aminophosphine: H_3NPH and $HNPH_3$*, Chem. Phys., **279**, 101-110 (2002)
[59] P. Skurski, J. Rak and J. Simons, *Is 9-acridinamine anion a dispersion-bound anion?*, J. Chem. Phys., **115**, 11193-11199 (2001)
[60] R. S. Mulliken, *Electronic Population Analysis on LCAO-MO Molecular Wave Functions. I*, J. Chem. Phys., **23**, 1833-1840 (1955)
[61] C. J. Cramer *Partial Atomic Charges* in *Essentials of Computational Chemistry: Theories and Models*; Second ed.; John Wiley & Sons: Chichester, 2004.
[62] F. Jensen *Wave Function Analysis* in *Introduction to Computational Chemistry*; Second ed.; John Wiley & Sons: Chichester, 2007.
[63] R. F. W. Bader, *Atoms in Molecules*, Acc. Chem. Res., **18**, 9-15 (1985)
[64] M. Jablonski and M. Palusiak, *Basis Set and Method Dependence in Atoms in Molecules Calculations*, J. Phys. Chem. A, **114**, 2240-2244 (2010)
[65] B. H. Besler, K. M. Merz and P. A. Kollman, *Atomic charges derived from semiempirical methods*, J. Comput. Chem., **11**, 431-439 (1990)
[66] L. E. Chirlian and M. M. Francl, *Atomic Charges Derived from Electrostatic Potentials - a Detailed Study*, J. Comput. Chem., **8**, 894-905 (1987)
[67] C. M. Breneman and K. B. Wiberg, *Determining Atom-Centered Monopoles from Molecular Electrostatic Potentials - the Need for High Sampling Density in Formamide Conformational-Analysis*, J. Comput. Chem., **11**, 361-373 (1990)

Chapter 3: Ammonia-Hydrogen Bromide and Ammonia-Hydrogen Iodide Complexes: Anion Photoelectron and *Ab Initio* Studies

Published in J. Phys. Chem. *A* vol. 114 pp. 1357–1363 (S. N. Eustis, A. Whiteside, D. Wang, M. Gutowski, and K. H. Bowen)

3.1. Abstract

The ammonia-hydrogen bromide and ammonia-hydrogen iodide, anionic hetero-dimers were studied by anion photoelectron spectroscopy. In complementary studies, these anions and their neutral counterparts were also investigated via *ab initio* theory at the coupled cluster level. In both systems, neutral $NH_3\cdots HX$ dimers were predicted to be linear, hydrogen-bonded complexes, whereas their anionic dimers were found to be proton-transferred species of the form, $(NH_4^+X^-)^-$. Both experimentally-measured and theoretically-predicted vertical detachment energies (VDE) are in excellent agreement for both systems, with values for $(NH_4^+Br^-)^-$ being 0.65 eV and 0.67 eV, respectively, and values for $(NH_4^+I^-)^-$ being 0.77 eV and 0.81 eV, respectively. These systems are discussed in terms of our previous study of $(NH_4^+Cl^-)^-$.

3.2. Introduction

Acid-base reactions between ammonia and hydrogen halides (HX) have fascinated generations of scientists, most of whom have seen the white fog that develops when vapors from ammonium hydroxide and hydrochloric acid intermingle. While reactions between ammonia and all the hydrogen halides readily form ammonium halide salts at significant reactant densities, their ability to proceed on the microscopic level with only one molecule of each reactant is another matter. Since the acidities of hydrogen halides increase consecutively from HF, to HCl, to HBr, to HI, the tendency for proton transfer to occur within the confines of isolated, neutral $NH_3\cdots HX$ complexes would also be expected to increase in that order. This expectation is somewhat quantified by the following semi-empirical condition for proton transfer in neutral base$\cdots$HX complexes,[1] $PA_{base} + \Delta H_{acid} + 102 > 0$, where PA is the proton affinity of base, ΔH_{acid} is the acidity of HX (the negative of the enthalpy of dissociation for the $HX \rightarrow H^+ + X^-$ reaction), and where both values are in units of kcal/mol. Applying this criterion to the $NH_3\cdots HX$ series yields negative values in all four cases , *viz.*, -65.4, -27.4, -17.4, and -8.3, where HX = HF, HCl, HBr, and HI, respectively. Furthermore, this outcome is

consistent with the preponderance of available experimental data and high level calculations on neutral NH_3···HX complexes, i.e., proton transfer between NH_3 and HX in an isolated interacting pair does not occur. Below, we briefly summarize the pertinent literature on NH_3···HCl, NH_3···HBr, and NH_3···HI neutral complexes.

In the case of NH_3 and HCl, early theoretical work suggested that their reaction would proceed with only a single molecule of each reactant.[2] Later theoretical studies, however, found that hydrogen bonding rather than proton transfer would likely dominate in complexes of ammonia and hydrogen chloride.[3,4] Experimental work including pulsed nozzle, Fourier-transform microwave studies,[5,6] matrix-isolated infrared investigations,[7-10] and Stark effect measurements[11] have since provided conclusive evidence that the neutral NH_3/HCl pair does not undergo proton transfer, preferring instead to form the linear hydrogen-bonded complex, NH_3···HCl. Modern theoretical predictions[12-21] are in accord with these results.

Fourier-transform microwave work showed the NH_3···HBr complex to be predominately hydrogen-bonded but with 11% ionic character.[6,22] Stark effect measurements were consistent with a linear, hydrogen bonded complex.[11] Matrix-isolated infrared studies in which NH_3 and HBr were co-deposited with the relatively non-perturbing host, neon, found the NH_3/HBr pair to form a hydrogen-bonded complex.[23-25] However, with more interactive hosts, such as Ar, Kr, and N_2, the infrared spectra were consistent with a growing degree of proton-transfer character in the NH_3···HBr complex.[25] Thus, the matrix environment was found to significantly influence the extent of proton transfer in the NH_3···HBr complex. Theoretical work was consistent with these experimental results, finding the isolated NH_3/HBr pair to form a linear, hydrogen-bonded complex with little to no proton transfer.[4,20,26-28]

While Fourier-transform microwave work suggested that the NH_3···HI complex is hydrogen-bonded rather than proton transferred,[6,29,30] matrix-isolated infrared studies found the level of proton transfer to be entirely dependent on the host.[31-33] Furthermore, different calculations found various degrees of proton transfer within the NH_3···HI complex,[26,27,34] these ranging from none to complete proton transfer. Clearly, the NH_3···HI complex is edging toward proton transfer even in the gas phase, and it is quite sensitive to changes in its environment.

Thus, in isolation, proton transfer does not spontaneously occur between a single molecule of ammonia and a single molecule of any of the three hydrogen halides considered here; these reactions, which occur so readily in bulk, do not have a true molecular level (two body) counterpart. Instead, they require the aide of external interactions, albeit to different extents, in order to initiate proton transfer and form ionic ammonium halides, $NH_4^+X^-$.

Among the simplest of perturbing agents is an electron, and through a combination of anion photoelectron spectroscopic experiments and high level *ab initio* calculations, in a previous study we showed that an excess electron is indeed enough to initiate proton transfer between ammonia and hydrogen chloride, forming the anion of ammonium chloride.[21] Our work further showed that the excess electron occupies a highly delocalized orbital surrounding the NH_4^+ cation, creating a Rydberg NH_4 moiety which itself interacts with and is distorted by the neighboring chloride anion, *i.e.*, $(NH_4^+Cl^-)^- = NH_4 \cdots Cl^-$. Thus, while the most stable form of the isolated neutral complex is likely hydrogen-bonded, the anionic complex prefers a proton-transferred configuration.

Our work with this system led us to examine analogous complexes between ammonia and the heavier hydrogen halides, HBr and HI. Two effects must be considered in the progression through the halogens. First, the larger halogens are better proton donors, which will affect the energetics of the electron-driven proton transfer. Second, the larger halogens show a tendency to form halogen bonds, resulting in a stable $NH_3 \cdots XH$ complex. However due to dipole cancellation such a complex would only weakly bind electrons, and would not undergo electron-driven proton transfer. Therefore this result will be discussed in a later publication.

Here, we present a synergetic experimental (anion photoelectron spectroscopy) and theoretical (coupled cluster level) study of both the anions and the corresponding neutral forms of ammonia-hydrogen bromide and ammonia-hydrogen iodide complexes.

3.3. Experimental

Anion photoelectron spectroscopy is conducted by crossing a mass-selected beam of negative ions with a fixed-frequency photon beam and energy-analyzing the resultant photodetached electrons. Photodetachment is governed by the energy-conserving

relationship, $h\nu$ = EBE + EKE, where $h\nu$ is the photon energy, EBE is electron binding energy, and EKE is electron kinetic energy. Knowing the photon energy and measuring the electron kinetic energy leads to the electron binding energies of the observed transitions.

The anionic complexes of interest were generated in a nozzle-ion source. In this device an ammonia/argon mixture (15%/85%) at 1-3 atm and 25°C was expanded through a 20 μm orifice (nozzle) into an operating vacuum of ~7 x 10^{-5} Torr, while an HX/argon (10%/90%) mixture at a few Torr was allowed to infuse into the expansion region immediately outside the nozzle. The stagnation chamber and nozzle were biased at -500 volts. Low energy electrons from an independently biased, thoriated-iridium filament were directed into the jet near the mouth of the nozzle. An axial magnetic field helped to form a micro-plasma just outside the nozzle orifice. Anions formed in this way were extracted through a 2 mm diameter skimmer into the ion optical system of the spectrometer. These were mass-analyzed by a 90° sector magnet (mass resolution = 400) before being mass-selected and directed into the ion-photon interaction region, where they interacted with ~200 circulating Watts of 2.540 eV photons from an argon ion laser operated intra-cavity. The resulting photodetached electrons were analyzed by a hemispherical electron energy analyzer (constant resolution throughout energy window) and counted by an electron multiplier. The photoelectron spectra were calibrated against the well-known photoelectron spectrum of O^-. Our apparatus has been described in detail previously.[35]

3.4. Computational Detail

The coupled cluster electronic structure method was used due to the significant contribution of electron correlation effects to the stability of weakly bound excess electron systems.[36,37] Geometry optimizations, dipole moment calculations, and vibrational zero-point energy corrections were performed at the coupled-cluster singles-doubles level of theory (CCSD). Single-point energy calculations were performed with perturbative triples (CCSD(T)), using the same basis sets, geometries, and tight convergence criteria.

The large, diffuse SOMO orbital in the anion would not be correctly described by conventional basis sets, even those augmented with conventional diffuse functions. Therefore the augmented, polarized, correlation-consistent basis set of double-zeta quality[38-40] was supplemented with an additional set of seven *s* and seven *p* diffuse functions.[41] The additional diffuse *s* and *p* functions were "even-tempered", *i.e.* their exponents form geometric progressions with the progression constant set to 2.5, and they used the most diffuse s and p functions on the conventional basis set as the zeroth functions in each progression. These extra functions are centered on the positive end of the complex's dipole, in this instance, on the nitrogen atom. Hereafter, these basis sets are referred to as "aug-cc-pvdz-2.5". Iodine, however, is an exception; there, the aug-cc-pvdz-PP basis set[42] (relativistic pseudopotentials for the core electrons on iodine) was used. All calculations were performed in the Gaussian 03 package.[43] Visualizations of molecules were generated in MOLDEN[44] with diffuse orbitals visualized as 50%-of-electron iso-surfaces using VMD.[45,46]

Adiabatic electron affinities (EA_a) for neutrals were computed as the energy of the anions subtracted from the energy of the neutrals at their optimized geometries, with zero-point energy corrections applied. Positive values therefore indicate that binding of an electron is exothermic, *i.e.*, the standard thermochemical definition. Vertical (electron) detachment energies (VDE) for anions were determined as the energy of the anion at its optimized geometry subtracted from the energy of the neutral at the same geometry. Likewise, vertical electron (attachment) affinities (EA_V) were computed as the energy of the anion at the neutral's optimized geometry, subtracted from the energy of the neutral at that same geometry. Positive values indicate that the anionic state is bound with respect to the neutral state.

Dissociation energies were determined as the energy of the relevant complex at its optimized geometry subtracted from the sum of the energies of its two separated fragments at their optimized geometries. The energy of the complex was determined using the dimer-centered basis set, with BSSE (by counterpoise) and vibrational zero-point energy corrections applied. Likewise, the monomer energies were determined with monomer-centered basis sets with vibrational zero-point corrections. Positive values indicate that fragmenting the complex is an endothermic process.

Proton affinities were determined as the energies of the protonated species subtracted from those of the deprotonated species at their optimized geometries, with (where necessary) zero-point energy and counterpoise corrections included. Positive values indicate that binding a proton is exothermic.

Relaxed potential energy curves for neutral species were calculated at the CCSD level with the aug-cc-pvdz-2.5 basis set described previously. The acidic proton, aligned with the C_3 axis and bridging the heavy atoms, is dubbed as "shuttling" because its position is profoundly affected by the excess electron attachment. The "shuttling" proton position was varied and all other coordinates relaxed. This proton's position is explicitly relative to either the nitrogen or the halogen, which each give a unique potential energy surface. At intermediate distances, the choice of coordinate does not influence the result, and the surfaces are identical. As the shuttling coordinate is extended, the other heavy atom is free to retreat from the advancing proton. Therefore we do not probe the proton shuttling potential energy surface near the other heavy atom, but instead probe the heavy atom-heavy atom breathing potential energy surface. For example at a high halogen-proton distance, the proton-nitrogen distance becomes constant, and the nitrogen-halogen distance varies. This was circumvented by combining surfaces created using both coordinates.

The potential energy curve for the anion was assessed as the vertical attachment energy at each point of the neutral potential energy curve, in order that the vertically-bound or –unbound nature of the anion would be obvious. This also avoided anticipated difficulties with spontaneous autodetachment of the electron during optimization in the weakly-bound region of the surface.

3.5. Results

The measured photoelectron spectra of $(NH_4^+Cl^-)^-$, $(NH_4^+Br^-)^-$, and $(NH_4^+I^-)^-$ are presented in Figure 3.1. Peak centers (EBE) for each of these spectra are tabulated in Table 3.1. Experimental and calculated values for vertical detachment energies (VDE) and electron affinities (EA_a) are presented in Table 3.2. Computed structures for the anions and their neutral counterparts are presented in Figure 3.2. In Table 3.3, the nitrogen-hydrogen and the halogen-hydrogen bond lengths in the free ammonium cation and the free hydrogen halides, respectively, are compared to the nitrogen-"shuttling

proton" and the halogen-"shuttling proton" bond lengths in both the neutral and anionic structures of the complexes under study here. Theoretical potential energy curves are presented in Figure 3.3 parts a and b.

Table 3.1: Experimental peak center positions (EBE's) for the photoelectron spectra, $(NH_4^+X^-)^-$ (X = Cl, Br, I), all data are in eV. $(NH_4^+Cl^-)^-$ data are taken from reference [21].

v'	$(NH_4^+Cl^-)^-$	$(NH_4^+Br^-)^-$	$(NH_4^+I^-)^-$
1	0.075	-	0.451
2	0.196	0.402	0.619
3	0.384	0.530	0.696
4	0.537	0.667	0.814
5	0.700	0.804	0.920
6	0.802	0.941	1.060
7	0.965	1.069	1.179
8	-	1.223	-

Table 3.2: The experimental and theoretical electron affinities (EA_a) and vertical detachment energies (VDE) for the $NH_3\cdots HBr/(NH_4^+Br^-)^-$ and the $NH_3\cdots HI/(NH_4^+I^-)^-$ systems. $NH_3\cdots HCl/(NH_4^+Cl^-)^-$ data are taken from reference [21].

Species	$NH_3\cdots HBr$	$(NH_4^+Br^-)^-$	$NH_3\cdots HI$	$(NH_4^+I^-)^-$	$NH_3\cdots HCl$	$(NH_4^+Cl^-)^-$
Expt. VDE (eV)		0.67		0.81		0.540
Theo. VDE (eV)		0.65		0.77		0.52
Expt. EA_a (eV)	0.28		0.45		0.075	
Theo. EA_a (eV)	0.26		0.47		0.068	

Table 3.3: Computed nitrogen-hydrogen and halogen-hydrogen distances for neutral and anionic complexes compared to computed values for the free ammonium cation and the free hydrogen halides. The hydrogen atoms being referred to here are the "shuttling protons", H_s, in both $\Delta(N\text{-}H_s)$ and $\Delta(X\text{-}H_s)$ (X=Br, I). Positive values indicate that the bond length or angle is greater in the anion than the complex than the free neutral monomer.

Species	$NH_3\cdots HBr$	$(NH_4^+Br^-)^-$	$NH_3\cdots HI$	$(NH_4^+I^-)^-$
$\Delta(N\text{-}H_s)$, Å	+0.836	+0.053	+0.943	+0.039
$\Delta(X\text{-}H_s)$, Å	+0.036	+0.634	+0.028	+0.714

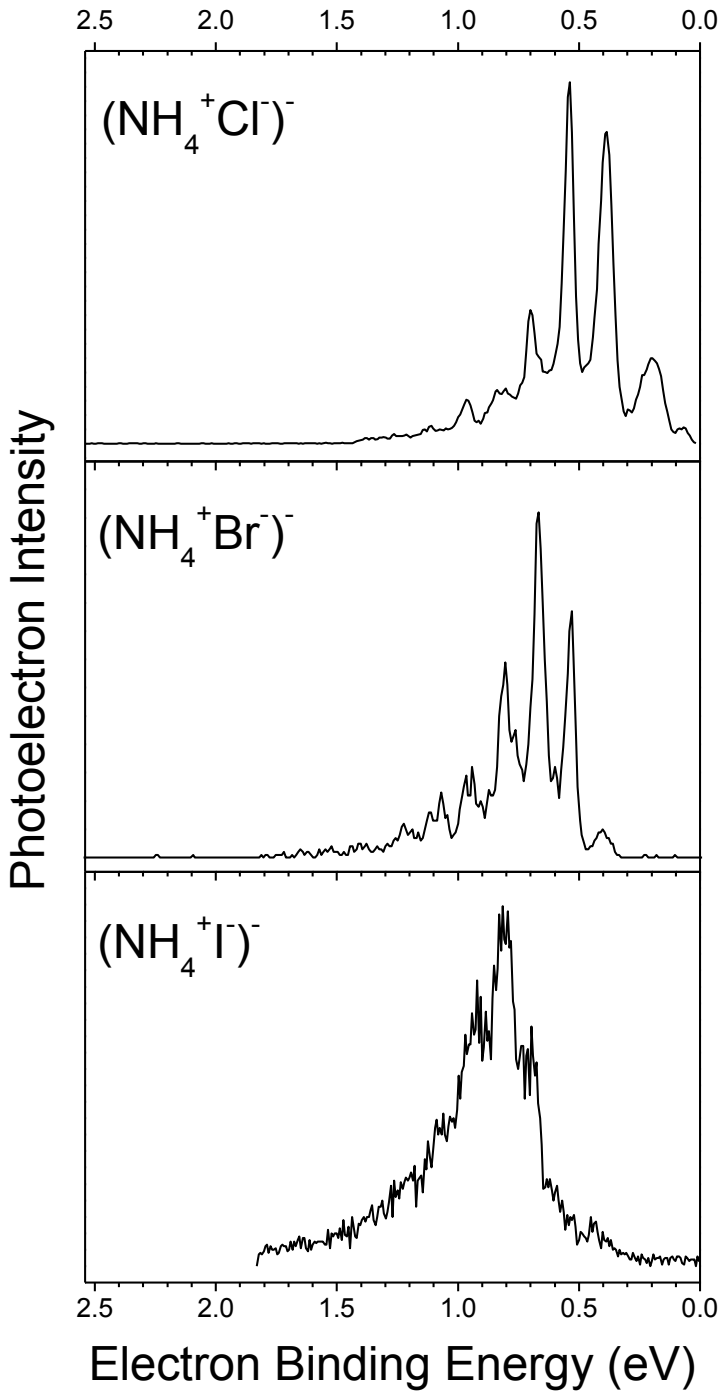

Figure 3.1: Photoelectron spectra of the ammonium chloride anion, the ammonium bromide anion, and the ammonium iodide anion each taken with 2.540 eV photons. The spectrum of the ammonium chloride anion[21] is presented here for comparison.

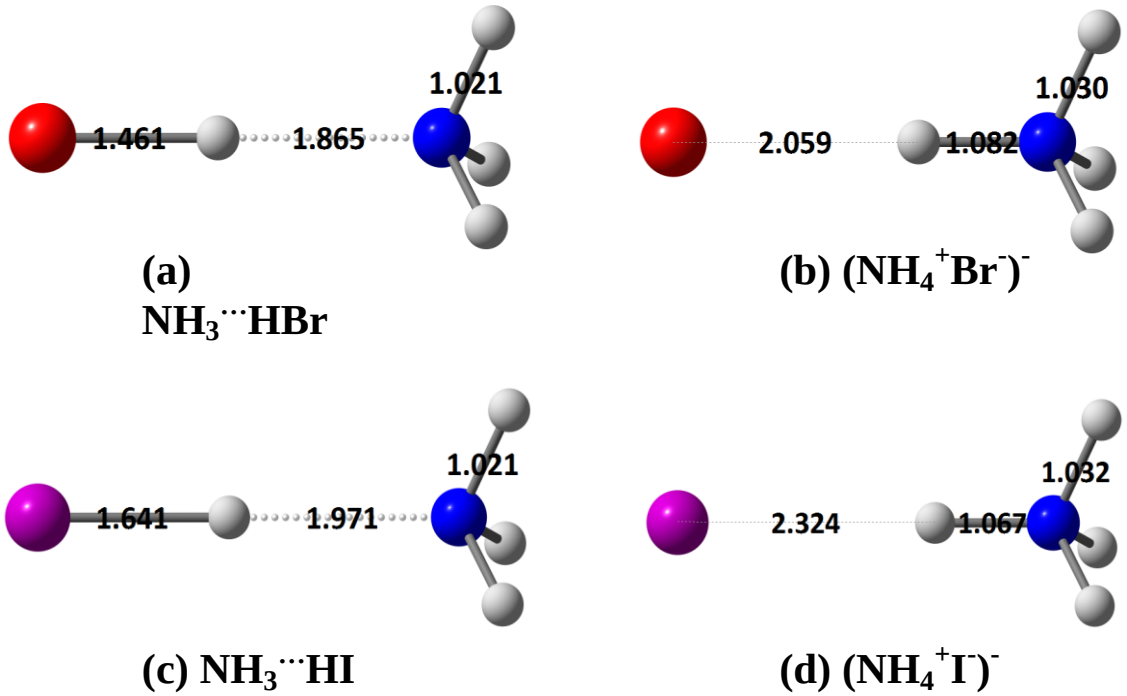

Figure 3.2: Calculated geometries for (a) NH_3···.HBr, (b) $(NH_4{+}Br^-)^-$, (c) NH_3···.HI, and (d) $(NH4^+I^-)^-$ at the CCSD/aug-cc-pvdz-2.5 level of theory. Blue for nitrogen, white for hydrogen, red for bromine, purple for iodine.

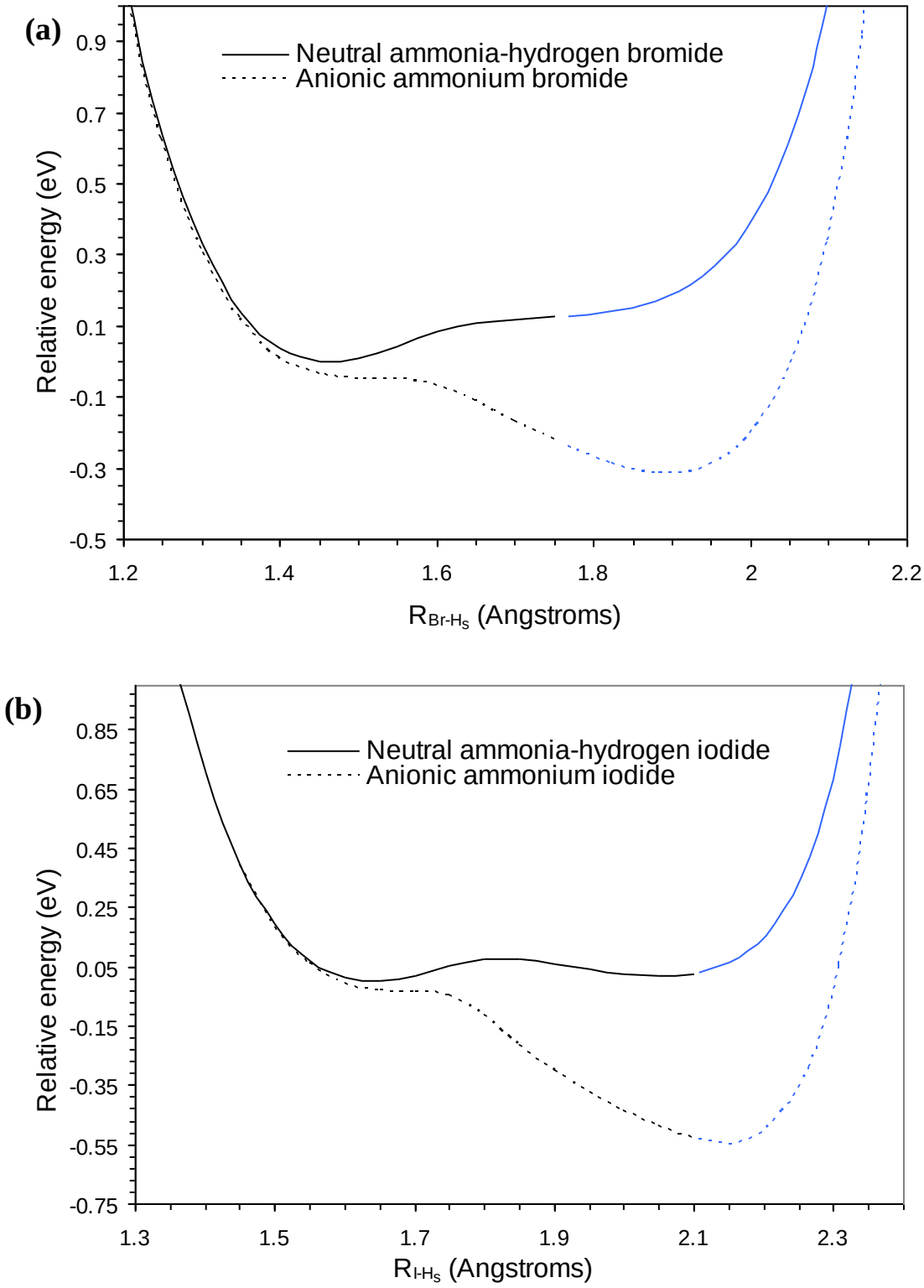

Figure 3.3, (a): Potential energy surfaces for the $(NH_4^+Br^-)^-$ anionic and the $NH_3\cdots HBr$ neutral complexes, dashed and solid lines respectively. (b): Potential energy surfaces for the $(NH_4^+I^-)^-$ anionic and the $NH_3\cdots HI$ neutral complexes, dashed and solid lines respectively. Calculated at the CCSD/aug-cc-pvdz-2.5 level of theory Black indicates surface evaluated from proton-halogen distance, blue indicates surface evaluated from proton-nitrogen distance

The photoelectron spectra of $(NH_4^+Br^-)^-$ and $(NH_4^+I^-)^-$, though different from one another, are nevertheless reminiscent of the spectrum of $(NH_4^+Cl^-)^-$, which we collected in our previous study.[21] The spectrum of $(NH_4^+Br^-)^-$ reveals a clear vibrational progression beginning with a peak at EBE ~0.4 eV and with the maximum in its fitted intensity envelope occurring at 0.67 eV. The spectrum of $(NH_4^+I^-)^-$ is similar in shape, with a maximum intensity occurring at 0.81 eV. In neither case did the spectral patterns change with source conditions, suggesting that none of the observed peaks are due to vibrational hot bands. While all of these ammonium halide anion photoelectron spectra are analogous to alkali halide anion photoelectron spectra in that they are anions of salts,[47] they are different in that the formation of ammonium halide anions involves proton transfers and in that the vibrational structure in their spectra are primarily due to shuttling proton motions. The related vibrational mode is a fully-symmetric stretching mode dominated by the motion of the "shuttling proton" along the C_3 axis, mirroring our earlier assessment of this motion in the case of the $(NH_4^+Cl^-)^-$ system.[21]

The results of our theoretical studies on these two systems are consistent with our experimental results. Theory predicts that for both systems the neutral complexes are linear and hydrogen-bonded, whereas for both anionic complexes the preferred configuration is the proton transferred ionic salt, $(NH_4^+X^-)^-$. As shown in Table 3.3, the halogen-hydrogen distances in the neutral complexes, although extended, are close to those of the free hydrogen halide. However, the distance from the nitrogen to the shuttling proton in each neutral complex is substantially larger than a nitrogen-hydrogen bond in the free ammonium cation. This indicates a covalently bonded hydrogen halide which is non-covalently bonded to an ammonia molecule. Conversely in the anions, the distance from the nitrogen to the shuttling proton is close to that seen in the ammonium cation, albeit slightly elongated. Furthermore, the distance from the halogen atom to this proton is much larger than that in the free hydrogen halides. This implies that the proton has been fully transferred and covalently bonded by the nitrogen, and that a non-covalent interaction exists between that hydrogen and the halide anion.

In the case of $(NH_4^+Br^-)^-$, there is excellent agreement between the experimental and theoretical VDE values (0.67 ± 0.02 eV vs. 0.65 eV, respectively). Initial assignments for the adiabatic electron affinity (EA_a) of ammonium bromide focused on the first visible peak centered at EBE = 0.41 eV. However, by subtracting the nearest vibrational spacing (0.131 eV) from the peak center at EBE = 0.41 eV, we arrived at a

value of 0.28 eV, which is consistent with the theoretically proposed value of 0.26 eV for the EA_a value of ammonium bromide. Furthermore, upon careful comparison of the peak patterns in the $(NH_4^+Cl^-)^-$ and the $(NH_4^+Br^-)^-$ photoelectron spectra, one sees that the $(NH_4^+Br^-)^-$ spectrum is missing the lowest EBE (origin) peak seen in the $(NH_4^+Cl^-)^-$ spectrum. This is likely caused by the relatively lower signal-to-noise ratio of the $(NH_4^+Br^-)^-$ spectrum as compared to the $(NH_4^+Cl^-)^-$ spectrum. Based on the foregoing, we put forth 0.28 ± 0.05 eV as the best value for the EA_a of ammonium bromide.

In the case of $(NH_4^+I^-)^-$, we again find excellent agreement between the experimental and calculated values of the VDE (0.81 ± 0.04 eV and 0.77 eV, respectively). In this case, the theoretically proposed EA_a value of 0.47 eV is consistent with the weak peak centered at EBE ~ 0.45 eV. We thus take the EA_a to be 0.45 ± 0.05 eV. Interestingly, despite a relatively strong $(NH_4^+I^-)^-$ ion signal, its photoelectron spectrum was weak by comparison with those of $(NH_4^+Cl^-)^-$ and $(NH_4^+Br^-)^-$, revealing a photodetachment cross section for $(NH_4^+I^-)^-$ that is roughly ten times less than that of $(NH_4^+Cl^-)^-$. (The fact that the photoelectron spectrum of $(NH_4^+Br^-)^-$ has a slightly lower signal-to-noise ratio than that of $(NH_4^+Cl^-)^-$ is mostly due to a lower $(NH_4^+Br^-)^-$ ion intensity rather than to a lower photodetachment cross section.)

3.6. Discussion

The results provide strong evidence that the anionic complexes of ammonia-hydrogen bromide and ammonia-hydrogen iodide are, in fact, the anions of the salts, $(NH_4^+Br^-)^-$ and $(NH_4^+I^-)^-$. Moreover, as in the ammonia-hydrogen chloride system reported previously,[21] their corresponding neutral complexes are linear and hydrogen-bonded, with little or no proton transfer. Consistent with these findings is the similarity, as mentioned above, between the photoelectron spectrum of $(NH_4^+Cl^-)^-$ and those of $(NH_4^+Br^-)^-$ and $(NH_4^+I^-)^-$. Comparing the experimental VDE and EA_a values, we see an increase from the chloride to the bromide case of 0.13 eV and 0.20 eV and from the bromide to the iodide case of 0.14 eV and 0.17 eV, respectively – a consistent yet relatively modest change. Similar comparisons are seen among the theoretically-predicted VDE and EA_a values, and these are plotted in Figure 3.4. Both the $(NH_4^+Br^-)^-$ and the $(NH_4^+I^-)^-$ photoelectron spectra also show vibrational progressions due to the proton shuttling mode ($N^{\cdots}H_s^{\cdots}X$). The vibrational spacings for the most intense peaks have shrunk from 0.154 eV (1242 cm^{-1}) in the $(NH_4^+Cl^-)^-$ spectrum to 0.135 eV (1089

cm^{-1}) in the $(NH_4^+Br^-)^-$ spectrum, largely reflecting the greater mass of bromine over chlorine. The vibrational spacings in the $(NH_4^+I^-)^-$ spectrum follow the same trend. The local minimum in the neutral potential energy surface of NH_3HI (Figure 3.3 (b)) around the proton-transferred geometry should be noted. This has a depth of approximately 50 meV. As the structure of the spectrum arises from the formation of a vibrationally excited neutral in this region of the potential energy surface upon removal of the electron, this complication may contribute to the poor resolution of the vibrational structure.

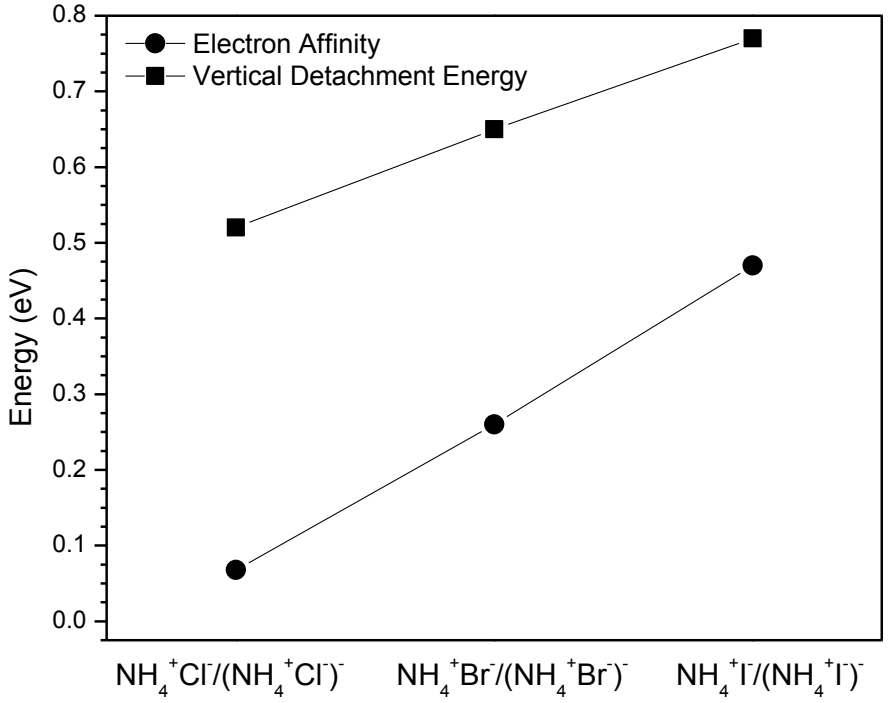

Figure 3.4: Comparison of computed EA_a and VDE values for $NH_3\cdots HCl$ and $(NH_4^+Cl^-)^-$, $NH_3\cdots HBr$ and $(NH_4^+Br^-)^-$, and $NH_3\cdots HI$ and $(NH_4^+I^-)^-$, respectively. Values for $NH_3\cdots HCl$ and $(NH_4^+Cl^-)^-$ were taken from reference 21.

Conceptually, the fact that proton transfer is made favorable by the addition of an excess electron can be rationalized in terms of the stabilization of the excess electron by the increased dipole moment on the ionic system versus the hydrogen-bonded one. This can be visualized by comparing the two plots in Figure 3.5, these depicting the volumes of 50% electron iso-surfaces for the LUMO of neutral $NH_3\cdots HBr$ and for the SOMO of anionic $(NH_4^+Br^-)^-$.

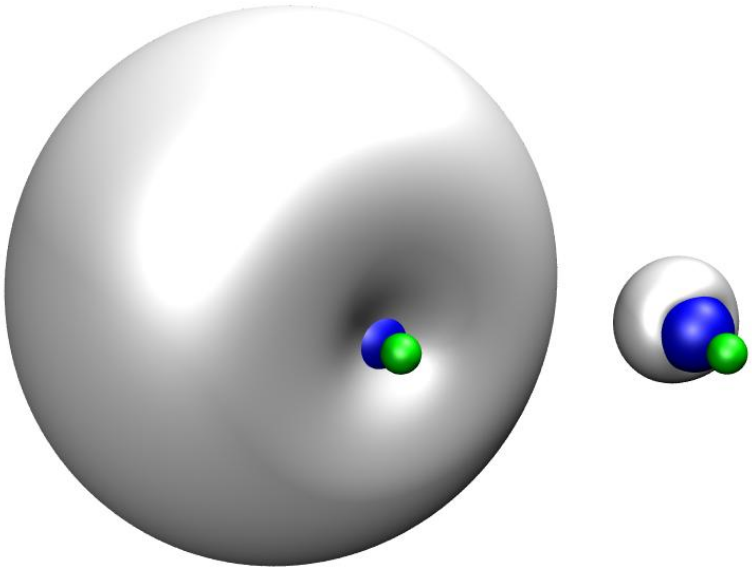

Figure 3.5: Plots depicting the volumes of 50% electron iso-surfaces for the LUMO of neutral NH_3···HBr on the left and for the SOMO of anionic $(NH_4^+Br^-)^-$ on the right.

Insight is also provided by considering the energetics of these systems. For example, consider forming the separated NH_4^+/Cl^- ion pair from NH_3 and HCl molecules. For proton transfer between the gas-phase, non-interacting acid and base, i.e., the transformation from NH_3 + HCl to NH_4^+ + Cl^- shown in Figure 3.6, the energy needed is the difference in the gas-phase proton affinities of ammonia and the chloride anion, calculated as 5.37 eV (5.58 eV, if we correct for zero-point energy and counterpoise). However, the transformation from the H_3N···HCl neutral complex to the net neutral H_3NH^+···Cl^- salt requires only 0.38 eV. This is a much lower energy than the proton transfer between the two isolated fragments. (Here, we used our *a priori* knowledge of the proton-transferred structure and disregarded the unavailable zero-point vibrational energy.)

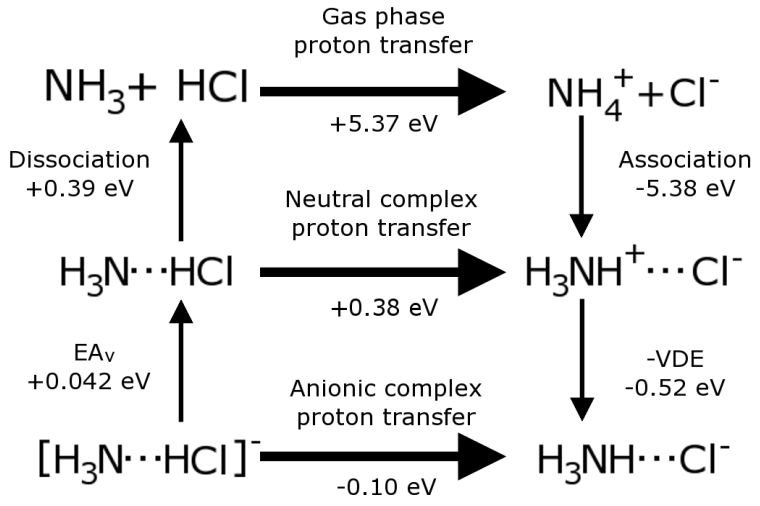

Figure 3.6: Energetic cycles relating to the formation of the ammonium chloride anion.

The reason for this is that the energy recovered by associating the ammonium chloride ion pair (NH_4^+ + Cl^- to $H_3NH^{+\cdots}Cl^-$) is significantly more than the energy needed to dissociate the ammonia-hydrogen chloride, hydrogen bonded, neutral complex ($H_3N^{\cdots}HCl$ to NH_3 + HCl). The difference in dissociation energies is 4.99 eV (4.97 eV with counterpoise, ZPE unavailable for $NH_4^+Cl^-$). If we traverse the diagram, we can see that the extra electrostatic stability accounts for the bulk of the energy needed to transfer the proton, dropping the endothermicity by 4.99 eV from 5.37 eV to 0.38 eV. However, proton transfer is still not spontaneous in the neutral.

The situation changes qualitatively with the addition of an excess electron. It can be seen that the vertical attachment energy of the excess electron to the neutral complex (EA_v = 0.042 eV, $H_3N^{\cdots}HCl$ to $[H_3N^{\cdots}HCl]^-$) is significantly lower than the vertical detachment energy from the anionic complex (VDE = 0.52 eV, $H_3NH^{\cdots}Cl^-$ to $H_3NH^{+\cdots}Cl^-$). That is to say, the extra electron is more stable by 0.482 eV when the anionic complex is of the ionic, proton-transferred type. This makes intuitive sense, given the larger dipole moment in the ionic form (4.31 D for the neutral at the hydrogen-bonded geometry, versus 10.01 D for the neutral at the ionic geometry). It is this extra 0.482 eV stabilization which "tips the balance" in favor of the electron-induced, proton transfer process, from endothermic by 0.38 eV to exothermic by 0.10 eV.

This scenario also holds for the bromide and the iodide. Similar schemes are provided in Figure 3.7 and Figure 3.8. Comparing the ammonia-hydrogen bromide complex to the ammonia-hydrogen chloride complex, a lessened proton affinity difference of 5.01 eV (5.20 eV with counterpoise and ZPE corrections) is partially counterbalanced by a lowered dissociation energy difference of 4.73 eV (4.69 eV with counterpoise), leaving a reduced endothermicity of 0.28 eV to proton transfer in the neutral complex. Formation of the ionic complex in the anion stabilizes the excess electron by 0.65 eV, resulting in an exothermicity of -0.33 eV for proton transfer in the anionic complex. The neutral dipole moment at the hydrogen-bonded geometry is 4.20 D, while that at the ionic geometry is 10.95 D.

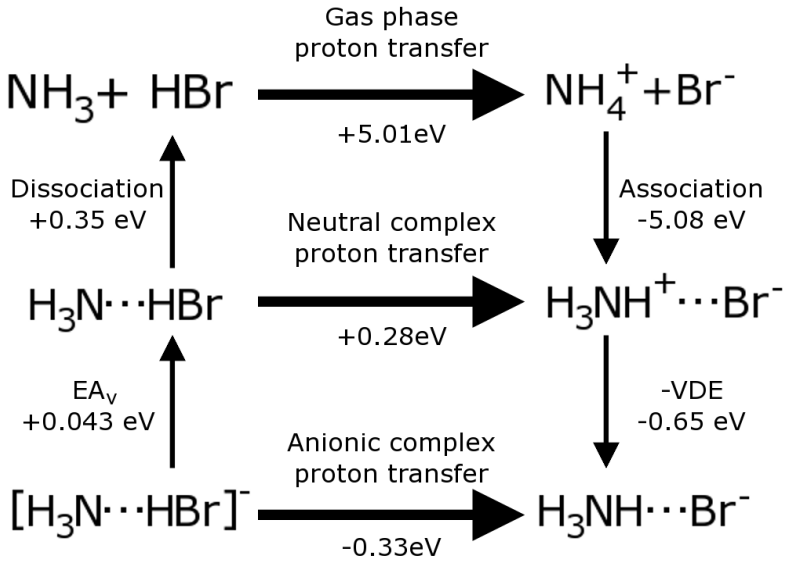

Figure 3.7: Energetic cycles relating to the formation of the ammonium bromide anion.

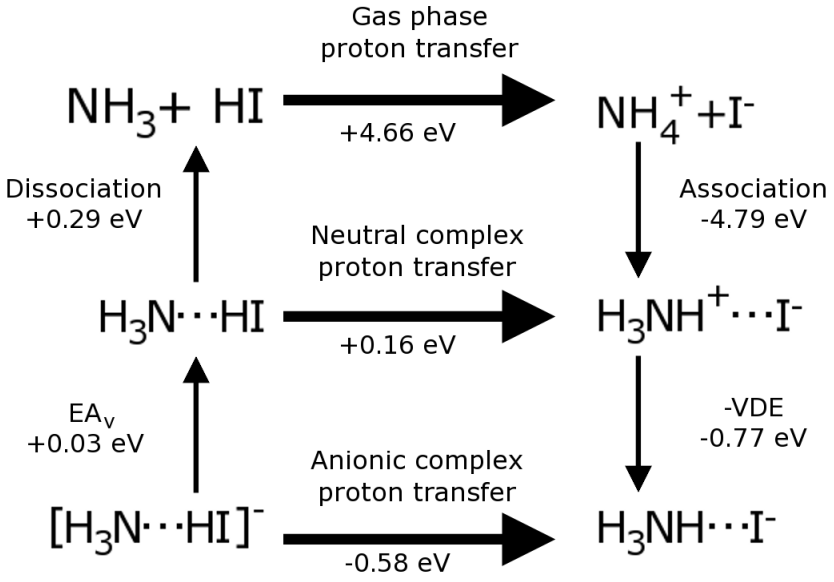

Figure 3.8: Energetic cycles relating to the formation of the ammonium iodide anion.

For iodine, the proton affinity difference is 4.66 eV (4.83 eV), with the dissociation energy difference for the neutral, ionic complex 4.50 eV (4.43 eV) higher than that of the hydrogen-bonded, neutral complex, resulting in a 0.16 eV endothermicity for proton transfer in the neutral complex. Forming the ionic complex in the anion stabilizes the excess electron by a net 0.74 eV, i.e., -0.77 - 0.03 eV, resulting in an exothermicity of -0.58 eV for proton transfer in the anionic complex. The neutral dipole moments are 3.74 D and 11.69 D for the hydrogen-bonded and ionic geometries, respectively.

Note that proton transfer in the neutral complexes approach spontaneity in all three systems as the halogen size, and thus acidity, increases. With increasing halogen size, the hydrogen halide becomes a stronger acid, and therefore proton transfer in the neutral becomes less endothermic. Therefore, it is expected that proton transfer will become spontaneous in the neutral with slightly stronger bases or acids than those considered here.

Furthermore, as reflected in both the experimental and the theoretical results, the stabilization of the excess electron, brought on by forming the anionic ionic complex, grows with increasing halogen size, making electron-induced, proton transfer increasingly exothermic.This is the dominant contribution to the trend. This stabilization arises in part due to the declining dipole moments of the hydrogen-bonded, neutral complexes (4.31 D, 4.20 D, and 3.74 D for NH_3···HCl, NH_3···HBr, NH_3···HI, respectively), and in part due to the increasing dipole moments of the ionic systems (10.01 D, 10.95 D, and 11.69 D for $NH_4^+Cl^-$, $NH_4^+Br^-$, and $NH_4^+I^-$, respectively). These, in turn, are due to the reduced polarization of the H-X bond in the hydrogen halides of the hydrogen-bonded complexes and to the increasing N-X distances in the ionic systems, respectively.

It is noteworthy from an "orbital taxonomy" perspective that in these proton transfer processes, the excess electron shifts from a distinctly dipole-bond orbital at the neutral equilibrium geometry to a much more compact orbital akin to a distorted valence *s* orbital (forming the distorted NH_4 Rydberg molecular moiety) at the anion equilibrium geometry.

3.7. References

[1] I. Alkorta, I. Rozas, O. Mo, M. Yanez and J. Elguero, *Hydrogen bond vs proton transfer between neutral molecules in the gas phase*, J. Phys. Chem. A, **105**, 7481-7485 (2001)

[2] E. Clementi and J. N. Gayles, *Study of the Electronic STructure of Molecules. VII. Inner and Outer Complex in the NH_4Cl Formation from NH_3 and HCl*, J. Chem. Phys., **47**, 3837-3841 (1967)

[3] Z. Latajka, S. Sakai, K. Morokuma and H. Ratajczak, *Possible Gas-Phase Ion-Pairs in Amine-HCl Complexes - an Ab initio Theoretical Study*, Chem. Phys. Lett., **110**, 464-468 (1984)

[4] A. Brciz, A. Karpfen, H. Lischka and P. Schuster, *A Candidate for an Ion-Pair in the Vapor-Phase - Proton-Transfer in Complexes $R_3N{\cdot}HX$*, Chem. Phys., **89**, 337-343 (1984)

[5] E. J. Goodwin, N. W. Howard and A. C. Legon, *The Rotational Spectrum of N-15-Ammonium Chloride Vapor - Characterization of the Hydrogen-Bonded Dimer $H_3N^{\cdots}HCl$*, Chem. Phys. Lett., **131**, 319-324 (1986)

[6] A. C. Legon, *The Nature of Ammonium and Methylammonium Halides in the Vapor-Phase - Hydrogen-Bonding Versus Proton-Transfer*, Chem. Soc. Rev., **22**, 153-163 (1993)

[7] B. S. Ault and G. C. Pimentel, *Infrared Spectra of the Ammonia-Hydrochloric Acid Complex in Solid Nitrogen*, J. Phys. Chem., **77**, 1649-1653 (1973)

[8] L. Andrews, X. F. Wang and Z. Mielke, *Infrared spectrum of the H_3N-HCl complex in solid neon*, J. Am. Chem. Soc., **123**, 1499-1500 (2001)

[9] L. Andrews, X. F. Wang and Z. Mielke, *Infrared spectrum of the H_3N-HCl complex in solid Ne, Ne/Ar, Ar, and Kr. Matrix effects on a strong hydrogen-bonded complex*, J. Phys. Chem. A, **105**, 6054-6064 (2001)

[10] A. J. Barnes and A. C. Legon, *Proton transfer in amine-hydrogen halide complexes: comparison of low temperature matrices with the gas phase*, J. Mol. Struct., **448**, 101-106 (1998)

[11] C. S. Brauer, M. B. Craddock, J. Kilian, E. M. Grumstrup, M. C. Orilall, Y. R. Mo, J. L. Gao and K. R. Leopold, *Amine-hydrogen halide complexes: Experimental electric dipole moments and a theoretical decomposition of dipole moments and binding energies*, J. Phys. Chem. A, **110**, 10025-10034 (2006)

[12] G. Corongiu, D. Estrin, G. Murgia, L. Paglieri, L. Pisani, G. S. Valli, J. D. Watts and E. Clementi, *Revisiting the potential energy surface for [$H_3N^{\cdots}HCl$]: An ab initio and density functional theory investigation*, Int. J. Quantum Chem, **59**, 119-134 (1996)

[13] M. Ramos, I. Alkorta, J. Elguero, N. S. Golubev, G. S. Denisov, H. Benedict and H. H. Limbach, *Theoretical study of the influence of electric fields on hydrogen-bonded acid-base complexes*, J. Phys. Chem. A, **101**, 9791-9800 (1997)

[14] R. Cazar, A. Jamka and F. M. Tao, *Proton transfer reaction of hydrogen chloride with ammonia: is it possible in the gas phase?*, Chem. Phys. Lett., **287**, 549-552 (1998)

[15] R. A. Cazar, A. J. Jamka and F. M. Tao, *Ab initio investigation of proton transfer in ammonia hydrogen chloride and the effect of water molecules in the gas phase*, J. Phys. Chem. A, **102**, 5117-5123 (1998)

[16] J. E. Del Bene and M. J. T. Jordan, *A comparative study of anharmonicity and matrix effects on the complexes XH : NH_3, X=F, CI, and Br*, J. Chem. Phys., **108**, 3205-3212 (1998)

[17] F. M. Tao, *Direct formation of solid ammonium chloride particles from HCl and NH_3 vapors*, J. Chem. Phys., **110**, 11121-11124 (1999)

[18] M. J. T. Jordan and J. E. Del Bene, *Unraveling environmental effects on hydrogen-bonded complexes: Matrix effects on the structures and proton-stretching frequencies of hydrogen-halide complexes with ammonia and trimethylamine*, J. Am. Chem. Soc., **122**, 2101-2115 (2000)

[19] B. Cherng and F. M. Tao, *Formation of ammonium halide particles from pure ammonia and hydrogen halide gases: A theoretical study on small molecular clusters $(NH_3\text{-}HX)_n$ (n=1, 2, 4; X = F, Cl, Br)*, J. Chem. Phys., **114**, 1720-1726 (2001)

[20] M. Biczysko and Z. Latajka, *Accuracy of theoretical potential energy profiles along proton-transfer coordinate for $XH\text{-}NH_3$ (X = F, Cl, Br) hydrogen-bonded complexes*, J. Phys. Chem. A, **106**, 3197-3201 (2002)

[21] S. N. Eustis, D. Radisic, K. H. Bowen, R. A. Bachorz, M. Haranczyk, G. K. Schenter and M. Gutowski, *Electron-Driven Acid-Base Chemistry: Proton Transfer from Hydrogen Chloride to Ammonia*, Science, **319**, 936-939 (2008)

[22] N. W. Howard and A. C. Legon, *An investigation of the hydrogen-bonded dimer H_3N-HBr by pulsed-nozzle, fourier-transform microwave spectroscopy of the ammonium bromide vapor.*, J. Chem. Phys., **86**, 6722-6730 (1987)
[23] B. S. Ault, E. Steinback and G. C. Pimentel, *Matrix Isolation Studies of Hydrogen Bonding. The Vibrational Correlation Diagram.*, J. Phys. Chem., **79**, 615-620 (1975)
[24] A. J. Barnes and M. P. Wright, *Strongly Hydrogen-Bonded Molecular-Complexes Studied by Matrix-Isolation Vibrational Spectroscopy .3. Ammonia-Hydrogen Bromide and Amine-Hydrogen Bromide Complexes*, J. Chem. Soc., Faraday Trans. 2, **82**, 153-164 (1986)
[25] L. Andrews and X. F. Wang, *Infrared spectra of the H_3N-HBr complex in solid Ne, Ne/Ar, Ar, Kr, and N_2. Strong matrix effects on a hydrogen-bonded complex*, J. Phys. Chem. A, **105**, 6420-6429 (2001)
[26] P. G. Jasien and W. J. Stevens, *Theoretical Studies of Potential Gas-Phase Charge-Transfer Complexes: NH_3+HCl,NH_3+HBr,NH_3+HI*, Chem. Phys. Lett., **130**, 127-131 (1986)
[27] Z. Latajka, S. Scheiner and H. Ratajczak, *The Proton Position in Amine HX (X = Br, I) Complexes*, Chem. Phys., **166**, 85-96 (1992)
[28] M. F. Ruiz-Lopez, F. Bohr, M. T. C. Martins-Costa and D. Rinaldi, *Studies of Solvent Effects Using Density Functional Theory. Cooperative Interactions in $H_3N^{\cdots}HBr$ Proton Transfer*, Chem. Phys. Lett., **221**, 109-116 (1994)
[29] A. C. Legon and D. Stephenson, *Is Ammonium Iodide an Ion Pair $H_3N^{+}H^{\cdots}I^{-}$ or a Hydrogen-bonded Species $H_3N^{\cdots}HI$ in the Gas Phase?*, J. Chem. Soc., Faraday Trans., **88**, 761-762 (1992)
[30] A. C. Legon, *Isolation and Characterization of Some Transient Complexes of Chemical Interest Using Pulsed-Nozzle, Fourier-Transform Microwave Spectroscopy*, J. Mol. Struct., **266**, 21-37 (1992)
[31] L. Schriver, A. Schriver and J. P. Perchard, *Spectroscopic Evidence for Proton-Transfer within the Bimolecular Complex HI-NH_3 Trapped in Cryogenic Matrices*, J. Am. Chem. Soc., **105**, 3843-3848 (1983)
[32] L. Schriver, *Comparison of the Proton and Deuteron Transfer in the Hydrogen (Deuterium) Iodide Ammonia or Trimethylamine Systems Trapped in Argon and Nitrogen*, Spectrochim Acta A, **43**, 1155-1160 (1987)
[33] L. Andrews and X. F. Wang, *Infrared spectrum of the H_3N-HI complex in solid Ne, Ar, Ne/Ar, Kr, and N_2. Comparisons of matrix effects on hydrogen-bonded complexes*, J. Phys. Chem. A, **105**, 7541-7550 (2001)
[34] P. Kollman, A. Dearing and E. Kochanski, *Ab Initio Self-Consistent Fieid Calculations on I_2-NH_3 and HI-NH_3. The Classic "Charge-Transfer" Interaction, an Example of Gas-Phase Proton Transfer, and the Duality of Lewis Acid Sites on HI*, J. Phys. Chem., **86**, 1607-1610 (1982)
[35] J. V. Coe, J. T. Snodgrass, C. B. Freidhoff, K. M. McHugh and K. H. Bowen, *Photoelectron spectroscopy of the negative cluster ions $NO^{-}(N_2O)_n$=1,2*, J. Chem. Phys., **87**, 4302-4309 (1987)
[36] M. Gutowski, P. Skurski, A. I. Boldyrev, J. Simons and K. D. Jordan, *Contribution of electron correlation to the stability of dipole-bound anionic states*, Phys. Rev. A, **54**, 1906-1909 (1996)
[37] M. Gutowski, K. D. Jordan and P. Skurski, *Electronic Structure of Dipole-Bound Anions*, J. Phys. Chem. A, **102**, 2624-2633 (1998)
[38] T. H. Dunning, *Gaussian basis sets for use in correlated molecular calculations. I. The atoms boron through neon and hydrogen*, J. Chem. Phys., **90**, 1007-1023 (1989)

[39] R. A. Kendall, T. H. Dunning and R. J. Harrison, *Electron affinities of the first-row atoms revisited. Systematic basis sets and wave functions*, J. Chem. Phys., **96**, 6796-6806 (1992)
[40] D. E. Woon and T. H. Dunning, *Gaussian basis sets for use in correlated molecular calculations. III. The atoms aluminum through argon*, J. Chem. Phys., **98**, 1358-1371 (1993)
[41] P. Skurski, M. Gutowski and J. Simons, *How to choose a one-electron basis set to reliably describe a dipole-bound anion*, Int. J. Quantum Chem, **80**, 1024-1038 (2000)
[42] K. Peterson, D. Figgen, E. Goll, H. Stoll and M. Dolg, *Systematically convergent basis sets with relativistic pseudopotentials. II. Small-core pseudopotentials and correlation consistent basis sets for the post-d group 16-18 elements*, J. Chem. Phys., **119**, 11113-11123 (2003)
[43] Gaussian 03, Revision C.02, M. J. Frisch, G. W. Trucks, H. B. Schlegel, G. E. Scuseria, M. A. Robb, J. R. Cheeseman, J. A. Montgomery Jr., T. Vreven, K. N. Kudin, J. C. Burant, J. M. Millam, S. S. Iyenga, J. Tomasi, V. Barone, B. Mennucci, M. Cossi, G. Scalmani, N. Rega, G. A. Petersson, H. Nakatsuji, M. Hada, M. Ehara, K. Toyota, R. Fukuda, J. Hasegawa, M. Ishida, T. Nakajima, Y. Honda, O. Kitao, H. Nakai, M. Klene, X. Li, J. E. Knox, H. P. Hratchian, J. B. Cross, C. Adamo, J. Jaramillo, R. Gomperts, R. E. Stratmann, O. Yazyev, A. J. Austin, R. Cammi, C. Pomelli, J. W. Ochterski, P. Y. Ayala, K. Morokuma, G. A. Voth, P. Salvador, J. J. Dannenberg, V. G. Zakrzewski, S. Dapprich, A. D. Daniels, M. C. Strain, O. Farkas, D. K. Malick, A. D. Rabuck, K. Raghavachari, J. B. Foresman, J. V. Ortiz, Q. Cui, A. G. Baboul, S. Clifford, J. Cioslowski, B. B. Stefanov, G. Liu, A. Liashenko, P. Piskorz, I. Komaromi, R. L. Martin, D. J. Fox, T. Keith, M. A. Al-Laham, C. Y. Peng, A. Nanayakkara, M. Challacombe, P. M. W. Gill, B. Johnson, W. Chen, M. W. Wong, C. Gonzalez and J. A. Pople, Gaussian, Inc., Wallingford CT, 2004
[44] G. Schaftenaar and J. H. Noordik, *Molden: a pre- and post-processing program for molecular and electronic structures*, J. Comput. Aided Mol. Des., **14**, 123-134 (2000)
[45] W. Humphrey, A. Dalke and K. Schulten, *VMD: Visual molecular dynamics*, J. Mol. Graphics Modell., **14**, 33-38 (1996)
[46] M. Haranczyk and M. Gutowski, *Visualization of molecular orbitals and the related electron densities*, J. Chem. Theory Comput., **4**, 689-693 (2008)
[47] T. M. Miller, D. G. Leopold, K. K. Murray and W. C. Lineberger, *Electron affinities of the alkali halides and the structure of their negative ions*, J. Chem. Phys., **85**, 2368-2375 (1986)

Chapter 4: Potential Energy Surfaces of the Neutral NH_3···HX (X=F, Cl, Br, I, At) Dimers

In preparation (A. Whiteside, M. Gutowski)

4.1. Abstract

The equilibrium structures and potential energy surfaces of the ammonia-hydrogen fluoride and ammonia-hydrogen astatide complexes are presented and characterised. NH_3HF is found to take a neutral pair structure at -1930 mH with respect to the free monomers, while NH_3HAt supports both a neutral pair and ion pair minimum at -6.31 mH and -2.16 mH respectively. The energetics of proton transfer in the full range of ammonia-hydrogen halide complexes are evaluated by investigating the forces acting upon the proton, as decomposed into one- and two-body terms. Halogen bonded structures of NH_3HX, where X is bromine, iodine, or astatine, are reported with energies of -1.03 mH, -2.83 mH, and -4.72 mH, respectively. These systems are characterised in depth.

4.2. Introduction

The ammonia-hydrogen halide systems have been of great theoretical interest to chemists since Mulliken first used ammonia-hydrogen chloride as an example charge-transfer complex in his early studies.[1] Early insights into intermolecular interactions and the challenges of experimental investigation led to a lengthy period of investigation into the degree of proton transfer within these systems.[2-12] In a recent paper[13] and the preceding chapter, we have discussed the role of an electron in triggering proton transfer in these complexes. However we have not directly addressed the issue of why and how proton transfer occurs in the corresponding neutrals. Furthermore, we have not discussed the possible alternative structures these systems may adopt.

The complexes of NH_3HX are experimentally known to adopt a C_{3v} hydrogen-bonded structure (Figure 4.1).[14,15] However the degree of proton transfer is highly matrix-dependent in experiment and method-dependent in theory.[2,16-32] Although it is now well-established that all of the systems adopt a neutral-pair ("N") structure NH_3…HX, [12,33-38] the matrix sensitivity of the results in matrix IR studies suggests that these systems are energetically close to proton transfer (PT) to form a zwitterionic ("Z") structure. What is the source of this careful balancing act? What factors are at play in

driving proton transfer? Are these systems qualitatively distinct, as suggested by the difference in the structures adopted, or is there an underlying commonality?

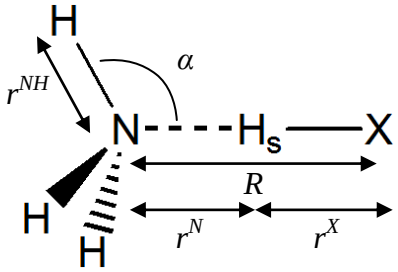

Figure 4.1: H_3N•••HX hydrogen bonded structure. "H_s" refers to the "shuttling proton".

Having described the relaxed potential energy surfaces of NH_3HBr and NH_3HI in the preceding chapter, and NH_3HCl in a past paper,[13] here we present the relaxed potential energy surfaces of NH_3HF and NH_3HAt, calculated with counterpoise corrections and careful consideration of how the systems can be best described to gain access to the proton transfer problem. Furthermore, the minima have been fully characterised at a high level of theory. These potential surfaces and minima can then be compared to the previous surfaces for Cl, Br, and I, which have been slightly improved with counterpoise corrections.

In investigating the heavier halides, it became clear that the dipole moment on NH_3HAt is very low, and the arrangement of charge is ambiguous. Astatine's electronegativity is similar to that of hydrogen, and therefore it is not obvious in which direction the dipole moment will lie. This is suggestive of a complex in which the *halogen* is the positively charged species directed at ammonia, which in turn is suggestive of halogen bonds. These counterintuitive interactions take advantage of the region of positive charge known as the "sigma hole" that appears on a halogen as the antipode of a covalent bond, and allow a *negatively* charged halogen to bond with an electron donor. By analogy to hydrogen bonds, the systems are identified as the halogen bond donor (electron acceptor) and halogen bond acceptor (electron donor).

To establish whether this is a plausible mode of interaction for the hydrogen halides, and to what degree it competes with the hydrogen-bonded structure, we computed potential energy surfaces for the "backwards" approach of H-X to NH_3, and attempted to find and characterise minima (Figure 4.2).

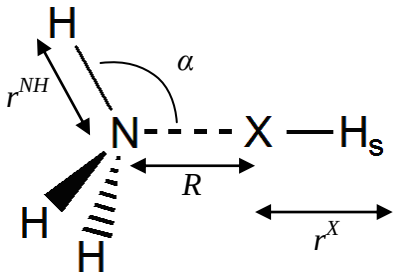

Figure 4.2: H_3N•••XH halogen bonded structure.

4.3. Computational methods

The energy of a neutral complex X-Y at a geometry G can be written as:

$$E_{X-Y}(G) = E_X(G_X) + E_Y(G_Y) + E^X_{1-b}(G) + E^Y_{1-b}(G) + E^{X-Y}_{2-b}(G) \qquad (111)$$

where $E_W(G_W)$ is the energy of the monomer (W= X or Y) at its equilibrium geometry G_W and

$$E^W_{1-b}(G) = E_W(G) - E_W(G_W) \qquad (112)$$

$$E^{X-Y}_{2-b}(G) = E_{X-Y}(G) - E_X(G) - E_Y(G) \qquad (113)$$

The first two terms on the right hand side of Equation 111 are the energies of the free relaxed monomers, and the sum of their energies constitutes the zero of energy in this analysis. The term $E^W_{1-b}(G)$ (Equation 112) is the one-body energy for monomer W; the increase of the energy as a result of its geometrical deformation (from G_W to G) when the complex is formed. $E^{X-Y}_{2-b}(G)$ (Equation 113) is the two-body interaction between the monomers X and Y after they adopt the geometry of the complex (G). The $E^W_{1-b}(G)$ term is positive or zero by definition (notwithstanding methodological limitations), while the sign of $E^{X-Y}_{2-b}(G)$ depends on the geometry of the complex; it is negative near the minimum energy structure of the X-Y complex.

The expression for the total energy $E_{X-Y}(G)$ can be rewritten as:

$$E_{X-Y}(G) = E_X(G_X) + E_Y(G_Y) + E_{stab}(G) \qquad (114)$$

where:

$$E_{stab}(G) = E^X_{1-b}(G) + E^Y_{1-b}(G) + E^{X-Y}_{2-b}(G) \qquad (115)$$

$E_{stab}(G)$ represents the stabilization energy of the X-Y complex at the geometry of the complex G. The force $F(G)$ (a vector) is defined as the finite difference approximation

to the derivative of the energy, where for a given pair of points G_n and G_{n+1} on the potential energy surface:

$$F\left(\frac{G_n + G_{n+1}}{2}\right) = \frac{E(G_{n+1}) - E(G_n)}{G_{n+1} - G_n} \tag{116}$$

E may be the stabilisation energy $E_{stab}(G)$, in which case this is the overall force drawing the monomers together; or it may be any one of $E_{1-b}^{W}(G)$ (the restoring force pulling the proton toward a particular monomer) or $E_{2-b}^{X-Y}(G)$ (the force drawing the two distorted monomers together). The sign of the displacement G to G_{n+1} was chosen in such a way that when the force is positive, it is directed towards the N structure (halogen atom), and when it is negative, it is directed toward the Z structure (nitrogen atom).

Depending on the region of the potential energy surface, the X and Y monomers can be NH_3 and HX or NH_4^+ and X^-. We will always use $E_{NH_3}(G_{NH_3}) + E_{HX}(G_{HX})$ as the zero of the energy and we will apply a constant energy shift of $E_{X^-} - E_{HX}(G_{HX}) - (E_{NH_3}(G_{NH_3}) - E_{NH_4^+}(G_{NH_4^+}))$ to the two-body term $E_{2-b}^{NH_4^+ - X^-}(G)$. This term is typically large and negative, as it characterizes the interaction between ions NH_4^+ and X^-; the "shift" is the energetic penalty required to perform proton transfer between the monomers.

The potential energy surfaces, optimised geometries and harmonic frequencies of the complexes were computed at the CCSD level[39] with standard Boys-Bernardi counterpoise corrections.[40-42] The geometric coordinates for the surfaces were defined as the shift of r^X or r^N from the equilibrium value for the free monomer. The monomers were NH_3 and HX in the case of N-type and halogen-bonded minima and NH_4^+ and X^- in the case of Z-type minima. The geometries of the monomers themselves were also optimised, and their vibrational frequencies computed. The CCSD density was used to calculate the dipole moments and effective charges by the Merz-Sing-Kollman method.[43,44] The charge transfer q^T is defined as the total charge on the NH_3 subunit of the NH_3HX molecule, regardless of the choice of N, or halogen-bonded structure, and the total charge on NH_4^+ for Z structures.

All electronic structure calculations were performed in the Gaussian 03[45] and Gaussian 09[46] codes. Tight SCF convergence criteria were imposed. Dunning-type

correlation consistent augmented double- and triple-zeta basis sets (aug-cc-pvdz, aug-cc-pvtz, respectively) were used,[47,48] with pseudopotentials in the case of astatine,[49] and further augmented with a set of 7s and 7p (F-I) or 12s and 11p (At) diffuse functions consistent with the preceding and following chapters, using a progression ratio of 2.5.[50] Henceforth, these basis sets are AVDZ+ and AVTZ+, respectively. AVDZ+ was used for halogen bonded structures, potential energy surfaces, and the hydrogen-bonded minima of the systems with Cl through I. AVTZ+ was used for the hydrogen-bonded minima of the new systems NH_3HF and NH_3HAt. The basis set and pseudopotential for astatine were obtained from the EMSL Basis Set Exchange.[51,52]

The most important geometric parameter in computing the proton transfer potential energy surface is the position of the "shuttling" proton H_s which is transferred between the two monomers. We could have fixed the other coordinates at some arbitrary value, and scanned the proton position to obtain the potential energy surface, but this procedure could lead to artefacts, such as a spurious local minimum for $NH_4^+\cdots Cl^-$.[32] Therefore a relaxed potential energy surface was necessary. However this introduces an additional difficulty: we must define the H_s position with respect to the heavy atom N or X (r^N and r^X in Figure 4.1), and each coordinate is only appropriate in the vicinity of the corresponding heavy atom. In the relaxed surface, at large values of r^N the intermonomer distance R relaxes and the region of the surface near X is not probed (and vice versa). Therefore as detailed in the preceding chapter and in the theory section it is necessary to combine two "complementary" potential energy surfaces. Furthermore, counterpoise corrections were applied with respect to the monomers implied by the choice of coordinate: when scanning r^N, the monomers were NH_4^+ and X^-, while when scanning r^X the monomers were NH_3 and HX (Figure 4.3).(The r^N potential surface for NH_3HF was counterpoise-corrected to NH_3 and HF for reasons apparent in the following chapter, but the forces computed in a separate scan corrected to NH_4^+ and X^-.)

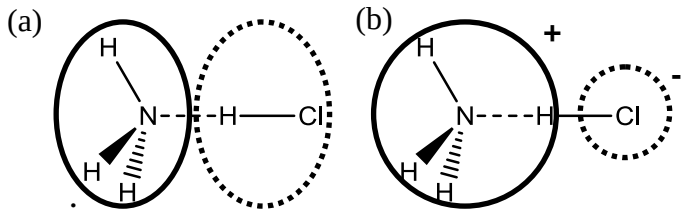

Figure 4.3: The two different monomer definitions used for counterpoise corrections, one with the neutral molecules (a) and one with the ions (b); notice that the same geometry is counterpoise corrected in two different ways

4.4. Results

4.4.1. Hydrogen bonded structures

An N structure was found for F, and both a global minimum N structure and a local minimum Z structure were found for At (Figure 4.4, Figure 4.5). Their relative energies and geometric parameters are summarised in through . The N structures are well-characterised as hydrogen-bonded dimers in which the X-H bond is elongated and softened by hydrogen bonding. Note the importance of the counterpoise correction in correctly determining the relative energies of the N and Z minima, albeit at the cost of potential energy surface discontinuity (Figure 4.6). The potential surface of NH_3HAt is highly anharmonic and therefore harmonic frequencies calculated upon it should be treated as suspect. Notwithstanding this, the Z structure of NH_3HAt is clearly an NH_4^+ cation hydrogen bonded with an astatide anion At^-, with the corresponding red-shift and stretch of the N-H bond.

Table 4.1: Stabilisation energies of N and Z structures of NH_3HF and NH_3HAt (mH)

	N	Z
NH_3HF	-19.295	
NH_3HAt	-6.314	-2.162

Table 4.2: Monomer geometric parameters (as in Figure 4.1), changes upon complex formation, and intermonomer distances, charge transfer (q^T) and dipole moments (μ) for complexes (Å, °, D, e)

	r^{NH}	α	r^X	R	μ	q^T
HF			**0.918**		1.810	
HAt			**1.688**		0.062	
NH_3	**1.012**	**112**			1.528	
NH_3HF	+0.000	-0.3	+0.028	2.671	4.544	0.143
NH_3HAt	+0.001	-0.2	+0.016	3.843	3.036	0.215
NH_4^+	**1.022**	**109.4**	**1.022**			
NH_4At	-0.006	-0.658	+0.097	3.307	10.134	0.475

Table 4.3: Monomer normal modes, changes on complex formation, and intermonomer normal modes for NH_3HF and NH_3HAt (cm^{-1})

	a_1 intermol. str.	e intermol. bend	e intermol. bend	a_1 NH_3 bend	e NH_3 bend	a_1 H-X str.	a_1 NH_3 str.	e NH_3 str.
HF						**4170**		
HAt						**2215**		
NH_3				**1064**	**1686**		**3500**	**3627**
NH_3HF	261	254	941	+97	-0	-624	+1	-2
NH_3HAt	87	136	416	-32	-3	-165	-5	-5

Table 4.4: Monomer normal modes, changes on complex formation, and intermonomer normal modes for NH_4At (cm^{-1})

NH_4^+			t_2 bend		e bend	a_1 str	t_2 str	
			1505	**1505**	**1753**	**3402**	**3520**	**3520**
NH_4At	a_1 intermol. str.	e intermol. bend	a_1 bend	e bend	e bend	a_1 str	a_1 str	e str
	278.3	247	-174	-47	-57	-1487	-52	+78

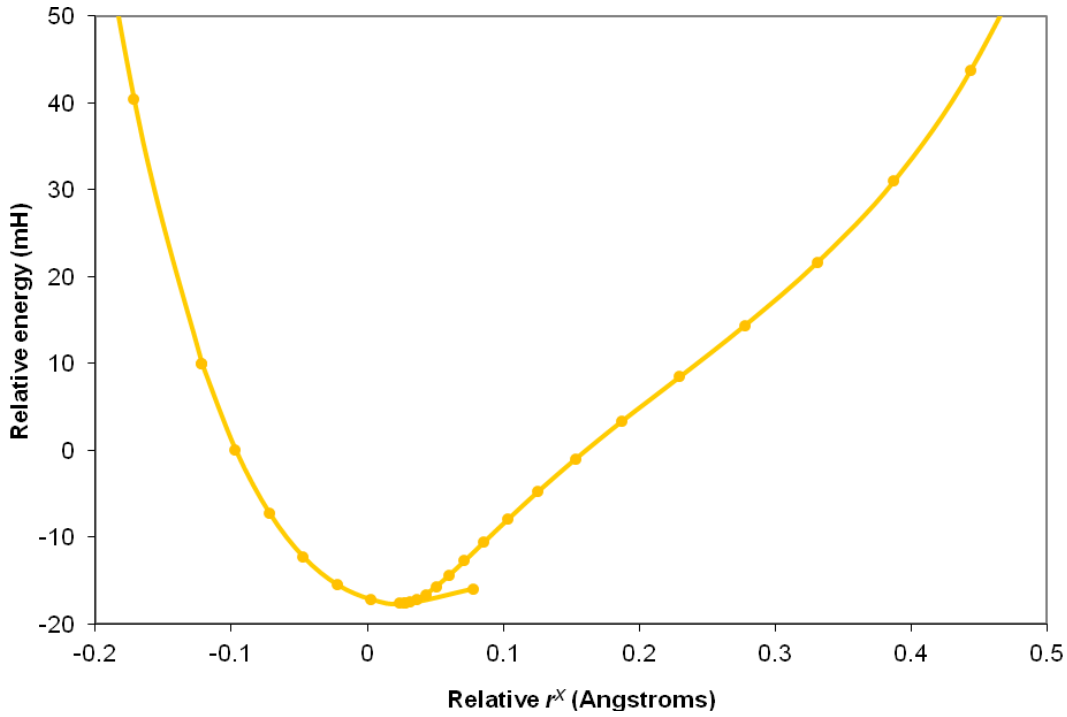

Figure 4.4: Hydrogen-bonding potential energy surface of NH_3HF; coordinates as in Figure 4.1

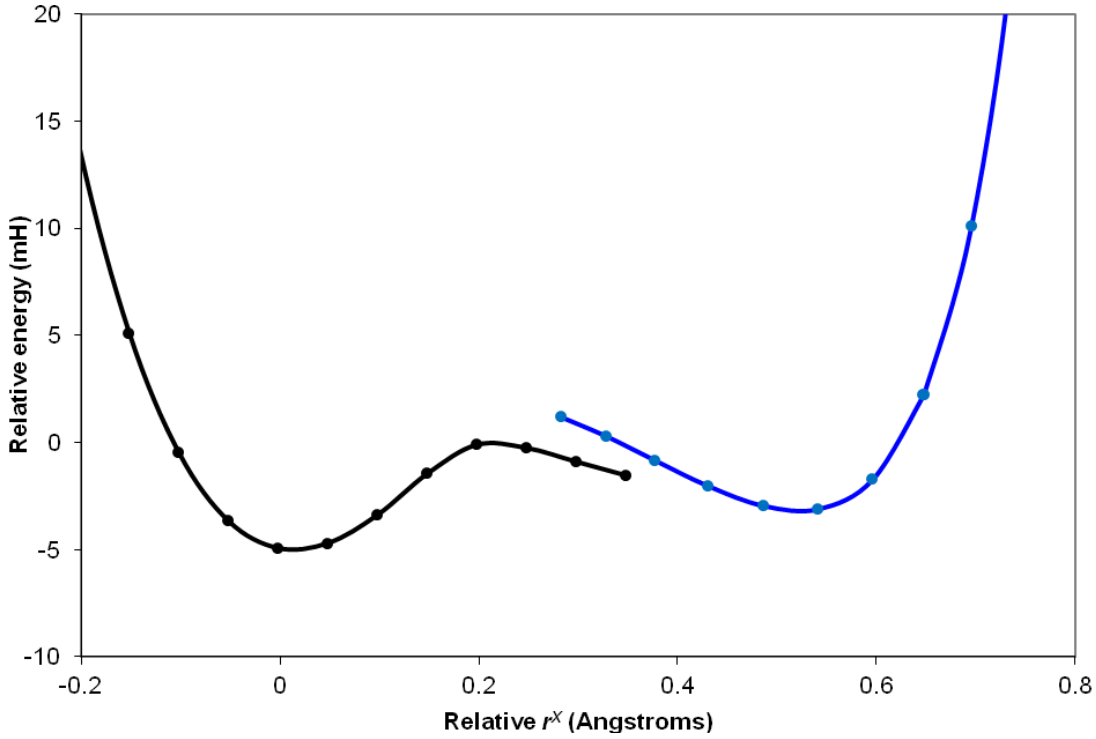

Figure 4.5: Hydrogen-bonding potential energy surface of NH_3HAt. Black and blue denote different counterpoise corrections; coordinates as in Figure 4.1.

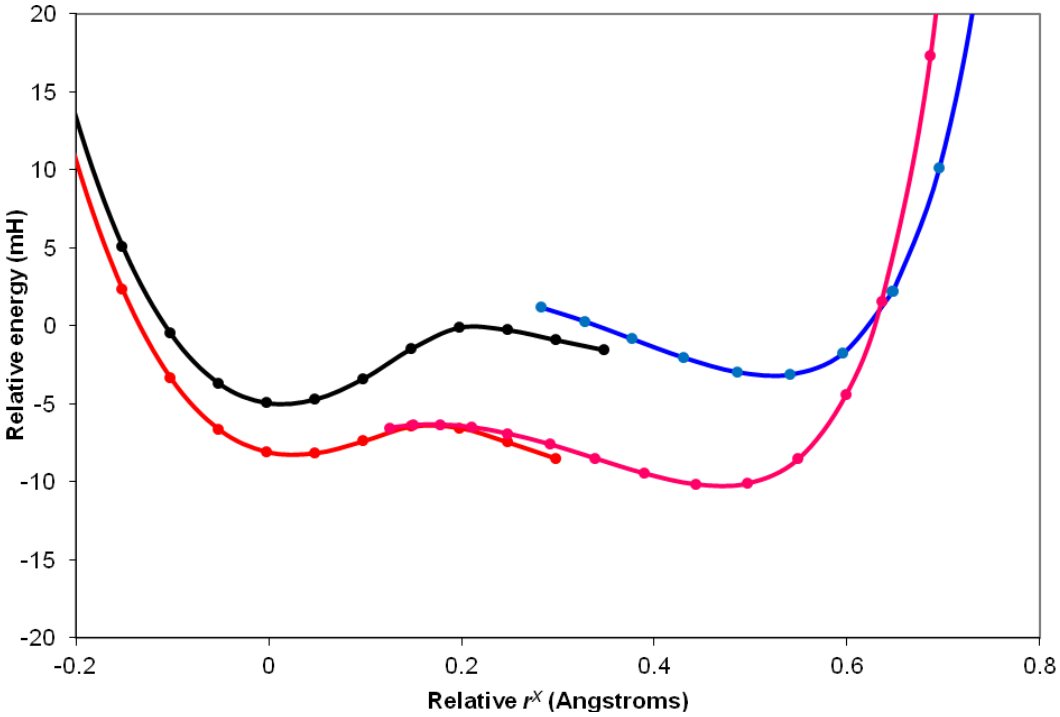

Figure 4.6: Comparison of counterpoise-corrected (black/blue) and counterpoise-uncorrected (red/pink) potential surfaces of NH_3HAt

4.4.2. Halogen bonded structures

Halogen bonded minima were located for the systems where X=Cl, Br, I, At (Figure 4.7). However the minimum for NH_3ClH is very shallow, and the intermolecular bending mode corresponding to the transition to the N structure is soft (actually imaginary, harmonic approximation notwithstanding) and the zero-point corrected energy is therefore only a fraction of a millihartree below the free monomer asymptote (Table 4.5). Therefore it is not likely to be physically meaningful. The remaining minima are modestly stable, and actually competitive in energy with the Z structure and approaching N for astatine (*c.f.*). Note the very small degree of monomer perturbation in geometric parameters and normal modes, particularly in comparison to the hydrogen-bonded structures (Table 4.6 and Table 4.7). Minima are increasingly stable with the increasing halide size, reflected in the stabilisation energy, the reducing R (despite the *increasing* halide size) and the gradual blue shift of the intermolecular stretching/bending modes due to the halogen bond's preference for linearity. These effects arise from the increasing polarisability and declining electronegativity of the halide, which increases the "depth" of the sigma hole. The degree of charge transfer increases with increasing halide size and bond strength, as anticipated (Table 4.5 and

Table 4.6) leading to a surprisingly large dipole moment for the complex with hydrogen astatide which would not be expected from dipole summation.

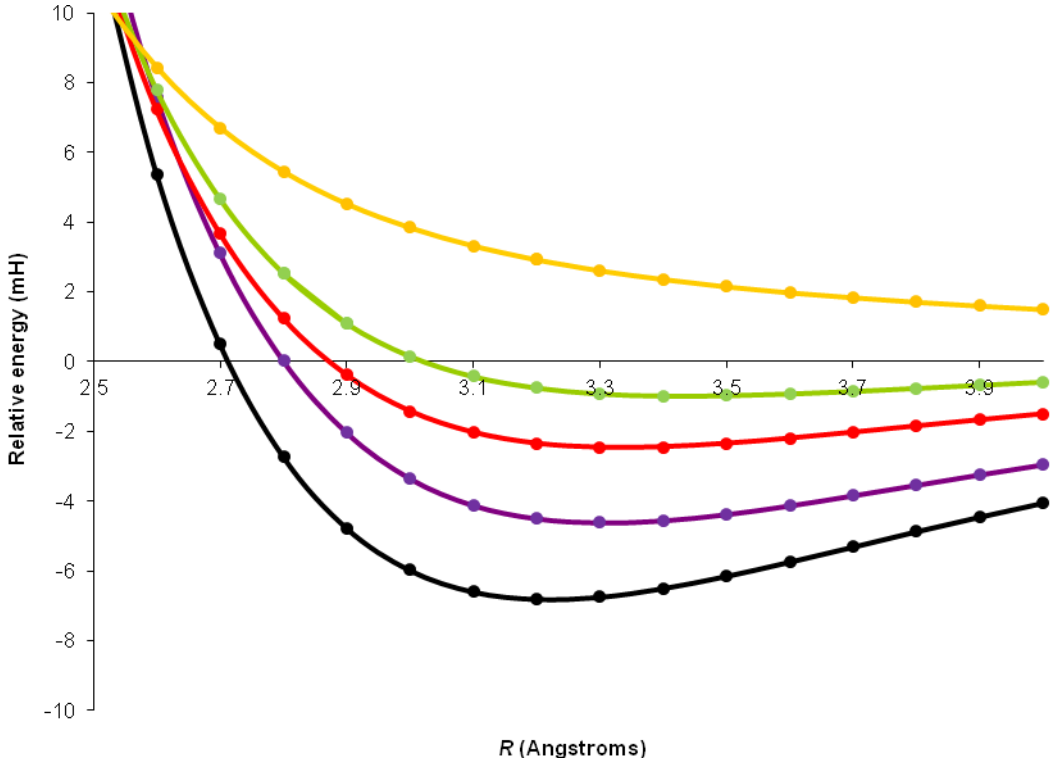

Figure 4.7: Halogen bonding potential energy surfaces for NH_3XH. Yellow=F, Green=Cl, Red=Br, Purple=I, Black=At

Table 4.5: Stabilisation energy of halogen-bonded structures (mH)

Halogen	Stabilisation energy
Cl	-0.064
Br	-1.031
I	-2.833
At	-4.720

Table 4.6: Geometric parameters of monomers (as in Figure 4.1), changes in halogen bond formation, and intermonomer distances, dipole moments and charge transfer in halogen bonded complexes (Å, °, D, e)

	r^{NH}	α	r^{X}	R	μ	q^{T}
HCl			**1.291**		**1.159**	
HBr			**1.425**		**0.887**	
HI			**1.613**		**0.446**	
HAt			**1.702**		**0.046**	
NH_3	**1.022**	**112.605**			**1.551**	
NH_3ClH	+0.000	-0.052	+0.001	3.430	0.660	0.101
NH_3BrH	+0.000	-0.028	+0.003	3.334	1.138	0.144
NH_3IH	+0.000	-0.104	+0.007	3.310	1.915	0.167
NH_3AtH	+0.000	-0.147	+0.012	3.221	2.591	0.200

Table 4.7: Normal modes of monomers, intermonomer modes in complexes, and changes in normal modes in complexes

	a_1 intermol. str.	e intermol. bend	e intermol. bend	a_1 NH_3 bend	e NH_3 bend	a_1 H-X str.	a_1 NH_3 str.	e NH_3 str.
HF						**4170**		
HCl						**2988**		
HBr						**2682**		
HI						**2347**		
HAt						**2215**		
NH_3				**1064**	**1686**		**3500**	**3627**
NH_3ClH	**(28*i*)**	**(27*i*)**	**220**	+11	-26	-10	-38	-29
NH_3BrH	**77**	**79**	**263**	+21	-26	-19	-38	-30
NH_3IH	**92**	**124**	**303**	+30	-27	-30	-37	-29
NH_3AtH	**108**	**165**	**337**	+42	-27	-101	-36	-29

4.5. Discussion

Now that the series NH_3HX has been completed by the addition of At and F, it can be evaluated globally. The N structures of the ammonia-hydrogen halides as a class show the typical qualities of the hydrogen bond: a red shift of the proton donor a_1 stretching mode, a corresponding increase in the bond length, and a modest degree of charge transfer from the proton acceptor to the proton donor (Table 4.8 through Table 4.10). The charge transfer increases the dipole moment of the complex beyond the sum of the monomer dipoles (even when extension of r^X is accounted for), without which these systems would be unlikely to bind an excess electron (see the preceding and following chapters, and [13]). The bond stretch distance and normal mode frequencies (*i.e.* the shapes of the potential surfaces) correlate with the strength (stabilisation energy) of the bond as anticipated for most of the halides (Table 4.9 and Table 4.10), however fluorine is an exception; the amount of bond stretching is less than chlorine, perhaps because of fluorine's genuinely exceptional affinity for its proton. The frequency of the

corresponding stretch is, however, strongly red-shifted (Table 4.10). The degree of charge transfer does not correlate with the strength of the bond as expected, for unknown reasons (Table 4.9).

Table 4.8: Stabilisation energies of N and Z hydrogen-bonded structures (mH)

	N	Z
F	-19.30	
Cl	-11.83	
Br	-9.92	
I	-6.85	-1.84
At	-6.31	-2.16

Table 4.9: Changes in geometric parameters upon complex formation, and intermonomer distances, charges and dipole moments for NH_3HX complexes (Å, °, D, e)

	r^{NH}	α	r^{X}	R	μ	q^{T}
NH_3HF	+0.000	-0.273	+0.028	2.671	+1.205	0.143
NH_3HCl	+0.009	-0.558	+0.031	3.221	+1.607	0.203
NH_3HBr	+0.009	-0.549	+0.028	3.416	+1.511	0.181
NH_3HI	+0.010	-0.367	+0.018	3.778	+1.340	0.209
NH_3HAt	+0.001	-0.237	+0.016	3.843	+1.446	0.215

Table 4.10: Changes in normal modes upon hydrogen bond formation for NH_3HX complexes (cm^{-1})

	a_1 NH_3 bend	e NH_3 bend	a_1 H-X str.	a_1 NH_3 str.	e NH_3 str.
NH_3HF	+97	-0	-624	+1	-2
NH_3HCl	+53	-4	-431	+3	+3
NH_3HBr	+43	-5	-346	+2	+4
NH_3HI	+28	-4	-181	-2	-1
NH_3HAt	+32	-3	-165	-5	-5

Although only two Z minima are found, and therefore it is inadvisable to draw trends from these results, the changes in the geometric parameters and vibrational frequencies are consistent with the picture of an NH_4^+ cation hydrogen bonded to a halide anion (Table 4.11, Table 4.12). The N-H distance (r^N) for the hydrogen-bonded proton is extended, and the stretching mode corresponding to this perturbation is red-shifted, while there low value of the charge on NH_4^+ is indicative of more than 0.5e charge transfer from the halide. These effects decline when moving from the lighter to the heavier halide.

Table 4.11: Changes in geometric parameters upon complex formation, and intermonomer distances, charges and dipole moments for NH_4X complexes (Å, °, D, e)

	r^{NH}	α	r^{N}	R	μ	q^{T}
NH_4I	-0.006	-0.391	+0.099	3.244	10.191	0.457
NH_4At	-0.006	-0.658	+0.097	3.307	10.134	0.475

Table 4.12: Changes in normal modes upon hydrogen bond formation for NH_4X complexes (cm^{-1})

	e NH_4 bend	a_1 NH_3 bend	e NH_3 bend	a_1 N-H_s str.	a_1 NH_3 str.	e NH_3 str.
NH_4I	-40	-185	-57	-1535	-65	+76
NH_4At	-47	-174	-57	-1487	-52	+78

Although the presence of the Z minimum is unique to NH_3HI and NH_3HAt, we argue that the molecular properties which cause this minimum to develop are intrinsic to this class of systems and can be seen throughout the system. The pending development of the Z minimum for NH_3HX is apparent even with NH_3HF; the nascent Z structure is apparent as a slight inflection of the potential energy surface between +0.3 Å and +0.4 Å r^X (Figure 4.4). As the series progresses, this part of the potential surface is "pulled down" until the surface is nearly flat in NH_3HBr and ultimately a second minimum is present (Figure 4.8).

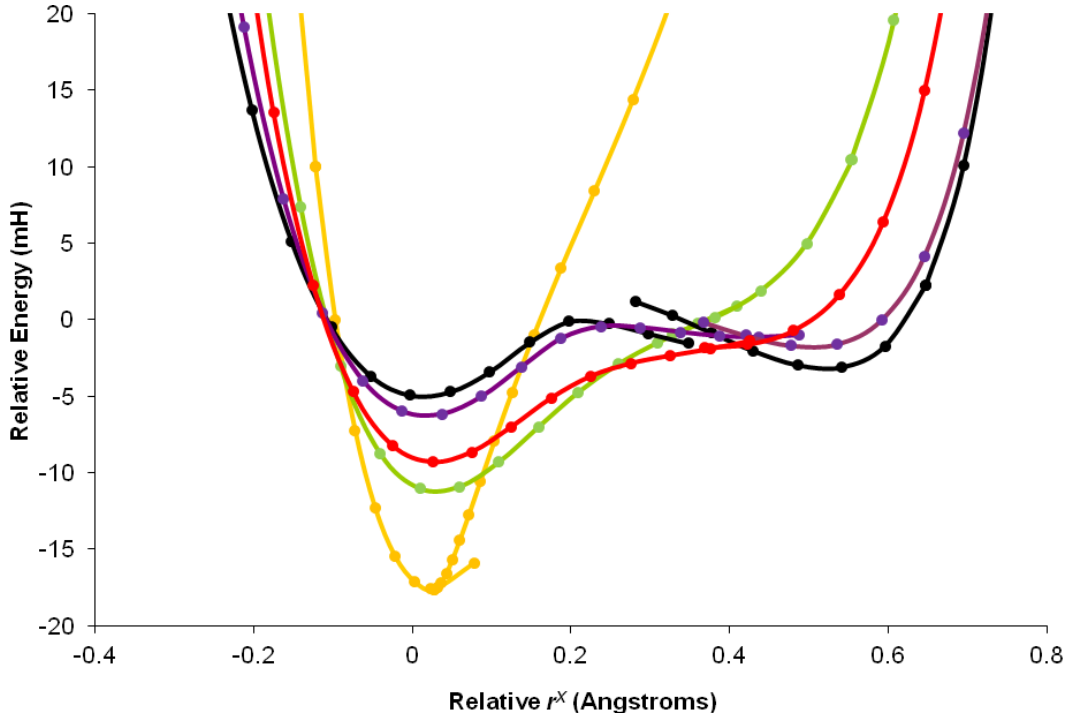

Figure 4.8: Hydrogen bonding potential energy surfaces for NH_3HX. Yellow=F, Green=Cl, Red=Br, Purple=I, Black=At

While the argument for the stability of the minima in NH_3HI and NH_3HAt may be made by comparing the stabilisation energy of the complex to the difference in the proton affinity of its monomers, as in the preceding chapter, this does not provide any information about the underlying origin of the distortion of the potential surface. It is more informative to evaluate the gradient of the energy with respect to proton position. This derivative is the vector force acting on the proton. Where it is positive, the force acts to the left, toward the N structure, and where it is negative, the force acts to the right, toward the Z structure. The other parameter of interest is the gradient of the force (second derivative of the energy), which determines how rapidly the force changes upon the proton motion. This is experimentally accessible around the minima, where it appears as the force constant in the harmonic vibrational frequencies.

Starting at the N structure, in all cases the system begins with negative force, then climbs to cross zero at some positive extension of HX corresponding to the N minimum. In this area, the second derivative is approximately constant. The force then climbs to a maximum around +0.2 Angstroms r^X, and then falls off (the second derivative becomes negative) as the proton approaches NH_3 to a distance of around +0.2 Angstroms r^N (Figure 4.9). The force then climbs again near the repulsive wall of NH_4^+. Although *all* of the complexes feel this effect, leading to the inflection point in F and Cl, only in the heavier complexes does the force drop near zero to give a plateau (Br) or cross zero to provide a barrier and second minimum (I, At). To understand why the surfaces differ, we must decompose the force into one- and two-body terms.

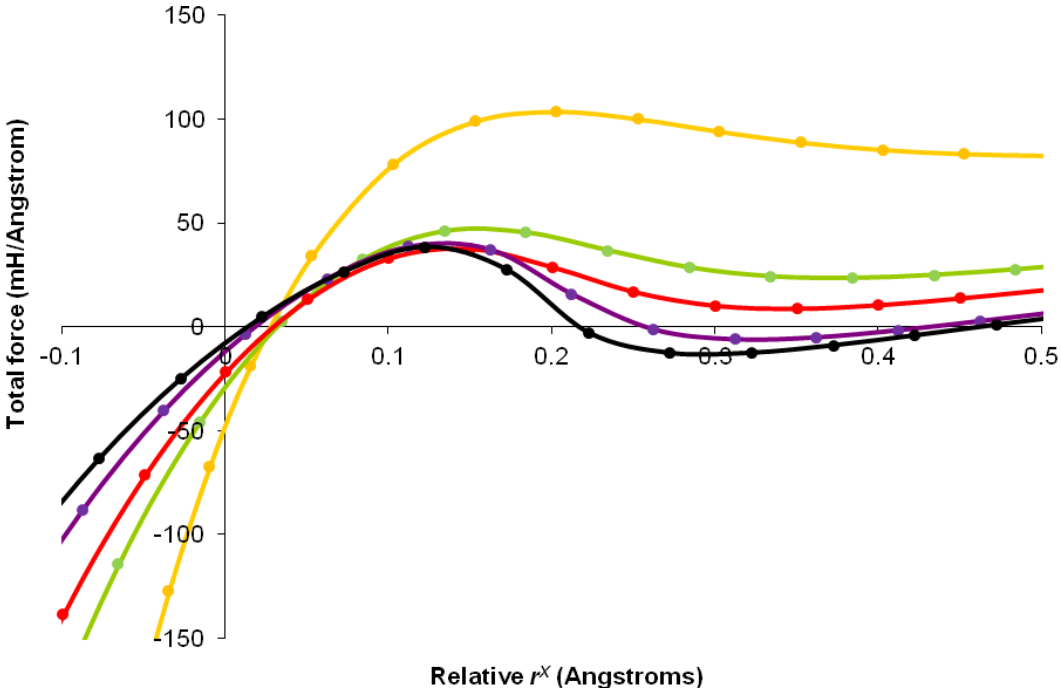

Figure 4.9: Derivative of the energy with respect to proton position, from perspective of NH_3-HX. Colours as in Figure 4.8.

From the perspective of the N structures, the one-body terms favour N (Figure 4.10). (Stretching the H-X bond is unfavourable, while NH_3 is not strongly distorted in the N or Z structure and does not have a significant role in the one-body energy.) The two-body terms favour Z (Figure 4.11), due to the increased electrostatic interaction from the elongated H-X and reduced proton-ammonia distance. From these plots we can see why the N structure has an extended H-X bond with respect to the monomer. The force upon the HX monomer is zero at equilibrium. The two-body force lies in favour extending H-X to increase the electrostatic interaction. Necessarily the sum of these forces favours extending H-X. However, the one-body force increases more rapidly (has a larger second derivative) than the two-body force with increasing r^X, and therefore the two opposing terms ultimately sum to zero at the slightly-increased r^X found in the N structure.

The most important factor for the development of the Z minimum is the rapid increase in the magnitude of the two-body force at around +0.2Å (Figure 4.11). It is this large negative contribution to the force that is largely responsible for the stagnation of the total force (Figure 4.9) and the corresponding droop in the potential surface (Figure 4.8).

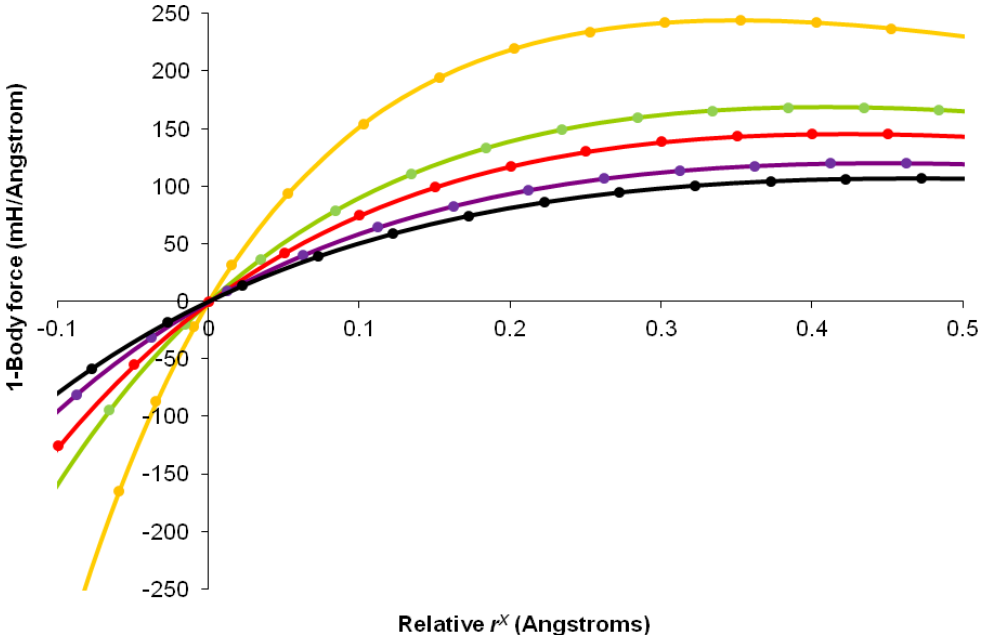

Figure 4.10: Derivative of the one-body energy with respect to proton position, from perspective of NH_3-HX. Colours as in Figure 4.8.

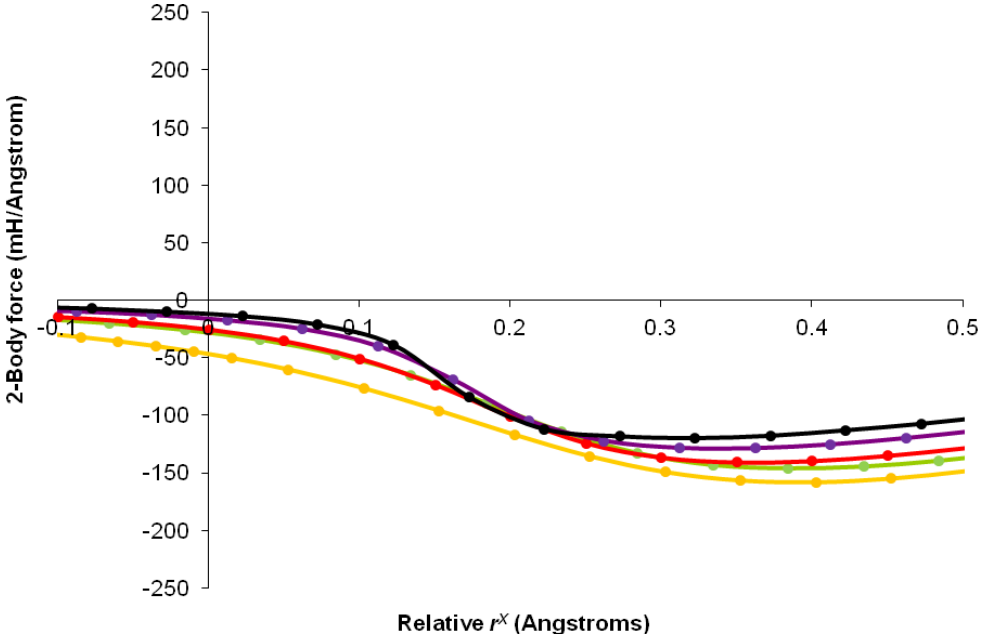

Figure 4.11: Derivative of the two-body energy with respect to proton position, from perspective of NH_3-HX. Colours as in Figure 4.8.

For NH_3HF, the two-body force and second derivative is the largest due to the large dipole moment of the monomer. However, the second derivative for HF is so exceptionally large that by +0.2 Å r^X the one-body force is too large to be much affected by the two-body term.

With progressively heavier halides, the one- and two-body terms act in opposite directions. The one-body force and second derivative become progressively smaller due to the softer hydrogen halide bond (Figure 4.10,), which allows the two-body term to have a greater influence. However the two-body force and second derivative are also becoming less negative, as the halide is softer and the hydrogen halide is less polar, and therefore the dipole moment is not enhanced as rapidly by the extending proton (Figure 4.11,). In practice, the balance lies in favour of the increasing influence of the two-body term, which continues to be large around +0.2 Å r^X, and "pulls down" the force curve, leading to the development of the inflection and plateau for heavier halides Cl and Br. For I and At it finally passes through zero, leading to a barrier and, beyond it, a net force toward the Z structure at large r^X.

Viewed from the perspective of the Z structure, there is a strong force towards increased r^N, *i.e.* the N structure (Figure 4.12). The one-body term is entirely due to the NH_4^+ stretch, which is almost constant from system to system and lies in favour of the Z structure (Figure 4.12). Therefore the variation in the ability to proton transfer is governed entirely by the two-body term, which is electrostatic in origin and is due to the halide anion's force upon the proton, and therefore favours the N structure.

The two-body force and second derivative are both larger for the lighter halides (Figure 4.14), due to the shorter internuclear distance (electrostatic interaction varies with $\frac{-1}{r}$ and its gradient with $\frac{1}{r^2}$) and the greater partial charge on the halide (the lighter halides are more electronegative). For NH_3HF, the two-body term always completely overbalances the one-body term, pulling the force curve up above zero for all values of r^N. For the rest, the two-body term is much smaller, and the one-body term has an opportunity to cancel it (Figure 4.12). For progressively heavier halides, the two-body force and second derivative become smaller. Therefore the one-body force is allowed to pull down the force curve. For the heavier halides, it passes through zero, and thereby

establishes a barrier to proton transfer at large r^N , and a negative force (toward Z) for small r^N, leading to the minimum.

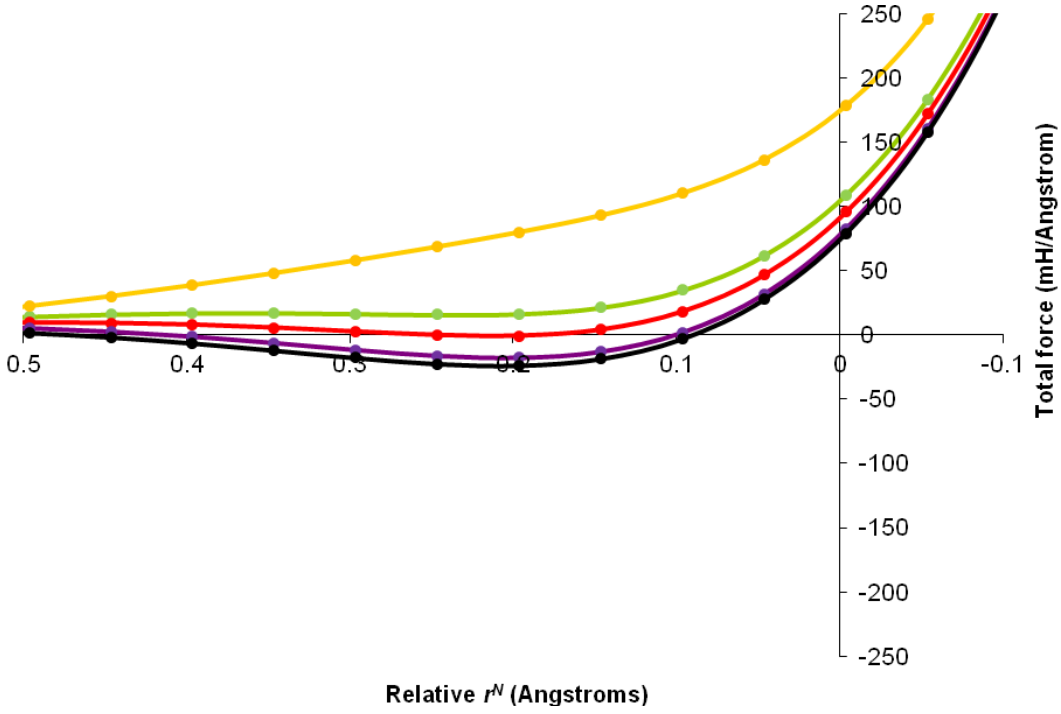

Figure 4.12: Derivative of the energy with respect to proton position, from perspective of $NH_4^+X^-$. Colours as in Figure 4.8.

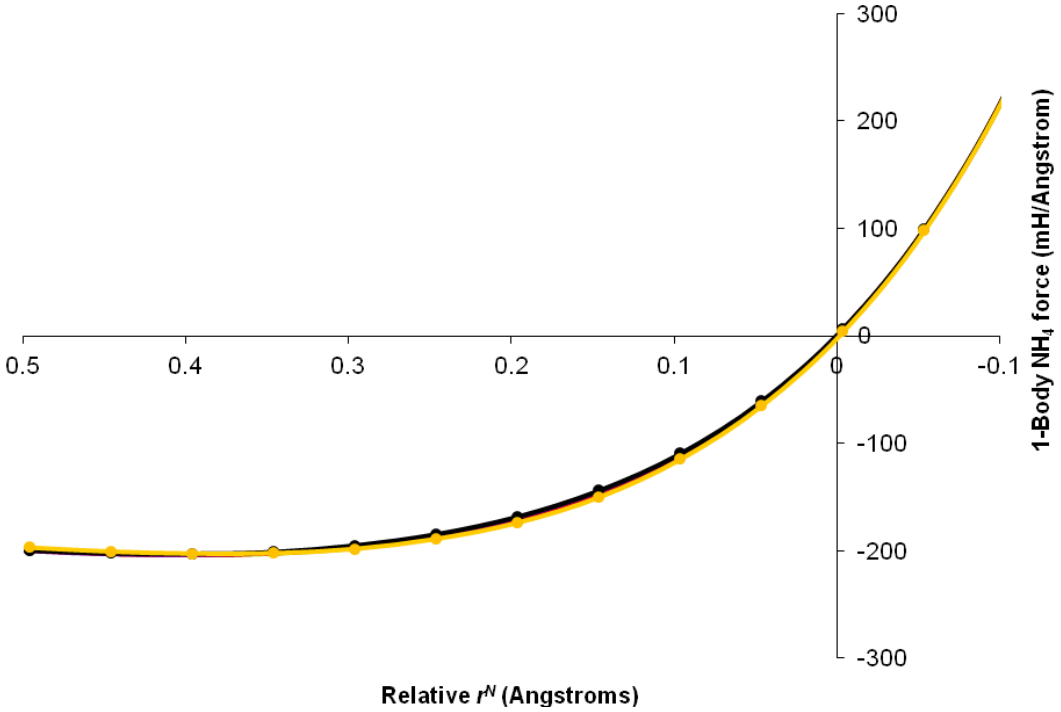

Figure 4.13: Derivative of the one-body NH_4^+ energy with respect to proton position, from perspective of $NH_4^+X^-$. Colours as in Figure 4.8.

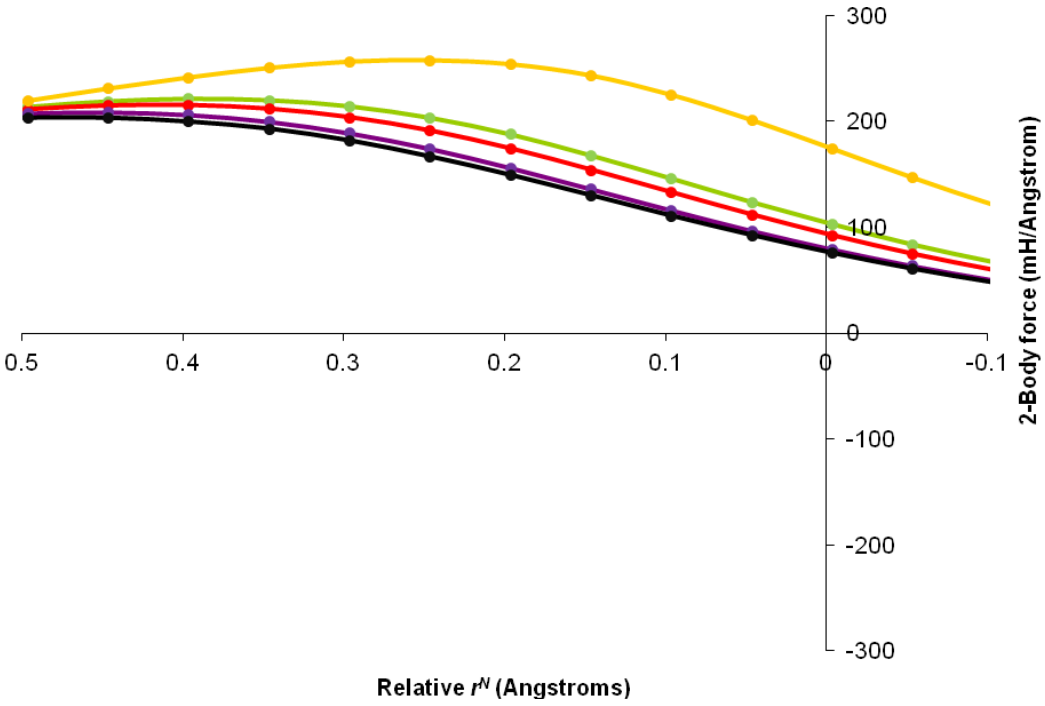

Figure 4.14: Derivative of the two-body energy with respect to proton position, from perspective of $NH_4^+X^-$. Colours as in Figure 4.8.

4.6. Summary

Three types of minima were sought on the potential energy surfaces of the C_{3v} NH_3HX (X=halogen) complexes: H_3N···HX "N" structures, proton-transferred NH_4^+…X^- "Z" structures, and H_3N···XH halogen-bonded structures. N structures were located for all of the halides F through At, at energies of -19.30 mH, -11.93 mH, -9.92 mH, -6.85 mH and -6.31 mH respectively. Their characteristics are consistent with hydrogen-bonded systems in general and the historically and chemically significant ammonia-hydrogen halides in particular. Z type minima are available to NH_3HI and NH_3HAt, at -1.84 mH and -2.16 mH respectively, and were successfully characterised as hydrogen bonded complexes of the ammonium cation with a halide anion.

The universality of the ammonia-hydrogen halide potential energy surfaces was demonstrated by examining the derivative of the energy with respect to proton position, i.e. the force on the proton. The force-geometry curves so developed were found to be qualitatively similar for all of the systems, with the quantitative changes in the shape of these curves determining whether one or two minima exist. Viewed from the perspective of the N complex, the one-body force governs the plausibility of proton transfer, with a large two-body term in its favour across all of the halides. Viewed from

the perspective of the Z complex, the two-body force governs the plausibility, with a strong effect from halide size and electronegativity.

It was found that the hydrogen halides heavier than HBr can form stable halogen bonded complexes with ammonia, and that these species show the classic trends of halogen-bonded complexes. In particular, the strength of the interaction increases with the size of the halide, even though this means a *reduction* in the intermonomer distance as the halide gets larger. For X=Br through At, their energies are 1.03mH, 2.83mH and 4.72 mH below the free monomer asymptote. Surprisingly, the ammonia-hydrogen astatide halogen bonded complex has a sufficiently large dipole moment that it may be able to bind an electron, although the experimental challenges of investigating astatine mean that this may not be confirmed for some time.

4.7. References

[1] R. S. Mulliken, *Molecular Compounds and Their Spectra. III. The Interaction of Electron Donors and Acceptors*, J. Phys. Chem., **56**, 801-822 (1952)

[2] L. Andrews and X. F. Wang, *Infrared spectrum of the H_3N-HI complex in solid Ne, Ar, Ne/Ar, Kr, and N_2. Comparisons of matrix effects on hydrogen-bonded complexes*, J. Phys. Chem. A, **105**, 7541-7550 (2001)

[3] M. J. T. Jordan and J. E. Del Bene, *Unraveling environmental effects on hydrogen-bonded complexes: Matrix effects on the structures and proton-stretching frequencies of hydrogen-halide complexes with ammonia and trimethylamine*, J. Am. Chem. Soc., **122**, 2101-2115 (2000)

[4] L. Andrews, X. F. Wang and Z. Mielke, *Infrared spectrum of the H_3N-HCl complex in solid neon*, J. Am. Chem. Soc., **123**, 1499-1500 (2001)

[5] E. Clementi, *Study of the Electronic Structure of Molecules. II. Wavefunctions for the NH_3+HCl → NH_4Cl Reaction*, J. Chem. Phys., **46**, 3851-3880 (1967)

[6] E. Clementi, *Study of the Electronic Structure of Molecules. VI. Charge Transfer Mechanism for the NH_3+HCl → NH_4Cl reaction*, J. Chem. Phys., **47**, 2323-2334 (1967)

[7] E. Clementi and J. N. Gayles, *Study of the Electronic STructure of Molecules. VII. Inner and Outer Complex in the NH_4Cl Formation from NH_3 and HCl*, J. Chem. Phys., **47**, 3837-3841 (1967)

[8] R. C. Raffenetti and D. H. Phillips, *Gaseous NH_4Cl revisited: A computational investigation of the potential energy surface and properties*, J. Chem. Phys., **71**, 4534-4540 (1979)

[9] A. Brciz, A. Karpfen, H. Lischka and P. Schuster, *A Candidate for an Ion-Pair in the Vapor-Phase - Proton-Transfer in Complexes R_3N·HX*, Chem. Phys., **89**, 337-343 (1984)

[10] P. Kollman, A. Dearing and E. Kochanski, *Ab Initio Self-Consistent Fieid Calculations on I_2-NH_3 and HI-NH_3. The Classic "Charge-Transfer" Interaction, an Example of Gas-Phase Proton Transfer, and the Duality of Lewis Acid Sites on HI*, J. Phys. Chem., **86**, 1607-1610 (1982)

[11] Z. Latajka, S. Scheiner and H. Ratajczak, *The Proton Position in Hydrogen Halide-Amine Complexes - $BrH-NH_3$ and $BrH-NH_2CH_3$*, Chem. Phys. Lett., **135**, 367-372 (1987)
[12] Z. Latajka, S. Scheiner and H. Ratajczak, *The Proton Position in Amine HX (X = Br, I) Complexes*, Chem. Phys., **166**, 85-96 (1992)
[13] S. N. Eustis, D. Radisic, K. H. Bowen, R. A. Bachorz, M. Haranczyk, G. K. Schenter and M. Gutowski, *Electron-Driven Acid-Base Chemistry: Proton Transfer from Hydrogen Chloride to Ammonia*, Science, **319**, 936-939 (2008)
[14] S. Shibata, *Structure of Gaseous Ammonium Chloride*, Acta Chem. Scand., **24**, 705-706 (1970)
[15] B. S. Ault and G. C. Pimentel, *Infrared Spectra of the Ammonia-Hydrochloric Acid Complex in Solid Nitrogen*, J. Phys. Chem., **77**, 1649-1653 (1973)
[16] Z. Latajka, S. Sakai, K. Morokuma and H. Ratajczak, *Possible Gas-Phase Ion-Pairs in Amine-HCl Complexes - an Ab initio Theoretical Study*, Chem. Phys. Lett., **110**, 464-468 (1984)
[17] S. Scheiner, *Theoretical Studies of Proton Transfers*, Acc. Chem. Res., **18**, 174-180 (1985)
[18] S. Scheiner and L. B. Harding, *Proton Transfers in Hydrogen-Bonded Systems. 2. Electron Correlation Effects in $(N_2H_7)^+$*, J. Am. Chem. Soc., **103**, 2169-2173 (1981)
[19] S. Scheiner and L. B. Harding, *Molecular Orbital Study of Proton Transfer in $(H_3NHOH_2)^+$*, J. Phys. Chem., **87**, 1145-1153 (1983)
[20] Y. Bouteiller, C. Mijoule, A. Karpfen, H. Lischka and P. Schuster, *Theoretical Vibrational Investigation of Hydrogen-Bonded Complexes - Application to $ClH-NH_3$, $ClH-NH_2CH_3$, and $BrH-NH_3$*, J. Phys. Chem., **91**, 4464-4466 (1987)
[21] P. G. Jasien and W. J. Stevens, *Theoretical Studies of Potential Gas-Phase Charge-Transfer Complexes: NH_3+HCl,NH_3+HBr,NH_3+HI*, Chem. Phys. Lett., **130**, 127-131 (1986)
[22] C. Chipot, D. Rinaldi and J. L. Rivail, *Intramolecular Electron Correlation in the Self-Consistent Reaction Field Model of Solvation - a MP2/6-31g** Ab Initio Study of the NH_3-HCl Complex*, Chem. Phys. Lett., **191**, 287-292 (1992)
[23] Z. Latajka and S. Scheiner, *Influence of Basis Set on the Calculated Properties of (H_3N-HCl)*, J. Chem. Phys., **82**, 4131-4134 (1985)
[24] A. J. Barnes and M. P. Wright, *Strongly Hydrogen-Bonded Molecular-Complexes Studied by Matrix-Isolation Vibrational Spectroscopy .3. Ammonia-Hydrogen Bromide and Amine-Hydrogen Bromide Complexes*, J. Chem. Soc., Faraday Trans. 2, **82**, 153-164 (1986)
[25] L. Schriver, A. Schriver and J. P. Perchard, *Spectroscopic Evidence for Proton-Transfer within the Bimolecular Complex HI-NH_3 Trapped in Cryogenic Matrices*, J. Am. Chem. Soc., **105**, 3843-3848 (1983)
[26] L. Andrews and X. F. Wang, *Infrared spectra of the H_3N-HBr complex in solid Ne, Ne/Ar, Ar, Kr, and N_2. Strong matrix effects on a hydrogen-bonded complex*, J. Phys. Chem. A, **105**, 6420-6429 (2001)
[27] L. Andrews, X. F. Wang and Z. Mielke, *Infrared spectrum of the H_3N-HCl complex in solid Ne, Ne/Ar, Ar, and Kr. Matrix effects on a strong hydrogen-bonded complex*, J. Phys. Chem. A, **105**, 6054-6064 (2001)
[28] A. J. Barnes, Z. Latajka and M. Biczysko, *Proton transfer in strongly hydrogen-bonded molecular complexes: matrix effects*, J. Mol. Struct., **614**, 11-21 (2002)
[29] A. J. Barnes and A. C. Legon, *Proton transfer in amine-hydrogen halide complexes: comparison of low temperature matrices with the gas phase*, J. Mol. Struct., **448**, 101-106 (1998)

[30] G. Q. Liu, Y. M. Zhao and Y. Yang, *Modeling Ar and Kr matrix effect on the ν_s (Cl - H) and ν_l (Cl - H) of Cl-H ··· NH_3 by the IEF-PCM method*, Struct. Chem., **19**, 659-663 (2008)

[31] J. E. Del Bene, M. J. T. Jordan, P. M. W. Gill and A. D. Buckingham, *An ab initio study of anharmonicity and matrix effects on the hydrogen-bonded BrH:NH_3 complex*, Mol. Phys., **92**, 429-439 (1997)

[32] A. Famulari, M. Sironi and M. Raimondi *BSSE-Free MCSCF method for strong hydrogen bonds: Investigation of H_2O-HCl and NH_3-HCl complexes* in *Quantum Systems in Chemistry and Physics, Vol. 1: Basic Problems and Model Systems*; Hernández-Laguna, A.; Maruani, J.; McWeeny, R.; Wilson, S., Eds.; Kluwer Academic Publishers: London, 2000, p 361-379.

[33] N. W. Howard and A. C. Legon, *Nature, Geometry, and binding strength of the ammonia-hydrogen chloride dimer determined from the rotational spectrum of the ammonium-chloride vapor*, J. Chem. Phys., **88**, 4694-4701 (1988)

[34] A. C. Legon, *The Nature of Ammonium and Methylammonium Halides in the Vapor-Phase - Hydrogen-Bonding Versus Proton-Transfer*, Chem. Soc. Rev., **22**, 153-163 (1993)

[35] E. J. Goodwin, N. W. Howard and A. C. Legon, *The Rotational Spectrum of N-15-Ammonium Chloride Vapor - Characterization of the Hydrogen-Bonded Dimer H_3N···HCl*, Chem. Phys. Lett., **131**, 319-324 (1986)

[36] M. Biczysko and Z. Latajka, *Accuracy of theoretical potential energy profiles along proton-transfer coordinate for XH-NH_3 (X = F, Cl, Br) hydrogen-bonded complexes*, J. Phys. Chem. A, **106**, 3197-3201 (2002)

[37] N. W. Howard and A. C. Legon, *An investigation of the hydrogen-bonded dimer H_3N-HBr by pulsed-nozzle, fourier-transform microwave spectroscopy of the ammonium bromide vapor.*, J. Chem. Phys., **86**, 6722-6730 (1987)

[38] A. C. Legon and D. Stephenson, *Is Ammonium Iodide an Ion Pair H_3N^+ H ··· I⁻ or a Hydrogen-bonded Species H_3N···HI in the Gas Phase?*, J. Chem. Soc., Faraday Trans., **88**, 761-762 (1992)

[39] R. J. Bartlett and M. Musial, *Coupled-cluster theory in quantum chemistry*, Rev. Mod. Phys., **79**, 291-352 (2007)

[40] H. B. Jansen and P. Ros, *Non-empirical molecular orbital calculations on the protonation of carbon monoxide*, Chem. Phys. Lett., **3**, 140-143 (1969)

[41] S. F. Boys and F. Bernardi, *The calculation of small molecular interactions by the differences of separate total energies. Some procedures with reduced errors.*, Mol. Phys., **19**, 553-556 (1970)

[42] S. Simon, M. Duran and J. J. Dannenberg, *How does basis set superposition error change the potential surfaces for hydrogen bonded dimers?*, J. Chem. Phys., **105**, 11024-11031 (1996)

[43] P. A. Kollman and S. U. Chandra, *An Approach to Computing Electrostatic Charges for Molecules*, J. Comput. Chem., **5**, 129-145 (1984)

[44] B. H. Besler, K. M. Merz and P. A. Kollman, *Atomic charges derived from semiempirical methods*, J. Comput. Chem., **11**, 431-439 (1990)

[45] Gaussian 03, Revision C.02, M. J. Frisch, G. W. Trucks, H. B. Schlegel, G. E. Scuseria, M. A. Robb, J. R. Cheeseman, J. A. Montgomery Jr., T. Vreven, K. N. Kudin, J. C. Burant, J. M. Millam, S. S. Iyenga, J. Tomasi, V. Barone, B. Mennucci, M. Cossi, G. Scalmani, N. Rega, G. A. Petersson, H. Nakatsuji, M. Hada, M. Ehara, K. Toyota, R. Fukuda, J. Hasegawa, M. Ishida, T. Nakajima, Y. Honda, O. Kitao, H. Nakai, M. Klene, X. Li, J. E. Knox, H. P. Hratchian, J. B. Cross, C. Adamo, J. Jaramillo, R. Gomperts, R. E. Stratmann, O. Yazyev, A. J. Austin, R. Cammi, C. Pomelli, J. W. Ochterski, P. Y. Ayala, K. Morokuma, G. A. Voth, P. Salvador, J. J. Dannenberg, V. G. Zakrzewski, S. Dapprich, A. D. Daniels, M. C. Strain, O. Farkas, D. K. Malick, A. D. Rabuck, K.

Raghavachari, J. B. Foresman, J. V. Ortiz, Q. Cui, A. G. Baboul, S. Clifford, J. Cioslowski, B. B. Stefanov, G. Liu, A. Liashenko, P. Piskorz, I. Komaromi, R. L. Martin, D. J. Fox, T. Keith, M. A. Al-Laham, C. Y. Peng, A. Nanayakkara, M. Challacombe, P. M. W. Gill, B. Johnson, W. Chen, M. W. Wong, C. Gonzalez and J. A. Pople, Gaussian, Inc., Wallingford CT, 2004

[46] Gaussian 09, Revision B.01, M. J. Frisch, G. W. Trucks, H. B. Schlegel, G. E. Scuseria, M. A. Robb, J. R. Cheeseman, G. Scalmani, V. Barone, B. Mennucci, G. A. Petersson, H. Nakatsuji, M. Caricato, X. Li, H. P. Hratchian, A. F. Izmaylov, J. Bloino, G. Zheng, J. L. Sonnenberg, M. Hada, M. Ehara, K. Toyota, R. Fukuda, J. Hasegawa, M. Ishida, T. Nakajima, Y. Honda, O. Kitao, H. Nakai, T. Vreven, J. J. A. Montgomery, J. E. Peralta, F. Ogliaro, M. Bearpark, J. J. Heyd, E. Brothers, K. N. Kudin, V. N. Staroverov, T. Keith, R. Kobayashi, J. Normand, K. Raghavachari, A. Rendell, J. C. Burant, S. S. Iyengar, J. Tomasi, M. Cossi, N. Rega, J. M. Millam, M. Klene, J. E. Knox, J. B. Cross, V. Bakken, C. Adamo, J. Jaramillo, R. Gomperts, R. E. Stratmann, O. Yazyev, A. J. Austin, R. Cammi, C. Pomelli, J. W. Ochterski, R. L. Martin, K. Morokuma, V. G. Zakrzewski, G. A. Voth, P. Salvador, J. J. Dannenberg, S. Dapprich, A. D. Daniels, O. Farkas, J. B. Foresman, J. V. Ortiz, J. Cioslowski and D. J. Fox, Gaussian, Inc., Wallingford CT, 2010

[47] T. H. Dunning, *Gaussian basis sets for use in correlated molecular calculations. I. The atoms boron through neon and hydrogen*, J. Chem. Phys., **90**, 1007-1023 (1989)

[48] R. A. Kendall, T. H. Dunning and R. J. Harrison, *Electron affinities of the first-row atoms revisited. Systematic basis sets and wave functions*, J. Chem. Phys., **96**, 6796-6806 (1992)

[49] K. Peterson, D. Figgen, E. Goll, H. Stoll and M. Dolg, *Systematically convergent basis sets with relativistic pseudopotentials. II. Small-core pseudopotentials and correlation consistent basis sets for the post-d group 16-18 elements*, J. Chem. Phys., **119**, 11113-11123 (2003)

[50] P. Skurski, M. Gutowski and J. Simons, *How to choose a one-electron basis set to reliably describe a dipole-bound anion*, Int. J. Quantum Chem, **80**, 1024-1038 (2000)

[51] K. Schuchardt, B. Didier, T. Elsethagen, L. Sun, V. Gurumoorthi, J. Chase, J. Li and T. Windus, *Basis Set Exchange: A community database for computational sciences*, J. Chem. Inf. Model., **47**, 1045-1052 (2007)

[52] D. Feller, *The role of databases in support of computational chemistry calculations*, J. Comput. Chem., **17**, 1571-1586 (1996)

Chapter 5: Electron-Driven Proton Transfer in Hydrogen Bonded Dimers

Submitted to the *Journal of the American Chemical Society* (Alexander Whiteside, Maciej Haranczyk, Maciej Gutowski, Jing Chen, Soren N. Eustis, Jay H. Hendricks, Kit H. Bowen).

5.1. Abstract

We have introduced a classification scheme for hydrogen-bonded dimers based on their preference to transfer a proton and form an ionic pair, a zwitterion. NH_3HF and H_2OHCl belong to class I, the least susceptible to proton transfer. These complexes do not proton transfer even upon the attachment of an excess electron but they support dipole-bound anions with electron vertical detachment energies (VDE) of 1.67 and 2.16 mH for $(NH_3HF)^-$ and $(H_2OHCl)^-$, respectively. Their PES spectra display very weak vibrational structures, if any. NH_3HCl belongs to class II: it does not support a zwitterionic minimum but it does proton transfer upon excess electron attachment. Its PES spectrum has very clear vibrational structure, dominated by a progression involving the H-Cl stretching mode. The excess electron binds to the NH_4^+ site forming a pair $NH_4\ldots Cl^-$, thus the VDE value of 19.88 mH is much larger than for the former systems. The last system, NH_3HAt, belongs to class III, the most susceptible to proton transfer. It supports a zwitterionic local minimum for the neutral complex and strongly binds an excess electron with a VDE of 30.80 mH. We have discussed the energetics of proton transfer in the NH_3HX complexes in terms of proton affinities, intermolecular interactions, and excess electron binding energies. We have reported opposed patterns of geometric distortions and vibrational shifts upon excess electron attachment to the complexes in class I and III, *i.e.* $H_3N\ldots HF$ and $NH_4^+\ldots At^-$. We have interpreted these patterns in terms of modifications of one- and two-body interaction energy terms and excess electron binding energies.

5.2. Introduction

The reaction of ammonia with hydrogen chloride provides an excellent example of the distinction between macroscopic solution-phase chemistry and microscopic bimolecular chemistry. In the solution phase, ammonia and hydrogen chloride react by proton transfer to form the salt ammonium chloride. However in the gas phase, the proton affinity (PA) of an ammonia molecule (854 kJ/mol[1,2]) is lower than that of a chloride

anion (PA Cl^- 1395 kJ/mol[3]), so in the bimolecular case the two molecules form a hydrogen-bonded complex of ammonia-hydrogen chloride ($H_3N\cdots HCl$). This is also expected of $H_3N\cdots HBr$ (PA Br^-: 1354 kJ/mol[4]) and $H_3N\cdots HI$ (PA I^-: 1315 kJ/mol[5]). Most of the endothermicity of proton transfer is compensated by intermolecular interactions when the molecules are brought together. These interactions are at least an order of magnitude greater for the proton-transferred "zwitterionic (Z)" complex than for the neutral (N) pair. However for the systems above, this is insufficient to make proton transfer (PT) favourable.[6,7]

In a recent publication and the preceding chapter (and corresponding publication) we examined the effect of a simple chemical perturbation, the addition of an electron, on $H_3N\cdots HCl$,[6] $H_3N\cdots HBr$ and $H_3N\cdots HI$.[7] It was found that binding an electron made proton transfer favourable in each case. Proton transfer approximately doubles the dipole moment of the neutral complex, and thus raises the binding energy of the electron. This increase in binding energy provides the additional drive toward PT which is necessary to tip the balance in favour of the Z complex. Upon electron detachment from the $(NH_4^+\cdots Cl^-)^-$ anion, a vibrationally excited neutral $H_3N\cdots HCl$ is formed (with the proton H_s shuttling between N and Cl, seeFigure 5.1, which gives rise to the vibrational structure in the photoelectron spectrum of the $(NH_4^+\cdots Cl^-)^-$ anion (Figure 5.2).

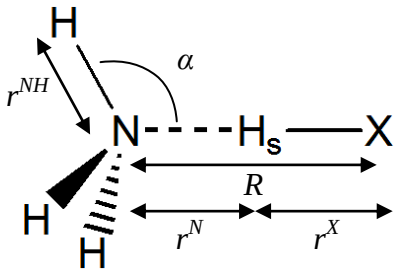

Figure 5.1: H_3N•••HX hydrogen bonded structure. "H_s" refers to the "shuttling proton".

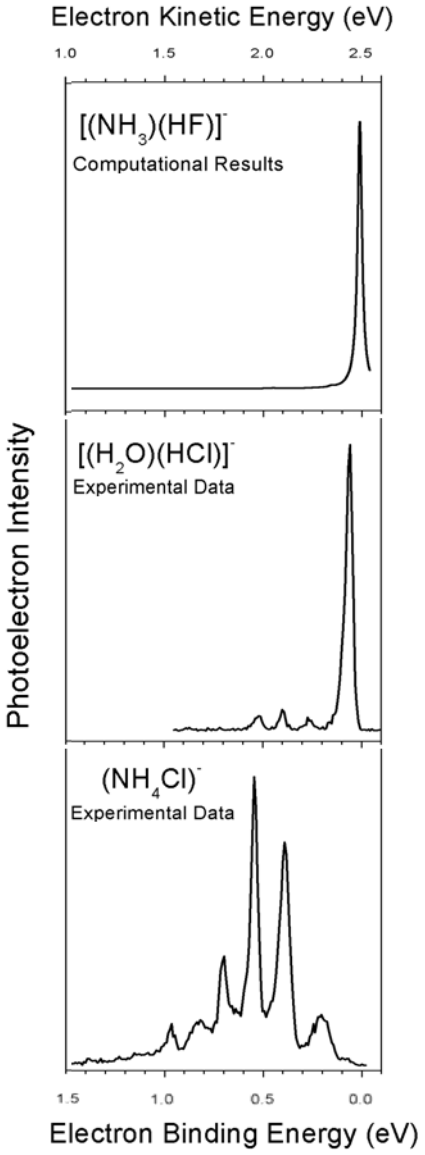

Figure 5.2: Photoelectron spectra of the dipole-bound ammonia/hydrogen fluoride and water/hydrogen chloride dimer anions ($NH3^{\cdots}HF^-$ and $H_2O\cdots HCl)^-$, and the electron-induced-proton-transferred ammonium chloride anion, $(NH_4Cl)^-$.

It can be inferred that when using a weaker base or acid, proton-transfer might not occur, even in the anion. Starting from a base that is weaker than NH_3, an earlier computational study by Skurski and Gutowski on the neutral and anionic H_2O...HCl identified that both forms have N-type structures.[8] The computed photoelectron spectrum was dominated by a single narrow peak at a low electron binding energy (EBE), and several weak peaks at higher EBEs. The main peak is associated with the transition from the vibrational ground state of the anion to the vibrational ground state of the neutral ("0-0"), while the weak peaks are associated with the intermolecular modes (H bond stretching and wagging of the H_2O monomer) and high energy combination transitions involving the aforementioned modes and the intramonomer

bending and stretching modes of H_2O. In this contribution, we report the experimental photoelectron spectrum of the $(H_2O\cdots HCl)^-$ anion and discuss the experimental data in terms of these computational predictions.[8]

We anticipate that using an acid that is weaker than HCl will have a similar effect of preventing proton transfer in the anion. Hydrogen fluoride (HF) is a famously weak acid (although its poor acidity belies its chemical activity); the fluorine anion has a proton affinity of 1555 kJ/mol.[9] The neutral $H_3N\cdots HF$ complex has been characterized by its infrared spectrum as a strong "type I" hydrogen-bonded species, with the HF stretching mode frequency red shifted by 921 cm^{-1} in the argon matrix-isolated species.[10] The structure of the complex and its polarity were probed in microwave spectroscopy experiments.[11] Those authors reported a relatively short N-F distance of 2.66 Å and a significant dipole moment of 4.448 D, the latter being 1.2 D larger than the sum of experimental dipole moments of NH_3 and HF. Unfortunately, our efforts to generate the $(H_3N\cdots HF)^-$ anion were unsuccessful, thus our investigation of $H_3N\cdots HF$ and its anion is purely computational. In particular, the dependence of anionic and neutral potential energies on the position of the proton H_s has been investigated, and the equilibrium structures, vibrational frequencies, and electron binding energies of the neutral $H_3N\cdots HF$ complex have been calculated. Finally, we modelled the photoelectron spectrum for its anionic complex.

Conversely, a hydrogen halide HX, where X^- has an exceptionally low proton affinity, may undergo proton-transfer in the *neutral* complex with ammonia. Astatide has the lowest proton affinity in water of all the halides,[12] and it is expected that astatide would also have the lowest proton affinity in the gas phase among all the halides, considering that the gas phase proton affinities of the remaining halides drop with increasing weight.[3-5,9] We have computationally studied the neutral $H_3N\cdots HAt$ and zwitterionic $NH_4^+\cdots At^-$ structures. The dependence of anionic and neutral potential energies on the position of the proton H_s was explored, and their equilibrium structures, vibrational frequencies, and vertical and adiabatic excess electron binding energies were calculated.

Hydrogen astatide (HAt) has a very low dipole moment of unconfirmed polarity,[13,14] owing to astatine's low electronegativity (2.2 in Pauling units), comparable with that of hydrogen (2.20 in Pauling units). On the other hand, the covalent radii of astatine (1.5 Å)[14] and hydrogen (0.31 Å)[15] and their polarisabilities differ drastically. As a

result, it is not obvious whether HAt would bond to NH_3 through a hydrogen bond ($H_3N\cdots HAt$ or $NH_4^+\cdots At^-$) or through a halogen bond ($HAt\cdots NH_3$). Due to dipole cancellation, such a complex is unlikely to bind an electron, and therefore this discussion is limited to the "N" ($H_3N\cdots HAt$) and "Z" ($NH_4^+\cdots At^-$) structures.

Hydrogen-bonded dimers can accommodate an excess electron on a π[16,17] or σ[18,19] orbital, but only the latter case is considered in this contribution. Our discussion is focused on the $H_3N\cdots HF$, $H_3N\cdots HCl$, $H_3N\cdots HAt$, and $H_2O\cdots HCl$ systems and their responses to the excess electron attachment, but it relies on and benefits from our past experience with dipole-bound anions supported by hydrogen-bonded systems[6,7,20-24] and amino-acids.[25-27]

The systems discussed here are representatives of three broad classes of hydrogen-bonded dimers characterised in Table 5.1. The class I systems do not support the Z-type minimum for the neutral complex and do not undergo proton transfer in the anion, *e.g.* $H_3N\cdots HF$ or $H_2O\cdots HCl$. The class II systems are the most affected by the excess electron attachment: they still do not support the Z-type minimum for the neutral complex, but they undergo proton transfer in the anion, *e.g.* $H_3N\cdots HCl$, $H_3N\cdots HBr$. The systems from this class have been studied in our earlier publications.[6,24] Finally, the class III neutral dimers support a Z-type minimum (local or global) and the minimum energy structure of the anion resembles the Z-type minimum of the neutral species, *e.g.* $NH_3\cdots HI$, $NH_3\cdots HAt$.

Table 5.1: Three classes of hydrogen-bonded dimers discussed in this chapter

Class	Characteristics
Class I	**No Z-type minimum for the neutral;**
Examples: $H_3N\cdots HF$, $H_2O\cdots HCl$	No proton transfer in the anion
Class II	**No Z-type minimum for the neutral;**
Examples: $H_3N\cdots HCl$, $H_3N\cdots HBr$	Proton transfer in the anion
Class III	**Z-type minimum for the neutral (local or global);**
Examples: $H_3N\cdots HI$, $H_3N\cdots HAt$	The minium energy structure of the anion resembles the Z-type minimum of the neutral

Hydrogen bonding favours linear arrangements between proton acceptors (A) and proton donors (HD). Thus the A···HD structures listed above are characterised by constructive superposition of dipoles of the interacting monomers. In fact, due to intermolecular charge transfer, dipole moments of the C_{3v} $H_3N\cdots HX$ dimers are larger than the sum of dipole moments of the isolated monomers. The dipole moments of hydrogen bonded dimers frequently exceed Fermi and Teller's critical dipole of 1.625 D[28] which is required to bind an excess electron. The resulting dipole-bound anionic states will be explored in this chapter.

The hydrogen-bonded DH and A units are prearranged for proton transfer ("zwitterionisation"):

$$A\cdots HD \leftrightarrow AH^+\cdots D^- \qquad (117)$$

In Table 5.2 we summarize experimental proton affinities of deprotonated proton donors, D^-, and proton acceptors, A. The differences between these quantities represent natural thermodynamic barriers for proton transfer. Intermolecular interactions compensate these barriers to a large extent. However for the class I and II complexes these interactions are insufficient to support a Z-type minimum. Excess electron attachment provides an additional driving force for proton transfer to occur, which is characteristic of the class II complexes.

Table 5.2: Proton affinities of deprotonated proton donors (PA D^-) and proton acceptors (PA A) and differences thereof (kJ mol^{-1})

A···HD	PA D^-	PA A	Difference
$H_3N\cdots HF$	1555[8]	854[1,2]	701
$H_2O\cdots HCl$	1395[3]	691[1]	704
$H_3N\cdots HCl$	1395	854	541
$H_3N\cdots HBr$	1353[4]	854	499
$H_3N\cdots HI$	1315[5]	854	461
$H_3N\cdots HAt$	1298 (Computed)	854	444

The classification presented in Table 5.1 is sufficient for the current project, although it could become more detailed based on the number of minima (one or two) supported by the neutral and the anion and their relative depth. Quite an extended study of anionic complexes of uracil with alcohols of various degree of acidity was presented by us in the past.[29]

This study has the following objectives:

I. To characterise the potential energy surfaces (and minima thereon) associated with the H_s position (Figure 4.1) in the neutral and anionic NH_3HF (class I) and NH_3HAt (class III).

II. To determine modifications of geometries and vibrational frequencies brought about by excess electron attachment to these complexes.

III. To predict the anion photoelectron spectrum of $H_3N\cdots HF$ and to analyze differences in experimental anion photoelectron spectra of $H_2O\cdots HCl$ and $H_3N\cdots HCl$.

5.3. Computational Methods

The one- and two-body energies of the neutral species are defined as in 4.3. The energy of the anion $(X\text{-}Y)^-$ can be written as

$$E_{(X-Y)^-}(G) = E_{(X-Y)}(G) - EBE(G) = E_X(G_X) + E_Y(G_Y) + E_{stab}(G) - EBE(G) \quad (118)$$

where EBE(G) is the vertical electron binding energy at the geometry G:

$$EBE(G) = E_{X-Y}(G) - E_{(X-Y)^-}(G) \quad (119)$$

The values of EBE are positive for vertically bound anionic states considered here.

In Sections 5.5 and 5.7 we will analyze two characteristic geometries, G_N and G_A, which are equilibrium geometries for the neutral complex X-Y and the anion $(X\text{-}Y)^-$, respectively. In Section 5.7 we will pay attention to the energy of the anion at these two geometries. It follows that the change in energy between the two structures can be written as:

$$\Delta E_{(X-Y)^-} = E_{(X-Y)^-}(G_A) - E_{(X-Y)^-}(G_N) \quad (120)$$

$$\Delta E_{(X-Y)^-} = \Delta E_{stab} - \Delta EBE \quad (121)$$

$$\Delta E_{stab} = E_{stab}(G_A) - E_{stab}(G_N) \quad (122)$$

$$\Delta EBE = EBE(G_A) - EBE(G_N) \quad (123)$$

$$\Delta E_{stab} = \Delta E_{1-b}^{X} + \Delta E_{1-b}^{Y} + \Delta E_{2-b}^{X-Y} \quad (124)$$

$$\Delta E_{1-b}^{W} = E_{1-b}^{W}(G_A) - E_{1-b}^{W}(G_N) \quad (125)$$

$$\Delta E_{2-b}^{X-Y} = E_{2-b}^{X-Y}(G_A) - E_{2-b}^{X-Y}(G_N) \quad (126)$$

The potential energy surfaces, optimised geometries and harmonic frequencies of the neutral and anion complexes were computed at the CCSD level[30] with standard Boys-Bernardi counterpoise corrections.[31-33] In the neutral complexes, the monomers were NH_3 and HX in the case of N-type structures and NH_4^+ and X^- in the case of Z-type structures. In the anionic complex, the monomers were NH_4^0 and X^- in the case of PT structures. The counterpoise correction for anionic non-PT structures presents a challenge, because neither NH_3 nor HX can retain an excess electron. On the assumption that the counterpoise correction would be little affected by the binding of the excess electron, the counterpoise correction for the non-PT anions was defined as exactly equal to that of the corresponding neutral. The geometries of the monomers themselves were also optimised, and their vibrational frequencies computed.

Once the optimised geometries were obtained for the neutral and anionic complexes, EBEs were computed at CCSD(T)[34] with counterpoise corrections analogous to those applied to the optimisations. The vertical attachment energy (VAE) is equivalent to EBE(G_N). The vertical detachment energy (VDE) is equivalent to EBE(G_A). The adiabatic electron affinity is defined as $AEA = E_{X-Y}(G_N) - E_{(X-Y)^-}(G_A)$.

Incremental contributions of each level of theory to the EBEs are defined as the difference between the affinity calculated at that level of theory, and the affinity calculated at the preceding level. A positive sign indicates that the electron is more strongly bound at the next level. Corrections from the vibrational zero-point energy (as computed from the above harmonic vibrational frequencies) were added to the final AEA values.

The CCSD density was used to calculate the dipole moments and effective charges by the Merz-Sing-Kollman method.[35,36] Orbitals were plotted from the same density, using MOLDEN[37] for contour plots and the OpenCubeMan tools[38] and VMD[39] (rendering in POVRay[40]) for isosurfaces.

All electronic structure calculations were performed in the Gaussian 03,[41] Gaussian 09[42] and Molpro[43] codes. Tight SCF convergence criteria were imposed. Dunning-type correlation consistent augmented double- and triple-zeta basis sets (aug-cc-pvdz, aug-cc-pvtz, respectively) were used,[44,45] with pseudopotentials in the case of astatine,[46] and further augmented with a set of 7s and 7p (F) or 12s and 11p (At) diffuse functions to bind the excess electron, using a progression ratio of 2.5.[47]

(Henceforth, these basis sets are AVDZ+ and AVTZ+, respectively.) The basis set and pseudopotential for astatine were obtained from the EMSL Basis Set Exchange.[48,49]

The most important geometric parameter in computing the potential energy surface is the position of the "shuttling" proton H_s which is transferred between the two monomers. We could have fixed the other coordinates at some arbitrary value, and scanned the proton position to obtain the potential energy surface, but this procedure could lead to artifacts, such as a spurious local minimum for $NH_4^+\cdots Cl^-$.[50] Therefore a relaxed potential energy surface was necessary. However this introduces an additional difficulty: we must define the H_s position with respect to the heavy atom N or X (r^N and r^X), and each coordinate is only appropriate in the vicinity of the corresponding heavy atom. Therefore as detailed in our previous chapter it is necessary to combine two "complementary" potential energy surfaces. Furthermore, for NH_3HAt counterpoise corrections were applied with respect to the monomers implied by the choice of coordinate: when scanning r^N, the monomers were NH_4^+ and At^-, while when scanning r^X the monomers were NH_3 and HAt. (The counterpoise correction was consistently to NH_3 and HF in NH_3HF).

The anion profiles were created by taking the neutral optimised geometry at each point, and calculating the counterpoise-corrected energy for the anion at that geometry. Therefore reading vertically between the two surfaces corresponds to the EBE at each point. The anion minimum is not necessarily included on this neutral profile, but given the limited number of degrees of freedom, the presence of a well on the anion profile can be read as an indication of the nearby minimum.

A fictitious $(NH_4^+\cdots F^-)^-$ structure was constructed in order to estimate energetics of proton transfer in NH_3HF. This was created by noting trends in the differences between anion and neutral geometries in the other NH_3HX systems (which did undergo proton transfer in anionic complex) and estimating a plausible magnitude for the changes that would occur between $H_3N\cdots HF$ and $(NH_4^+\cdots F^-)^-$. The geometrical parameters of the fictitious system are given in the Supplimentary Information (section 5.9).

A simulated photoelectron spectrum was created for $(H_3N\cdots HF)^-$ because this system is amenable to future experimental verification. The $(NH_3HAt)^-$ system, on the other hand, is not only experimentally challenging because of the relatively short half-lives of all isotopes of At (the longest is 8.1 hours)[14] but also methodologically more

challenging because of the strongly anharmonic potential energy surfaces, in particular of the neutral complex. The Frank-Condon (FC) factors, *i.e.* the squares of the overlap integrals between vibrational wave functions of the neutral and anionic $H_3N^{\cdots}HF$, were calculated in the harmonic approximation at the CCSD/AVTZ+ level with counterpoise-corrected equilibrium geometries and hessians. Both equilibrium geometrical parameters and curvatures are affected by the excess electron attachment and the resulting FC factors might contribute to vibrational structure in the photoelectron spectrum.[8,20,51] The polyatomic FC factors were calculated using Doktorov and co-workers' relations[52] as implemented in the code of Roy,[53] and assuming a temperature of 100 K in the mass selected ion beam.[21] The intensity of the 0-0 transition was set to one and all other intensities were scaled accordingly. The notation n_i^j indicates that for the *n*th mode there is an excitation from the *i*th to the *j*th quantum state and 0_0^0 stands for the 0-0 transition. The calculated FC factors were convoluted with Lorentzian line shapes (full width at half-maximum equal to 218 cm^{-1}).[21]

5.4. Experimental methods

Mixed dimer anions composed of both ammonia/hydrogen chloride and water/hydrogen chloride molecules were generated and studied by anion photoelectron spectroscopy (PES). This technique is conducted by crossing a mass-selected beam of negative ions with a fixed-frequency photon beam and energy-analyzing the resultant photodetached electrons. The photodetachment process is governed by the energy-conserving relationship, hν = EBE + EKE, where hν is the photon energy, EBE is the electron binding energy, and EKE is the electron kinetic energy. Since the photon energy is known and the electron kinetic energies are measured, electron binding energies (transitions from an anion to its neutral counterpart) are determined.

Both anionic complexes of $H_2O\cdots HCl$ and $H_3N\cdots HCl$ were generated in a supersonic expansion nozzle-ion source. To produce NH_4Cl^- anions, an NH_3/Ar gas mixture (15%/85%) at 1-3 atmospheres and 25°C was expanded through a 20 μm diameter orifice into vacuum (~7 × 10^{-5} Torr), while a few Torr of a HCl/Ar gas mixture (10%/90%) was leaked through a small tube (0.125" OD) into the supersonic expansion region immediately outside the nozzle. To produce $(H_2O\cdots HCl)^-$ anions, an HCl/Ar gas mixture (10%/90%), sitting over ~5 ml liquid H_2O (at 25°C) on the floor of the nozzle's stagnation chamber, was expanded (along with H_2O vapor) through a 20 μm diameter orifice into a ~1 × 10^{-4} Torr vacuum. In both cases, negative ions were formed by

injecting low energy electrons from a negatively-biased thoriated-iridium filament into the expanding jet, where a microplasma was formed in the presence of a weak axial magnetic field. These anions were then extracted, collimated, and transported by ion optics into the flight tube of a 90° magnetic sector, mass spectrometer with a mass resolution of ~400. The mass-selected anions of interest were then crossed with the intra-cavity laser beam of an argon ion laser, and the photodetached electrons were energy-analyzed in a hemispherical electron energy analyzer with a resolution of ~30 meV. The photoelectron spectra reported here were recorded with ~180 circulating watts of 2.540 eV/photon light and calibrated against the well-known photoelectron spectrum of O^- anion.[54] A detailed description of this apparatus has been presented previously.[55] Efforts to generate $(H_3N\cdots HF)^-$ anions were unsuccessful.

5.5. Computational results for $(H_3N\cdots HF)^-$ and $(NH_4^+\cdots At^-)^-$

The neutral and anionic C_{3v} complexes of NH_3 with HF do not support minima for PT structures. By contrast, the neutral hydrogen bonded complex of NH_3 with HAt supports two minima: N and Z. The anion of this complex supports only one minimum related to the zwitterionic (PT) structure.

5.5.1. Effect of excess electron on the geometry and frequencies

Binding of an electron results in subtle geometric changes in the $H_3N\ldots HF$ complex, as depicted in Table 5.3 and Figure 5.3. The NH_3 molecule bends away from planarity by additional 0.6°, the HF bond length increases by 0.006 Å, and the R distance decreases by 0.020 Å. There is also an elongation of the NH bonds in ammonia by 0.002 Å. All these geometrical changes lead to an increase of the dipole moment of the neutral complex by 0.09 D and therefore stabilize the dipole-bound anionic state.

Table 5.3: Geometric parameters (as Figure 55). dipole moments and charge transfer of NH_3HF and NH_3HAt , and changes upon electron binding and proton transfer as appropriate. Å, °, D and e.

	r^{NH}	α	r^{X}	r^{N}	R	μ^{N}	q^{T}
HF			**0.918**			**1.810**	
HAt			**1.689**			**0.062**	
NH_3	**1.012**	**112.1**				**1.528**	
NH_4^+	**1.022**	**109.471**		**1.022**			
NH_4^0	**1.038**	**109.471**		**1.038**		**0**	
NH_3HF	**1.012**	**111.8**	**0.946**	**1.725**	**2.671**	**4.544**	**0.143**
$(NH_3HF)^-$	+0.002	+0.6	+0.006	-0.026	-0.020	+0.088	+0.013
NH_3HAt	**1.013**	**111.9**	**1.705**	**2.138**	**3.843**	**3.036**	**0.215**
$NH_4^+At^-$	+0.003	-3.1	+0.483	-1.019	-0.537	+7.099	+0.261
$(NH_4^+At^-)^-$	+0.011	+2.0	+0.275	-0.062	+0.212	+1.823	+0.097

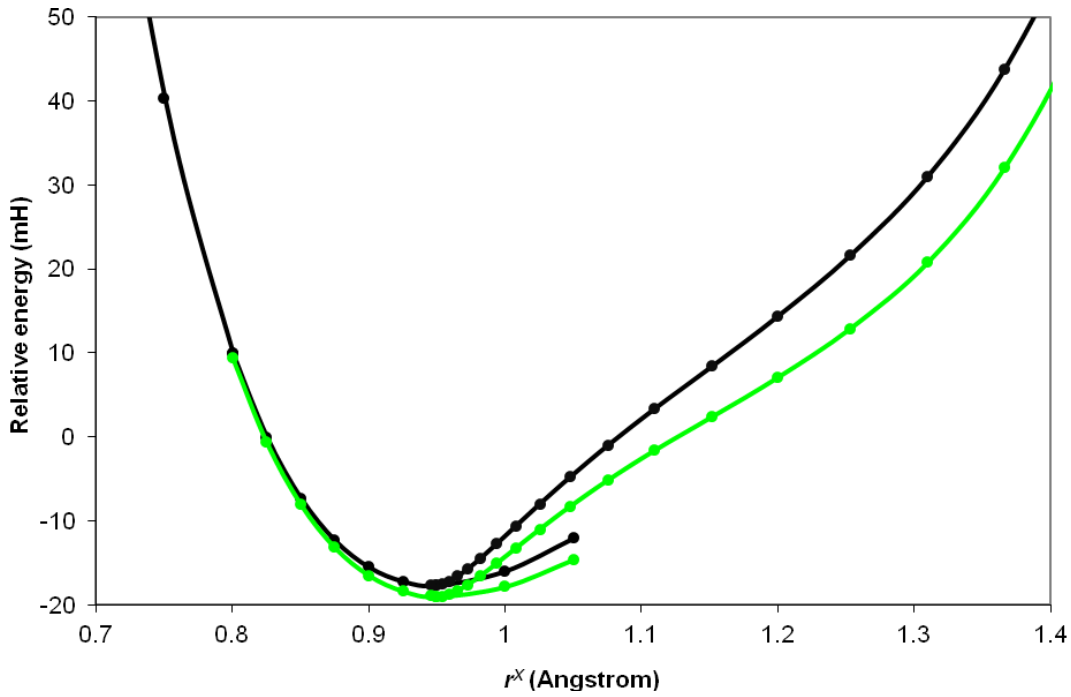

Figure 5.3: Counterpoise-corrected neutral potential energy surface (black) and anion energy profile (green) of NH_3HF.

The presence of an excess electron favours a more polar structure for the complex, as this binds the electron more strongly. Even though the Z type minimum does not exist for this complex due to the large proton affinity of fluoride, the structural reorganization is in the direction of zwitterion formation, *i.e.* r^N reduces by 0.029 A and r^F increases by 0.006 A. There is also a transfer of 0.013 *e* within the neutral complex from NH_3 to

HF upon this geometrical relaxation. This nascent proton transfer is responsible for the redshift of the H-F stretching mode by 122 cm^{-1} (Table 5.4).

Table 5.4: Normal mode frequencies of NH_3HF and changes upon electron binding (cm^{-1})

Mode #	Description	ν (NH_3HF)	δν(NH_3HF)$^-$
1	a_1 Intermolecular str.	261	+8
2,3	e Intermolecular bend	254	+30
4,5	e Intermolecular bend	941	+46
6	a_1 NH_3 bend	1161	+15
7,8	e NH_3 bend	1686	-5
9	a_1 H_s-F str. (some NH_3)	3546	-164
10	a_1 NH_3 str. (some H_s-F)	3502	-22
11,12	e NH_3 str.	3626	-27

The stretching modes localized on ammonia, a_1 and e, are also redshifted by 55 and 26 cm^{-1}, respectively (Table 5.4). These shifts might be associated with the nature of the orbital occupied by the excess electron, which is weakly antibonding across the N-H bonds (Figure 5.4). The redshifts in frequencies of the stretching modes are paralleled by blueshifts in the a_1 NH_3 umbrella bending mode and in all the intermolecular modes, in particular the bending e modes (Table 5.4). The blueshift for the NH_3 umbrella mode is consistent with the fact that planarization of ammonia decreases the dipole moment of the neutral complex and therefore destabilizes the anion, *i.e.* raises the energy to a greater degree (and therefore is associated with a stronger force) than the same perturbation in the neutral.

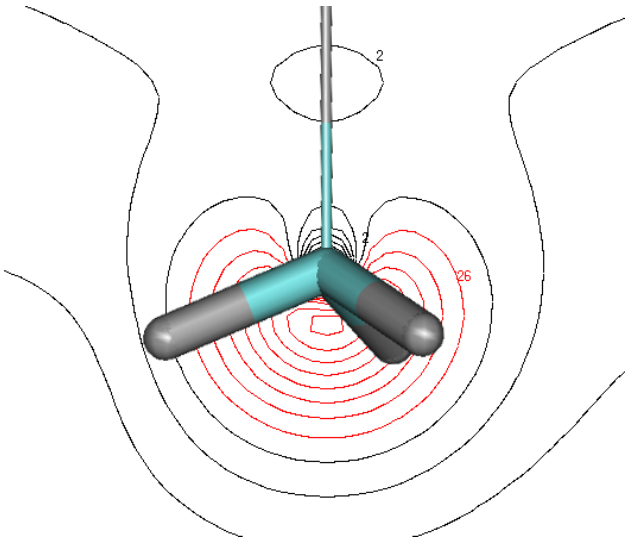

Figure 5.4: Contour plot of the lowest unoccupied orbital the NH_3HF molecule in the region near NH_3. Only one of the N-H bonds is in the plane of the plot. The change in phase (red to black) along the bond indicates that the orbital is antibonding with respect to this bond, and therefore forming the anion will weaken it.

In contrast to NH_3HF, two hydrogen bonded minima were identified for NH_3HAt: N and Z (Figure 5.5). The relative stability of these two minima is very sensitive to the level of theory; it requires the counterpoise correction and a highly correlated treatment to unravel that the non-PT minimum is the global minimum (as detailed in the preceding chapter). With respect to the isolated NH_3 and HAt, the N complex is at -6.3 mH, the transition state is at +2.1 mH, and the Z complex is at -2.2 mH, all results at the CCSD(T) level of theory. It goes without saying that the double well potential for the NH_3HAt neutral will result in anharmonicity and the quantitative values of the harmonic frequencies quoted in the following should be treated as suspect, especially for the mode corresponding to proton transfer. Notice that the counterpoise method is needed to pin down the relative stability of the N and Z structures, but it introduces a discontinuity between the "left" and "right" branches due to different offsets to energy resulting from the different counterpoise corrections (Figure 5.5). This discontinuity has to be removed before solving the anharmonic vibrational problem.

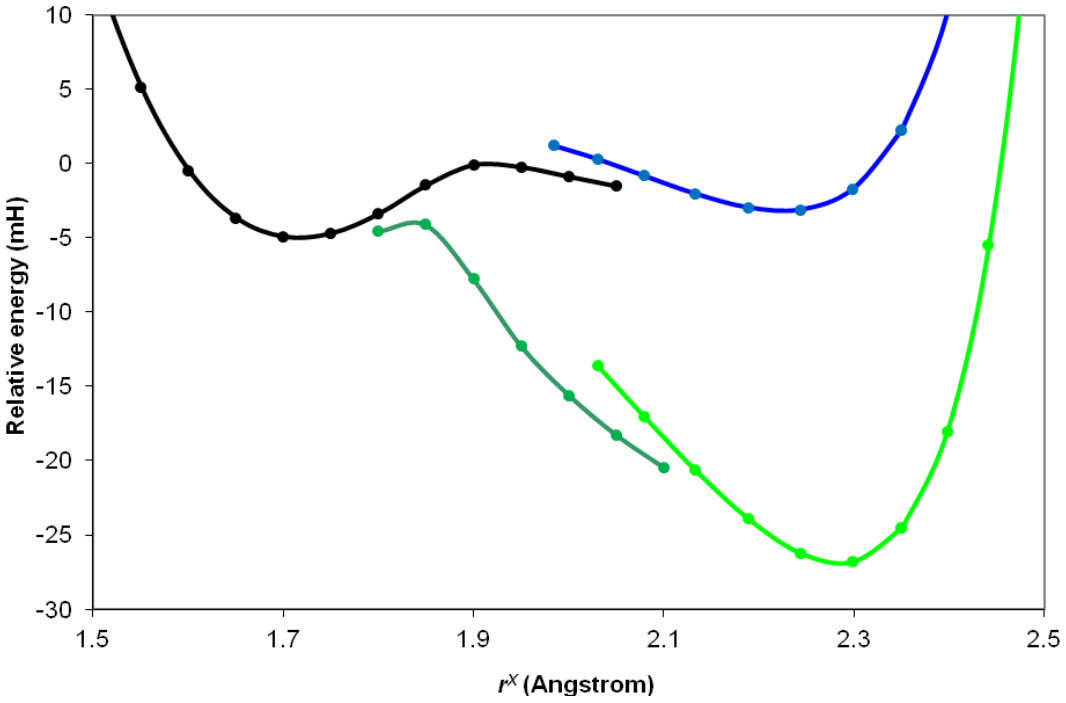

Figure 5.5: Counterpoise-corrected potential energy surface for NH_3HAt neutral (black/blue), and profile for the anion (dark green/light green). Colours indicate coordinate choice for scan.

The detailed discussion of the N and Z neutral structures of NH_3HAt is briefly summarized in Table 5.3, Table 5.5 and Table 5.6. Here we focus on their ability to vertically bind an excess electron. Starting from the N structure, its dipole moment of

3.036 D is smaller by 1.508 D than the dipole moment of $H_3N\cdots HF$. The difference results primarily from the small dipole moment of isolated HAt (0.062 D, with the positive pole on the hydrogen) when compared with 1.810 D for HF. The sum of dipole moments of the isolated monomers in NH_3HAt (1.528 D (for NH_3) + 0.062 D = 1.590 D) is smaller than Fermi and Teller's 1.625 D critical dipole.[28] However, there is a significant charge transfer of *ca.* 0.2 e from NH_3 to HAt upon formation of the N complex and the resulting dipole of 3.036 D becomes sufficient to vertically bind an electron, though the value of VAE is smaller than 0.6 mH. (This is why characterization of this region of the potential energy surface for the anionic NH_3HAt required additional *s* and *p* diffuse basis functions.) Despite the small value of VAE, the potential energy surface of the anionic complex does not support the N-type minimum, *i.e.* the energy of the anionic dimer decreases as the r^{At} coordinate increases from 1.71 A until the $NH_4^{\cdots}At^-$ minimum is reached (Figure 5.5).

Table 5.5: Normal mode frequencies of NH_3HAt, and changes upon proton transfer and electron binding (cm^{-1})

Mode #	Description (NH_3HAt)	ν (NH_3HAt)	Description ($NH_4^+At^-$)	ν($NH_4^+At^-$)	δν($NH_4^+At^-$)$^-$
1	a_1 Intermol. str.	87		278.3	-99
2,3	e Intermol. bend	136		246.8	-27
4	a_1 NH_3 bend	1096	a_1 NH_3 bend + H_s-N str.	1331	+55
5,6	e Intermol. bend	416	e NH_4 bend	1458	-6
7,8	e NH_3 bend	1684		1696	-12
9	a_1 H_s-At str.	2051	a_1 H_s-N str.	1914	+938
10	a_1 NH_3 str.	3495		3468	-182
11,12	e NH_3 str.	3623		3598	-240

Table 5.6: Normal mode frequencies of NH_4^+, and changes upon hydrogen bonding to At^- and electron binding(cm^{-1}). Mode numbers to match Table 5.5.

Mode #	Description (NH_4^+)	ν(NH_4^+)	Description ($NH_4^+At^-$)	δν ($NH_4^+At^-$)	δν ($NH_4^+At^-$)$^-$	ν(NH_4^0)
4	t_2 bend	1505	a_1 NH_3 bend + H_s-N str.	-174	+55	1348
5,6	″	″	e NH_4 bend	-46	-6	″
7,8	e bend	1753	e NH_3 bend	-57	-12	1638
9	a_1 str.	3402	a_1 H_s-N str.	-1487	+938	3091
10	t_2 str.	3520	a_1 NH_3 str.	-52	-182	3117
11,12	″	″	e NH_3 str.	+78	-240	″

The low-barrier proton-transfer in the neutral complex changes the identities of the constituent monomers (Figure 5.5). The resulting neutral Z structure $NH_4^+\cdots At^-$ is

characterized by a dipole moment of 10.135 D (Table 5.3). The NH_4^+ monomer is significantly distorted from the relaxed T_d structure: r^N is increased by 0.097 Å, r^{NH} decreased by 0.006 Å, and α decreased by 0.7°. Stronger intermolecular interactions in $NH_4^+ \cdots At^-$ than in $H_3N \cdots HAt$ must be responsible for the shortening of R by 0.537 Å (Table 5.3).

The excess electron attaches to the NH_4^+ site of the Z complex leading to $NH_4 \cdots At^-$, where NH_4 is the ammonium Rydberg radical characterized by Herzberg,[56] here geometrically and electronically distorted by the interaction with At^- (see also the following chapter). The geometric distortions resulting from binding an excess electron are significant and lead to an increase of the dipole moment of the neutral complex by 1.823 D (Table 5.3). Of particular interest is the evolution of the R parameter, which increases by 0.212 Å in the anionic complex involving At but decreases by 0.020 Å in the anionic complex involving F (Table 5.3). In parallel, all of the intermolecular modes are redshifted for the former but blueshifted for the latter (Table 5.4 and Table 5.5). These results suggest that the excess electron attachment weakens intermolecular interactions in $NH_4^+ \cdots At^-$ but strengthens them in $H_3N \cdots HF$. These observations illustrate qualitative differences between the anions based on the class I and III dimers.

Another striking feature is a partial reversal of the distortion of the NH_4^+ unit upon the excess electron attachment: r^N decreases by 0.062 Å (Table 5.3), thus significantly compensates an increase by 0.095 Å reported above between the relaxed NH_4^+ and the Z neutral complex. This geometric change is paralleled by a large blueshift (938 cm^{-1}) of the a_1 N-H_s stretching mode (Table 5.5), i.e., there is a significant compensation of a redshift of 1487 cm^{-1} experienced by the a_1 mode of NH_4^+ upon formation of the hydrogen bond with At^-; the resultant mode is close to that of the free ammonium radical (Table 5.6).

Other distortions of the NH_4^+ moiety and frequency shifts upon the excess electron attachment (Table 5.3 and Table 5.5) are analogous to those reported for $H_3N \cdots HF$ and have a similar interpretation. They are, however, enhanced by the stronger interaction between the excess electron and the dimer. Thus the r^{NH} distance increases by 0.011 Å and the NH stretching modes are redshifted by 182 and 240 cm^{-1} for the a_1 and e modes, respectively. The α angle increases by 2 ° and the a_1 NH_3 umbrella bending mode is blueshifted by 55 cm^{-1}.

5.5.2. Vertical and adiabatic excess electron binding energies

Incremental contributions to the vertical and adiabatic electron binding energies, starting from the Koopmans' theorem and Hartree-Fock terms and ending up at the CCSD(T) level, are collected in Table 5.7 and Table 5.8 for NH_3HF and NH_3HAt, respectively. This format exposes the role of electron correlation, the investigation of which can be simplified to two tasks:[57-60] (i) reproduce the dynamical correlation between the excess electron and electrons of the neutral dimer, and (ii) reproduce the correlated electron distribution in the neutral complex, in these specific cases a reduction of the Hartree-Fock dipole moment of the neutral complex brought about by electron correlation effects. Electron correlation effects reduce the Hartree-Fock dipole moment by *ca.* 0.15 and 0.18 D for the N-type neutral complexes $H_3N\cdots HF$ and $H_3N\cdots HAt$, respectively, and by ca. 0.50 D for the Z complex $NH_4^+\ldots At^-$. These reductions should reduce the excess electron binding energy. The results reported in Table 5.7 and Table 5.8 demonstrate, however, an increase of electron binding energies upon inclusion of electron correlation effects. Clearly, the dynamic correlation between the excess electron and electrons of the neutral dimer is more important than the reduction of dipole moment. In the case of HAt, we report the VAE and AEA values with respect to two minimum energy structures of the neutral complex, $H_3N\cdots HAt$ and $NH_4^+\cdots At^-$ (Table 5.8).

Table 5.7: Electron binding energies for NH_3HF and its anion (mH). Koopmans' theorem values in brackets.

	HF	δMP2	δCCSD	δ(T)	Total	δZPE	Total	Total (meV)
VDE	0.595 (0.56)	0.445	0.485	0.140	1.666	N/A	1.666	45.3
VAE	0.526 (0.50)	0.400	0.459	0.131	1.516	N/A	1.516	41.2
AEA	0.037	1.029	0.381	0.222	1.669	0.171	1.840	50.1

Table 5.8: Electron binding energies for NH_3HAt and NH_4At, and the NH_4At^- anion (mH). Koopmans' theorem values in brackets. AEA values are from NH_4At^- to NH_3HAt or NH_4At.

	HF	δMP2	δCCSD	δ(T)	Total	δZPE	Total
VDE	22.701 (19.56)	6.197	1.153	0.746	30.796	N/A	30.796
NH_3HAt							
VAE	0.039 (0.040)	0.081	0.483	0.1464	0.750	N/A	0.750
AEA	28.446	-6.212	-0.789	0.285	21.723	-6.112	15.618
NH_4At							
VAE	15.257 (12.82)	4.981	1.266	0.696	22.199	N/A	22.199
AEA	21.449	1.836	2.293	0.305	25.883	-0.320	25.563

HF, MP2, and CCSD contribute approximately equally to VDE and VAE for $H_3N^{\cdots}HF$ (Table 5.7), with a non-negligible contribution from triple excitations (>8% of the total CCSD(T) value). Due to the small dipole moment of $H_3N\ldots HAt$ the convergence of VAE is very slow (Table 5.8). The CCSD term proves to be dominant (64.4%) followed by a contribution from triple excitations (19.5%), while the Hartree-Fock contribution represents only 5.2 % of the total CCSD(T) value. The electron binding energies are much larger for the high-dipole Z structure, $NH_4^+\ldots At^+$. Note the dramatic contraction of the orbital occupied by the excess electron upon the proton transfer (Figure 5.6). The Hartree-Fock term proves to be dominant for the VDE, VAE and AEA values (more than 69%). The incremental MP2 term is the second most important (more than 20%) for the vertical energies VDE and VAE, with smaller contributions from CCSD and CCSD(T). Once again, it is confirmed that highly correlated methods are needed to reproduce electron binding energies for neutral systems with dipole moments less than 5 D.[57-60] On the other hand, electron binding to ionic pairs with dipole moments larger than 9 D is methodologically much less demanding.[25-27] Orbital relaxation effects associated with polarization of the neutral dimer by the excess electron and backpolarisation, which are quantified by a difference between the Hatree-Fock and Koopmans' terms, are negligible for the N-type structures, $H_3N^{\cdots}HF$ and $H_3N^{\cdots}HAt$, but they represent more than 10% of the total CCSD(T) value of VAE and VDE for the Z structure, $NH_4^{+\cdots}At^+$.

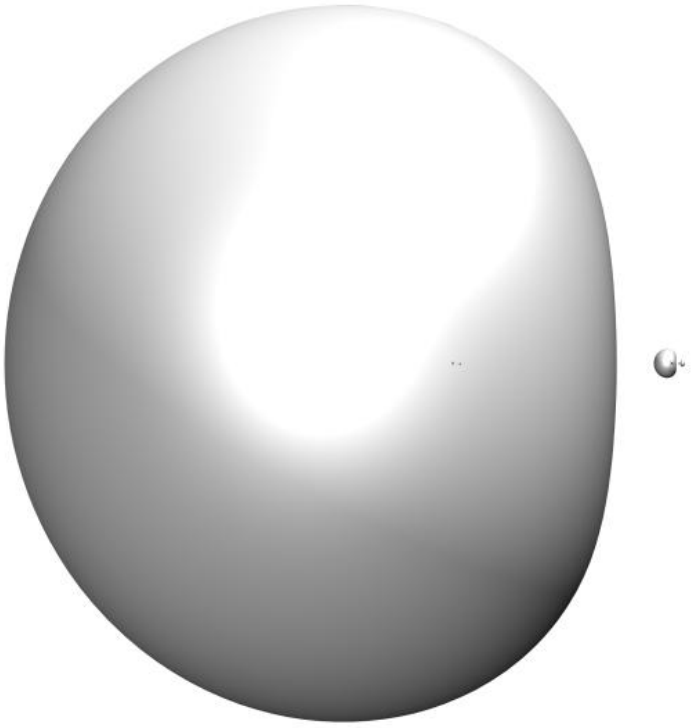

Figure 5.6: Left and right: 0.9-electron isosurfaces of neutral NH_3HF LUMO at neutral and anion equilibrium geometries respectively (to scale).

Contributions from zero-point vibrations typically stabilize a dipole-bound anion with respect to the neutral. The stabilization results from red shifts for specific intramonomer modes brought about by the excess electron (see Section 5.5.1 for a detailed discussion of the nature of these modes). Indeed, a contribution from zero-point vibrations contributes 9% to the total AEA of $H_3N\cdots HF$ (Table 5.7). However, the zero-point vibrational contribution destabilizes $(NH_4^+\cdots At^-)^-$ (Table 5.8). In the case of AEA defined with respect to $NH_4^+\ldots At^-$, it is a blue shift in the frequency of the H_s-N stretching mode, which is responsible for a negative contribution to AEA. The contribution is even more destabilizing for AEA defined with respect to $H_3N\ldots HAt$ (Table 5.8). This is due to the fact that the zero point energy increases for the $H_3N\ldots HAt \rightarrow NH_4^+\ldots At^-$ transformation, because a soft intermolecular e mode morphs into a more rigid intramonomer e NH_4^+ bending mode (Table 5.5).

5.5.3. Computational photoelectron spectrum of $(H_3N\cdots HF)^-$

The predicted anion photoelectron spectrum for NH_3HF^- (Figure 5.2) is dominated by a transition at 404 cm^{-1} between the vibrational ground states of the anion and neutral (which is set as the zero energy point for the figure by convention). The position of this transition is equivalent to AEA. It is determined based on the CCSD(T) electronic energies of the anion and neutral at their minimum energy structures and a correction for zero-point vibrations determined at the CCSD level. In view of small differences in geometries (Table 5.3) and frequencies (Table 5.4) between the neutral and the anion complex, the FC factors strongly favour transitions with the anion and the neutral in the same vibrational state (Table 5.9; 3_0^2 denotes the transition from the second excited state of the third mode in the anion, to the ground vibrational state of that mode in the neutral, *etc.*).

Table 5.9: Peak assignment for computed NH_3HF spectrum (cm^{-1})

Energy (cm^{-1})	Transition	Description	F-C factor	Intensity
373	$2_1^1; 3_1^1;$	e_2 intermolecular bend (hot band)	0.996	0.017
396	1_1^1	a_1 intermolecular str. (hot band)	0.975	0.02
404	0_0^0	AEA	1	1
665	1_0^1	a_1 intermolecular str.	0.013	0.013
910	$2_0^2; 3_0^2$	e_2 intermolecular bend	0.002	0.002
1565	6_0^1	a_1 NH_3 bend	0.005	0.005
3949	9_0^1	a_1 F-H_s str.	0.001	0.001

The only vibrational excitation of the neutral species, with an intensity exceeding 1% of the 0-0 transition, is associated with the a_1 intermolecular stretching mode (1_0^1). This is consistent with a contraction of R upon the anion formation by 0.02 Å. 6_0^1 is next in intensity (0.5% of the 0-0 transition) and reflects an increase in α by 0.6° and a small blue shift for the a_1 NH_3 bending mode upon the anion formation. This transition is far enough from the 0-0 transition and sufficiently strong to perhaps account for the small maximum in the PES spectrum at 0.19 eV. Other transitions, with intensities exceeding 0.1% of the 0-0 transition, involve an intermolecular e mode (blueshifted by 30 cm^{-1} upon the anion formation) and an intramolecular a_1 F-H_s stretching mode (r^F increased by 0.006 A and the mode redshifted by 163 cm^{-1} upon the anion formation). The latter is the "proton shuttling" mode but the intensity of the 6_0^1 transition is very weak indeed, and the peak can barely be resolved at the foot of the spectrum. Of particular interest are the intermolecular hot bands, which lie close in energy but *below* the AEA as a consequence of the blue shift of the intermolecular modes in the anion (Table 5.9). The transitions involving the a_1 stretching and e bending modes have FC factors very close to 1, but their intensities are strongly dampened by Boltzmann factors. Due to small values of blueshifts (< 30 cm^{-1}) they merge into the "foot" of the 0-0 peak and are unlikely to be resolved as separate peaks, though they should bias the measured AEA to a lower energy. At the assumed temperature of 100 K the maximum of the PES spectrum still coincides with the position of the 0-0 transition and the full width at half-maximum of the dominant peak remains 218 cm^{-1}. Increased temperature should enhance the population of the anion excited states, giving a temperature-dependent red-shift of the AEA.

5.6. Experimental results for $(H_2O\cdots HCl)^-$ and $(NH4^+\cdots Cl^-)^-$

The photoelectron spectrum of the $(H_2O\cdots HCl)^-$ anion displayed the distinctive spectral signature of a dipole-bound anion, in which the spectrum is dominated by a single, narrow peak at low electron binding energy (EBE) with much weaker molecular vibrational features located at slightly higher EBE values (Figure 5.2). This spectral pattern implied nearly perfect Franck-Condon overlap between the anion and its corresponding neutral and thus suggested a high structural similarity between the anion and its neutral counterpart. By contrast, the photoelectron spectrum of the ammonia/hydrogen chloride dimer anions was very different. It displayed a well-developed vibrational envelope, implying a significant structural difference between the

anion and its corresponding neutral. In addition, EBE value of the maximum in its vibrational envelope is an order of magnitude larger than that for the dipole-bound, water/hydrogen chloride dimer anion. As has been described previously, the excess electron in the ammonia/hydrogen chloride dimer anion induced proton transfer from the hydrogen chloride molecule to the ammonia molecule.[6] Thus, ammonia/hydrogen chloride dimer anions are best characterized as ammonium chloride anions, $(NH_4Cl)^-$, whereas water/hydrogen chloride dimer anions are best characterized as dipole bound anions, $(H_2O\cdots HCl)^-$, with no excess electron induced proton transfer.

5.7. Discussion

To evaluate the reasons why proton-transfer does or does not occur, the energetics for the overall process were assessed for the model class I (NH_3HF) and III (NH_3HAt) dimers and the results are presented in Figure 5.7a and b. In the case of HF, this involved the construction of the fictitious PT structure discussed in Section 5.3.

As discussed in the Introduction, the fluoride anion's proton affinity is much higher than that of ammonia (Table 5.2), and therefore proton transfer between an isolated HF molecule and an isolated NH_3 is strongly disfavoured by 269 mH. The electrostatic interaction between the NH_4^+ and F^- ions is much stronger than that between the NH_3 and HF molecules, and as a consequence the association energy for assembling those ions (224 mH) is much larger than the energy required to dissociate the NH_3HF complex (14 mH), and therefore proton transfer in the neutral complex is only disfavoured by 57 mH. However this is still quite a large barrier to overcome.

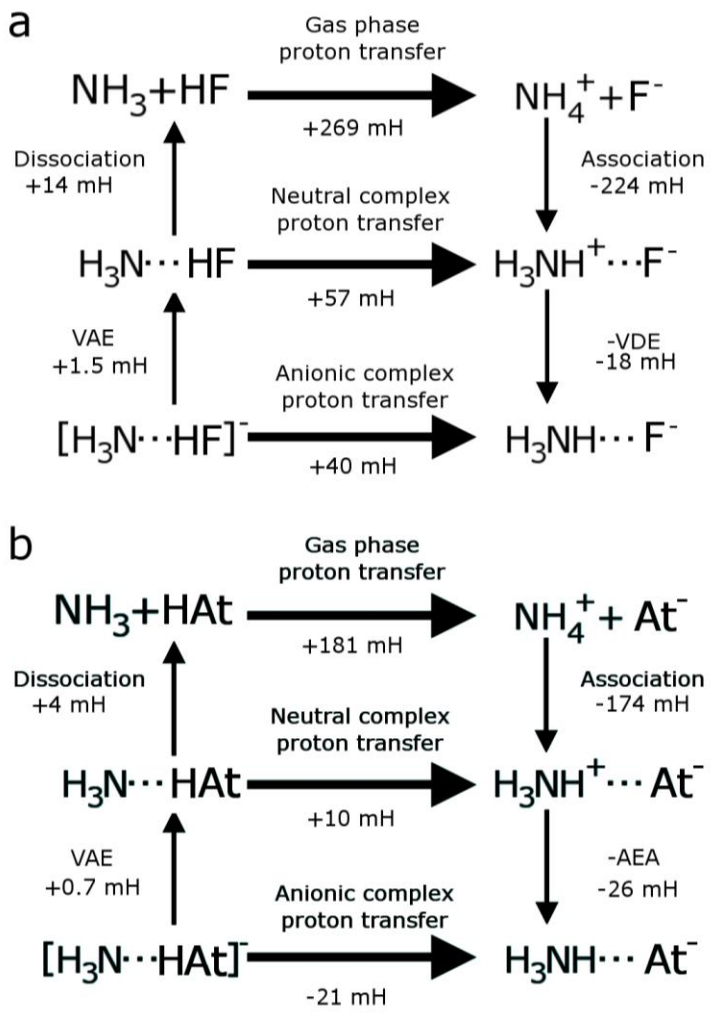

Figure 5.7: Decomposition of the energetics of proton transfer between NH_3 and HX in the isolated monomers, neutral complex, and anionic complex. X=F for a, X=At for b. Counterpoise and (where start and end are minima) zero-point energy corrections have been applied to the energies.

Binding an electron also tips the balance towards the ionic complex. The dipole moment in the N-type NH_3HF complex is 4.544 D, and the dipole moment in the proposed Z-type $NH_4^+F^-$ complex is much larger at 10.025 D. As a consequence, the electron is 17.5 mH more strongly bound in the Z-type complex. However this still leaves a 40 mH shortfall. Proton transfer is therefore not favourable, even for the anion. This is consistent with the trend observed in the previous chapter. In that case, the heavier halides displayed a progressively smaller shortfall in proton affinity in the gas phase, and a progressively greater difference between the electron affinities of the hydrogen-bonded and proton-transferred structures. (Conversely, heavier halides show a steadily smaller difference between hydrogen-bonded and proton-transferred dissociation energies, diminishing an effect which favours proton transfer in the neutral species.)

In NH_3HAt, as in the other NH_3HX, proton-transfer is not favourable in the neutral complex. However, the shortfall in energy is much smaller than in NH_3HF (+10 mH). . The computed proton affinity of astatide is much lower than that of fluoride (494 mH, versus 588 mH for F^-; Table 5.2), and thus the proton transfer between the isolated monomers is less unfavourable. However note that the gain in association energy from proton transfer is smaller, 170 mH in this case *versus* 210 mH in NH_3HF, due to the increased internuclear distance between the NH_4^+ and X^- fragments. As the electron binding energy of the N-type neutral is much lower in this case (due to the very weak polarisation of the H-X bond by astatine; the dipole is 3.036 D), and the electron binding energy of the PT-type anion is much higher (due to the increased internuclear separation by the larger halide; the dipole is 11.957 D), there is a large enough energetic benefit from proton transfer in the anion to make this highly favourable.

The evolution of VDE and VAE in the NH_3HX complexes is summarised in Figure 5.8. X=F breaks from the trend of VDEs quite dramatically because it lacks a PT-type anion. Still, the hypothetical Z structure for the HF complex matches the trend of VDE values. Other VDE values exceed 19 mH and systematically increase along the halogen series. These anions are based on PT structures characterised by dipole moments larger than 10 D. The increasing values of VDE reflect the fact that the distance between X^- and NH_4 increases along the halogen series. As a consequence, the unpaired electron in the NH_4 radical is less destabilized as X^- becomes more distant. The VAE values are small and decrease along the halogen series. The decreasing value of VAE reflects the fact that the polarity of the N-type complexes decreases along the halogen series. This in turn reflects a decreasing polarity of the HX molecules along the halogen series. The VDE and VAE values for the HF complex are indistinguishable in Figure 5.8.

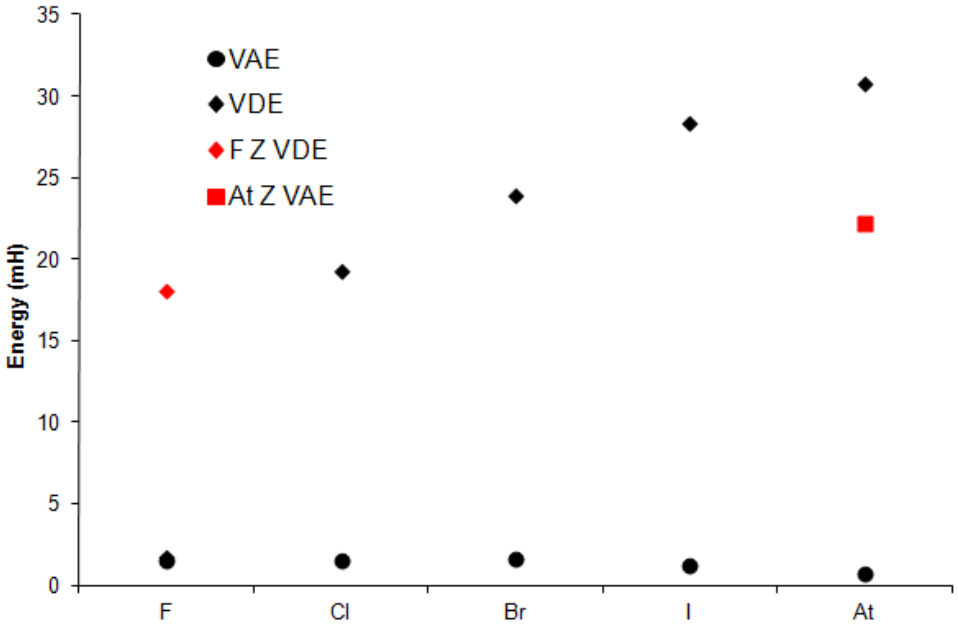

Figure 5.8: Comparison of computed electron affinities of NH_3HX (X=F, Cl, Br, I, At) complexes. The VAE and VDE for F are coincident.

In Section 5.5 we noted that excess electron attachment to the $H_3N\cdots HF$ and $NH_4^+\cdots At^-$ complexes leads to qualitatively different geometric distortions and vibrational shifts. First, the R distance decreases for the non-PT complex, but increases for the PT-type complex. Second, the intermolecular vibrational modes are blueshifted in the N-type complex but redshifted in the PT-type complex. Third, NH_4^+ unit is strongly distorted in the neutral complex with At^-, in particular the N-H_s bond is elongated. However, upon excess electron attachment, the NH_4 unit distorts back towards a tetrahedral structure, i.e., N-H_s bond contracts and the associated stretching mode blueshifts by 938 cm^{-1}.

The values of ΔE_{1-b}^{X}, ΔE_{1-b}^{Y}, ΔE_{2-b}, and ΔEBE terms defined by Eqs. 9-15 and collected in Table 5.10 allow us to interpret the above results. In the case of the PT-type complex in systems with a Z minimum, the lowering of the energy of the anion upon relaxation from the G_N to G_A geometry is accomplished through weakening of the 2-body interaction between NH_4^+ and X^-, a significant increase of the EBE, and a significant decrease of the $\Delta E_{1-b}^{NH_4^+}$ term. An increase of the R distance stabilizes the unpaired electron in NH_4 at the expense of weakening of the 2-body term. As a consequence, the EBE is enhanced and the intermolecular vibrational modes are redshifted. A partial restoration of the tetrahedral geometry of NH_4 leads to a decrease of the $\Delta E_{1-b}^{NH_4^+}$ term and a significant blueshift in the N-H_s stretching mode. Reducing the one-body term in NH_4^+ corresponds to relaxing the NH_3-H^+ bond toward the

equilibrium tetrahedral geometry; such a motion raises the overall dipole moment of the complex and is therefore favoured in the anion. The same pattern is observed for both NH_4At and NH_4I, which also supports a Z minimum and a PT anion (Table 5.10, Table 5.11, Table 5.12).

Table 5.10: Change in one- and two-body energies, and electron binding energy, between neutral and anion geometries (mH)

	ΔE_{2-b}	$\Delta E_{1-b}^{HX/X^-}$	$\Delta E_{1-b}^{NH_3/NH_4^+}$	ΔEBE	ΔE
NH_3HF	**-0.34**	**0.36**	**-0.02**	**-0.15**	**-0.15**
NH_4At	**9.7**	**0.0**	**-4.7**	**-8.5**	**-3.6**
NH_4I	**10.0**	**0.0**	**-5.0**	**-9.1**	**-4.0**

Table 5.11: Geometric parameters of NH_4I (as in Figure 5.1) and changes upon electron binding in Å, ° and Debye.

	r^{NH}	α	r^N	R	μ^N
$NH_4^+I^-$	**1.023**	**109.1**	**1.128**	**3.244**	**10.191**
$(NH_4^+I^-)^-$	+0.010	+1.9	-0.05	+0.222	+1.935

Table 5.12: Normal mode frequencies of NH_4^+, and changes upon hydrogen bonding to I^- and electron binding

Mode #	Desc. (NH_4^+)	$\nu(NH_4^+)$	Description ($NH_4^+At^-$)	$\delta\nu$ ($NH_4^+At^-$)	$\delta\nu$ $(NH_4^+At^-)^-$	$\nu(NH_4^0)$
1			a_1 intermol str.		-103	
2,3			e intermol. bend		-25	
4	t_2 bend	1505	a_1 NH_3 bend + H_s-N str.	-185	+67	1348
5,6	″	″	e NH_4 bend	-40	-7	″
7,8	e bend	1753	e NH_3 bend	-57	-8	1638
9	a_1 str.	3402	a_1 H_s-N str.	-1535	+993	3091
10	t_2 str.	3520	a_1 NH_3 str.	-64	-181	3117
11,12	″	″	e NH_3 str.	+76	-235	″

The evolution of the 1- and 2-body terms is opposite in the case of the N-type complex NH_3HF. The lowering of the energy of the anion is accomplished through strengthening of the 2-body interaction between NH_3 and HF and an increase of the electron binding energy EBE at the expense of increase of the repulsive ΔE_{1-b}^{HF} term. Contrary to NH_3-H^+, extending the H-F bond will contribute positively to the total dipole moment, and therefore the energetic penalty of such a stretch is compensated for by the electron in the anion. The increased 2-body interaction is responsible for the shortening of R and blueshifting of intermolecular modes. The geometrical distortions, in particular an

increase of r^F (Table 5.3), are responsible for enhancement of the dipole moment of the neutral complex by 0.088 D and thus for enhanced EBE. An increase in r^F is penalized by the ΔE_{1-b}^{HF} term and is followed by a red shift in the F-H_s stretching mode (Table 5.10).

We believe that modifications of the 1-body, 2-body, and EBE terms brought about by the excess electron attachment and demonstrated for the NH_3HF and NH_4At/NH_4I systems are characteristic for the class I and III hydrogen bonded complexes. The geometric distortions reported in the past for the anions of $(HF)_2$,[20] NH_3H_2O[61] and H_2OHCl[8] match the geometric pattern for the class I systems. These systems should be revisited to quantify the 1-body and 2-body terms. The geometric distortions reported in the past for zwitterions of amino acids[25-27] match the geometric pattern for the class III systems.

In section 5.5 we also noted that excess electron attachment leads to longer r^{NH} distances and red shifts in the stretching NH modes of a_1 and e symmetry. We discussed these changes in terms of the nodal structure of an orbital occupied by the excess electron. Another way of looking at these shifts is to recognize that the excess electron is tethered to the protic hydrogens of the NH_3 group. One can view $e^{-}\cdots H_3N$-HF as a hydrogen bonded system, in which the excess electron acts an acceptor of the protic H(N)s.[51] If so, then the redshifts of the NH stretches upon binding an electron are analogous to redshifts for stretching modes of proton donors in hydrogen bonded systems, though diminished by a smaller strength of "intermolecular" interactions: the energy of a typical hydrogen bond is *ca.* 8 mH, whereas the VDE value for this anionic complex is 1.666 mH.

5.8. Summary

We have introduced a classification scheme for the hydrogen-bonded dimers $A\cdots H_DD$ based on their preference to transfer H_D^+ from D and form a zwitterion $AH_D^+\ldots D^-$. The systems studied, NH_3HF, H_2OHCl, and NH_3HAt, belong to the extreme classes I and III. The first two belong to class I, the least susceptible to proton transfer: they do not support a zwitterionic minimum and do not transfer H_D even upon the attachment of an excess electron. The two systems support dipole-bound anions with VDEs of 1.67 and 2.16 mH for $(NH_3HF)^-$ and $(H_2OHCl)^-$, respectively. The third system, NH_3HAt, belongs to class III, the most susceptible to proton transfer. It supports a zwitterionic

local minimum for the neutral complex, and strongly binds an excess electron with a VDE of 30.80 mH.

The computational results for $(NH_3HF)^-$ and $(H_2OHCl)^-$[8] and the experimental PES spectrum of $(H_2OHCl)^-$ demonstrate that these molecular frameworks are only weakly affected by excess electron attachment. No vibrational structure is present in the computed spectrum of $(NH_3HF)^-$ (Figure 5.2). It is weak but clearly visible in the experimental spectrum of $(H_2OHCl)^-$ (Figure 5.2) and the corresponding computational results.[8] The difference in the strength of the vibrational structure in the PES spectra of $(H_2OHCl)^-$ and $(NH_3HF)^-$ correlates with the magnitude of electron binding energies (1.67 vs. 2.16 mH).

The NH_3HCl system belongs to the middle class, II: it does not support a zwitterionic minimum but it does transfer H_D upon excess electron attachment. Thus the structures of the neutral and anionic complex differ *qualitatively*. As a consequence, the PES spectrum has very clear vibrational structure, dominated by a progression involving the H-Cl stretching mode (Figure 5.2). The excess electron binds to the NH_4^+ site forming a pair $NH_4^{\cdots}Cl^-$. Hence, the VDE value of 19.88 mH is much larger than for the class I systems, though no stable neutral Z structure is present.

We discussed the energetics of proton transfer in the NH_3HX complexes and the additional driving force for proton transfer resulting from an excess electron attachment. In view of the fact that the proton affinity of D^- is typically larger than that of A by 400-700 kJ mol^{-1}, the shortfall needs to be compensated by additional interactions. Firstly, intermolecular interactions favour the ionic pair $AH^+ \ldots D^-$ over the neutral pair A…HD. Still, they are not able imprint a local minimum for $AH^+ \ldots D^-$ on the potential energy surface in the complexes with F, Cl, and Br (the preceding chapter). Only with I and At, for which the shortfall in proton affinities is the smallest, can we witness such a minimum. In this context, with the subtle balance between one-and two-body forces, the excess electron can exert a powerful influence. A barrier to proton transfer disappears for Cl and all the heavier halogens, as illustrated by our calculations and photoelectron spectra ([6,24]; Figure 5.2). The binding of the excess electron is much stronger for $NH_4^+ \ldots X^-$ than for $H_3N \ldots HX$. The anion of the former can be viewed as a complex of the NH_4 radical with X^-, whereas for the latter the anion is dipole-bound and the vertical attachment energy does not exceed 1.5 mH.

We reported opposed patterns of geometric distortion and vibrational shifts upon excess electron attachment to the complexes in class I and class III, i.e. $H_3N^{\cdots}HF$ and $NH_4^{+\cdots}At^-$. For example, the distance between the heavy atoms *decreases* in the F complex but *increases* in the At complex, and the intermolecular vibrational modes are *blue*shifted in the former but *red*shifted in the latter. We interpreted these patterns in terms of modifications of one- and two-body interaction energy terms and excess electron binding energies. Of particular interest is partial restoration of the tetrahedral geometry of NH_4 in the anionic complex and a significant blueshift of the N-H stretching mode by 938 cm^{-1}. By contrast, in the neutral $NH_4^{+\cdots}At^-$ complex the same N-H bond is strongly elongated away from T_d symmetry and the stretching mode is redshifted by 1487 cm^{-1}.

5.9. Appendix: Supplementary Information

Table 5.13: Geometric parameters of extrapolated NH_4F Z complex..(Å and °)

	r^{NH}	α	r^X	r^N	R
NH_4F (Z)	1	111.3	1.6	1.1	2.7

5.10. References

[1] E. P. L. Hunter and S. G. Lias, *Evaluated gas phase basicities and proton affinities of molecules: An update*, J. Phys. Chem. Ref. Data, **27**, 413-656 (1998)

[2] E. P. Hunter and S. G. Lias *Proton Affinity Evaluation* in *NIST Chemistry WebBook, NIST Standard Reference Database Number 69*; Linstrom, P. J.; Mallard, W. G., Eds.; National Institute of Standards and Technology: Gaithersburg MD, 20899, 2011.

[3] J. D. D. Martin and J. W. Hepburn, *Determination of bond dissociation energies by threshold ion-pair production spectroscopy: An improved D-0(HCl)*, J. Chem. Phys., **109**, 8139-8142 (1998)

[4] C. Blondel, P. Cacciani, C. Delsart and R. Trainham, *High-Resolution Determination of the Electron-Affinity of Fluorine and Bromine Using Crossed Ion and Laser-Beams*, Phys. Rev. A, **40**, 3698-3701 (1989)

[5] R. J. Pelaez, C. Blondel, C. Delsart and C. Drag, *Pulsed photodetachment microscopy and the electron affinity of iodine*, J. Phys. B: At., Mol. Opt. Phys., **42**, 125001 (2009)

[6] S. N. Eustis, D. Radisic, K. H. Bowen, R. A. Bachorz, M. Haranczyk, G. K. Schenter and M. Gutowski, *Electron-Driven Acid-Base Chemistry: Proton Transfer from Hydrogen Chloride to Ammonia*, Science, **319**, 936-939 (2008)

[7] S. N. Eustis, A. Whiteside, D. Wang, M. Gutowski and K. H. Bowen, *Ammonia−Hydrogen Bromide and Ammonia−Hydrogen Iodide Complexes: Anion Photoelectron and Ab Initio Studies*, J. Phys. Chem. A, **114**, 1357-1363 (2009)[8] P. Skurski and M. Gutowski, *Ab initio study of the dipole-bound anion $(H_2O...HCl)^-$*, J. Chem. Phys., **111**, 3004-3011 (1999)

[9] J. E. Bartmess *Negative Ion Energetics Data* in *NIST Chemistry WebBook, NIST Standard Reference Database Number 69*; Linstrom, P. J.; Mallard, W. G., Eds.; National Institute of Standards and Technology: Gaithersburg MD, 20899, 2012.
[10] G. L. Johnson and L. Andrews, *Matrix Infrared Spectrum of the H_3N-HF Hydrogen-Bonded Complex*, J. Am. Chem. Soc., **104**, 3043-3047 (1982)
[11] V. A. Clements, P. R. R. Langridge-Smith and B. J. Howard In *OSU International Symposium on Molecular Spectroscopy* 1980.
[12] M. Swart, E. Rosler and F. M. Bickelhaupt, *Proton affinities in water of main group element hydrides - effects of hydration and methyl substitution*, Eur. J. Inorg. Chem., **2007**, 3646-3654 (2007)
[13] T. Saue, K. Faegri and O. Gropen, *Relativistic effects on the bonding of heavy and superheavy hydrogen halides*, Chem. Phys. Lett., **263**, 360-366 (1996)
[14] J. S. Thayer *Relativistic Effects and the Chemistry of the Heavier Main Group Elements* in *Relativistic Methods for Chemists*; Barysz, M.; Ishikawa, Y., Eds.; Springer: London, 2010, p 79.
[15] B. Cordero, V. Gomez, A. E. Platero-Prats, M. Reves, J. Echeverria, E. Cremades, F. Barragan and S. Alvarez, *Covalent radii revisited*, Dalton Trans., 2832-2838 (2008)
[16] M. Gutowski, I. Dabkowska, J. Rak, S. Xu, J. M. Nilles, D. Radisic and K. H. Bowen, *Barrier-free intermolecular proton transfer in the uracil-glycine complex induced by excess electron attachment*, Eur. Phys. J. D, **20**, 431-439 (2002)
[17] R. A. Bachorz, M. Haranczyk, I. Dabkowska, J. Rak and M. Gutowski, *Anion of the formic acid dimer as a model for intermolecular proton transfer induced by a π^* excess electron*, J. Chem. Phys., **122**, 204304 (2005)
[18] J. Simons, *Molecular anions*, J. Phys. Chem. A, **112**, 6401-6511 (2008)
[19] M. Gutowski and P. Skurski, *Electron binding energies in linear dipole-bound $(HCN)_n^-$ (n=2-5) anions*, Chem. Phys. Lett., **300**, 331-338 (1999)
[20] M. Gutowski and P. Skurski, *Theoretical study of the dipole-bound anion $(HF)_2^-$* , J. Chem. Phys., **107**, 2968-2973 (1997)
[21] J. H. Hendricks, H. L. deClercq, S. A. Lyapustina and K. H. Bowen, *Negative ion photoelectron spectroscopy of the ground state, dipole-bound dimeric anion, $(HF)_2^-$*, J. Chem. Phys., **107**, 2962-2967 (1997)
[22] G. H. Lee, S. T. Arnold, J. G. Eaton and K. H. Bowen, *Electronic properties of dipole-bound $((H_2O)_2)^-$, $((D_2O)_2)^-$, $(((H_2O)_2)^-$ Ar(n=1,2,3), and $((D_2O)_2)^-$ Ar(n=1,2,3) using negative ion photoelectron spectroscopy*, Chem. Phys. Lett., **321**, 333-337 (2000)
[23] M. Gutowski, C. S. Hall, L. Adamowicz, J. H. Hendricks, H. L. de Clercq, S. A. Lyapustina, J. M. Nilles, S. J. Xu and K. H. Bowen, *Solvated electrons in very small clusters of polar molecules: $((HF)_3)^-$*, Phys. Rev. Lett., **88**, 143001 (2002)
[24] S. N. Eustis, A. Whiteside, D. Wang, M. Gutowski and K. H. Bowen, *Ammonia−Hydrogen Bromide and Ammonia−Hydrogen Iodide Complexes: Anion Photoelectron and Ab Initio Studies*, J. Phys. Chem. A, **114**, 1357-1363 (2009)
[25] M. Gutowski, P. Skurski and J. Simons, *Dipole-bound anions of glycine based on the zwitterion and neutral structures*, J. Am. Chem. Soc., **122**, 10159-10162 (2000)
[26] J. Rak, P. Skurski and M. Gutowski, *An ab initio study of the betaine anion-dipole-bound anionic state of a model zwitterion system*, J. Chem. Phys., **114**, 10673-10681 (2001)
[27] P. Skurski, J. Rak, J. Simons and M. Gutowski, *Quasidegeneracy of zwitterionic and canonical tautomers of arginine solvated by an excess electron*, J. Am. Chem. Soc., **123**, 11073-11074 (2001)
[28] E. Fermi and E. Teller, *The Capture of Negative Mesotrons in Matter*, Phys. Rev., **72**, 399-408 (1947)

[29] M. Haranczyk, J. Rak, M. Gutowski, D. Radisic, S. T. Stokes and K. H. Bowen, *Intermolecular proton transfer in anionic complexes of uracil with alcohols*, J. Phys. Chem. B, **109**, 13383-13391 (2005)
[30] R. J. Bartlett and M. Musial, *Coupled-cluster theory in quantum chemistry*, Rev. Mod. Phys., **79**, 291-352 (2007)
[31] H. B. Jansen and P. Ros, *Non-empirical molecular orbital calculations on the protonation of carbon monoxide*, Chem. Phys. Lett., **3**, 140-143 (1969)
[32] S. F. Boys and F. Bernardi, *The calculation of small molecular interactions by the differences of separate total energies. Some procedures with reduced errors.*, Mol. Phys., **19**, 553-556 (1970)
[33] S. Simon, M. Duran and J. J. Dannenberg, *How does basis set superposition error change the potential surfaces for hydrogen bonded dimers?*, J. Chem. Phys., **105**, 11024-11031 (1996)
[34] J. A. Pople, M. Head-Gordon and K. Raghavachari, *Quadratic configuration interaction - a general technique for determining electron correlation energies*, J. Chem. Phys., **87**, 5968-5975 (1987)
[35] P. A. Kollman and S. U. Chandra, *An Approach to Computing Electrostatic Charges for Molecules*, J. Comput. Chem., **5**, 129-145 (1984)
[36] B. H. Besler, K. M. Merz and P. A. Kollman, *Atomic charges derived from semiempirical methods*, J. Comput. Chem., **11**, 431-439 (1990)
[37] G. Schaftenaar and J. H. Noordik, *Molden: a pre- and post-processing program for molecular and electronic structures*, J. Comput. Aided Mol. Des., **14**, 123-134 (2000)
[38] M. Haranczyk and M. Gutowski, *Visualization of molecular orbitals and the related electron densities*, J. Chem. Theory Comput., **4**, 689-693 (2008)
[39] W. Humphrey, A. Dalke and K. Schulten, *VMD: Visual molecular dynamics*, J. Mol. Graphics Modell., **14**, 33-38 (1996)
[40] Persistence of Vision Raytracer, 3.6, Persistence of Vision Pty. Ltd., Williamstown, Victoria, Australia, 2004
[41] Gaussian 03, Revision C.02, M. J. Frisch, G. W. Trucks, H. B. Schlegel, G. E. Scuseria, M. A. Robb, J. R. Cheeseman, J. A. Montgomery Jr., T. Vreven, K. N. Kudin, J. C. Burant, J. M. Millam, S. S. Iyenga, J. Tomasi, V. Barone, B. Mennucci, M. Cossi, G. Scalmani, N. Rega, G. A. Petersson, H. Nakatsuji, M. Hada, M. Ehara, K. Toyota, R. Fukuda, J. Hasegawa, M. Ishida, T. Nakajima, Y. Honda, O. Kitao, H. Nakai, M. Klene, X. Li, J. E. Knox, H. P. Hratchian, J. B. Cross, C. Adamo, J. Jaramillo, R. Gomperts, R. E. Stratmann, O. Yazyev, A. J. Austin, R. Cammi, C. Pomelli, J. W. Ochterski, P. Y. Ayala, K. Morokuma, G. A. Voth, P. Salvador, J. J. Dannenberg, V. G. Zakrzewski, S. Dapprich, A. D. Daniels, M. C. Strain, O. Farkas, D. K. Malick, A. D. Rabuck, K. Raghavachari, J. B. Foresman, J. V. Ortiz, Q. Cui, A. G. Baboul, S. Clifford, J. Cioslowski, B. B. Stefanov, G. Liu, A. Liashenko, P. Piskorz, I. Komaromi, R. L. Martin, D. J. Fox, T. Keith, M. A. Al-Laham, C. Y. Peng, A. Nanayakkara, M. Challacombe, P. M. W. Gill, B. Johnson, W. Chen, M. W. Wong, C. Gonzalez and J. A. Pople, Gaussian, Inc., Wallingford CT, 2004
[42] Gaussian 09, Revision B.01, M. J. Frisch, G. W. Trucks, H. B. Schlegel, G. E. Scuseria, M. A. Robb, J. R. Cheeseman, G. Scalmani, V. Barone, B. Mennucci, G. A. Petersson, H. Nakatsuji, M. Caricato, X. Li, H. P. Hratchian, A. F. Izmaylov, J. Bloino, G. Zheng, J. L. Sonnenberg, M. Hada, M. Ehara, K. Toyota, R. Fukuda, J. Hasegawa, M. Ishida, T. Nakajima, Y. Honda, O. Kitao, H. Nakai, T. Vreven, J. J. A. Montgomery, J. E. Peralta, F. Ogliaro, M. Bearpark, J. J. Heyd, E. Brothers, K. N. Kudin, V. N. Staroverov, T. Keith, R. Kobayashi, J. Normand, K. Raghavachari, A. Rendell, J. C. Burant, S. S. Iyengar, J. Tomasi, M. Cossi, N. Rega, J. M. Millam, M. Klene, J. E. Knox, J. B. Cross, V. Bakken, C. Adamo, J. Jaramillo, R. Gomperts, R. E. Stratmann,

O. Yazyev, A. J. Austin, R. Cammi, C. Pomelli, J. W. Ochterski, R. L. Martin, K. Morokuma, V. G. Zakrzewski, G. A. Voth, P. Salvador, J. J. Dannenberg, S. Dapprich, A. D. Daniels, O. Farkas, J. B. Foresman, J. V. Ortiz, J. Cioslowski and D. J. Fox, Gaussian, Inc., Wallingford CT, 2010

[43] MOLPRO, a package of ab initio programs, version 2010.1, H.-J. Werner, P. J. Knowles, G. Knizia, F. R. Manby, M. Schütz, P. Celani, T. Korona, R. Lindh, A. Mitrushenkov, G. Rauhut, K. R. Shamasundar, R. D. A. T. B. Adler, A. B. A. Bernhardsson, D. L. Cooper, M. J. O. Deegan, A. J. Dobbyn, F. Eckert, E. Goll, C. Hampel, A. Hesselmann, G. Hetzer, T. Hrenar, G. Jansen, C. Köppl, Y. Liu, A. W. Lloyd, R. A. Mata, A. J. May, S. J. McNicholas, W. Meyer, M. E. Mura, A. Nicklass, D. P. O'Neill, P. Palmieri, K. Pflüger, R. Pitzer, M. Reiher, T. Shiozaki, H. Stoll, A. J. Stone, R. Tarroni, T. Thorsteinsson, M. Wang and A. Wolf, Cardiff, UK, 2011

[44] T. H. Dunning, *Gaussian basis sets for use in correlated molecular calculations. I. The atoms boron through neon and hydrogen*, J. Chem. Phys., **90**, 1007-1023 (1989)

[45] R. A. Kendall, T. H. Dunning and R. J. Harrison, *Electron affinities of the first-row atoms revisited. Systematic basis sets and wave functions*, J. Chem. Phys., **96**, 6796-6806 (1992)

[46] K. Peterson, D. Figgen, E. Goll, H. Stoll and M. Dolg, *Systematically convergent basis sets with relativistic pseudopotentials. II. Small-core pseudopotentials and correlation consistent basis sets for the post-d group 16-18 elements*, J. Chem. Phys., **119**, 11113-11123 (2003)

[47] P. Skurski, M. Gutowski and J. Simons, *How to choose a one-electron basis set to reliably describe a dipole-bound anion*, Int. J. Quantum Chem, **80**, 1024-1038 (2000)

[48] K. Schuchardt, B. Didier, T. Elsethagen, L. Sun, V. Gurumoorthi, J. Chase, J. Li and T. Windus, *Basis Set Exchange: A community database for computational sciences*, J. Chem. Inf. Model., **47**, 1045-1052 (2007)

[49] D. Feller, *The role of databases in support of computational chemistry calculations*, J. Comput. Chem., **17**, 1571-1586 (1996)

[50] A. Famulari, M. Sironi and M. Raimondi *BSSE-Free MCSCF method for strong hydrogen bonds: Investigation of H_2O-HCl and NH_3-HCl complexes* in *Quantum Systems in Chemistry and Physics, Vol. 1: Basic Problems and Model Systems*; Hernández-Laguna, A.; Maruani, J.; McWeeny, R.; Wilson, S., Eds.; Kluwer Academic Publishers: London, 2000, p 361-379.

[51] M. Haranczyk and M. Gutowski, *Effect of excess electron and one water molecule on relative stability of the canonical and zwitterionic tautomers of glycine*, J. Chem. Phys., **128**, 125101 (2008)

[52] E. V. Doktorov, I. A. Malkin and V. I. Manko, *Dynamical Symmetry of Vibronic Transitions in Polyatomic-Molecules and Franck-Condon Principle .2.*, J. Mol. Spectrosc., **64**, 302-326 (1977)

[53] D. S. Yang, M. Z. Zgierski, D. M. Rayner, P. A. Hackett, A. Martinez, D. R. Salahub, P. N. Roy and T. Carrington, *The Structure of Nb_3O and Nb_3O^+ Determined by Pulsed-Field Ionization-Zero Electron Kinetic-Energy Photoelectron-Spectroscopy and Density-Functional Theory*, J. Chem. Phys., **103**, 5335-5342 (1995)

[54] D. M. Neumark, K. R. Lykke, T. Andersen and W. C. Lineberger, *Laser Photodetachment Measurement of the Electron-Affinity of Atomic Oxygen*, Phys. Rev. A, **32**, 1890-1892 (1985)

[55] J. V. Coe, J. T. Snodgrass, C. B. Friedhoff, K. M. McHugh and K. H. Bowen, *Photoelectron spectroscopy of the negative ion SeO^-*, J. Chem. Phys., **84**, 618-625 (1986)

[56] G. Herzberg, *Rydberg Spectra of Triatomic Hydrogen and of the Ammonium Radical*, Faraday Discuss., **71**, 165-173 (1981)

[57] M. Gutowski, P. Skurski, A. I. Boldyrev, J. Simons and K. D. Jordan, *Contribution of electron correlation to the stability of dipole-bound anionic states*, Phys. Rev. A, **54**, 1906-1909 (1996)
[58] M. Gutowski, P. Skurski, K. D. Jordan and J. Simons, *Energies of dipole-bound anionic states*, Int. J. Quantum Chem, **64**, 183-191 (1997)
[59] M. Gutowski and P. Skurski, *Dispersion Stabilization of Solvated Electrons and Dipole-Bound Anions*, J. Phys. Chem. B, **101**, 9143-9146 (1997)
[60] M. Gutowski, K. D. Jordan and P. Skurski, *Electronic Structure of Dipole-Bound Anions*, J. Phys. Chem. A, **102**, 2624-2633 (1998)
[61] P. Skurski and M. Gutowski, *Theoretical study of the dipole-bound anion* $(H_2O...NH_3)^-$, J. Chem. Phys., **108**, 6303-6311 (1998)
[62] A. Whiteside, M. Gutowski, V. A. Clements, P. R. R. Langridge-Smith and B. J. Howard (to be published)

Chapter 6: Is Electronegativity a Useful Descriptor for the Pseudo-Alkali Metal NH_4?

Published in *Chemistry - A. European. Journal* vol. 17 pp. 13197–13205 (Alexander Whiteside, Sotiris S. Xantheas, and Maciej Gutowski)

6.1. Abstract

Molecular ions in the form of "pseudo-atoms" are common structural motifs in chemistry, with properties that are transferrable between different compounds. We have determined one such property – the electronegativity – for the "pseudo-alkali metal" ammonium (NH_4), and evaluated its reliability as a descriptor versus the electronegativities of the alkali metals. The computed properties of ammonium's binary complexes with astatine and of selected borohydrides confirm the similarity of NH_4 to the alkali metal atoms, although the electronegativity of NH_4 is relatively large in comparison to its cationic radius. We have paid particular attention to the molecular properties of ammonium (angular anisotropy, geometric relaxation, and reactivity), which can cause deviations from the behaviour expected of a conceptual "true alkali metal" with this electronegativity. These deviations allow for the discrimination of effects associated with the molecular nature of NH_4.

6.2. Introduction

Electronegativity is the ability of an atom to attract electrons from its neighbours. This concept has been of great utility in explaining and predicting chemistry, from the polar covalent bond that is formed between two atoms of unlike electronegativity,[1] to directing effects in aromatic substitution reactions.[2] Central to this concept is the assumption that electronegativity is a consistent property regardless of the atom's environment, *i.e.* it is transferable. Further development in this area has questioned whether chemical functional groups and certain molecular ions – "pseudo-atoms" – are sufficiently well-defined and well-behaved to have electronegativities of their own.

Electronegativity was first given a quantitative definition by Pauling in 1932, during the period in which theoretical chemistry (as we now understand it) was first being formulated.[3] This definition was based upon the resonance model of polar bonding and experimental thermochemical data, and inferred the value of electronegativity from

the energetics of the bonds being formed. In 1934 Mulliken redirected Pauling's argument to define electronegativity as an absolute property of the atom, equal to one half of the *sum* of the atom's gas-phase ionisation energy and its electron affinity.[4] (This was later conceptually refined as a property of the corresponding orbitals that either gain or lose the electrons.[5]) A caveat of this latter definition is that an atom must be in its proper *valence state* to form specific chemical bonds, and therefore a value for the electronegativity obtained from ground state electron affinities and ionization energies might be invalid. It is therefore understood that electronegativity is *not* strictly transferable and depends upon an atom's environment.[4]

Sanderson initially proposed[6] and various groups ultimately applied (e.g. Reference [7,8]) the "electronegativity equalisation principle". This principle observes that as an electronegative atom accumulates negative charge, its electronegativity will tend to decrease. Conversely its less electronegative neighbours will gain positive charge and increase in their electronegativity. An equilibrium is reached when the electronegativities are equal. Therefore a molecule has its own well-defined electronegativity, which is constant across the molecule. Parr ultimately confirmed this principle by demonstrating the equivalence between the electronic chemical potential (*i.e.* the energy change of a physical system upon the gain or loss of electrons) and the electronegativity.[9]

Related to electronegativity is the concept of hardness. Pearson proposed chemical hardness qualitatively in his hard-soft acid-base (HSAB) theory, as an intuitive combination of several related concepts such as the electronegativity, the polarisability, and the valence orbital energies of an atom.[10] This model was very successful in developing the understanding of reactivity. In the 1980s, Parr and Pearson formalized a quantitative definition of "absolute hardness", equal to one half the *difference* between the ionisation energy and the electron affinity of the atom. Whereas the Mulliken electronegativity is the finite-difference approximation to the first derivative of the energy with respect to the number of electrons, the hardness is the approximation to the second derivative.[11]

Since molecules have well-defined ionization energies and electron affinities, we propose that the Mulliken electronegativity and the Pearson hardness of a molecule can be calculated from these quantities. (We note that the Mulliken definition of

electronegativity was used by Leyssens *et al*[12] to discuss changes in electronegativity of parts of a molecule, *i.e.*its constituent chemical groups).

The electronegativity and hardness are expected to vary with a molecule's charge, electronic state and geometry, and geometrical relaxation can be expected to occur when a molecule's charge changes. In order to systematically investigate the molecular electronegativity and hardness, it is instructive to start from molecular systems whose geometry is not significantly altered upon the change of their total charge. In addition, complications resulting from the involvement of excited valence electronic states should be avoided.

Ammonium meets both of these criteria. The parent species, the "pseudo-atom" for which the electronegativity and hardness are calculated, is the ammonium radical. This unusual molecule consists of a tetrahedrally symmetric ammonium cation binding one electron to a diffuse, full-symmetric orbital using its positive charge.[13] First definitively identified by Herzberg in 1980,[14] this "Rydberg molecule" was of considerable interest as a molecular analogue for the alkali metals. For example, it was predicted by Boldyrev and Simons[15] that the ammonium radical would form a dimer similar in properties to the alkali metal dimers. Wright and McKay indicated that spontaneous decomposition to ammonia and molecular hydrogen would occur when the ammonium molecules rotated in such a way that two hydrogen atoms were in proximity,[16] but a later study found that mixed alkali metal-ammonium dimers would be stable.[17]

The ammonium radical can bind a second electron in its fully-symmetric orbital to form an ammonium anion[18-20] dubbed the "double-Rydberg anion" NH_4^-.[18] The process is akin to an alkali metal cation binding a first and a second electron to its *s* valence orbital. The tetrahedrally-symmetric ammonium radical and anion are metastable with respect to decomposition to an ammonia molecule plus a hydrogen radical and anion, respectively. The nitrogen-hydrogen bond distance is predicted to change by less than 0.02 Å between the cation and the neutral,[21,22] and only to a small degree between the neutral and anion,[18] meeting the first criterion. Like the alkali metals,[23] the ground electronic states of the neutral, cation, and anion are proper for the determination of the electronegativity and hardness of NH_4, therefore meeting the second criterion.

Notwithstanding its compliance with the basic requirements for determining electronegativity, ammonium is not an atom. Ammonium is not isotropic with respect to orientation, as the alkali metals are. Ammonium can distort geometrically, while the alkali metals cannot. And ammonium can donate one or more of its protons, a capacity that is unavailable to the alkali metals in the chemical regime. Therefore it was anticipated that ammonium would not behave as an ideal "pseudo-atom" in all conditions.

In this study we have computationally evaluated properties connected with ammonium's electronegativity in order to determine similarities and differences with the alkali metals. Firstly, we probed ammonium's behaviour in the gas phase to elucidate these effects in a clear, well-defined model. Using these insights, we then investigated ammonium's behaviour in solids to determine how these effects influence bulk materials.

6.2.1. Selection of Systems

Ammonium is a "pseudo-alkali metal", and therefore its electronegativity and properties were compared to those of the true alkali metals. In the first instance, accurate values for the ionization energy (*IE*) and electron affinity (*EA*) were calculated for the ammonium and sodium radicals at a high level of theory. In the case of *IE*, a positive value indicates that removal of an electron is endothermic. In the case of *EA*, a positive value indicates that addition of an electron is exothermic. From these values the Mulliken electronegativity, defined as one half of the sum of the *IE* and *EA*, and the Pearson hardness, defined as one half of the magnitude of the difference between the *IE* and *EA*, were calculated.

To identify similarities and differences between NH_4 and alkali metals, we compared the polarity of complexes containing ammonium with the polarity of analogous complexes containing the alkali metals (for Li, Na, and K). The dipole moment across a bond is expected to vary linearly with the "ionicity" of the bond,[1] and this bond ionicity is approximately proportional to the difference between the electronegativities of the two atoms (or an atom and a pseudo-atom, in this instance), as noted by Dailey and Townes.[24] We therefore computed the dipole moment and effective atomic charges of selected alkali and ammonium complexes.

NH_4^+ is a conjugate Brønsted-Lowry acid, and consequently it can interact by hydrogen bonding or proton donation with other chemical species. For this study it is important to maintain the identity of NH_4^+, which would be disrupted by proton transfer. We have therefore modelled NH_4^+ and alkali metal cations complexed with a weak Brønsted-Lowry base, astatide (At^-). (Complexes of NH_4^+ with stronger bases were discussed elsewhere.)[25,26] The choice of astatine as an electronegative probe of NH_4 ensures the geometrical stability of the cation-anion pair against proton transfer to the astatide. This results from astatide's low proton affinity (the lowest of any of the halides except the ununseptide[27] anion). The ionicity of ammonium astatide was then compared to the ionicities of the alkali metal astatides.

Ammonium is neither spherically symmetric nor rigid, and therefore it is expected to behave differently in different orientations or geometries. We probed ammonium with astatine in several structures. The C_{3v} structures depicted in Figure 6.1 ("structure A" and "structure B") were the prototypes. In structure A, a vertex of the tetrahedron is directed toward astatine. In structure B, a face of the tetrahedron is directed toward astatine. The orientation of the ammonium provides the first degree of freedom, and by evaluating each structure with a rigid tetrahedral "pseudo-atom" we could determine the effect of the orientation of ammonium on the ionicity.

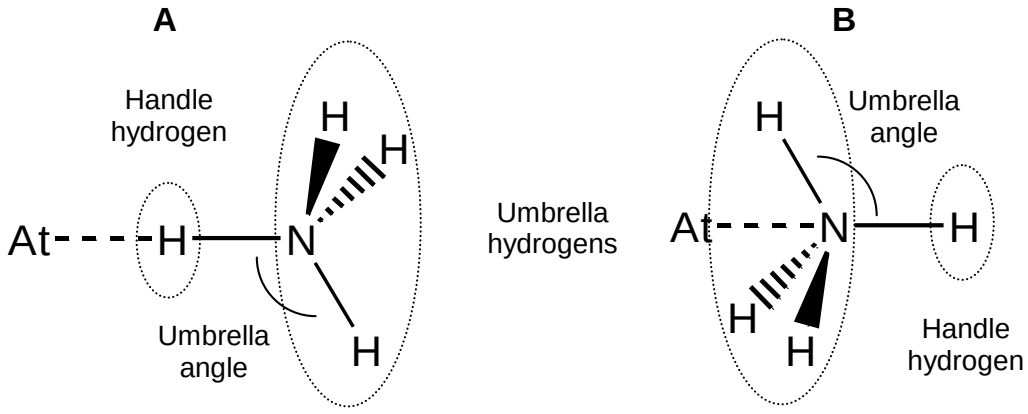

Figure 6.1: Structures of ammonium astatide complexes, indicating the terms used in the text.

As the next degree of freedom, we permitted ammonium to relax, *i.e.* to distort from the perfect tetrahedral structure. By comparing the dipole moment and charge for the rigid and relaxed geometries in the A and B structures we could investigate the effect of ammonium's internal geometric relaxation on the ionicity.

Finally, changes in the distance between the astatide and its partner cation cause compound variations in the dipole moments. First, there is a direct dependence of the dipole moment on the separation between effective positive and negative charges. In addition, effective atomic charges vary with the interionic distance. To isolate these two effects, we evaluated the ionicities of the alkali and ammonium astatides with either a relaxed or a fixed distance between the astatide and its partner. For ammonium, both rigid and deformable "pseudo-atoms" were considered in the A- and B-type orientations. When maintaining a fixed interionic distance for the alkali and ammonium astatides, we used the optimal astatine-nitrogen distance obtained for structure B when ammonium was rigid. This was selected based on the conjecture that ammonium in this geometry would behave most similarly to an alkali metal atom (as elaborated in the Results section). In summary, a total of eight structures were calculated for ammonium astatide (A vs. B, rigid vs. deformable NH_4, optimized vs. fixed interionic distance), and two for each alkali metal astatide (optimized vs. fixed interionic distance).

A single astatine atom used as a probe of the properties of NH_4 provides a demanding test of the usefulness of the electronegativity concept for molecular species. On the one hand, astatine seems to be quite benign, because At^- is a weak Brønsted-Lowry base. On the other hand, At^- creates a strong electrostatic field and acts as a potential donor of electron density. These features lead to a geometrical relaxation of NH_4^+ paralleled by a partial intermolecular charge transfer, which counteract effects associated with the electronegativity difference between At and an isolated NH_4. One could expect that electronegativity would be a more robust descriptor in the case of NH_4 engaged in a highly symmetric crystalline lattice. We investigated the borohydrides of the alkali metals and ammonium to assess whether the ammonium borohydride fits the electronegativity-property correlations that are characteristic of the corresponding alkali crystals.

Orimo *et al* studied the relationship between electronegativity of the metal site and properties of the alkali metal borohydrides,[28] which are of considerable interest as hydrogen storage materials for fuel cell vehicles. These borohydrides decompose upon heating to release hydrogen gas. They demonstrated that the more electronegative alkali metals form less stable borohydrides (as determined by the heat of formation), which decompose at lower temperatures. They proposed that the stability of a borohydride is dependent upon placing a negative charge upon the BH_4^- unit, and that the use of more

electronegative metals reduces this charge, leading to instability in the borohydride and a lower temperature of dehydrogenation. However even the borohydride of lithium decomposes at such a high temperature that it is impractical for on-board applications.[28,29] Ammonium borohydride, by contrast, releases hydrogen at relatively moderate temperatures.[30] Once the electronegativity of ammonium had been computed, we could assess whether the electronegativity of ammonium is high enough to be the cause of this behaviour, or whether the effect arises from other properties or molecular nature of ammonium.

Ammonium borohydride's crystal structure is a matter of some interest and ongoing debate.[30] Two structures have been proposed: a zinc blende structure in which the vertices of ammonium tetrahedra are directed at the faces of borohydride tetrahedra, and an orientationally disordered rock salt structure. The zinc blende crystal's N-H···H_3B dihydrogen bonded structure A (Figure 6.2) is akin to the "structure A" indicated in the preceding ammonium astatide detail (Figure 6.1). We can propose a complementary structure (zinc blende "structure B", Figure 6.2) in which borohydride tetrahedral vertices are directed towards the ammonium tetrahedral faces, B-H···H_3N. In this structure, ammonium's proton donor role is reduced. By computing the ionicity of ammonium borohydride in these zinc blende structures, we could assess whether links between the ionicity and the orientation of ammonium carry over to the solid phase. Furthermore, by comparing the ionicity and stability of the zinc blende structures, we could assess whether the more ionic structures are the more stable, as expected by the rule for the alkali metal borohydrides, or whether other effects overrule ionicity.

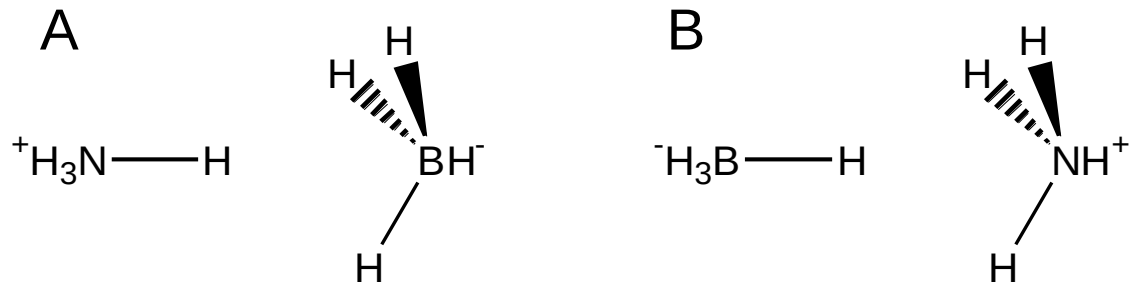

Figure 6.2: The preferred (A) and unpreferred (B) dihydrogen bonding structures in zinc blende ammonium borohydride.

6.3. Computational Detail

For isolated ammonium and the ammonium astatides, the coupled cluster method,[31] with singles and doubles (CCSD) or with singles, doubles and perturbative triples (CCSD(T)) was used. The Gaussian 03 package was used for these calculations.[32] The core orbitals of nitrogen and the alkali metals were not frozen, *i.e.* core-valence correlation was permitted. Dunning-type augmented, correlation-consistent, polarized valence double- triple- and quadruple-zeta basis sets (aug-cc-pVnZ, n=D, T, Q)[33] were used for hydrogen. Their core-valence analogues (aug-cc-pCVnZ)[33-37][2] were used for alkali metals and, while valence basis sets coupled with pseudopotentials (aug-cc-pVTZ-pp)[40] were used for astatine. These basis sets were obtained from the EMSL basis set library.[38,39] The basis sets for sodium were further augmented with one diffuse *s* function centered on the atom, whereas for nitrogen they were augmented with an even-tempered set of three *s* functions, in order to adequately describe the valence electron(s).[41] Each additional function had an exponent equal to that of the most diffuse function divided by 2.5.

The geometry of tetrahedral ammonium was optimised at the CCSD and CCSD(T) levels with triple- and quadruple-zeta basis sets. The geometries of the astatide complexes were optimised (or partially optimised) at the CCSD level with the triple-zeta basis set. Dipole moments, effective atomic charges determined by the Merz-Singh-Kollman method,[42-44][3] vibrational frequencies and harmonic zero-point vibrational energy corrections were calculated at the same level of theory, the latter for fully optimized geometries only. Effective charges reported are the negative of the charge at the astatine atom, q_{At}. Hartree-Fock (HF), Møller-Plesset second-order perturbation theory (MP2), CCSD, and CCSD(T) contributions to the energy were recorded. Hartree-Fock energies were extrapolated to the basis set limit by Halkier's method[45] using three points, and correlation energies by Helgaker's method[46] using two points. In each case, the highest extrapolation point was the energy obtained with the quadruple-zeta basis set.

[2] Woon and Dunning's core-valence basis set for sodium and Feller's core-valence basis set for potassium are are not yet published in the literature, but has been made available on the EMSL basis set library (the latter as "Feller misc. CVnZ").[38,39]

[3] Given that ammonium astatide is expected to be highly ionic in character, the ionic radius of the ammonium cation (1.46Å) and an estimate of the ionic radius of astatide (2.25Å) were used, in place of the covalent radii.

Optimised geometries and electronic structures for crystalline ammonium borohydride were calculated with the PW91 functional[47] and PAW-GGA pseudopotentials[48] using VASP.[49-52] Partial charges were calculated by Bader's analysis[53] using software developed by Henkelman *et al.*[54-56] Bratsch's half-power scheme[23] was chosen to convert the Mulliken electronegativity in eV (χ_M) to the electronegativity on the Pauling scale (χ_P): $\chi_P = 1.35\sqrt{\chi_M} - 1.37$.

Chemical structure diagrams were created using ChemDraw.[57]

6.4. Results

Astatine's Mulliken electronegativity was computed as 6.22 eV based on literature values for the ionisation energy[58] and electron affinity.[59] This is equivalent to 2.00 on the Pauling scale (via the equation in the Computational Detail section). We have tested that the ionic complex of NH_4^+ and At^- is stable with respect to the hydrogen bonded complex of HAt with NH_3, which contrasts At with lighter halogen atoms.[25,26]

The computed results for isolated Na and NH_4 are summarised in Table 6.1 and Table 6.2 respectively. HF indicates the Hartree-Fock (uncorrelated) energy, ΔMP2, ΔCCSD, and Δ(T) indicate the incremental contributions to the correlation energy at the respective level of theory, and ΔZPE indicates the zero-point vibrational energy correction to the adiabatic properties. At the CCSD(T) level of theory the calculated values of the ionisation energy (*IE*) and electron affinity (*EA*) of sodium were within 0.01 eV and 0.0002 eV of the experimental data, respectively. The error bars in experimental values of *IE* and *EA* for NH_4 are larger than those for Na. The CCSD(T) *IE* and *EA* of NH_4 are marginally outside of the error bars. Note that the second electron is unbound for both species at the Hartree-Fock level, and that more than 10% of the *EA* of NH_4 is recovered by the perturbative triples correction used at the CCSD(T) level, a fact that further emphasises the importance of electron correlation in the proper description of the anions.

Table 6.1: Calculated sodium radical ionization energy (IE), electron affinity (EA), electronegativity and hardness calculations (values in eV). HF indicates the Hartree-Fock (uncorrelated) energy, ΔMP2, ΔCCSD, and Δ(T) indicate the incremental contributions to the correlation energy at the respective level of theory (MP2, CCSD, and CCSD(T)).

	HF	ΔMP2	ΔCCSD	Δ(T)	Total	Experimental
IE	4.954	0.156	0.008	0.011	5.130	5.13908 [60]
EA	-0.104	0.473	0.155	0.024	0.548	0.547949 +/- 0.000044[61]
Electronegativity	2.425	0.315	0.082	0.018	2.839	2.844 from expt. data 2.84 from literature [23]
Hardness	2.529	-0.158	-0.073	-0.006	2.291	2.296 from expt. data 2.30 from literature[11]

Table 6.2: Calculated ammonium radical ionization energy (IE), electron affinity (EA), electronegativity and hardness (values in eV). HF indicates the Hartree-Fock (uncorrelated) energy, ΔMP2, ΔCCSD, and Δ(T) indicate the incremental contributions to the correlation energy at the respective level of theory (MP2, CCSD, and CCSD(T)) and ΔZPE indicates the zero-point vibrational energy correction to the adiabatic values.

	HF	ΔMP2	ΔCCSD	Δ(T)	ΔZPE	Total	Expt.
IE (adiabatic)	4.001	0.469	-0.011	0.058	0.138	4.656	4.73 +/- 0.06[13]
IE (vertical)	4.062	0.440	-0.010	0.053	N/A	4.545	N/A
EA (adiabatic)	-0.103	0.424	0.086	0.063	-0.012	0.458	0.472 +/- 0.003[18],4
EA (vertical)	-0.102	0.424	0.086	0.063	N/A	0.470	N/A
Electronegativity from adiabatic energies	1.949	0.447	0.037	0.061	0.063	2.556	N/A
Electronegativity from vertical energies	1.980	0.432	0.038	0.058	N/A	2.507	N/A
Hardness from adiabatic energies	2.052	0.022	-0.049	-0.002	0.075	2.099	N/A
Hardness from vertical energies	2.082	0.008	-0.048	-0.005	N/A	2.037	N/A

The resulting Mulliken electronegativity values are 2.839 eV for Na, and 2.556 eV (adiabatic), and 2.507 eV (vertical) for NH_4. For reference, the literature value for sodium is 2.84 eV.[23] Using Bratsch's scheme, values of 0.77 (vertical) and 0.79 (adiabatic) are obtained for ammonium on the Pauling scale. The corresponding hardnesses of ammonium are 2.098 eV (adiabatic) and 2.037 eV (vertical). Boldyrev and Simons have previously estimated sodium's electronegativity to be approximately 1.3 times that of ammonium using the available data on the latter,[17] putting ammonium's electronegativity around 2.1 eV. That underestimate resulted from the value of *EA* used in the prediction.

[4] Snodgrass et al[18] report the vertical detachment energy of the ammonium anion, but conclude that "because of the high degree of structural similarity between this anion and its corresponding neutral, the adiabatic electron affinity of [tetrahedral ammonium] has the same value"

The fully relaxed structure A for ammonium astatide was found to be the global minimum, while fully relaxed structure B was a second-order saddle point. Two degenerate negative frequencies exist for the fully relaxed structure B, corresponding to rotation of the ammonium molecule perpendicular to the C_3 symmetry axis (i.e. toward structure A). The fully relaxed structure A was 0.26 eV more stable than the fully relaxed structure B at the level of theory used for the optimization.

The effective charges q_{At} of the binary complexes have been plotted as a function of the difference in electronegativity between astatine and either the alkali atom or ammonium. The results for complexes with fixed and relaxed interionic distances are displayed in Figure 6.3 and Figure 6.4, respectively. Analogous plots for dipole moments are displayed in Figure 6.5 and Figure 6.6. All complexes proved to be highly ionic. For the alkali astatides, the dipole moments ranged from 7.3 to 11.5 D, and q_{At} ranged from 0.61 to 0.75 e. For the ammonium astatide structures, the dipole moments ranged from 9.1 to 10.9 D, and the charges from 0.53 to 0.70 e.

For the alkali (Li, Na, K) astatides (diagonal crosses "×" in Figure 6.3 to Figure 6.6) there are clear correlations between the q_{At} or the dipole moments and the difference in electronegativity between the astatine and the metal. These correlations are denoted with straight lines. A superior correlation was found when the alkali-astatine distance was fixed (Figure 6.3, Figure 6.4). The ammonium astatide with the rigid tetrahedron at the B orientation, labelled with "+", is typically the closest to the lines determined by the alkali astatides. The matching is better for dipole moments than for q_{At} , with the latter being too small with respect to the trend lines. We conclude that ammonium radicals are the most similar to the alkali atoms when they are constrained to the rigid tetrahedral geometry and their ability to engage in chemical interactions involving their hydrogen atoms is suppressed by the B orientation.

Changing the ammonium orientation from B to A, while keeping the tetrahedron rigid and the interionic distance fixed, lowers the ionicity of the complex (asterisks "*" in Figure 6.3, Figure 6.4). A clear deviation from the straight line can be seen for q_{At} (Figure 6.3) and the dipole moment (Figure 6.4). We ascribe the drop in q_{At} to the direct chemical interaction between the "handle" hydrogen of NH_4 and At. The A structure ensures a perfect collinear alignment of the "handle" hydrogen with N and At and facilitates a charge transfer from the idealized At^- to NH_4^+. As a consequence, the q_{At}

value is lower by 0.12 e for A than for B. The dipole moment then declines by 0.9 D as a result. This illustrates that the iconicity of ammonium can be substantially quenched upon its engagement in hydrogen bonding.

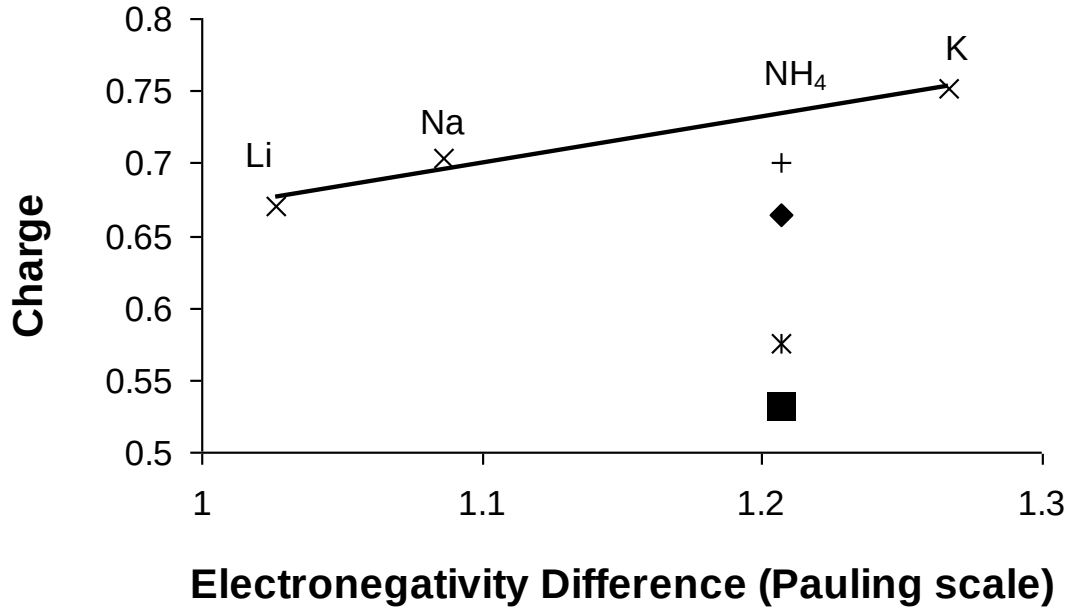

Figure 6.3: Correlation between the electronegativity difference (Pauling scale) and charge (in e) of astatide complexes, with alkali-astatide and nitrogen-astatide distances (R_{NAt}) fixed to that obtained for structure B with rigid NH_4 at 3.1293 Å. Diagonal crosses (×) indicate the alkali metals, to which a least-squares fit line is applied. The vertical cross (+) indicates the rigid ammonium astatide in structure B. The diamond (♦) indicates the relaxed ammonium astatide in structure B. The asterisk (*) indicates the rigid ammonium astatide in structure A. The square (■) indicates the relaxed ammonium astatide in structure A.

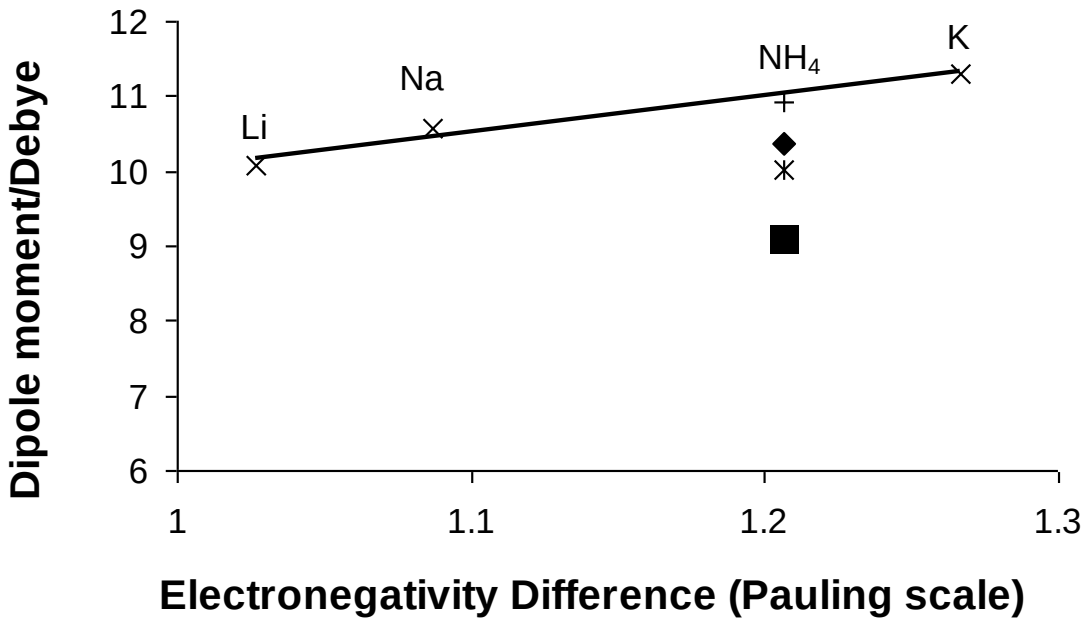

Figure 6.4: Correlation between the electronegativity difference (Pauling scale) and dipole moment (Debye), with alkali-astatide and nitrogen-astatide distances (R_{NAt}) fixed to that obtained for structure B with rigid NH_4 at 3.1293 Å. Symbols as in Figure 6.3.

In the next step we considered the effect of the geometrical relaxation of the NH_4^+ unit caused by the interaction with At^-, while the interionic distance remains fixed. This partial geometrical relaxation causes a drop in dipole moment and q_{At} (symbols "♦" for B and "■" for A in Figure 6.3 and Figure 6.4). For the B orientation, the dipole moment dropped by 0.55 D while the q_{At} value was reduced by 0.035 e. The most profound geometrical change is the widening of the "umbrella" angle by 5.4°, i.e., moving the "umbrella" hydrogens toward astatine. In addition, the umbrella and handle hydrogen-nitrogen distances lengthened by 0.004 Å and shortened by 0.003 Å, respectively, with respect to the isolated ammonium cation.[5] Thus all the hydrogen atoms have relaxed closer to astatine. Given that the hydrogen atoms carry partial positive charges, this relaxation contributes to the reduction in the dipole moment of the complex. The reduction in q_{At} and the dipole moment with respect to the "+" values provides direct evidence for quenching the iconicity of the complex resulting from the structural flexibility of ammonium.

The relaxation of NH_4^+ causes similar changes in structure A (* versus ■ in Figure 6.3 and Figure 6.4). The dipole moment declined by 0.95 D while q_{At} was reduced by 0.045 e. The most profound geometrical change is the elongation of the "handle" hydrogen-

[5] CCSD with a triple-zeta basis set.

nitrogen distance by 0.11 Å with respect to the isolated ammonium cation. This change is consistent with a hydrogen-bonding interaction between ammonium cation and astatide. In addition, the "umbrella" hydrogen-nitrogen distance decreased by 0.007 Å and the umbrella angle is reduced by 0.4° versus the tetrahedral angle. The net result of these rearrangements is again to move the hydrogens toward the astatide and reduce the overall dipole of the complex. The reduction in q_{At} and the dipole moment with respect to the rigid values values ("*") provides further evidence for quenching the iconicity of the complex resulting from structural flexibility of ammonium.

In the final step we allow for the relaxation of the interionic distance in both the alkali and ammonium astatides and the resulting q_{At} values and dipole moments are presented in Figure 6.5 and Figure 6.6, respectively. The trend lines are again based on the results for alkali astatides. As the "fixed" interionic distance used in Figure 6.3 and Figure 6.4 was optimal for the B structure with the rigid tetrahedron, it is the A structure of ammonium astatide which is primarily affected by relaxation of this degree for freedom. Indeed, the dipole moment for the A orientation, rigid tetrahedron ("*" in Figure 6.6) lies just on the trend line! This results from the compound nature of the dipole moment. The value of q_{At} is too small with respect to the trend line by over 0.1 e, see Figure 6.4, but this deficiency in polarity is compensated by a relatively large interionic distance (3.25 vs. 3.13 Å for A and B, respectively) and the resulting dipole moment closely matches the trend line. The preference for a larger interionic distance in A is a reflection of the internal structure of NH_4, specifically of the repulsive steric interaction between the "handle" hydrogen and At. Notice that the values of q_{At} are only modestly affected by the relaxation of the interionic distance.

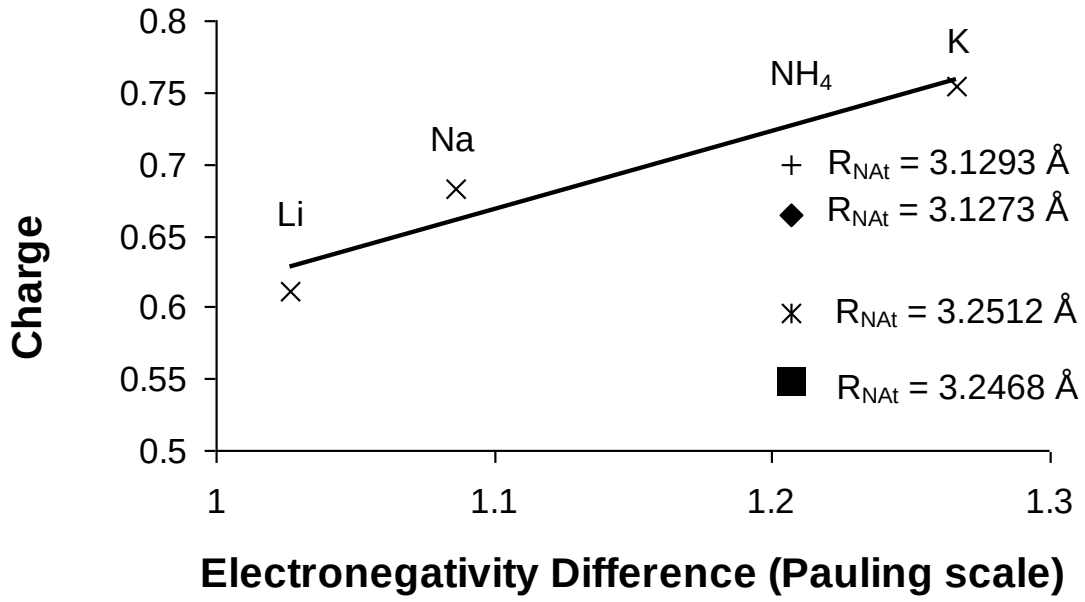

Figure 6.5: Correlation between the electronegativity difference (Pauling scale) and charge (in e) of astatide complexes, with optimum alkali-astatide and nitrogen-astatide distances (R_{NAt}). Symbols as in Figure 6.3.

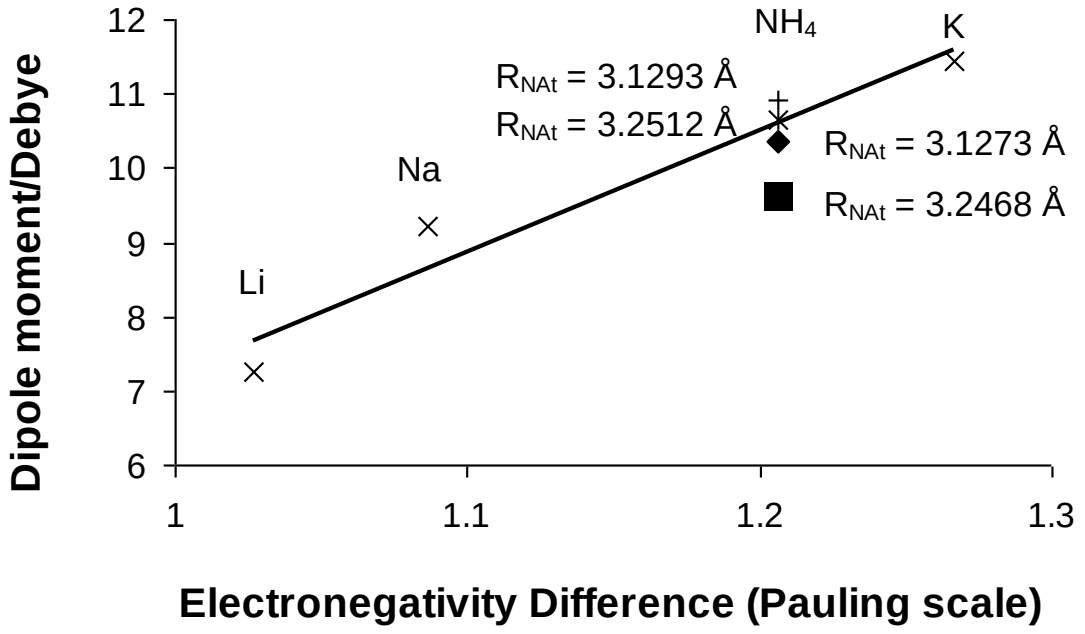

Figure 6.6: Correlation between the electronegativity difference (Pauling scale) and dipole moment (Debye), with optimal alkali-astatide and nitrogen-astatide distances (R_{NAt}). Symboles as in Figure 6.3.

The ionicities of the ammonium borohydride zinc blende crystal structures are consistent with the conclusions drawn from the gas phase study. Zinc blende structure B, which has less hydrogen bonding character, is more ionic (with a partial charge of

0.84 e on each ion) than structure A (0.77 e). This agrees with our gas-phase observation that permitting the use of ammonium's hydrogen-bonding ability leads to a reduction in the ionicity of its compounds. Therefore our conclusion regarding the effect of ammonium orientation upon the ionicity of its compounds has transferred from the gas phase to the crystal.

The relationship between improved stability and increased ionicity for the alkali metal borohydrides[28] does not follow for the relative energies of these ammonium borohydride structures. The more ionic structure B is less stable (by 1.1 eV per formula unit) than the less ionic structure A, which is contrary to the rule formulated for metal borohydrides, but consistent with the relative stability of the A and B complexes of NH_4^+ with At^-. The behaviour expected by considering ammonium as an atomic pseudo-alkali ion is trumped by its preferences with regard to intermolecular, i.e., dihydrogen, bonding.

The correlation between alkali metal borohydride decomposition temperatures and electronegativity of the metal is summarised in Figure 6.7.[6] The plot suggests that an alkali metal with an electronegativity higher than lithium is needed for more favourable hydrogen release. Ammonium's electronegativity of 0.77 to 0.79 on the Pauling scale would be too low for favourable hydrogen release if ammonium borohydride obeyed the electronegativity vs. temperature of dehydrogenation relation indicated by the black trend line on this chart, which predicts a release temperature on the order of 850 K.

[6] Note the correlation in the work of Orimo et al is made with the Pauling electronegativity, which has a thermochemical basis, while our calculated electronegativity for ammonium is the Mulliken electronegativity, which is electronic in nature. We plotted our own correlation using the Mulliken electronegativities of the alkali metals and ammonium, converted to the Pauling scale using Bratsch's method as outlined previously. The converted Mulliken electronegativities of the alkali metals are lower than the Pauling electronegativites. The discrepancy is 0.01 for lithium, 0.02 for sodium, 0.09 for potassium, and 0.12 for rubidium.

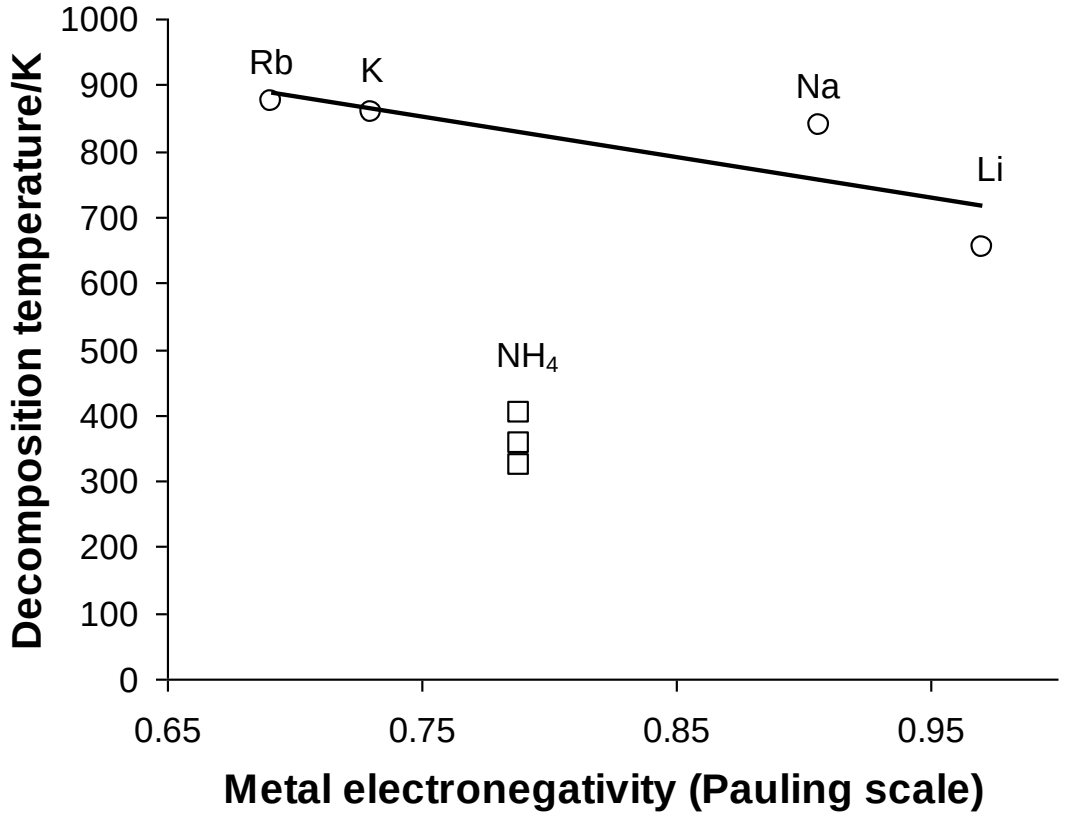

Figure 6.7: Correlation between the decomposition temperatures of alkali metal and ammonium borohydrides, and the electronegativities of the alkali metal atoms and the ammonium radical. Circles (○) denote results for alkali metal borohydrides from Orimo *et al.*[62] The line represents a least-squares fit to these points. Squares (□) denote three hydrogen release temperatures of ammonium borohydride,[30] plotted against the adiabatic electronegativity of NH_4.

However, ammonium borohydride's first hydrogen release temperature,[7] indicated with the lowest square (□),[30] is significantly lower than those of the alkali metal borohydrides. This is due to the substantially different mechanism of hydrogen release. Ammonium borohydride's decomposition reaction takes advantage of the presence of protic hydrogens on ammonium, which can interact with the hydridic hydrogens on borohydride for the facile release of molecular hydrogen.[30] Therefore the electronegativity of ammonium is not a suitable descriptor for the hydrogen release temperature of NH_4BH_4, due to its molecular nature.

[7] Ammonium borohydride can release up to four equivalents of molecular hydrogen per formula unit, with increasing temperature. The experimentally reported temperatures for some of these decompositions are plotted with the additional squares, but do not correspond to any borohydride. Note that the adiabatic electronegativity of ammonium has been used for the plot.

6.5. Discussion

The calculated electronegativity of 2.556 to 2.507 eV for ammonium lies between the values for sodium (2.84 eV[23]) and potassium (2.42 eV[23]) on the Mulliken scale. Similarly, ammonium's hardness of 2.098 eV to 2.037 eV is between that of sodium (2.30 eV)[60,61] and potassium (1.92 eV) [60,61] As anticipated, structural relaxation in isolated ammonium upon the change in the number of electrons was very minor at the CCSD and CCSD(T) levels and does not exceed 0.016 and 0.017 Å, respectively (see the Supporting Information).

The similarity in the structures corresponding to the different charge states is reflected in the similarity of the adiabatic and vertical electronegativities and hardnesses. In fact, the majority of the difference is due to the inclusion of a zero-point vibrational energy correction in the adiabatic calculations. The adiabatic electronegativity and hardness were higher than the vertical electronegativity and hardness in each case. Ammonium's effective cationic radius is 1.46 Å,[44] which is significantly larger than that of potassium (1.38 Å[44]) and near that of rubidium (1.52 Å[44]). Therefore if ammonium were an alkali metal, it would have an unusually high electronegativity and hardness for the size of its cation, and *vice versa* (see Figure 6.8).

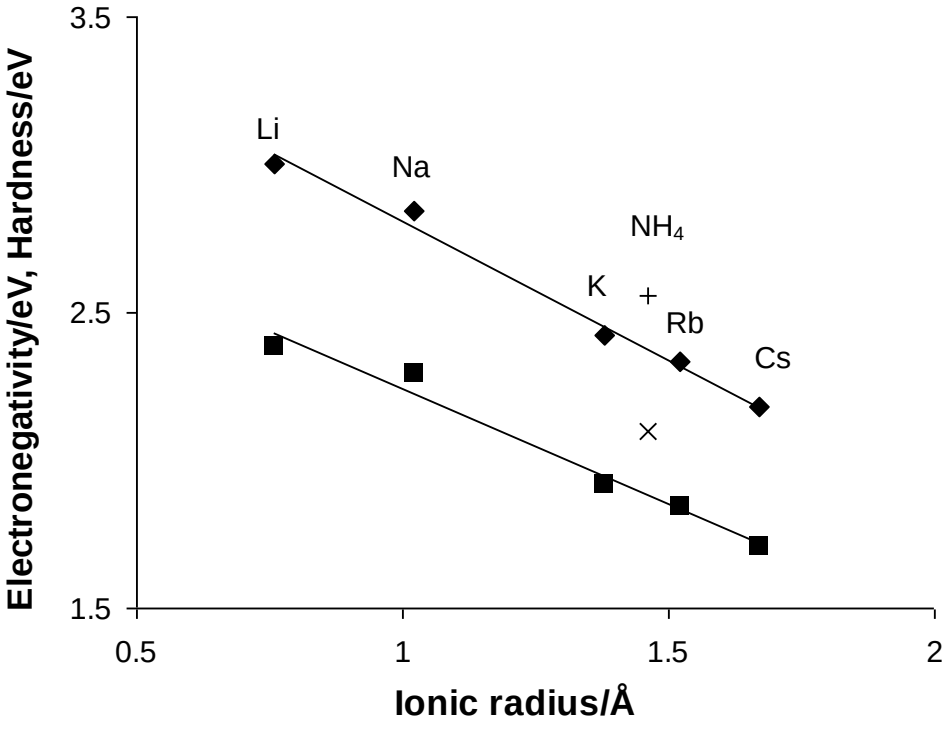

Figure 6.8: Neutral electronegativity and hardness versus cation radius[44] for the alkali metals and ammonium. Electronegativity as diamonds ("♦") for alkali metals and vertical cross ("+") for NH_4. Hardness as squares ("■") for alkali metals and diagonal cross ("x") for NH_4.

With regard to the electronegativity-ionicity relations, note that the values of q_{At} are systematically below the trend lines, irrespective of the orientation of the tetrahedron, its deformation, or interionic relaxation (Figure 6.3 and Figure 6.4). However the effective cationic radius of NH_4 is large for its electronegativity (Figure 6.8). This increases the equilibrium cation-anion distance, and consequently the dipole moments, which end up, fortuitously, close to the alkali trend lines (Figure 6.6).

The calculated Mulliken electronegativity of 2.5 eV for NH_4 justifies a high polarity of its complexes with astatine (χ_M = 6.2 eV), as reflected by their significant dipole moments (9.1 to 10.9 D). There are, however, other factors that partially quench the ionicity of these complexes. These are: (i) participation of NH_4 in hydrogen bonding and (ii) geometrical distortion of NH_4 away from the tetrahedral structure. Both are manifestations of the molecular (polyatomic) nature of NH_4 and the availability of protic hydrogens. Similarly, in the ammonium borohydride zinc blende crystals, allowing ammonium to act as a hydrogen bond donor reduced the ionicity of the crystal. The structure of ammonium borohydride, given ammonium's high electronegativity, is worthy of further discussion. The alkali metal borohydrides, with the exception of lithium, adopt a cubic rock salt structure with orientational disorder of the hydrogen atoms around the boron atoms.[63] These are the same structures as the corresponding bromides, which given the borohydride anion's comparable radius (2.03 Å[64] for BH_4^- versus 1.96 Å[44] for Br^-) is not surprising (lithium borohydride adopts a cubic zinc blende structure, in which the faces of borohydride tetrahedra are oriented toward alkali metal atoms,[65] while lithium bromide adopts the rock salt structure.) Given that Rb^+ has a similar radius to NH_4^+ (Figure 6.8), that rubidium borohydride has the rock salt structure, and that most of the alkali borohydrides adopt the rock salt structure, we may assume that ammonium borohydride would also adopt this structure. However, theoretical results in this study and prior work[30] indicate that the zinc blende structure has a lower electronic energy than the rock salt structure.

Mooser and Pearson's empirical rules for binary crystals suggest that for ions of a given size, decreasing the electronegativity difference tends to favour the zinc blende and wurtzite structures over the rock salt and caesium chloride structures.[66] Starting from rubidium borohydride structure, we may replace rubidium with ammonium, which is of a similar size but which is much more electronegative (see Figure 6.8). Therefore the

electronegativity difference between "metal" and borohydride is reduced, and the balance is tipped in favour of the zinc blende structure. We therefore conjecture that the relatively large electronegativity of ammonium for its size contributes to the similarity in stability of the zinc blende and rock salt structures of its borohydride.

The relative stability of the zinc blende and rock salt structures is a complex problem.[30] Calculations indicate that entropic factors arising from the orientational disorder of the ammonium and borohydride ions will cause ammonium borohydride to favour the rock salt structure.[30] Once again, effects arising from the polyatomic nature of NH_4 and BH_4 would be acting contrary to the effects associated with the electronegativity difference.

6.6. Conclusions

We have computed the Mulliken electronegativity of the ammonium radical as 2.507 eV based on the vertical ionization potential and electron affinity (assuming rigidity) and 2.556 eV based on adiabatic data (allowing relaxation). We have also computed the Pearson hardness as 2.037 eV in the vertical case, and 2.098 eV in the adiabatic case. These values are intermediate between those of sodium and potassium, although ammonium has an effective cationic radius between potassium and rubidium. In comparison with alkali atoms, ammonium's electronegativity "punches above" its effective cationic radius

We have identified in what ways ammonium's molecular nature competes with its pseudo-atom nature. Allowing ammonium to act as a hydrogen bond donor, or to geometrically distort causes a partial quenching of its ionicity in a heterodimer or crystal. The equilibrium interionic distance of its heterodimer, and thus the dipole moment, depends upon whether the ammonium tetrahedral face or vertex is directed at its neighbour. And in the borohydrides, allowing ammonium to act as a source of hydrogen opens up new reaction mechanisms for decomposition that are unavailable to the alkali metals, leading to a markedly different decomposition temperature.

In conclusion, it has been shown that that ammonium's electronegativity remains the dominant factor in determining polarity, or iconicity, of its compounds. The deviations from the behaviour expected of a conceptual "true alkali metal" with this

electronegativity allow for the discrimination of effects associated with the polyatomic nature of NH_4.

6.7. Appendix: Supplementary Information

Table 6.3: Structural parameters of tetrahedral ammonium optimised at CCSD(T) with a quadruple-zeta basis set

Ammonium species	N-H distance (Å)
Cation	1.020793
Neutral radical	1.037817
Anion	1.038075

Table 6.4: Structural parameters of tetrahedral ammonium optimised at CCSD with a triple-zeta basis set

Ammonium species	N-H distance (Å)
Cation	1.020699
Neutral radical	1.036253
Anion	1.035621

Table 6.5: M-At distances (Å) of alkali metal astatides optimised at CCSD with a triple-zeta basis set.

Species	M-At distance
LiAt	2.473519
NaAt	2.807132
KAt	3.161683

Table 6.6: Optimised structural parameters of ammonium astatide complexes, with fixed N-At distance of 3.129267Å.. Computed at CCSD with a triple-zeta basis set, parameters as defined in Figure 6.1,

Structure	Relaxed ammonium	N-H distances (Å)		Umbrella angle (degrees)
		Umbrella	Handle	
A	No	1.037817	1.037817	109.4712
A	Yes	1.014029	1.130603	109.0492
B	No	1.037817	1.037817	109.4712
B	Yes	1.024800	1.017454	114.9086

Table 6.7; Optimised structural parameters of ammonium astatide complexes, with a relaxed N-At distance. Computed at CCSD with a triple-zeta basis set., parameters as defined in Figure 6.1.

Structure	Relaxed ammonium	N-H distances (Å)		N-At distance (Å)	Umbrella angle (degrees)
		Umbrella	Handle		
A	No	1.037817	1.037817	3.251229	109.4712
A	Yes	1.013987	1.136430	3.246783	108.7977
B	No	1.037817	1.037817	3.129266	109.4712
B	Yes	1.024780	1.017470	3.127330	114.9240

Table 6.8: Unit cell of ammonium borohydride zinc blende structure A, optimised with PW91 using PAW pseudopotentials.

Cell vectors (Å):
a 5.1335458009040660 -0.0235500354008238 -0.3840658446176553
b -0.0234581092507503 5.1341681061017880 -0.3847550083818576
c 2.8075901210810380 2.8073247543690010 3.1185642438214990

Atomic positions in direct coordinates:
N 0.7645084075436205 0.1365109104196390 0.7252345451772200
B 0.0162160596308303 0.8846295454023274 0.2253354923674998
H 0.7243882807774787 0.7866911824164417 0.3935680891969809
H 0.0794643625683199 0.7544305207815673 0.4554915226582984
H 0.1141412715356508 0.1763894293011204 0.0571941765710051
H 0.1464594710835674 0.8214898946290582 0.9950531025575302
H 0.8095448760549329 0.0174138822250706 0.9278414962412535
H 0.5188492228553107 0.0549971046902061 0.8565992035943381
H 0.8461970998700018 0.3821304376452062 0.5938638112811853
H 0.8835388217802667 0.0914321907893582 0.5226394197546850

Table 6.9: Unit cell of ammonium borohydride zinc blende structure B, optimised with PW91 using PAW pseudopotentials.

Cell vectors (Å):
a 5.6816776657229870 -0.0374515339523117 -0.4484371799942925
b -0.0374086411750119 5.6801086497665860 -0.4497660063360067
c 3.0858164994323410 3.0839471627306210 3.4387573934370530

Atomic positions in direct coordinates:
B 0.7629498571604868 0.1380393340593030 0.7253395255202859
N 0.0178154174742070 0.8830633138588478 0.2252323846805541
H 0.7968699186728154 0.8094338041799586 0.3556057830276947
H 0.0713153219913259 0.7891914383901534 0.3955783686828067
H 0.0914391699808737 0.1040140188264751 0.0948301956265480
H 0.1118118727685051 0.8294701601228478 0.0548911835306147
H 0.8448870474690436 0.0472910609805322 0.9081742031031389
H 0.5012086543776734 0.0499240144996494 0.9010391041630239
H 0.8516011282287041 0.3997635968797088 0.5495656056200135
H 0.8534094855763659 0.0559243565024760 0.5425645054452943

6.8. References

[1] L. Pauling *The Partial Ionic Character of Covalent Bonds and the Relative Electronegativity of Atoms* in *The Nature of the Chemical Bond*; Third ed.; Cornell University Press: Ithaca New York, 1960.

[2] R. W. Taft, *Concerning the Electron-Withdrawing Power and the Electronegativity of Groups*, J. Chem. Phys., **26**, 93-96 (1957)

[3] L. Pauling, *The Nature of the Chemical Bond. IV. The Energy of Single Bonds and the Relative Electronegativity of Atoms.*, J. Am. Chem. Soc., **54**, 3570-3582 (1932)

[4] R. S. Mulliken, *A New Electroaffinity Scale; Together with Data on Valence States and on Valence Ionization Potentials and Electron Affinities*, J. Chem. Phys., **2**, 782-791 (1934)

[5] J. Hinze and H. H. Jaffe, *Electronegativity. I. Orbital Electronegativity of Neutral Atoms*, J. Am. Chem. Soc., **84**, 540-546 (1962)

[6] R. T. Sanderson, *Electronegativities in inorganic chemistry: (II)*, J. Chem. Educ., **31**, 2-7 (1954)

[7] J. E. Huheey, *The Electronegativity of Groups*, J. Phys. Chem., **69**, 3284-3291 (1965)
[8] S. G. Bratsch, *Electronegativity equalization with Pauling units*, J. Chem. Educ., **61**, 588-589 (1984)
[9] R. G. Parr, R. A. Donnelly, M. Levy and W. E. Palke, *Electronegativity: The density functional viewpoint*, J. Chem. Phys., **68**, 3801-3807 (1978)
[10] R. G. Pearson, *Hard and Soft Acids and Bases*, J. Am. Chem. Soc., **85**, 3533-3539 (1963)
[11] R. G. Parr and R. G. Pearson, *Absolute Hardness: Companion Parameter to Absolute Electronegativity*, J. Am. Chem. Soc., **105**, 7512-7516 (1983)
[12] T. Leyssens, P. Geerlings and D. Peeters, *The Importance of the External Potential on Group Electronegativity*, J. Phys. Chem. A, **109**, 9882-9889 (2005)
[13] G. I. Gellene, D. A. Clearly and R. F. Porter, *Stability of the ammonium and methylammonium radicals from neutralized ion-beam spectroscopy*, J. Chem. Phys., **77**, 3471-3477 (1982)
[14] G. Herzberg, *Rydberg Spectra of Triatomic Hydrogen and of the Ammonium Radical*, Faraday Discuss., **71**, 165-173 (1981)
[15] A. I. Boldyrev and J. Simons, *Rydberg Bonding in $(NH_4)_2$*, J. Phys. Chem., **96**, 8840-8843 (1992)
[16] J. Wright and D. McKay, *Stability of the Rydberg dimer $(NH_4)_2$*, J. Phys. Chem., **100**, 7392-7397 (1996)
[17] A. I. Boldyrev and J. Simons, *On the possibility of mixed Rydberg-valence bonds*, J. Phys. Chem. A, **103**, 3575-3580 (1999)
[18] J. T. Snodgrass, J. V. Coe, C. B. Freidhoff, K. M. McHaugh and K. H. Bowen, *Photodetachment spectroscopy of cluster anions. Photoelectron spectroscopy of $H^-(NH_3)_1$, $H^-(NH_3)_2$ and the tetrahedral isomer of NH_4^-*, Faraday Discuss., **86**, 241-256 (1988)
[19] J. V. Ortiz, *Vertical and adiabatic ionization energies of NH_4^- isomers via electron propagator theory and many-body perturbation-theory calculations with large basis-sets*, J. Chem. Phys., **87**, 3557-3562 (1987)
[20] M. Gutowski, J. Simons, R. Hernandez and H. L. Taylor, *"Double-Rydberg" Molecular Anions*, J. Phys. Chem., **92**, 6179-6182 (1988)
[21] K. W. Sattelmeyer, H. F. Schaefer and J. F. Stanton, *The eqiulibrium structure of the ammonium radical Rydberg ground state*, J. Chem. Phys., **114**, 9863-9865 (2001)
[22] M. W. Crofton and T. Oka, *Observation of forbidden transitions of ammonium ion (NH_4^+) v_3 band and determination of ground state rotational constants. Observation of v3 band allowed transitions of ND_4^+*, J. Chem. Phys., **86**, 5983-5988 (1987)
[23] S. G. Bratsch, *Revised Mulliken electronegativities: I. Calculation and conversion to Pauling units*, J. Chem. Educ., **65**, 34-41 (1988)
[24] B. P. Dailey and C. H. Townes, *The Ionic Character of Diatomic Molecules*, J. Chem. Phys., **23**, 118-123 (1955)
[25] S. N. Eustis, D. Radisic, K. H. Bowen, R. A. Bachorz, M. Haranczyk, G. K. Schenter and M. Gutowski, *Electron-Driven Acid-Base Chemistry: Proton Transfer from Hydrogen Chloride to Ammonia*, Science, **319**, 936-939 (2008)
[26] S. N. Eustis, A. Whiteside, D. Wang, M. Gutowski and K. H. Bowen, *Ammonia−Hydrogen Bromide and Ammonia−Hydrogen Iodide Complexes: Anion Photoelectron and ab Initio Studies*, J. Phys. Chem. A, **114**, 1357-1363 (2009)
[27] Y. T. Oganessian, F. S. Abdullin, P. D. Bailey, D. E. Benker, M. E. Bennett, S. N. Dmitriev, J. G. Ezold, J. H. Hamilton, R. A. Henderson, M. G. Itkis, Y. V. Lobanov, A. N. Mezentsev, M. K. J., S. L. Nelson, A. N. Polyakov, C. E. Porter, A. V. Ramayya, F. D. Riley, J. B. Roberto, M. A. Ryabinin, K. P. Rykaczewski, R. N. Sagaidak, D. A. Shaughnessy, I. V. Shirokovsky, M. A. Stoyer, V. G. Subbotin, R. Sudowe, A. M.

Sukhov, Y. S. Tsyganov, V. K. Utyonkov, A. A. Voinov, G. K. Vostokin and P. A. Wilk, *Synthesis of a New Element with Atomic Number Z=117*, Phys. Rev. Lett., **104**, 142502 (2010)

[28] Y. Nakamori, K. Miwa, A. Ninomiya, H. Li, N. Ohba, S.-i. Towata, A. Züttel and S.-i. Orimo, *Correlation between thermodynamical stabilities of metal borohydrides and cation electronegativitites: First-principles calculations and experiments*, Phys. Rev. B: Condens. Matter, **74**, 045126 (2006)

[29] A. Züttel, A. Borgschulte and S. Orimo, *Tetrahydroborates as new hydrogen storage materials*, Scripta Mater., **56**, 823-828 (2007)

[30] A. Karkamkar, S. Kathmann, G. Schenter, D. Heldebrant, N. Hess, M. Gutowski and T. Autrey, *Thermodynamic and Structural Investigations of Ammonium Borohydride, a Solid with a Highest Content of Thermodynamically and Kinetically Accessible Hydrogen*, Chem. Mater., **21**, 4356-4358 (2009)

[31] R. J. Bartlett and M. Musial, *Coupled-cluster theory in quantum chemistry*, Rev. Mod. Phys., **79**, 291-352 (2007)

[32] Gaussian 03, Revision C.02, M. J. Frisch, G. W. Trucks, H. B. Schlegel, G. E. Scuseria, M. A. Robb, J. R. Cheeseman, J. A. Montgomery Jr., T. Vreven, K. N. Kudin, J. C. Burant, J. M. Millam, S. S. Iyenga, J. Tomasi, V. Barone, B. Mennucci, M. Cossi, G. Scalmani, N. Rega, G. A. Petersson, H. Nakatsuji, M. Hada, M. Ehara, K. Toyota, R. Fukuda, J. Hasegawa, M. Ishida, T. Nakajima, Y. Honda, O. Kitao, H. Nakai, M. Klene, X. Li, J. E. Knox, H. P. Hratchian, J. B. Cross, C. Adamo, J. Jaramillo, R. Gomperts, R. E. Stratmann, O. Yazyev, A. J. Austin, R. Cammi, C. Pomelli, J. W. Ochterski, P. Y. Ayala, K. Morokuma, G. A. Voth, P. Salvador, J. J. Dannenberg, V. G. Zakrzewski, S. Dapprich, A. D. Daniels, M. C. Strain, O. Farkas, D. K. Malick, A. D. Rabuck, K. Raghavachari, J. B. Foresman, J. V. Ortiz, Q. Cui, A. G. Baboul, S. Clifford, J. Cioslowski, B. B. Stefanov, G. Liu, A. Liashenko, P. Piskorz, I. Komaromi, R. L. Martin, D. J. Fox, T. Keith, M. A. Al-Laham, C. Y. Peng, A. Nanayakkara, M. Challacombe, P. M. W. Gill, B. Johnson, W. Chen, M. W. Wong, C. Gonzalez and J. A. Pople, Gaussian, Inc., Wallingford CT, 2004

[33] T. H. Dunning, *Gaussian basis sets for use in correlated molecular calculations. I. The atoms boron through neon and hydrogen*, J. Chem. Phys., **90**, 1007-1023 (1989)

[34] D. E. Woon and T. H. Dunning, *Gaussian basis sets for use in correlated molecular calculations. V. Core-valence basis-sets for boron through neon*, J. Chem. Phys., **103**, 4572-4585 (1995)

[35] R. A. Kendall, T. H. Dunning and R. J. Harrison, *Electron affinities of the first-row atoms revisited. Systematic basis sets and wave functions*, J. Chem. Phys., **96**, 6796-6806 (1992)

[36] A. Schafer, H. Horn and R. Ahlrichs, *Fully optimized contracted Gaussian basis sets for atoms Li to Kr*, J. Chem. Phys., **97**, 2571-2577 (1992)

[37] D. Feller, E. D. Glendening, D. E. Woon and M. W. Feyereisen, *An extended basis set ab initio study of alkali metal cation–water clusters*, J. Chem. Phys., **103**, 3526-3542 (1995)

[38] K. Schuchardt, B. Didier, T. Elsethagen, L. Sun, V. Gurumoorthi, J. Chase, J. Li and T. Windus, *Basis Set Exchange: A community database for computational sciences*, J. Chem. Inf. Model., **47**, 1045-1052 (2007)

[39] D. Feller, *The role of databases in support of computational chemistry calculations*, J. Comput. Chem., **17**, 1571-1586 (1996)

[40] K. Peterson, D. Figgen, E. Goll, H. Stoll and M. Dolg, *Systematically convergent basis sets with relativistic pseudopotentials. II. Small-core pseudopotentials and correlation consistent basis sets for the post-d group 16-18 elements*, J. Chem. Phys., **119**, 11113-11123 (2003)

[41] M. Gutowski, K. D. Jordan and P. Skurski, *Electronic Structure of Dipole-Bound Anions*, J. Phys. Chem. A, **102**, 2624-2633 (1998)
[42] P. A. Kollman and S. U. Chandra, *An Approach to Computing Electrostatic Charges for Molecules*, J. Comput. Chem., **5**, 129-145 (1984)
[43] B. H. Besler, K. M. Merz and P. A. Kollman, *Atomic charges derived from semiempirical methods*, J. Comput. Chem., **11**, 431-439 (1990)
[44] R. D. Shannon, *Revised effective ionic-radii and systematic studies of interatomic distances in halides and chalcogenides*, Acta Crystallogr. Sect. A: Found. Crystallogr., **A32**, 751-767 (1976)
[45] A. Halkier, T. Helgaker, P. Jørgensen, W. Klopper and J. Olsen, *Basis-set convergence of the energy in molecular Hartree–Fock calculations*, Chem. Phys. Lett., **302**, 437-446 (1999)
[46] T. Helgaker, W. Klopper, H. Koch and J. Noga, *Basis-set convergence of correlated calculations on water*, J. Chem. Phys., **106**, 9639-9646 (1997)
[47] J. P. Perdew, J. A. Chevary, S. H. Vosko, K. A. Jackson, M. R. Pederson, D. J. Singh and C. Fiolhais, *Atoms, molecules, solids, and surfaces: Applications of the generalized gradient approximation for exchange and correlation*, Phys. Rev. B: Condens. Matter, **46**, 6671-6687 (1992)
[48] G. Kresse and D. Joubert, *From ultrasoft pseudopotentials to the projector autmented-wave method*, Phys. Rev. B: Condens. Matter, **59**, 1758-1775 (1999)
[49] G. Kresse and J. Hafner, *Ab initio molecular dynamics for liquid metals*, Phys. Rev. B: Condens. Matter, **47**, 558-561 (1993)
[50] G. Kresse and J. Hafner, *Ab initio molecular dynamics simulation of the liquid-metal-amorphos-semiconductor transition in germanium*, Phys. Rev. B: Condens. Matter, **49**, 14251-14269 (1994)
[51] G. Kresse and J. Furthmüller, *Efficiency of ab-initio total energy calculations for metals and semiconductors using a plane-wave basis set*, Comput. Mater. Sci., **6**, 15-50 (1996)
[52] G. Kresse and J. Furthmüller, *Efficient iterative schemes for ab initio total-energy calculations using a plane-wave basis set*, Phys. Rev. B: Condens. Matter, **54**, 11169-11186 (1996)
[53] R. F. W. Bader, *Atoms in Molecules*, Acc. Chem. Res., **18**, 9-15 (1985)
[54] G. Henkelman, A. Arnaldsson and H. Jónsson, *A fast and robust algorithm for Bader decomposition of charge density*, Comput. Mater. Sci., **36**, 254-360 (2006)
[55] E. Sanville, S. D. Kenny, R. Smith and G. Henkelman, *An improved grid-based algorithm for Bader charge allocation*, J. Comput. Chem., **28**, 899-908 (2007)
[56] W. Tang, E. Sanville and G. Henkelman, *A grid-based Bader analysis algorithm without lattice bias*, J. Phys.: Condens. Matter, **21**, 084204 (2009)
[57] CS ChemDraw Std, Version 5.0, Cambridgesoft Corporation, Cambridge, MA, 02140, 1998
[58] P. Atkins and J. de Paula *Physical Chemistry*; Ninth ed.; Oxford University Press: Oxford, 2010.
[59] H. Hotop and W. C. Lineberger, *Binding energies in atomic negative ions*, J. Phys. Chem. Ref. Data, **4**, 539-576 (1975)
[60] S. G. Lias *Ionization Energy Evaluation* in *NIST Chemistry WebBook, NIST Standard Reference Database Number 69*; Linstrom, P. J.; Mallard, W. G., Eds.; National Institute of Standards and Technology: Gaithersburg MD, 2012.
[61] J. E. Bartmess *Negative Ion Energetics Data* in *NIST Chemistry WebBook, NIST Standard Reference Database Number 69*; Linstrom, P. J.; Mallard, W. G., Eds.; National Institute of Standards and Technology: Gaithersburg MD, 20899, 2012.
[62] S. Orimo, Y. Nakamori and A. Züttel, *Material properties of MBH_4 (M = Li, Na, and K)*, Mater. Sci. Eng., B, **108**, 51-53 (2004)

[63] G. Renaudin, S. Gomes, H. Hagemann, L. Keller and K. Yvon, *Structural and spectroscopic studies on the alkali borohydrides MBH_4 (M = Na, K, Rb, Cs)*, J. Alloys Compd., **375**, 98-106 (2004)
[64] S. C. Abrahams and J. Kalnajs, *The Lattice Constants of the Alkali Borohydrides and the Low-Temperature Phase of Sodium Borohydride*, J. Chem. Phys., **22**, 434-436 (1954)
[65] J. P. Soulie, G. Renaudin, R. Cerny and K. Yvon, *Lithium boro-hydride $LiBH_4$ I. Crystal Structure*, J. Alloys Compd., **346**, 200-205 (2002)
[66] E. Mooser and W. B. Pearson, *On the crystal chemistry of normal valence compounds*, Acta Crystallogr., **12**, 1015-1022 (1959)

Chapter 7: Summary

The ammonium-hydrogen halide systems have been extensively discussed in the context of the degree of proton transfer that they undertake. It has been demonstrated that the proton transfer in the neutral complex is actually driven by a common underlying balancing act between the one- and two-body forces upon the proton, a balancing act that is close to shifting in these species. The mild perturbation of the addition of a dipole-bound electron (a very weak interaction) can drive proton transfer in all of these systems save ammonium fluoride, and it has been demonstrated that this is driven by the electron's own demands upon the one- and two-body energy of the complex, which are likely to manifest as a force upon the proton if investigated using the techniques described in Chapter 4.

In view of this, it is hoped that such an analysis of proton transfer could be extended to other hydrogen-bonded systems, in particular those containing different bases. The balance of one- and two-body terms may suggest ways to control the PT properties of economically significant systems such as photoelectric devices and fuel cells, or biologically relevant materials, such as ion channels. Deeper analysis of the two-body term through techniques such as symmetry-adapted perturbation theory (SAPT) would be particularly enlightening. Furthermore, the close coupling of electron- and proton-transfer in these systems is suggestive of deeper subtleties. How to the terms binding the electron vary in these proton transfer systems? As suggested in the penultimate research chapter, describing the excess electron as an interacting third body – perhaps also via SAPT – would provide insight.

This analysis also provided the unexpected discovery of halogen-bonded systems for NH_3HX. Of particular interest is the ammonia-hydrogen astatide system, which has a dipole moment of over 2.6 D due to charge transfer from ammonium *in spite* of the halogen's proximity to it. A dipole of this magnitude should vertically bind an electron. While experimental verification of this system is unlikely to be forthcoming, a theoretical analysis would be intriguing.

Throughout this thesis, a constant theme has been the identity of ammonium. In the proton-transferred anions NH_4X^-, we can make the case that the system is actually an ammonium radical bound to a halide anion in much the same way as the alkali halide

anions, and is not a dipole-bound anion at all. Given this, the case has been made that ammonium is a well-defined pseudo-atom, and it has been tested by assigning it an electronegativity and exploring how its molecular and pseudo-atom natures compete. Could other molecules be engineered with such a split identity, carrying advantageous molecular *and* atomic properties? And how widely does this concept of the pseudo-atom with electronegativity carry? Many other plausible pseudo-atom units exist, such as the hydronium radical, the BH_4^- in alkali metal borohydrides, the B_{12} and B_2 "ions" suggested for a high-pressure phase of boron[1] and perhaps even fullerenes. It is not obvious what results might be found by the investigation of these species as atoms-and-molecules

In brief, it is anticipated that the generalisations presented here may be carried forward and exploited to better the understanding of intermolecular interactions and molecular anions.

7.1. References

[1] A. R. Oganov, J. H. Chen, C. Gatti, Y. Z. Ma, Y. M. Ma, C. W. Glass, Z. X. Liu, T. Yu, O. O. Kurakevych and V. L. Solozhenko, *Ionic high-pressure form of elemental boron*, Nature, **457**, 863-867 (2009)

Chapter 8: Glossary of Abbreviations

AIM	atoms in molecules; also known as "Bader's analysis", a method of defining and characterising the volumes of and interactions between atoms soley on the basis of the topology of the electron density (section 1.1)
BSSE	basis set superposition error; an error in computing interaction energies (section 2.6)
BCP	bond critical point; a point in a molecule lying between two atoms where the gradient of the density is zero, and the curvature is negative only along the internuclear axis
CI	configuration interaction; a post-Hartree-Fock method for computing electron correlation (section 2.3.2.1)
CIS/D/T	configuration interaction with single/double /triple excitations
CC	coupled cluster; a post-Hartree-Fock method for computing electron correlation (section 2.3.2.2)
CCS/D/T/(T)	coupled cluster method using single/double/triple/perturbative triple excitations
DFT	density functional theory; an electron correlation method in which the electron correlation energy is defined soley based on the electrn density
IR	infra-red; in this context, infra-red vibrational spectroscopy
mH	millihartree; a unit of energy equal to the product of the Rydberg constant, the Planck constant, and the speed of light (0.027 electron volts)
MPn (n=1,2,3...)	Møller-Plesset perturbation theory of order n; a post-Hartree-Fock method for computing electron correlation (section 2.3.2.3)
MCSCF	multi-configurational SCF; method for computing electron correlation by operating on a linear combination of determinants
NBO	natural bond order analysis; a method for describing the involvement of particularly orbitals in bonds by analysis the distribution of electron density between the basis functions
SCF	self-consistent field; in this context, the Hartree-Fock self-consistent field procedure (section 2.2)
SAPT	symmetry-adapted perturbation theory; an application of

perturbation theory, properly adapted to the antisymmetry of the electronic wavefunction, to decompose monomer interaction energies into electrostatic, induction etc. components